Production of a Non-Isocyanate Polyurethane (NIPU) Polymeric Material for Adhesive or Plasticizer Applications from Castor Oil and Chitosan

Andrés Felipe Guzmán Agudelo

Tesis doctoral presentada para optar al título de Doctor en Ingeniería Química

Directores
Luis Alberto Rios, Doctor (PhD) en Ciencias Naturales

Julian Antonio Restrepo, Doctor (PhD) en Química Sostenible

Universidad de Antioquia
Facultad de Ingeniería

Doctorado en Ingeniería Química

Medellín, Antioquia, Colombia

2024

Cita	(Guzmán, 2024)
Referencia **Estilo APA 7 (2020)**	Guzmán A. (2024). *Production of a Non-Isocyanate Polyurethane (NIPU) Polymeric Material for Adhesive or Plasticizer Applications from Castor Oil and Chitosan* [Tesis doctoral]. Universidad de Antioquia, Medellín, Colombia.

Doctorado en Ingeniería Química, Cohorte X.

Grupo de Investigación Procesos Químicos Industriales.

Sede de Investigación Universitaria (SIU).

Dedicatoria

A mi hija Amelie quien ha traído una inyección divina de fuerza vital a mi vida. A mi compañera de vida Sofía quien ha sido uno de mis grandes soportes y guías durante los últimos años. A mi madre Elvia cuyo apoyo, acompañamiento y amor ha sido fundamental para mí, siempre. Sin ellas tres nada hubiera sido posible.

A mis hermanos, mi padre y mis amigos, cuyas palabras de aliento nunca me dejaron caer.

Agradecimientos

Agradezco a mis directores de tesis, Doctor Luis Alberto Rios y Doctor Julián Antonio Restrepo por su acompañamiento y guía. A los profesores del departamento de ingeniería química quienes hicieron parte del programa de formación del Doctorado en Ingeniería química. A mis colegas del grupo de Procesos Químicos Industriales PQI por su valiosa ayuda en temas técnicos y de caracterización. A la facultad de ingeniería. A nuestra amada Alma Mater Universidad de Antioquia. Gracias por todo lo que me has brindado desde que ingresé como estudiante de ingeniería.

Un grand merci au Professeur Sébastien Leveneur pour son soutien lors du stage de recherche à l'Institut INSA de Rouen, France. Merci également au Professeur Nasreddine Kebir et à Wander Pérez, chercheur, pour leur aide précieuse.

Agradecimiento especial a Colciencias-Colfuturo y Sapiencia-Medelín por la financiación recibida para el desarrollo de ese programa.

.

TABLE OF CONTENTS

TABLE OF FIGURES

ABREVIATIONS AND SYMBOLS

%wt: Weight Percentage
%C: Conversion Percentage
%S: Selectivity percentage
%Y: Yield Percentage
$[NaOH]$: NaOH concentration (mol/L)
$\overline{\boldsymbol{\nu}}$: Wavenumber
AA: Acetic Acid
AA_n: Acetic Acid mol
AD:. Apparent Density (g/mL)
ANOVA: Analysis of variance
ASTM: American Society for Testing and Materials
AU: Arbitrary Units
AV: Acid Value (mg KOH/ g sample)
AVE: average
BA: n-butylamine
BDA: 1,4-Butylenediamine
C: Concentration
CC: Cyclic Carbonate
CCO: Carbonated Castor Oil
CH: Chitosan
CH_3COONa: Sodium Acetate
CLSO: Carbonated Linseed Oil
CMO: Carbonated Methyl Oleate
CNMR: Carbon Nuclear Magnetic Resonance
CO: Castor Oil
COFAME: Castor oil fatty acid methyl esters
CO_M: Castor Oil mass (g)
COOH: carboxylic acid group
CSBO: Carbonated Soybean Oil
CV: Coefficient of variation (%)
d: Doublete
DB: Double Bonds
DBA: Dibutyl amine
DB_n: Double Bond mol
DD: De-acetylation degree (%)
DDe: De-acetylation degree estimated by elemental analysis (%)
DDp: De-acetylation degree estimated by potentiometric analysis (%)
DMSO: Dimethyl sulfoxide
EBA : Ethyl butyl amine
ECO: Epoxidized Castor Oil
ECOFAME: Epoxidized castor oil fatty acid methyl esters
EDA: 1,2 Ethylenediamine
EFAD: Epoxidized Fatty Acid Diester

ESBO: Epoxidized Soybean Oil
EC: exchange capacity in equivalents/L
E_n: Epoxide mol
FA: Formic acid
FAME: Fatty Acid Methyl Esther
FFA: Free Fatty Acids
FTIR: Fourier Transformed Infrared spectroscopy
g: grams
GC: Gas chromatography
GC-MS: Gas chromatography-Mass spectrometry coupled technique
GLH: Glucosamine hydrochloride
HEX: Hexane
HMDA: 1,6-hexamethylenediamine
HNIPU: Hybrid Non-Isocyanate
HNMR: Proton or Hydrogen Nuclear Magnetic Resonance
HP: Hydrogen Peroxide
HP_n: Hydrogen Peroxide mol
η_r : Relative Viscosity
η_{sp}: Specific Viscosity
IER: Ion Exchange Resin
IER_M: Mass of Amberlite ® IR120 catalyst (g).
IEFAD: Internal Epoxidized Fatty Acid Diesters
IPDA: Isophorone-diamine
IV: Iodine value (g I_2 / 100 g sample) measured according to the ASTM D 5554 standard (ASTM, 2006).
IV_i: Initial Iodine Value
IV_f: Final Iodine Value
Krt: Kurtosis coefficient
L: Liters
LiTOf : Lithium triflate
LPT: Linear Potentiometric Titration
μ: Dynamic Viscosity
MBA: Methyl butyl amine
mL: Milliliters
Mv: Viscous Molecular Mass
Mw: Molecular Mass (g/mol)
Mw_{CO}: Castor Oil Molecular Mass
n: sample size
NaOH: Sodium Hydroxide
NaCl: Sodium Chloride
$NaCl_M$: Mass of NaCl in g.
$NaOH_V$: NaOH solution volume in mL
NH_2: Amino group
NIPU: Non-Isocyanate Polyurethane
OH: Hydroxyl groups

OOC: Oxirane-Oxygen Content Percentage measured according to the ASTM D 1652-04 standard (ASTM, 2004).
OOC_T: Theoretical Oxirane-Oxygen Content Percentage
PHU: Polyhydroxyurethane
PVC: Polyvinyl Chloride
PU: Polyurethane
RA: Ricinoleic Acid
RPM: revolutions Per Minute
s: Singlet
s.d: Standard Deviation
s.e: Standard Error
Skew: Skewness coeficcient
SS: Stirring Speed in RPM
SD: Standard Deviation
T: Temperature in °C
t: time
TA: tris(2-aminoehtyl) amine
TBABr: Tetrabuthylammonium Bromide
TBD: Triazabicyclodecene
TEFAD: Terminal Epoxidized Fatty Acid Diester
Tg: Glass Transition Temperature
TGA: Thermal Gravimetric Analysis
TOF: Turnover Frequency

1. ABSTRACT

A new bio-based non-isocyanate polyurethane (NIPU) material was developed from castor oil (Ricinus communis) and chitosan through various adequation steps and a polymerization reaction. The main research problem tackled in this project was the possibility of the reaction between amino groups of chitosan and cyclic carbonate groups through an aminolysis reaction to yield urethane or carbamate bonds. Many reports have been published about this reaction with different substrates, mainly in homogeneous conditions using carbonated and aminated substrates. Carbamate bond production from amine groups of polysaccharides like chitosan has been broadly studied through the reaction with chloroformates (chloroformic acid esters), but only one report was found on the attempt to produce carbamate through carbonate-amine aminolysis (Aiba, 1993). Indeed, this work uses chitosan as an aminated substrate and linear carbonates such as diethyl and dimethyl pyrocarbonates. To the best of the author's knowledge, this is the closest study to what was intended to be done in this project, as no cyclic carbonates have been used in this reaction. In the project, several defined processing steps for castor oil can be identified: epoxidation and carbonation. In the epoxidation step, the mass transfer limitation involved in the performance of the catalyst was studied. A factor significance study and an optimization of the reaction parameters were carried out using response surface experimental designs. Some pilot-scale runs were also done to study the behavior and the evolution of temperature. At the epoxidized castor oil carbonation step, the apparent improving effect of water in the reaction was studied. The aminolysis reaction was studied using a simple fatty-carbonated substrate like carbonated methyl oleate and short amines like n-butylamine and its derivatives. Kinetic studies were conducted at this stage. Then, carbonated methyl oleate and carbonated castor oil were reacted with glucosamine hydrochloride, which is the monomeric unit of chitosan. Characterization by nuclear magnetic resonance and Fourier transform infrared spectroscopy allowed the identification of carbamate bond production. Finally, carbonated castor oil was reacted with aqueous chitosan in an emulsion system, and the product was used as an additive for a commercial adhesive product, Autodhesan®, from ANDERCOL Co., an Akzo Nobel team member. The final product showed improved performance characteristics for the adhesive.

2. RESEARCH PROBLEM

Aminolysis reaction between cyclic carbonates and amines for urethane bond production have been broadly studied mainly with simple molecules an in homogeneous systems. It has been used also for non-isocyanate polyurethane (NIPU) production, commonly, from petroleum-derived compounds. Although renewable bio-based materials like vegetable oils, as the carbonated substrate, have been used in this process, they almost always are reacted with simple bi-functional amines from fossil sources, like ethylenediamine, hexamethylenediamine etc. As the best of the knowledge of the author, there is no report of a completely bio-based NIPU where both, cyclic carbonate and aminated substrates have origin in natural renewable sources.

Castor oil is a very versatile raw material that can be taken to the cyclic-carbonate form through epoxidation and carbonation processes. Although epoxidation of vegetable oils has a wide scientific background, castor oil epoxidation is a process needing more insight since castor oil has a different physicochemical behavior compared to the other common vegetable species due to the presence of hydroxyl group in ricinoleic acid, the main fatty acid of castor oil. Since one can find various reports of carbonation of some epoxidized ricinoleic-derived products, it is not the case for epoxidized castor oil. On the other hand, chitosan is a polysaccharide with multiple amine groups in its structure. Its solubility in water depends on the water pH, chitosan molecular mass and degree of de-acetylation. The challenge of making the carbonated castor oil oleaginous phase compatible with the chitosan aqueous phase in order to carry out a successful aminolysis reaction, becomes on of the basic facts sustaining the research question of this project. Furthermore, due to the great abundance of hydroxyl in both raw materials, as well as to the fact that aminolysis reaction produces hydroxyl groups as byproduct also, the expected product can be consistently thought as a material proper for adhesive or plasticizer applications. Taking into account all these elements, the author proposes the following research question: Is it possible to produce a Castor oil-Chitosan-based NIPU with special properties for adhesive or plasticizer applications?

2.1 Hypothesis

It is possible to carry out the aminolysis reaction between carbonated castor oil and aqueous chitosan in an emulsion system for producing a NIPU material for adhesive or plasticizer applications.

2.2 Objectives

General objective

To develop a castor oil / chitosan-based NIPU material for adhesive or plasticizer applications.

Specific objectives

- To determine the mass transfer effect involved in the catalysis of the epoxidation of castor oil.
- To determine the improving effect of water on the carbonation of epoxidized castor oil.
- To determine the kinetics aspects of the aminolysis of a simple fatty-carbonated substrate with different simple amines
- To test the NIPU material as an additive for adhesive or plasticizer applications in order to inquire its effect on performance features.

3. GENERALITIES

3.1 CASTOR OIL - MARKET AND APPLICATIONS

Castor oil (CO) is a vegetable oil produced from castor plant beans (*Ricinus Communis*). It is a viscous, pale-yellow liquid with a particular taste and odor. Compared with other vegetable oils, it has a good shell life and it does not turn rancid unless subjected to excessive heat. On average, castor seeds contain about 46-55% oil by weight. Castor seeds are poisonous to humans due to the presence of ricin and ricinine allergens that are extremely toxic with a small lethal dose of around 1 mg for an adult person (Ogunniyi, 2006). India is the largest producer of castor beans with around 6.000.000 tons in the period 2019-2022 followed by Mozambique and Brazil (FAO, 2024). Table 1 shows the castor bean production of various countries in the period 2019-2022. Brazil and Paraguay appear as the main Latin-American producers.

Table 1. Castor bean production of various countries, period 2019-2022

Country	Production (Ton)
India	6.304.420
Mozambique	293.910
Brazil	123.896
China	98.000
Myanmar	48.219
Ethiopia	43.000
Vietnam	27.000
Paraguay	25.000

Source: FAO Statistics, http://www.fao.org/faostat/en/#data

Colombia does not have an important production but also an infinite potential to do it. Figure 1 shows the Colombian castor bean production in the period 2014-2020.In the period 2019-2022, India was the largest castor oil been producer with 6.304.420 tones. At the same period, the largest exporter of castor bean was Ethiopia with 16264,71 ton (Table 2). Paraguay appears like the Latin-American largest exporter of castor bean. China appears like the largest importer (Table 3). Brazil also showed a notorious value. Values in Table 3 suggest the importance and size of the chemical industry around castor oil in China and Brazil (FAO, 2024). It is not a coincidence the large offer of castor oil-derived products like sebacic acid, hydrogenated and ethoxylated castor oil coming from these countries.

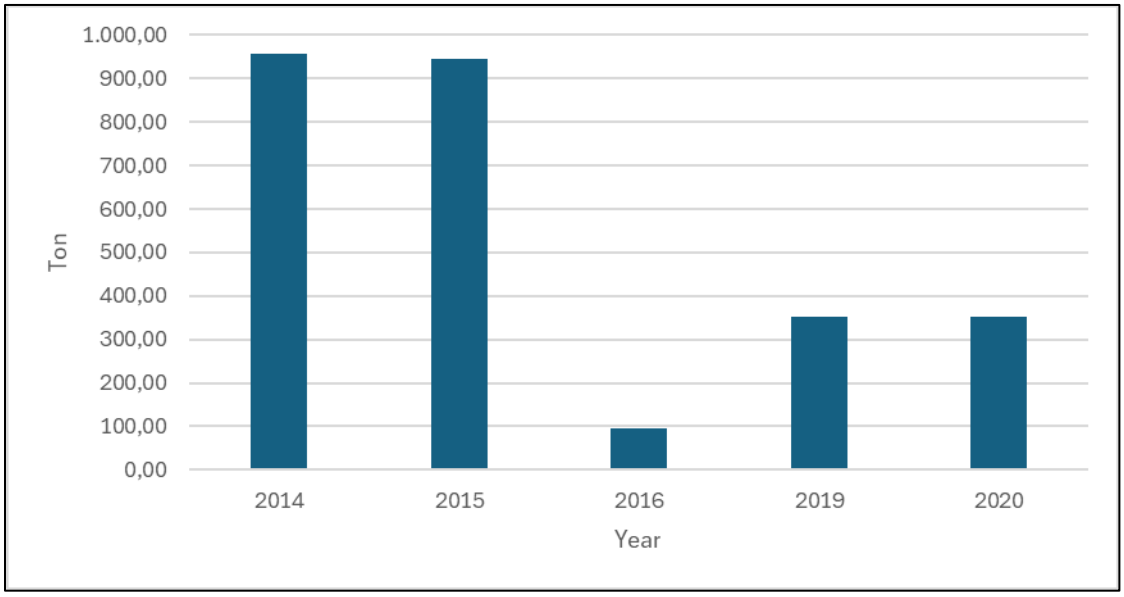

Figure 1. Colombian castor bean production, period 2014-2020

Source: Colombian Agricultural Ministry-AGRONET system, https://www.agronet.gov.co/Paginas/inicio.aspx

Table 2. Castor bean exportation of various countries, period 2019-2022

Country	Exportation (Ton)
Ethiopia	Ţ16264,71
Myanmar	15619,04
India	13026,39
Paraguay	4020

Source: FAO Statistics, http://www.fao.org/faostat/en/#data

Table 3. Castor bean importation of various countries, period 2019-2022

Country	Importation (Ton)
China	73661,89
Brazil	4198,13

Source: FAO Statistics, http://www.fao.org/faostat/en/#data

Due to its particular composition, CO is a very versatile raw material for many industrial, agricultural and pharmaceutical applications: Some derived products of castor oil include ointments, nylon, varnishes, lubricants, hydraulic fluids, dyes, detergents, plastics, synthetic leather, adhesives, paints, lacquers, plasticizers, coatings, inks, cosmetics and perfumes. The castor cake is mainly used as a fertilizer and it is unsuitable for animal feeding because of the presence of a very toxic protein called ricin and other allergens (Ogunniyi, 2006; Yeboah et al., 2020). Generalities

on the CO extraction, modification and applications are exposed in various reviews (Chauke et al., 2019; Mutlu & Meier, 2010; Patel et al., 2016).

3.2 CASTOR OIL PROPERTIES AND MODIFICATION

The extraction of castor oil (CO) can be carried out by mechanical means and/or solvent extraction. The mechanical extraction with a hydraulic press removes around 45% of the oil content of the seed (Ogunniyi, 2006). The refining process includes: settling/filtration, water and acid degumming and neutralization steps. CO physicochemical characteristics may vary according to the specie, type of extraction (solvent, cold pressing, hot pressing) and the quality of the oil (crude or refined). There are many reports about the physicochemical properties of CO. Table 4 compares the refined CO properties reported in various research works and the ASTM (American Society for Testing and Materials) specifications for the quality of CO.

Compared with other vegetable oils like palm or soybean, CO has high viscosity and affinity to water, due to its high content of ricinoleic acid (RA) (around 90%) in the triglyceride, which is a fatty acid with a hydroxyl group in the 12th position of the carbon chain. This hydroxyl group (OH) makes oil more hydrophilic than other vegetable oils and it tends to make hydrogen bonds, increasing viscosity. The average number of hydroxyl groups (OH) per triglyceride molecule is 2,7 (Bhaskar et al., 2018). Ricinoleic acid (RA) has also an unsaturation or double bond (DB) on the 9th position, which is the functional group to be modified in the epoxidation and carbonation steps. Figure 2 shows the RA structure as the main component of the castor oil trygliceride. The typical CO fatty acid composition ranges are shown in Table 5.

Table 4. Castor oil typical physicochemical characteristics

	REFERENCE					
PROPERTY	**(Ogunniyi, 2006)**	**(Akpan et al., 2006)**	**(Shridhar et al., 2010)**	**(Patel et al., 2016)**	**(Yeboah et al., 2020)**	**ASTM specification (Bhaskar et al., 2018)**
Specific gravity	0.961-0.963	0,9587	0,95	0,959	0,961	0,957-0,961
Acid value (mg KOH/g sample)	3	0,869	2,2	-	1,34	≤ 2
Iodine value (g I_2/100 g sample)	82-88	84,8	87	-	83	83-88
Saponification value (mg KOH/g sample	179-185	181,55	181	-	165,50-187,46	176-184
Hydroxyl value (mg KOH/g sample)	-	-	-	-	-	160-168
Kinematic Viscosity (St)	-	6,4842 (28°C)	6,9 (25°C)	8,893	1,86 St/dPas (30°C) 9,3-10 St/dPas (25°C)	6,3-8,9
Refractive index	-	1,4674	-	1,480	1,476	1,4764-1,4778

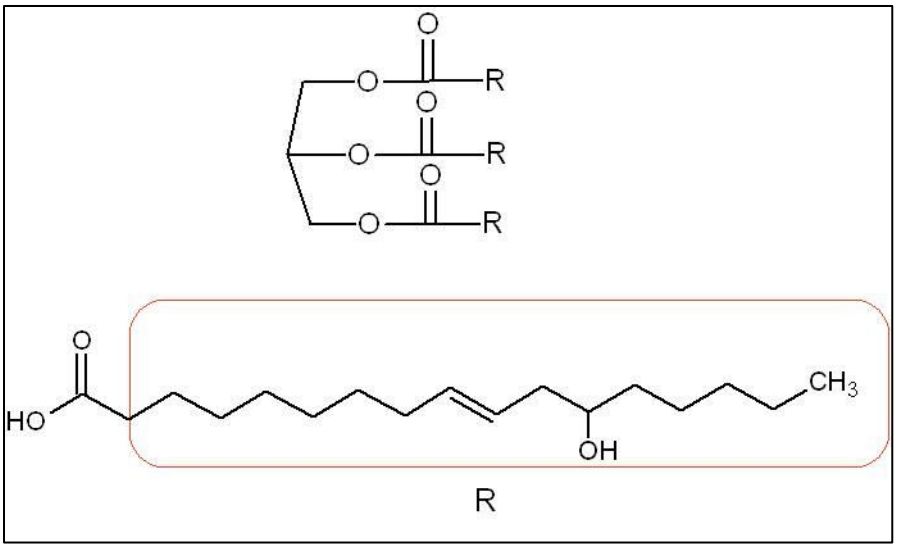

Figure 2. Ricinoleic acid structure

Table 5. Castor oil typical fatty acid composition range

Fatty acid	Composition range (%)
Ricinoleic	87,7 - 90,4
Linoleic	4,1 - 4,7
Oleic	2,2 – 3,3
Stearic	0.7 – 1,0
Palmitic	0,8 – 1,0
Linolenic	0,5 – 0,7

Source: (Mutlu & Meier, 2010)

Because of its particular composition, CO has a broad range of chemical transformation possibilities that are used to produce the derivatives used in the applications quoted before. Among them, the most important reactions are (Mutlu & Meier, 2010):

Ester reactions: Hydrolysis, esterification, alcoholysis, saponification, reduction, amidation and halogenation.

Double bond reactions: Oxidation, polymerization, hydrogenation, epoxidation, halogenation, addition reactions, sulfonation and metathesis.

Hydroxyl group reactions: Dehydration, hydrolysis, caustic fusion, pyrolysis, alkoxylation, esterification, halogenation, urethane formation and sulfonation.

3.3 EPOXIDATION OF CASTOR OIL

The three-member-cyclic-ether formation from castor oil (CO) double bonds (epoxidation) is carried out with a peroxyacid according to the Prilezhaev reaction. The peroxyacid is formed *in situ* by the contact between an organic acid like acetic or formic acid, hydrogen peroxide (HP) and an acid catalyst. For other vegetable oils, formic acid can be used instead acetic without any catalyst. For vegetable oil epoxidation with acetic acid, sulfuric acid is the most common catalyst, but not for CO. Since it is too hydrophilic, it is necessary to use a heterogeneous acid catalyst and some organic non-polar solvent. Previous experiments have shown that CO epoxidation without any solvent like benzene, toluene or hexane, can cause partial or total emulsification of the system. Although CO is just partially soluble in hexane, this solvent acts as a barrier to avoid emulsification and it is very easy to remove due to its low boiling point and high volatility. On the other hand, homogeneous aqueous acid catalysts like sulfuric acid could cause epoxide ring opening, decreasing the selectivity (%S) to epoxide. Indeed, carboxylic acetic acid (AA) and peroxyacid could also open the epoxide ring. Campanella and Baltanás (Campanella & Baltanás, 2005) showed this fact and focused on the study of the ring opening of epoxidized soybean (*Glycine max*) oil by AA and peracetic acid (PAA) on the presence of sulfuric acid as catalyst. They found that the ring opening is mostly influenced by the carboxylic acid than the peroxyacid. Another interesting result is the fact that the ring degradation increases at lower pH's. Regarding the kinetic facts, they concluded that the PAA concentration is very low in any moment and the AA concentration is essentially constant during all the reaction. In other study, the same authors worked with Amberlite® IR-120 ion exchange resin (IER) as acid catalyst for the study of the epoxide ring opening of epoxidized soybean oil (Campanella & Baltanás, 2004). There, they concluded that the ring opening is kinetically first order with respect to the epoxide oxirane ring group concentration and second order with respect to the AA concentration. They found also that the ring opening increases with the increasing of the mass of catalyst and the decreasing of the particle size. As well as with the homogeneous mineral acid catalyst, they conclude also that the most important degradation reaction of the oxirane ring with the IER is the opening by AA.

Castor oil (CO) epoxidation has been worked by many authors in different contexts. Kinetics and parameter optimization are the main topics developed by different authors. Among the first documented works, it is the patent developed by Crivello and Chakrapani (Crivello & Chakrapani, 2000). In this work, it is proposed a method to carry out the CO epoxidation with a phase transfer catalyst as novel tungsten peroxo-complexes and/or crown ethers. Specifically, they propose the methyltri-n-octylammonium diperoxotungstophosphate (MTTP) and the 18-crown-6-ether as the preferred phase transfer catalyst. As oxidizing agent, they use 30% HP. On a typical process, CO is mixed with the catalyst and the temperature is raised to around 60

°C. Then HP is added over the course of 4 hours and then vigorously stirred for another 4 hours before allowing cooling to room temperature. The epoxidized castor oil (ECO) obtained by this way has around 3,6% of oxirane-oxygen content (OOC) with a 75% of double bond (DB) conversion. Another research using a phase transfer catalyst is the one reported by Luo and colleagues (Luo et al., 2011) where the obtained ECO was used in the development of waterborne polyurethanes (WPU). In this work, the catalyst is a preparation based in cetylpyridiniuammonium chloride, tungstic and phosphoric which is then used on an oil/catalyst defined ratio in the epoxidation reaction along with 1 atm of O_2 and cyclohexene as solvent, 35 °C and 2,5 hours of reaction time. There is no report on conversion, selectivity or yield. Another type of catalyst is the used in a Brazilian work (Nunes et al., 2008). Here, the authors explored the epoxidation of castor oil with a vanadium acetylacetonate / t-butil hydroperoxide system ($VO(acac)_2$/TBHP) using 20% excess of TBHP and 1% (substrate based) of $VO(acac)_2$ by 3 hours under toluene reflux. It was obtained ECO with 88% %C and 82% %S. Hernandez and colleagues (Hernandez et al., 2017) reported a non-toxic and green ECO production reaction to produce bio-materials proposed for medical, odontological and pharmaceutical applications, using alumina as catalyst and HP as oxidizing agent. To optimize the process, it was developed a central composite design experiment 2^3 + 6 axial points + 3 central points with methyl-ricinoleate as the model substrate. After the optimization, the best parameters were used to epoxidize CO with 94% %C and of 89% %S, reducing wastewater treatment and purification steps. The epoxide ring opening could be observed by the HNMR signal at δ= 3,6 ppm. It could be observed also by FTIR with the increasing of the absorption band at 3400 cm^{-1}.

The first reported CO epoxidation with IER as catalyst is the work of Park and colleagues (Park et al., 2004). They prepared ECO with Amberlite® IR-120 as catalyst at 55 °C and 7 hours of reaction obtaining 84% of yield (%Y) and ECO with an average molecular mass (Mw) of 1518 g/mol. After that, they polymerized the ECO with N-benzylpyrazinium hexafluoroantimonate as catalyst and the obtained material was thermally characterized by Diferential Scanning Calorimetry (DSC), Dynamic Mechanical Analysis (DMA) and Thermal Mechanical Analysis (TMA).

Goud and co-workers (Goud et al., 2006) made also the epoxidation of castor oil with Amberlite® IR-120 to propose a simple kinetic model assuming a complete homogeneous system where the conversion of DB is of first order respect to DB concentration. They compared acetic and formic acid and used hydrogen peroxide at different temperatures, 30 °C, 50 °C, 70 °C, 85°C with a molar ratio of DB: organic acid: HP of 1:0,5:1,5. The authors found that the activation energy is 48,2 KJ/mol with AA and 35,4 KJ/mol for formic acid (FA). Two curious facts of this work are: they found that at lower temperatures FA has a faster kinetic in converting double bonds into epoxide groups so it is more efficient than AA, which in turn becomes more efficient at the highest temperature (85 °C). This is explained by the hypothesis that due to the higher activity of FA at 85°C, some HP is decomposed, depleting the

oxygen availability for the epoxidation reaction. They provide no experimental evidence of this hypothesis. On the other hand, the authors claimed also that the Amberlite ® ion exchange resin has the same effect as an inert solvent in protecting the oxirane groups to avoid side undesirable reactions hence they use no solvent in the reaction. They provided no evidence of this claim either. According to the practical experience of the author of this PhD thesis, when the CO epoxidation is carried out without an inert solvent, the system becomes an emulsion that is hard to reverse, due to the hydroxyl ricinoleic group causing high affinity of castor oil with aqueous systems. A more elaborated kinetic model was proposed by Sinadinović-Fišer and colleagues (Sinadinović-Fišer et al., 2012). In this work, it was found an optimal ECO production under the following conditions: 1/0,5/1,5 molar ratio DB/AA/HP (glacial AA and 30% aqueous HP drip added), 10% of Amberlite catalyst (based on the joint mass of AA and HP), 100% (oil weight based) benzene as solvent and a reaction temperature of 323 K, giving a maximum %Y to epoxide groups of 77,91%, it means, an OOC of 3,81%. For real, it was obtained a maximum ECO %Y of 78,32% with an OOC of 3,83% with 15% (%wt oil base) of Amberlite® IER catalyst but, since the increasing of the oxirane ring cleavage with the increasing of the catalyst amount, it was defined 10% as the best parameter for the catalyst, due to the fact that the yield is only 0,52% lower. The proposed kinetic model is based on the reaction scheme of Figure 3 and it considers the HP incremental addition and the occurrence of all the reactions during this period, as well as the influence of the catalyst amount. With kinetic rate expressions, a re-parameterized Arrhenius equation and mass balances, the authors obtained a superior model with a very good fit to the experimental data. Some of these same authors developed later a new kinetic model considering the chemisorption phenomena at the solid catalyst phase and assuming all the liquid as a pseudo-homogenous phase (Janković et al., 2014). There, it was considered the adsorption and desorption of all species (AA, HP, PAA and water) in the reaction of PAA formation. With the experimental data, it was fitted a model to obtain the dependence with temperature of the acetic acid adsorption rate coefficient (as the rate-determining step in this reaction), the adsorption equilibrium constants for all the species, as well as the rate coefficients of epoxy ring formation and ring cleavage reactions (reactions II and III in Figure 3). In this later reaction, the order of the hydroxyl acetate formation is one respect to acetic acid, instead of two, the used one in the previous work. With all these modifications, this model seems to fit better the experimental data than the one obtained in the previous work of 2012.

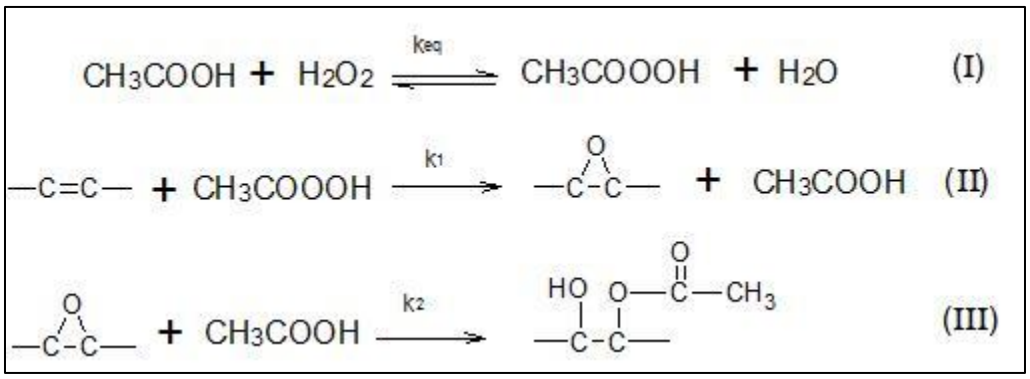

Figure 3. Epoxidation reaction system of castor oil with peracetic acid generated in situ

On a very non-coherent and misspelled way, an experimental work about the optimization of castor and jojoba oils was reported on a paper by El-Adly and colleagues (El-Adly et al., 2014). In this work, it is claimed that the optimum predicted CO %C through a polynomial regression involving AA/DB, HP/DB ratios, temperature and time of reaction, is 53,24% using 1,32% wt. HP/DB; 0,37% wt. AA/DB at 61 °C and 8 hours of reaction. No reports on solvent uses, %C measurement or experimental design can be found at the manuscript. Anyway, as it is reported below in this work, it is possible to carry out better processes to obtain %C above 90%.

Fu and colleagues (Fu et al., 2019) carried out the epoxidation of CO with an unspecified cation exchange resin in order to produce plasticizers for PVC. The approximated reactant molar ratios were AA:DB=0,05:1 and PH:DB=1,11:1 were and, respectively, %wt catalyst = 5% and %wt solvent=107%. No reports on %C, %Y or %S are found in the work. For this application, the authors claim that epoxy groups improve the compatibility of the plasticizer with PVC. On the other hand, OH groups from CO reduce the compatibility of the plasticizer with PVC so, modifications on this functional group like acetylation or benzoylation were tested.

Seralite ® SRC-120 appears as another H^+ form ion exchange resin equivalent to Amberlite ® in ECO production. Sudha and colleagues (Sudha et al., 2017) reported the *in situ* epoxidation of CO with this catalyst using AA (0,9 mol/mol DB), HP (1,6 mol/mol DB) and toluene as solvent (43,5% %wt oil-based) with 92% %C but with very questionable and doubtful %S and %Y results: CO iodine value (IV) of 83-96 g I_2/100 g and ECO OOC of 6,5% were reported, but the maximum theoretical oxirane oxygen content that might be calculated from this IV is around 5,14%, i.e. 137% %S and 126% %Y which makes no sense (in appendix 6.5 it is possible to check the way to calculate these values). ECO was also transesterified and acrylated and the products were characterized by FTIR and HNMR.

From the previous master degree work of the author of the current research (Guzmán, 2016), it is well known that it is possible to use hexane as solvent for the CO epoxidation with very good conversion and yield to oxirane groups and the

additional fact that it is easier to separate from the system by means of rotary evaporation than aromatic solvents like benzene or toluene used in previous works. From this experience also and off course from the literature, it is clear that an IER heterogeneous catalyst like Amberlite ® IR120 is better than the homogeneous sulfuric acid for CO epoxidation.

Reports on the epoxidation of CO fatty acid methyl esters (COFAME) and ricinoleic acid RA can be found also. Borugada and colleagues (Borugada & Goud, 2014) produced epoxidized COFAME (ECOFAME) as a renewable lubricant base fluid with enhanced thermal and oxidative stability. The epoxidation was carried at 1,5:1 PH:DB and 0,5:1 AA:DB molar ratios, 15% of Amberlite® IR-120 (COFAME %wt.-based), 60 °C and 10 hours. An ECOFAME with 4,86% OOC and 96,04% yield over the theoretical content was obtained. With TGA and DTG analysis, it was found that ECOFAME exhibits improved thermal and oxidative stabilities than COFAME and a commercial lubricant oil. In order to produce biolubricant basestocks, Salimon and coworkers (Salimon et al., 2012) made the epoxidation of RA by dropping slowly 8 mL of 30% HP to a stirred solution 90% RA (15 g) and 88% AA (14 mL) at 4 °C. The reaction proceeded at room temperature by 2-5 hours, and the product obtained was a white powdery solid. No reports on conversion, yield or selectivity are found in the report.

3.4 CARBONATION OF EPOXIDIZED VEGETABLE OILS

Five-membered cyclic carbonate is a ring-shaped chemical functionality were the one-bonded oxygen atoms are linked to two adjacent carbon atoms that can be part of a larger molecule. Cyclic carbonate (CC) production from epoxidized substrates is the selective cyclo-addition of CO_2 to epoxide groups from a substrate as it is shown in Figure 4. This reaction has been an interesting topic of study since it consumes CO_2, a greenhouse effect gas as well as the produced cyclic carbonates are very useful raw materials for important applications as electrolyte battery solvents, fuel additives, polycarbonates and glycols production, and environmental friendly organic solvents for chemistry (Zalomaeva, Chibiryaev, et al., 2013; Zalomaeva, Maksimchuk, et al., 2013).

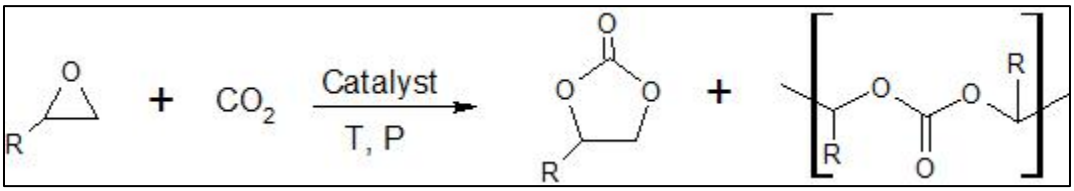

Figure 4. Carbonation of epoxidized substrate

Depending on the nature and/or composition of the catalytic system, the reaction might produce also polycarbonate compounds. The most common catalytic systems to carry out this reaction are composed by Lewis bases acting as nucleophiles, sometimes assisted by a Lewis acid. Quaternary ammonium salts, phosphonium salts and ionic liquids are typical for this process. When compounds as tetrabutylammonium halides, imidazolium halides, iminium halides and 4-dimethylaminopyridine are employed in the absence of a Lewis acid, the reaction becomes selective to CC product. The use of Lewis base homogeneous catalysts may have some drawbacks also: purification by distillation of the produced cyclic carbonates is difficult since they have high boiling points and for example, tetraalkylammonium halides, tend to degrade with high temperatures. The selectivity can be tuned by varying the type of nucleophilic specie, the nucleophilic-to-metal ratio and temperature. Another homogeneous catalysts that have been studied and used by itself or combined, are: metal-porphyrins, metal complexes with salen/salphen-based ligands, zinc β-diiminates, iron and magnesium bimetallic macrocyclic phenolate complexes, aluminium and iron based amino triphenolate and bis(phenolate) complexes, onium salts, ionic liquids containing hydroxyl, carboxylic acid or amino moieties such as protic tetraalkylammonium halides, protic phosphonium halides, protic imidazolium compounds, functionalized 4-dimethylaminopyridine. Different type of organo-catalysts has also been used, like onium salts, ionic liquids containing hydroxyl, carboxylic acid or amino moieties such as protic tetra-alkyl-ammonium halides, protic phosphonium halides, protic imidazolium compounds and functionalized 4-dimethylaminopyridine. Combined

with Lewis bases, several protic compounds containing hydroxyl or carboxylic acid moieties have been employed, including bio-based compounds as pyrogallol, gallic acid, tannic acid, water, as well as phenolic compounds, silanediol complexes, fluorinated alcohols, boronic acids, carboxylic acid-containing amines, simple alcohols and cavitand-based polyphenols. Heterogeneous catalysts have been studied also. Polymers and silica-based materials including ordered mesoporous silica with high specific surface area such as MCM-41 and SBA-15 have been studied as supports to immobilize various Lewis bases as ionic liquids, onium salts and non-ionic organic bases. The immobilization is carried out through robust, covalent bonding to prevent the leaching of active species into the reaction mixture. These heterogeneous catalysts solve the separation problems associated with homogeneous catalytic systems but they need high temperatures (≥ 100 °C) in order to reach high conversions. Metal-organic frameworks and metal-functionalized porous organic polymers have been studied also as supports, as well as bio-based compounds as cellulose and chitosan which have been functionalized to introduce quaternary ammonium or imidazolium moieties as metal-free heterogeneous catalysts (Kamphuis et al., 2019).

Although petroleum-derived ethylene carbonate and propylene carbonate are the most used five-membered CC worldwide, bio-based CC have had increasing attention from the academy and industry. Different bio-based sources have been used as limonene oxide, limonene dioxide, bio-butadiene and 1,4 cyclohexadiene (a by-product of the self-metathesis of some polyunsaturated fatty acids derived from plant oils) and vegetable oils. These bio-based sources bring the challenge of being economically feasible since there are a lot of issues related with their availability and production costs (Kamphuis et al., 2019). Very interesting and remarkable works on the carbonation of triglyceride and lipidic substrates from bio-based sources have been done.

Kathalewar and colleagues (Kathalewar et al., 2014) made the carbonation of a commercial epoxy resin derived from cardanol, a phenolic lipid from cashew tree (*Anacardium occidentale*), to produce NIPU's. The reaction was carried out in a high pressure autoclave with mechanical stirrer with 5% TBABr catalyst, 120 °C, 1000 psi CO_2 pressure and 10 hours of reaction. Because of the reaction, the epoxy content moved from 2,5 (epoxy resin) to <0,1 mmol/g (carbonated product), confirming the CO_2 fixation on the epoxy moieties. Viscosity changed also, moving from 49 to 5600 Pa s @ 25°C.

The first epoxidized-vegetable oil carbonation was reported by Tamami and colleagues (Tamami et al., 2004). Epoxidized soybean oil (ESBO) was carbonated at 110 °C, 5% mol of catalyst, atmospheric pressure with continuous CO_2 flow by 70 hours, to produce carbonated soybean oil (CSBO). Various catalysts were used: NaI, LiBr, benzyltrimethylammonium, Amberlite IR 400 (Cl) and Tetrabuthylammonium Bromide (TBABr). The best conversion to CSBO was obtained with TBABr (94%). The reaction was monitored by FTIR: carbonate group

appearance at 1805 cm^{-1} and oxirane group disappearance at 823 and 845 cm^{-1} and by HNMR considering the signal about 2,70-3,00 ppm from the –CH groups of the epoxy ring. The catalyst was removed by dissolving the reaction mixture in ethyl acetate and extracting twice with water. The viscosity of the product was 13200 cP at 25 °C, very much higher than the value for the epoxidized soybean oil (450 cP), due to the enhanced intermolecular interactions caused by the polar cyclic carbonate groups. Two years later, Parzuchowski and colleagues (Parzuchowski et al., 2006) produced CSBO using KI activated by 18-crown-6 as catalyst in a high pressure reactor at 6 MPa of CO_2 pressure and 130 °C. They claimed an improvement in the process since they report that using tetraalkylammonium salts (benzyl-trietylammonium chloride or TBABr) at 6 MPA CO_2 pressure and 130 °C leads to a poor conversion lower than 10% after 5 days of reaction, compared with an almost complete conversion at the same conditions using KI activated with 18-crown-6 as catalyst. The complete conversion of epoxy groups yielded a product with a viscosity of 2'0 Pa*s at 20 °C. HNMR-$CDCl_3$-400 MHz showed signals at 4.45-4.95 ppm due to protons of CC ring. Then, in 2008, Li and colleagues (Z. Li et al., 2008) also produced CSBO from ESBO using a catalytic mix of $SnCl_4 \cdot 5H_20$ and TBABr at high temperature and pressure in a stainless steel autoclave with mechanical stirrer. They found that the best conversion (89,2%) was obtained with a 3% mol of catalyst with a ratio of 1:3 $SnCl_4 \cdot 5H_20$ to TBABr at 120 °C and 1,0 MPa. They explain that the synergetic effects of $SnCl_4 \cdot 5H_20$ Lewis acid which activates the epoxy groups from ESBO and TBABr Lewis base which activates the CO_2 is the reason of the improvement on the catalytic behavior of this mix. Then, with this "optimum" mix ratio of catalysts, they found that it is possible to reach higher conversions with higher temperatures, pressures and reaction times (140 °C, 1,5 MPa and 40 hours). The CSBO obtained had a viscosity of 19320 cP. FTIR characterization shows the same results of Tamami et al. HNMR-300 MHz results showed that in addition to the disappearing of epoxy groups signals around 2,80-3,00 ppm, there is the appearance of carbonate groups signals at 4,45-4,90 ppm. Crown-type catalysts for carbonation of vegetable oil substrates have been studied by various authors. Schäffner and co-workers (Schäffner et al., 2014) carried out a catalytic screening on the carbonation of epoxidized methyl oleate at 100 °C, 17 hours, 100 bar CO2 and 5% w. of catalyst combined with 3,5% w. of a phase transfer catalyst. They obtained high conversions around 90-94% with an alkali halide catalyst accompanied with a crown ether-type phase transfer catalyst. Interestingly, they developed a life cycle analysis to determine the real CO_2 saving from this reaction. It was concluded that CO_2 utilization in the carbonation reaction has a minor impact on the final CO_2 savings. Longwiz and colleagues (Longwitz et al., 2018) developed the carbonation of different bio-derived epoxidized substrates like fatty acids, oil and terpenes with different calcyum-based catalysts with crown ethers as ligands in combination with various co-catalysts. The most active system consisted of a dicyclohexyl functionalized 18-crown-6 ether and triphenyl phosphane in addition to calcium iodide. They reported the carbonation of internal epoxide groups at mild

conditions: 45 °C, 0,5 Mpa CO_2 pressure, 5% mol of catalys loading and 24 h of reaction, with yields up to 98%. Substrates like epoxidized ethyl oleate, erucic acid, methyl-O-acetyl ricinoleate, methyl soyate, high oleic sunflower, soybean and lidseed oil, were used. Conversions up to 99% were obtained.

Not only oil but fatty acid methyl esters have been carbonated too. Doll and colleagues (Doll & Erhan, 2005) reported the synthesis of carbonated methyl oleate (CMO) and carbonated methyl linoleate using supercritical CO_2 and TBABr as catalyst. The fatty acid methyl ester material was heated in a warm water bath and the poured into a high-pressure reactor vessel. Next 5% mol of TBABr was dissolved and the reactor was pressurized with CO_2 to 500 psi, then heated to 100 °C and then the pressure was further increased to 1500 psi and maintained at this value by a pressure-controlling pump for 15 hours of reaction. The product obtained was a light brown viscous liquid (the increasing in the viscosity is not as large as the observed in the carbonation of epoxidized triglyceride materials as soybean oil) with a yield of 93%. The catalyst was removed by a water-washing and sonication process. The product losses in this step were minor than 3% giving an overall experimental yield of 90%. The products were characterized by HNMR, CNMR, FTIR and TGA. For CMO, HNMR-500 MHz showed a characteristic signal at 4,63-4,22 ppm as a singlet for CC ring protons. CNMR signal at 154 ppm corresponding to CC carbons and at 79-82 ppm corresponding to cyclic ring carbon. FTIR showed a band at 1793 cm^{-1} from the CC carbonyl group. TGA showed a superior 50%-weight loss temperature of 251 °C compared to ordinary methyl oleate (187 °C) which brings to CMO a higher potential in lubricant or fuel additive applications. Holser (Holser, 2007) developed a similar experience with epoxidized methyl soyate at atmospheric pressure. The reaction was carried out by bubbling carbon dioxide gas to the epoxidized methyl soyate in the presence of 1% (weight-base) TBABr catalyst. In this experience it was observed that 42% of the epoxide groups were carbonated after 18 hours of reaction. Carbonation of oligomeric ricinoleic acid for NIPU production was carried out by Ren and colleagues (Ren et al., 2021). Ricinoleic acid was oligomerized through esterification reaction between the carboxylic acid and hydroxyl group, then the terminal acid groups were esterified with methanol followed by the epoxidation of double bonds in the oligomer. The carbonation of the epoxide groups was carried out with TBABr catalyst at 140 °C, 3,6-3,8 MPa of CO_2 and 24 hours of reaction.

Carbonation of vegetable oils has been made out not only for producing NIPU´s but producing polyols for polyurethane production through the conventional route. This is the case of Jalilian and colleagues (Jalilian et al., 2008). They carried out the carbonation of ESBO at 110 °C, TBABr/$CaCl_2$ co-catalyst couple (5%/2,5% mol epoxy) and ambient pressure. The product was purified by water-washing, sonication, decantation and vacuum-drying at 90°C. The obtained CSBO had 15400 cP at 25°C viscosity and 98% yield. It took around 24 hours to reach 85% conversion approximately. They claimed that the modified catalyst system with $CaCl_2$ as co-catalyst causes a considerable reduction in time reaction compared with the TBABr-

ambient pressure technology reported by Tamami and colleagues. HNMR-$CDCl_3$-400 MHz: 4,43-4,71 ppm, CC ring protons.

The use of water as an improving medium for epoxide cyclic carbonation has been reported also. Jian and colleagues (Jian et al., 2009) reported the carbonation of propylene oxide with CO_2 in the presence of water, with various catalysts among which the Lewis base-type butyl-triphenilphosphonium iodide catalyst showed the best results with an optimal water/oxirane molar relationship of 0,33 and 0,2 mol of propylene oxide, 1 mmol of catalyst , 2 MPa CO_2 and 125 °C. At these conditions they found a reaction rate as much as 7 times higher than the one without water in the first 30 minutes of reaction. Furthermore, after 4 hours of reaction the yield to CC without water was around 50-60% compared to almost 100% with water. A further increasing in the water content caused a decrease in the yield and selectivity because of the side reaction between water and the oxirane to produce 1,3-propyleneglycol. This improvement in the catalytic activity was explained by the synergistic effect between the OH-water moiety and the Lewis base catalyst in the oxirane ring opening, accelerating the reaction rate. This was confirmed by testing the reaction with OH and non-OH containing solvents. Conversion, selectivity and yield was noticeable superior with solvents like phenol, acetic acid, propylene-glycol, ethanol and 2-propanol compared to N,N-dimethylformamide, acetone, cyclohexane and dichloromethane, among others. As an interesting fact for the current work, it was found that the reaction with TBABr was significantly improved with the presence of water since the conversion increased from 56% to 95%, the yield to CC from 54% to 86% and the turnover frequency (TOF) from 11 to 175 (mol of synthesized carbonate per mol of catalyst per hour), using 0,2 mol of propylene oxide, 0,067 mol of water 1 mmol of TBABR catalyst, 2 MPa CO_2, 125 °C and 1 hour of reaction. As it will be shown later, such improvement was not observed from the experimental results of this work. This could be explained from the fact that in this case the epoxidized substrate is not as simple as the propylene oxide in terms of molecular size and compatibility of reaction phases. Vegetable oils show a greater steric hindrance and water incompatibility so these effects could be the reason why a significant improving effect was no observed.

Besides water, other modifications as microwave radiation have been tested to improve the carbonation reaction. Mazo and Rios (Mazo & Rios, 2012) developed the carbonation of ESBO adding water and microwave radiation and they found that both factors improve on a significant way conversion, selectivity and reaction times. They found that microwave heating reduces time reaction from ¼ to 1/3 times the reaction required using conventional heating under similar reaction conditions (140 °C, 5% mol TBABr and H_2O/epoxide 1/3 mol). Specifically, for example, they obtained conversions of 95% at 70 hours and 25 hours with conventional and microwave heating, respectively. They reported also that the addition of water increased the conversion around 10% with microwave heating and 5% for conventional heating. In a subsequent work (Mazo & Rios, 2013) they reported that

adding water on a 1/3 molar ratio the reaction proceeded 70% faster than without water. They found also that 5% TBABr catalyst is the optimum quantity and that the reaction followed a first-order kinetic respect to epoxide at 100-140 °C. Another experience with microwave was carried out by Zheng and co-workers (J.-L. Zheng et al., 2018). Approximately 150 g of epoxidized cottonseed oil methyl ester was charged in an autoclave reactor with an amount of TBABr catalyst between 4-8%, temperatures, CO_2 pressures and microwave power in the ranges 100-120 °C, 2,5-6 bar and 80-300 W, respectively, were used as reaction parameters. After 7 hours, conversions up to 64% were obtained and kinetic results showed a slight increasing in the reaction rate. HNMR-$CDCl_3$-400 MHz:4,40-4,95 ppm (4 peaks)-protons of CC ring.

The first visible review about carbonation of epoxidized vegetable oils was reported by Miloslavskiy and colleagues (Miloslavskiy et al., 2014). Although it is a nice review job, there are some inaccuracies and lack of information that can be pointed. A stowaway common edition mistake was found related with reference 7, a publication of Javni and colleagues (Javni et al., 2003) that it is supposed to work on the epoxidation of ESBO with TBABr catalyst, when for real, it is a publication dealing with a soy-based conventional polyurethane formulation with different isocyanates and its characterization. No information about ESBO carbonation can be found in this work. It is possible that the authors confounded this paper with other one published by Javni also, where it is developed a soy-based NIPU through the carbonation of ESBO (Javni et al., 2008). Another fact: being from 2014, the review work failed to report a 2007 important work (Holser, 2007). As an interesting and redeemable fact, the authors put on the table the discussion about the importance of removing the catalyst after the reaction. In the conclusions it is claimed that there is ambiguity on the information about this topic and it can be inferred that it is not necessarily mandatory to remove the catalyst from the system since the information is not sufficient to prove the importance of this step. Nohra and colleagues touch the problem of the carbonation of vegetable oils for NIPU production (Nohra et al., 2013) as well as Błażek and Datta (Błażek & Datta, 2019). Carré and colleagues published a review focused on the CC production from renewable sources (Carré et al., 2019). A more recent review was published by Aomchad and colleagues (Aomchad et al., 2021). In this work there is a broad review on carbonation of epoxidized bio-based substrates like glycerol, terpenes and vegetable oils. Nice remarks on process condition, catalytic performance and reaction yield, conversion and selectivity were collected and systematically organized and presented.

Soybean oil has been the most used for this purpose but other species like linseed (*Linum usitatissimum*), Cottonseed (*Gossypium*), sunflower (*Helianthus annus*) and castor, have been tried also. Javni and colleagues (Javni et al., 2008) reported the optimal production of CSBO from ESBO with 0,025 mol TBABr/mol epoxy, 140 °C and 1,03 MPa of CO_2 obtaining a product with 96% of conversion, 32 Pa.S viscosity, after 23 hours. It is not clear why they considered these conditions as optimal since

they reported an even better conversion of 97,8% using a higher CO_2 pressure of 5,65 MPa after 22 hours. After the reaction, the product was diluted in ethyl acetate, washed three times with water and dried on rotary evaporator before using it on NIPU formulations. As a remarkable fact, they follow the reaction kinetic by measuring viscosity and OOC and proposed a plot of them as a way to estimate conversion by measuring viscosity. In fact, with this correlation they proposed an explanation for the low mechanical properties of the NIPU's obtained by Tamami (Tamami et al., 2004) since a medium-conversion carbonated oil was used. Boyer and co-workers (Boyer et al., 2010) prepared carbonated fatty acid diester sunflower oil-derivatives with terminal and internal carbonate groups from terminal epoxidized fatty acid diesters (TEFAD) and internal epoxidized fatty acid diesters (IEFAD), respectively. Carbonation was carried out at temperatures ranging from 60-140 °C and pressures from 5-18 MPa in the presence of 3% TBABr catalyst. A study on the CO_2-EFAD (Epoxidized fatty acid diester) mutual solubility was done as well as a kinetic monitoring of the reaction. As expected, CO_2 solubility in EFADs increased with pressure and decreased with temperature. They found also that TEFAD have faster kinetics than IEFAD due to the higher reactivity of terminal epoxide groups compared to internal ones. For complete conversion IEFAD required temperatures as high as 140 °C compared with TEFAD that required 120 °C. An interesting finding was that at a fixed temperature of 120 °C, IEFAD reached maximal conversion (90%) at 10 MPa. Above this value, increasing the pressure did not enhance the epoxide conversion. Conversion of TEFAD (94%-100%) is almost unaffected by CO2 pressure changes. No clear explanation is proposed for this phenomenon.

Following the methodology of Tamami, Mahendran and colleagues (Mahendran et al., 2012) produced carbonated linseed oil for NIPU production and reported an increasing in viscosity from 1,05 Pa*s (epoxidized oil) to 163 Pa*s (Carbonated oil) and in average molecular mass from 1100 to 2600 g/mol. Linseed oil was used also by Pouladi and colleagues (Pouladi et al., 2021). They carried out the carbonation of epoxidized linseed oil with 5% wt of TBABr catalyst at 140 °C and 30 mL/min of CO_2 flow by 48 hours. Conversions up to 100 % were obtained. González and colleagues (González Martínez et al., 2021) carried out the carbonation of epoxidized linseed oil by placing 5g of oil with TBABr catalyst (2,5%-5% mol epoxy content -based) in a 500 mL Teflon vessel inserted into a stainless steel reactor. The system was purged three times with CO_2 and then the reaction conditions were adjusted: 90-120 °C temperature, 60-120 psi CO_2 pressure and 12-92 hours of reaction. They found a high performance at 90 °C, 60 psi and 5% TBABr: 96% conversion, yield 95% and selectivity 99%.

Bähr and Mülhaupt (Bähr & Mülhaupt, 2012) produced carbonated soybean oil (CSBO) and carbonated linseed oil (CLSO) to formulate NIPU materials. The carbonation reaction was carried out with 3% mol of catalyst (TBABr or heterogeneous-silica-supported 4-pyrrolidinopyridinium iodide), 140 °C and pressures ranging from atmospheric, 10 bar and 30 bar of CO_2. They found that

TBABr has better catalytic activity than the silica-supported one, reaching complete epoxide conversion in shorter times (20 hours for TBABr compared with 45 hours for silica-supported). The advantage of the heterogeneous one is that it is easy to recover but its lower activity is a notorious drawback. The activity of both catalysts increased with the increasing of CO_2 pressure. HNMR-$CDCL_3$-300MHz showed signal around 4,45-5,10 ppm corresponding to the two hydrogens of CC ring. Heterogeneous catalyst was also used by Wang and colleagues (J. Wang et al., 2012). They used a Pt doped $H_3PW_{12}O_{40}/ZrO_2$ kegging-type hetero-polyacid catalyst to make the cyclic addition of CO_2 to ESBO. The optimal reaction conditions were: 150 °C, 1 MPa CO2 pressure, 50% DMF solvent and 30 hours of reaction time obtaining 91,6 % of epoxide conversion. They found also that viscosity increased from 418 cP (soybean oil) to 15400 cp (CSBO) at 25 °C. As an interesting fact, they claimed that the reusability capacity of the catalyst was improved by the Pt doping of the catalyst. On a patent of the same year (Birukov et al., 2012b) reacted ESBO with CO_2 at 1 MPa and 120 °C with 0,5% w/w TBABr catalyst by 40 hours and CSBO was obtained with 85% conversion. Other experiences were carried out to obtain ESBO partially carbonated with conversions of 60% and 35% for hybrid NIPU production. Ammonium halides-based mixed catalyst systems have been tried aso. It is the case of Langanke and colleagues (Langanke et al., 2013). In this work, the solvent-free catalytic synthesis of a variety of oleochemical-based CC was carried out by employing various organic halides and polyoxometales, single or mixed, as catalysts. Mehtyl oleate, methyl linoleate and soybean oil were some of the used oleaginous substrates. It was found that the catalyst system composed by TBABr and Cr(III)-substituted silicotungstate can yield better performance than the individual TBABr thanks to a synergistic catalytic effect over the two reactants: TBABr opens the epoxide ring by foming Br-alkoxide intermediate and the silicotungstate interacts with CO_2 enhancing its nucleophilicity. Conversions and selectivities over 95% were obtained. Levina and co-workers (Levina et al., 2015) carried out the carbonation of epoxidized sunflower oil by loading 200 g of epoxidized sunflower oil into a high-pressure reactor and 3% TBABr catalyst (epoxy mol-based). The reaction was carried out by 20 hours at 140 °C and 0,8 Mpa CO_2 pressure. A conversion of 95% of epoxy groups was obtained. Yu and co-workers prepared CSBO for NIPU applications from commercial ESBO (Vikoflex 7170 ®, Arkema, Philadelphia, PA, USA) using 5% TBABr catalyst, 152 bar of CO_2, 140 °C, 22 RPM and 18 hours. They reported a 0,75% of epoxy content in the final product (Yu et al., 2018).

Not only NIPU but other applications have been proposed for carbonated vegetable oils. According to Zhang and colleagues (L. Zhang et al., 2014) it is well known the high potential of vegetable oil-based lubricants due to their excellent lubricity properties, high flash point, favorable viscosity-temperature behavior and compatibility with mineral oils. In this sense, they made the epoxidation and then the carbonation of cottonseed oil for lubricant applications. The carbonation reaction was carried out in a stainless-steel autoclave at temperatures between 100-150 °C,

CO_2 pressures from 1 to 3 MPa and catalyst ratios from 0,0125 to 0,0625 mol of TBABr per epoxide mol. The results suggest that the best conditions were: 140 °C, 3 MPa, 0.04 mol TBABr/epoxide mol and 24 hours of reaction. After the reaction the product was purified by dissolving it in ethyl acetate and washing three times with water. The raw material as well as the epoxidized intermediate and the final product were characterized by FTIR and ^{1}HNMR. By the way, the paragraph entitled "Characteristics of CCSO" of the paper explaining these results shows a repetitive explanation of the signals. Since in this paragraph one can read the exact words two times, it does not seem intentional but a common copy-paste mistake that lower the editorial quality of the text. What concerns to the lubricity properties, carbonated oil with 100% epoxide conversion showed the highest oxidation stability compared with epoxidized and unmodified oil as well as improved friction-reducing and anti-wear properties, with a flash point of 250 °C, pour point of 0 °C, viscosity of 1142,3 mm^2/s at 40 °C and 64,7 mm^2/s at 100°C and a viscosity index of 109.

Alves and colleagues (Alves et al., 2015) studied a bicomponent organocatalyst to be used for carbonation of lindseed oil, specifically a combination of organic salts and/or ionic liquids combined with a hydrogen bond donnor activator derived from multiphenolic compounds or fluoroalcohols. It was found that the onium, phosphonium and imidazolium salts exhibited the highest catalytic activity with a 25% of conversion after 5 hours at 100 °c and 10 MPa. Guanidinum salt was found to be the best. It was found that multiphenolic activators derived from catechol, pyrogallol and fluoroalcohols were also to have the highest co-catalytic activity increasing the conversion by 1,85 to 2-fold. 1,3-(bis-2-hydroxyhexafluoroisopropyl)benzene, hexafluoro-2-(p-toluyl)isopropanol, perfluoro-tert-butanol and pyrocatechol were the most efficient. An additional kinetic study showed optimal conditions for the reaction at TBABr/activator=1, 2.2 mol% TBABr, 120 °C and 5 MPa.

Zheng and colleagues (J. L. Zheng et al., 2015) published the results of a very complete research work providing first, a nice short review on epoxidized vegetable oil carbonation and then a complete analysis about the influence on the kinetics of epoxidized cottonseed oil carbonation of various factors like temperature, stirring speed, catalyst amount, temperature, pressure. They determined also the gas-liquid mass transfer coefficient, CO_2 solubility and the catalyst thermal stability involved in the reaction. They found that the optimum reaction conditions were: 130°C, 50 bar and 3,5% mol of TBABr catalyst with a conversion of 85% and selectivity of 96% for 7 hours of reaction, and the reaction temperature should not exceed 130 °C because of the stability of the catalyst. CO_2 solubility was 0,57 $mol*L^{-1}$ and it is independent of epoxide conversion. On the other hand, the mass-transfer coefficient increased with temperature and decreased with the epoxide conversion, because of the viscosity increasing. The same research team developed a later work (X. Cai et al., 2017) where they proposed a kinetic study including mass transfer phenomena for the carbonation of epoxidized cottonseed oil at different temperatures (110-140°C),

0,06-0,3 mol/L of TBABr catalyst and CO2 pressures between 21,1-49,7 Bar. They found that the carbonation reaction rate constant at a reference temperature of 403 K is 2,07e-4 $L^2mol^{-2}s^{-1}$ with an activation energy of 50,0 KJ/mol. They demonstrated also that the larger the carbonate group concentration the lesser the gas-liquid CO_2 mass transfer coefficient. This fact explains the stabilizing trend of conversion with time and why it is necessary to use high pressures for the reaction. An interesting fact is that as opposite to their previous work, they demonstrated that at 140 °C the decomposition of TBABr can be assumed negligible.

Epoxides based on renewable olechemicals were carbonated by Thenumberg and colleagues (Tenhumberg et al., 2016) using tetra-n-butylphosphonium salts in combination with metal-based co-catalysts. Reactions were carried out at 100 °C, 50 bar CO_2 and 20 hours of reaction. As model substrate epoxidized methyl oleate was utilized but other oleaginous derivatives like epoxidized high-oleic sunflower, sunflower, soybean, linseed, mehtyl soyate and methyl ricinoleate, were used too. As an interesting fact this work revealed that mehtyl ricinoleate seems to be a challenging substrate since it produces a 5-membered ether isomer-byproduct from the intramolecular substitution reaction of the ricinolecic hydroxyl group and the epoxide. It is proposed also that if this hydroxyl group is protected with an acetyl group, selectivity to carbonated product was increased considerably from 42 to 63%. Tetra n-buthyl phosphonium bromide - Molybdenum trioxide (MoO_3) catalytic system was found as highly active for the synthesis of oleochemical CC with high yield and selectivity (>99%). A further investigation was carried out by Büttner and colleagues (Büttner et al., 2016). Various iron salts as Lewis acidic co-catalyst were screened in the carbonation of epoxidized methyl oleate using 2 % mol of TBABr catalyst, 2 % mol of co-catalyst, 100 °C, 16 h and 5,0 Mpa CO_2 pressure. $FeCl_3$ co-catalyst showed the best performance with 84% yield and >99% chemoselectivity. A reduction of co-catalyst amount from 2 % to 0,25% resulted in a decrease of conversion rate but in a increase of selectivity also. Increasing the catalyst amount from 2 % to 3 % resulted in full conversion and a slight decrease of selectivity from 99 % to 94 %. With a 3 % TBABr / 0,25 % $FeCl_3$ system, the optimal conditions were: 100 °C, 24 h and 5,0 MPa CO_2 pressure. Instead of TBABr, tetra-n-octylphosphonium Bromide $(Oct_4P)Br$ was tried as catalyst and it showed interestingly higher rates of conversion, yield and selectivity compared to TBABr. 2,0 % mol of $(Oct_4P)Br$ and 0,25 % mol of $FeCl_3$ co-catalyst showed 99% conversion and 96% selectivity at 100 °C, 24 h and 5,0 MPa CO_2 pressure. Under these optimized reaction conditions, different substrates like carbonated ethyl oleate, iso-octyl olate, methyl eicosenoate, methyl erucate and methyl ricinoleate, were evaluated. They found that methyl ricinoleate showed full conversion but just a 40 % yield. This is explained by an isomerization intramolecular side reaction between the -OH ricinoleic group and the oxirane group to produce a tetrahydrofuran-derivative. The study revealed also that if the OH- moiety is protected by an acetyl group the reaction proceeds smoothly with 85% conversion and 81 % yield. Epoxidized vegetable oils like lindseed oil, high-oleic sunflower oil, soybean oil and methyl

soyate were studied also as substrates. Conversions above 99% were obtained and very interesting yields like 94 % for soybean oil and 90 % for linseed oil were obtained too. Lamarzelle and coworkers (Lamarzelle et al., 2016) produced cyclic carbonate from undecanoic, oleic and sebacic acid substrates trough two ways: high pressure reaction with TBABr catalyst and glycerol carbonate addition. They carbonated a substrate-ether-epoxide with 3% TBABr catalyst and 40 bars CO_2 pressure at 80 °C for 3 days , obtaining substrate-ether-cyclic-carbonate with 82% yield. They used also other route by producing the chloroformate-derived substrate and then mixing it with glycerol carbonate obtaining substrate-ester-cyclic carbonate with 73% yield. Different methyl ester were used as substrate In the work of Cai and colleagues (T. Cai et al., 2020), like epoxidized o-acetyl methyl ricinoleate, methyl oleate, methyl linoleate, methyl linolenate and methyl estearate were carbonated using CO_2 and the acid-base pair UiO-66-NH_2 to produce cyclic carbonate with epoxy conversion around 94%. The reaction was carried out at temperatures between 80-160 °C and 3-15 h wit 0-0,6 MPa of CO_2 pressure.

Poussard and coworkers (Poussard et al., 2016) produced CSBO with different cyclic carbonate content by varying the time reaction for NIPU formulation. The reaction was carried out under spercritical CO_2 conditions at 120 °C and 100 Bar and 2,65 wt% of TBABr catalyst. Complete conversion was reached after 9 hours and this was explained by the supercritical CO_2 decreasing effect on the oil viscosity, facilitating the CO_2 coupling. Alternative species as jatropha (*Jatropha curcas*) have been used also. Hannifa and colleagues (Haniffa et al., 2017) carried out the epoxidation and carbonation of epoxidized Jatropha oil for NIPU formulation. The production of carbonated jatropha oil was carried out with 3,5 w% of TBABr and temperatures from 110-140 °C and 1-2 Mpa of CO_2. They found that the better yields (around 99%) were obtained at 120 °C and 2 Mpa after 30 hours of reaction.

Carrodeguas and co-workers (Peña Carrodeguas et al., 2017) propposed the use of a catalytic dual system composed by Al(III) amionotriphenolate complexes (0,1-1 mo %) and different nucleophiles (2-5 mol%) like bis(triphenylphosphine)iminium chloride, tetrabutylammonium chloride and TBABr for the carbonation of various fatty acid-derived epoxidized compounds as methyl oleate, methyl linoleate, methyl linolenate, methyl erucate, methyl elaidate and methyl ricinoleate, under mild conditions (70-85 °C and 10 bar CO_2). The use of chloride-based nucleophiles proved to be high stereo-selective to produce cis-configured CC for all substrates except for ricinoleic acid which followed a trans-configured selectivity due to the influence of the OH ricinoleic group on the reaction mechanism. Conversion above 99% and selectivity between 87-99% was obtained with this substrate. Ricinoleic substrate was used also by Ren and co-workers (Ren et al., 2021). In this work, carbonation of epoxidized oligomeric ricinoleic acid was carried out by loading an autoclave with 2 g of this substrate, 0,2 mmol of TBABr catalyst and 5 mL of dimethylformamide. The system was filled with 3 MPa of CO_2 and heated to 140 °C to reach a pressure between 3,6-3,8 MPa. The reaction was maintained for 24 hours.

After the reaction, the mixture was washed with water to remove the solvent and the catalyst. A yield of 90% was obtained.

Farhadian and colleagues carried out the carbonation of epoxidized sunflower oil for hybrid NIPU networks production with different bio-based amines (Farhadian et al., 2018). Epoxidized sunflower oil carbonation was carried out with a porphyrin-based catalyst system (manganese tetra (4-methoxy) phenyl porphyrin chloride/TBABr) in a molar ratio 4/4, in a system connected to a balloon full of CO_2 gas at atmospheric pressure, 100 °C of temperature and 30 hours of reaction with 100% conversion. An interesting modified TBABR-based catalytic system was proposed by Liu & Lu (Liu & Lu, 2018). The catalyst was prepared as a deep eutectic solvent, based on a hydrogen bond acceptor (TBABr) and hydrogen bond donors (ethylene glycol, 1,2-propanediol, triethylene glycol, levulinic acid, decanoic acid and oleic acid) through a mixing-heating step at 80 °C, until a homogeneous stable liquid was formed. The carbonation reaction was carried out in an autoclave PARR® reactor at different CO2 pressures, temperatures and reaction times. They found that the system composed by TBABr/Triethylene glycol had the best catalytic activity at the following reaction parameters: 100 °C, 1,0 MPa CO2, 400 rpm, 0,04 mol TBABR/mol epoxide and 10 hours. Then, experiments were carried out to find the following optimum values: 0,12 mol catalyst/epoxide mol, 120 °C, 10 hours reaction and 1,0 MPa CO2 pressure. They demonstrated also that the TBABr-eutectic solvent has better catalytic activity than the TBABr alone.

Mathematical and statistical methods have been applied also in the carbonation of epoxidized vegetable oils. It is the case of Mendes and colleagues (dos Santos et al., 2020).They developed a catalyst screening by the modeling and exploratory analysis of the quantitative structure-property relationship of different organo-catalyst molecules. By a mathematical and statistical analysis of different structure parameters as molecular arrangement, chain size, substituent type and other, it was possible to conclude that cetyltrimethylamonium bromide can be proposed as a good catalyst for the synthesis of oleochemical carbonates. Validation reactions were carried out with three different vegetable oils (canola, rice and soybean) at 120 °C, 48 hours, 5% catalyst and butanol as solvent obtaining conversions up to 99%.

3.5 CHITOSAN

Chitin is the second most abundant polysaccharide bio-polymer from nature, behind cellulose. It is present in cell walls in fungi, shrimp-shells, exoskeletons of arthropods crustacean and insects among others, and it is a chain of N-acetylglucosamine units (Figure 5).

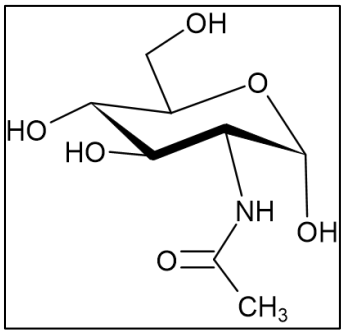

Figure 5. N-acetylglucosamine unit

Chitosan (CH) is obtained from the chitin de-acetylation reaction promoted by a strong alkali compound and converting to a chain of fully or partially de-acetylated units, called glucosamine units. Figure 6 shows on a comparative way, the structures of chitin, CH and cellulose.

CH degree of de-acetylation (DD) in percentage, is the glucosamine to N-acetylglucosamine ratio. There are many attempts to measure and calculate the DD. One can classify them in elemental analysis-based, potentiometric-conductimetric-based and spectrophotometric-based methods. The degree of acetylation (DA) is understood as the complement of DD, so

$$DA=100-DD \quad (1)$$

The potentiometric method basically consists in dissolving CH with a known excess of acid solution and then to titrate with a basic solution like NaOH following the pH evolution. From the two inflection points of the titration curve it is possible to estimate the amount of free amino groups thus CH DD. Since CH precipitates in the neutral zone, causing some error in the determination of the second inflection point, a variation in the DD calculation called “Linear Potentiometric Titration” (LPT) has been proposed and used by various authors (Jiang et al., 2003; Tan et al., 1998).

CH solubility has been broadly studied and some reports can be mentioned in order to gain clarity of some key factors about this aspect. CH solubility depends on different factors such as polymer molecular weight, degree of acetylation, pH, temperature, polymer crystallinity and N-acetyl-D-glucosamine and D-glucosamine units distribution on the main chain (Aiba, 1991; Anthonsen et al., 1993). The presence of large amounts of protonated -NH_2 groups on the CH structure determine its solubility in acid aqueous media. When around 50% of all amino groups are protonated, CH becomes soluble. Lowering the molecular weight helps to improve solubility too (Kubota & Eguchi, 1997; Aranaz et al., 2021). In the work of Kurita and co-workers (Kurita et al., 1977) it was showed that heterogeneous deacetylation of chitin produces block-type copolymers of N-acetyl-glucosamine and D-glucosamine units making the CH product insoluble in water. On the other hand, homogeneous deacetylation produced random distribution structure and a water-soluble product at 50% DD. Vårum and colleagues carried out a similar experience and they found that with a DD of 50%, CH is soluble at neutral pH no matter the method of preparation: homogeneous or heterogeneous deacetylation (Vårum et al., 1991b, 1991a). In this case, they obtained a randomly distributed structure with the homogeneous process and a slightly blockwise structure, not so different, with the heterogeneous one. In acid-aqueous media, solubility is determined also by the concentration ratio between acid equivalents and free amino groups as it was found in the work of Rinaudo and colleagues (Rinaudo et al., 1999). Using acetic acid, they found complete solubilization of chitosan with 50% of amino groups protonation and a molar ratio of acid to fee amino groups of 0,6. With a strong acid as HCl the acid to free amino groups ratio must be nearly to 1 (Rinaudc et al., 1999). Lu and colleagues determined that CH with a DD between 46,7-64,4 % is completely soluble in water (Lu et al., 2003). For higher DD it is necessary to protonate amino groups on an acid medium, to become CH water-soluble. According to Il'ina and Varlamov, the complete protonation of CH amino groups takes place at pH=4,0 (Il'ina & Varlamov, 2005). This pH criteria must be handled very carefully since neutralized CH may show molecular aggregation phenomena with time which induces pH values higher than those for fresh solutions (Domard, 1987).

Chitosan and polysaccharides in general have been polymerized or crosslinked through well-known techniques for producing special materials called hydrogels. Hydrogels consists of three-dimensional flexible polymeric networks that are able to absorb large quantities of water due to the presence of a large number of hydrophilic groups in the network. They are similar to ion-exchange resins since they act through electrostatic interactions but unlike resins, hydrogels are flexible structures (Khan & Lo, 2016). They are produced through different methods like solvent evaporation, neutralization, chemical or physical crosslinking and ionotropic gelation. The chemical crosslinking can be carried out by different ways like radical polymerization, high energy irradiation, enzyme utilization and chemical reaction with complementary groups through addition, nucleophilic addition or condensation reactions (Ahmadi et al., 2015; Krajewska, 2004; Sadeghi et al., 2016). Aiba (Aiba,

1989) studied the reactivity of CH solutions with different DA using methyl-4-azidobenzoimidate (MABI) and ethylene glycol diglycidyl ether in homogeneous states. It was found that MABI reacted with amino groups of CH only at neutral pH. This reaction is well known as one of the reactions of bioconjugation to crosslink amino-acids and it takes place between imido-ester functional group of MABI and NH_2 functional group of chitosan to produce an amidine linkage. The most common CH crosslinking agents are aldehydes as glutaraldehyde which react with the CH amino group yielding an imide or Schiff base group (Kildeeva et al., 2009; Mitura et al., 2020). Among the various mechanisms to produce hydrogels, the covalent linkage between complementary functional groups like NH_2-COOH or isocyanate-OH/NH_2 is well known (Ullah et al., 2015). A special kind of hydrogels called lipopolysaccharides are based on the crosslinking through carbamate bond formed from the reaction of the NH_2 group of amino-saccharides and different reagents, especially chloroformates (chloroformic acid esters), due to the high preference of these esters for amines. This kind of process will be analyzed in detail in the next section. About the CH-NH_2 group reactivity, it was found an interesting fact in the work of Pestov and colleagues (Pestov et al., 2022), where it is shown that In the chitosan crosslinking process via Schiff-base reaction with aldehydes, a protoned chitosan-amine group in acidic media generates an ionic interaction with acetate ion. It would be an impediment for the reaction of the amine group in a potential aminolysis reaction process. As it was mentioned in the abstract, no reports of crosslinking of CH through the reaction of the amino groups with cyclic carbonated substrates, were found.

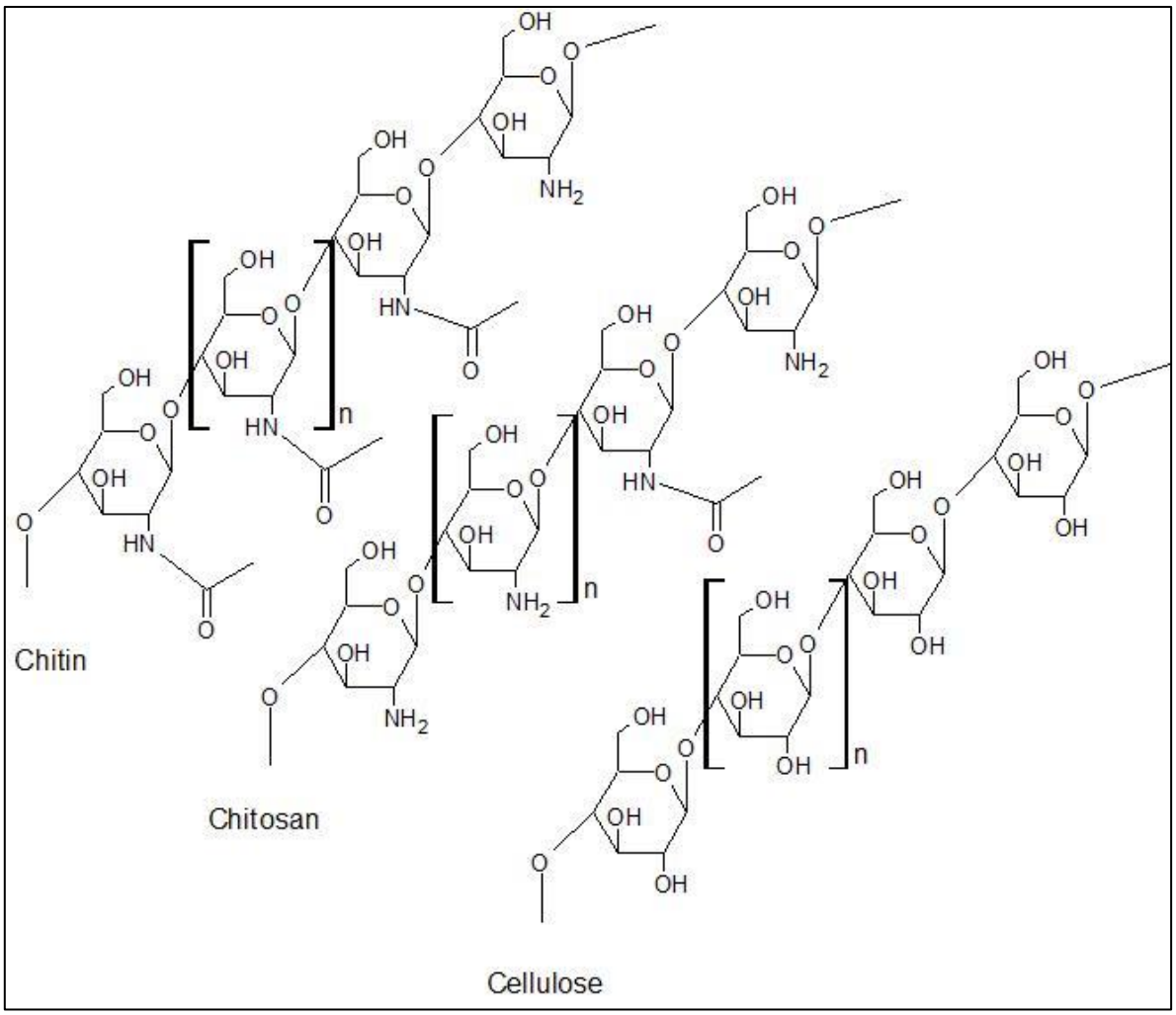

Figure 6. N-Chitin, chitosan and cellulose

3.6 AMINOLYSIS REACTION

Aminolysis of cyclic carbonates (CC) is the production of hydroxy-urethane or hydroxy-carbamate groups from the reaction of CC with amines as it is shown in **Figure 7**. Since the CC ring can be opened through two sides, two products: one with a primary OH group (1°OH) and other with a secondary OH group (2°OH) can be obtained. Steblyanko and colleagues found that the product with the secondary alcohol is preferred since it is thermodynamically more stable, with a 1°OH: 2°OH production ratio of 1:4,43 (Steblyanko et al., 2000).

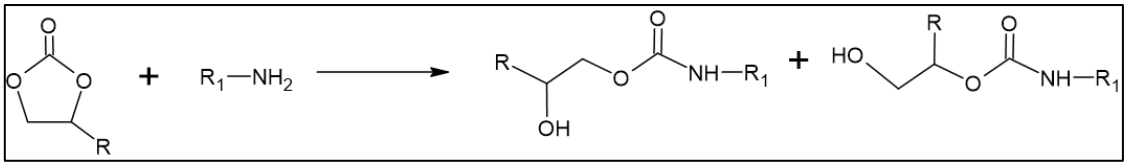

Figure 7. Aminolysis of cyclic carbonate with amine

If the CC group is located on an ester-containing chain like FAME or triglyceride, there are at least three possible products: two hydroxy-urethane molecules and one undesirable amide molecule produced by the side reaction of the ester group and the amine, according to Figure 8.

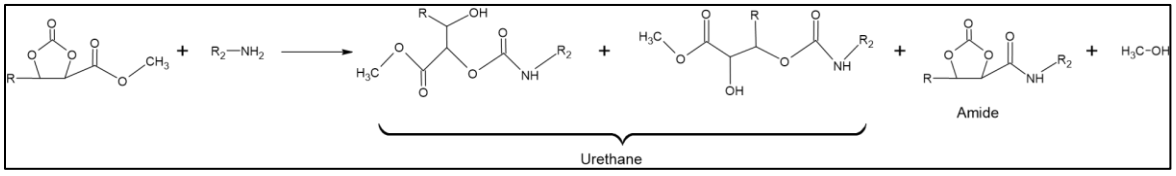

Figure 8. Aminolysis of ester-cyclic carbonate with amine

The evolution degree of this reaction depends on various factors like CC type and size, CC substituents type and size, temperature and presence of solvents. The five membered CC is the most stable; therefore, its reactivity is lower compared with six- and seven-membered CC's. The larger the size of the CC ring the greater its instability therefore, its reactivity. It has been demonstrated that a six-membered CC may be 29 to 62 times more reactive than five-membered CC (Tomita et al., 2001).

Cornille and colleagues (Cornille, Blain, et al., 2017) studied the reactivity of cyclic carbonate (CC) in aminolysis at room temperature with different CC sizes and substituents, and different solvents. They concluded that conversion is blocked by the decreasing of the amine diffusion, probably due to hydrogen bonds of the OH group at α position of carbamate group generated in the reaction. Steric hindrance

from the CC substituents plays an important role in reactivity hence in the conversion too. It was found that esther and ether substituents in CC provide more reactivity, as well as the presence of protic solvents in the system, like methanol. Oxygen from ether and esther groups increases the unstability of the CC ring, favoring the reaction with amines. Methanol interacts with the polyhydroxyurethane (PHU) reducing inter and intra hydrogen bonding between PHU chains, increasing the mobility of the polymer. Protic solvents inhibit also side undesirable reactions, like urea formation, amidification or dehydration which could be favored by the esther substituents in CC. Conversions of CC around 80% were obtained after 6 hours of reaction at room temperature using methanol as solvent.

Jalilian and colleagues (Jalilian et al., 2008) made the aminolysis of CSBO with ethanolamine in order to produce a polyol for polyurethane production. The reaction was carried out at 1,3 mol of amine to carbonate excess, LiCl catalyst (9,6% mol epoxide) and THF solvent (40 % v/w) to produce two hydroxyl groups linked to the backbone chain per carbonate group reacted. The reaction was completed after 9 hours. The product was dissolved in chloroform, extracted twice with slightly acidic aqueous solution, decanted and dried (yield=95%). ^{1}HNMR signals appeared at 3,86 and 3,69 ppm due to C groups attached to hydroxyl and urethane oxygen atoms, respectively. CNMR showed the appearance of urethane carbonyl peak at 157,69 ppm and disappearance of CC carbonyl peak at 153,88 ppm.

Aminolysis reaction between sunflower oil-derived carbonated fatty acid diester with terminal and internal carbonate groups, and different amines (EDA and IPDA) was studied by Boyer and colleagues (Boyer et al., 2010) at different temperatures in the absence of catalyst. The progress of the reaction was monitored by ATR-FTIR spectroscopy by following the disappearance of carbonate bands at 1803 cm-1 and 772 cm-1 and the appearance of new bands at 3330 cm-1 (hydroxyl group), 1714 cm-1 (carbonyl group) and 1530 cm-1 (N-H deformation of urethane group). It was revealed that an increase in temperature makes easier the aminolysis reaction and terminal carbonated fatty acid derivatives are more reactive than the internal ones. It was showed also that aminolysis kinetics is more sensitive to temperature increase in the case of internal carbonated fatty acid derivatives. The side reaction between carbonate groups and glyceride ester function to yield amide groups was observed only when primary EDA was used. Secondary IPDA is less reactive then more selective to aminolysis reaction. HNMR spectrum showed new signal at 3,6 and 4,6 ppm revealing the formation of urethane linkages and hydroxyl groups, respectively.

Levina and colleagues (Levina et al., 2015) studied the reactivity of carbonated sunflower oil using n-butylamine in DMSO at 55 °C. They found that at a CC concentration of 1,5-5,0 x 10^{-2} mol/L and in excess of amine between 0,1-0,75 mol/L, the aminolysis reaction proceeded in pseudo first-order-mode. As an interesting fact, from the kinetic study they concluded that there is not an evident effect of the TBABr presence in the aminolysis of carbonated substrate, it means it would be not necessary to remove the catalyst after carbonation reaction. A very interesting

complementary study was carried out by the same research group (Zabalov et al., 2020) . In this publication, a comparative study of reactivity was done between carbonated oleic, linoleic and linolenic-based substrates in the reaction process production of their hydroxyurethane derivatives through DFT quantum-chemical calculations. In this study it was concluded that carbonated linolenic fragments of the triglyceride chains are the most reactive. A nice review on aminolysis reaction mechanism was published by Tiger and colleagues (Tiger et al., 2021). In this work, it is claimed that vegetable-derived CC's have a 2-3 times lower reactivity than some oil-based carbonated model compounds and oligomers. It is a confirmation of the big challenge in making to react carbonated lipidic-derived substrates in aminolysis reaction for NIPU production.

Mono and Poly-amino-saccharide carbamates

The aminolysis using the NH_2 groups of amino-saccharide substrates to produce carbamate compounds has been studied by various authors, mainly, throughout the reaction with chloroformates (chloroformic acid esters). The first report is the one of Ikeda and co-workers (Ikeda et al., 1971). In this study they used GLH and methoxycarbonyl chloride as reactives, Na_2CO_3 to de-protonate the NH_2 group and a 50% aqueous solution of acetone as solvent. In the experience, GLH (2 g) is dissolved in 40 mL of the solvent and then 1,5 g of Na_2CO_3 and 1,9 mL methoxycarbonyl chloride were added successively under stirring and the mixture was stirred by 1 hour at room temperature. Then the solution was evaporated and the residue was extracted with methanol. The evaporation of the extract gave a brown powder, which as dissolved in a 4% HCl-methanol solution and then refluxed by 20 hours. The resulting solution was neutralized with lead carbonate, filtered and evaporated. HNMR in D_2O revealed 3H s. corresponding to $NHCOOCH_3$ proton at 6,31 ppm. As the best knowledge of the present work, the possibility of the reaction between saccharide-NH_2 and lipidic-CC groups has not been studied. The nearest report came from one author: Sei-ichi Aiba (Aiba, 1993), where it was evaluated the reactivity of the NH_2 group of chitosan with different reagents like derivatives of chloroformic acid esters, epoxides, cyanuric chloride, nicotinic acid and linear carbonates. In the experimental methodology, 10 mg of CH (670000<Mv(g/mol)<980000) were dissolved in 1,8 mL of a 0,11M AA aqueous solution, then, 1,05 equivalents of NaOH were added through a 1M aqueous solution. The solution is cooled in ice bath and an ethanolic solution of dimethyl or diethyl pyrocarbonate was added at room temperature with constant stirring until complete homogeneity of the system which was then let overnight in a refrigerator. After that, pH was measured and methanolic NaOH was added to precipitate the products which were centrifugated and washed with aqueous methanol. The product was characterized by elemental analysis, colloid titration and FTIR and it was

reported a urethane vibration band at 1700 cm^{-1}. It was reported that the maximum reactivity with pyrocarbonates was reached at slightly alkaline pH obtaining degrees of NH_2 substitution around 28-30% what made the product water-insoluble and gel-like form.

As Aiba (Aiba, 1993), the work of Cárdenas and colleagues (Cárdenas et al., 2002) deserves a special mention because it uses CH as saccharide amino-containing substrate too. In this case, unlike Aiba, they used only ethyl and methyl chloroformates as substitution reactants and sodium acetate as auxiliary reagent/catalyst. In the experience, an excess (1,2,5 and 10 molar respect o CH) of ethyl or methyl chloroformate dissolved in ethanol is added to a defined amount of CH (84% deacetylation degree, Mv=81250 g/mol) in a bottom rounded flask. Then, a 0,05 M sodium acetate solution is added and the pH is adjusted to 3. The mixture is stirred for 12 hours at room temperature and then neutralized. The product is separated by centrifugation, washed tree times with acetone and dried at 40°C in vacuum. When the product was water-soluble it was dialyzed for 3 days and then lyophilized. They pointed that after the sodium acetate, it was necessary to add some drops of NaOH 1M to rise pH to 3, in order to partially neutralize the acetic and hydrochloric acids from the main reaction, stabilizing and regenerating the acetate media and avoiding these acids to protonate the CH-amino group what it would be an impediment for the substitution reaction. From these experiences It is clear that CH-NH_2 groups must be de-protoned in order to enhance its reactivity, but at the same time, it collides with the necessity of protonate them to enhance CH water-solubility. In this same sense, another interesting work is the one of Alvárez and colleagues (Alvárez-Paino et al., 2014) because they carried out the reaction between GLH and a linear carbonate prepared from poly(ethylene glycol) methacrylate and p-nitrophenyl chloroformate. In the experience, 3 g (5,7 mmol) of the linear carbonate and 0,01 g of hydroquinone were dissolved in 6 mL of dimethyl sulfoxide DMSO at room temperature. Then, 0,88 g of triethylamine and 1,23 g of GLH were added and the system was let to react for 24 hours. After that, the triethylamine chlorhydrate byproduct was removed by filtration and the carbamate product was precipitated using a 4/1 mixture of diethyl ether/chloroform and purified by successive solubilization-precipitation processes. Finally, the product was dried in vacuum at room temperature in the presence of phosphorus pentoxide. 50% yield was reported.

As it was mentioned before, this reaction has been carried out mainly between a saccharide amino-containing substrate like GLH and chloroformic acid esters like 2,2,2 Trichloro-ethoxycarbonyl chloride (Imoto et al., 1987), p-Nitrobenzyl chloroformate (Qian & Hindsgaul, 1997) and methyl-chloroformate (Bauer et al., 2002). Wang and colleagues (G. Wang et al., 2009) carried out the reaction using various chloroformates. Other related works using the same technique are: Birchall and coworkers (Birchall et al., 2011) using fluorenyl methyl oxy carbonyl, Higashi and Ikeda (Higashi & Ikeda, 2021) with 4-nitrophenyl methoxycarbonyl chloride and

a reported yield of 74% yield, Bietsch and colleagues (Bietsch et al., 2023) using ethyl, isopropyl and isobutyl chloroformates and reported yields around 96%.

3.7 WATERBORNE POLYURETHANES AND NIPU FROM VEGETABLE OILS AND CHITOSAN

Conventional PU's come from a well-known technique and because of the use of castor oil and chitosan, many reports deserve to be mentioned here. Castor oil and chitosan have been used together to produce PU through the conventional way (Uscátegui et al., 2019) for biomedical applications. Polyol from castor oil improved the mechanical properties of the polymer as well as its bio-compatibility. In the work of Gallego and co-workers (Gallego et al., 2013), chitin and chitosan were functionalized with reactive isocyanate groups in order to use these products as thickening agents in castor oil. The final product known as oleo-gel was prepared by adding slowly the isocyanate-functionalized chitin/chitosan to the castor oil while it was mixed with an anchor-shaped impeller. The mixing process was maintained at 70 RPM for 24 hours at room temperature. Then, the mixture was homogenized with a rotor-stator turbine at 8800 RPM during 1 min. The product showed high stability and improved thermophysical properties what make it a good candidate as a biodegradable lubricant grease. Due to its functionality, castor oil can be modified to increase its hydroxyl functionality in order to produce PU through the conventional way. It is the case of the work of Rihayat and colleagues (Rihayat et al., 2020) where CO is treated with H_2O_2, AA and H_2SO_4, methanol and glycerin to obtain a polyol. Then, this polyol is mixed with toluene diisocyanate and Montmorillonite to produce a PU coating with improved thermal resistance due to the Montmorillonite filler and antimicrobial properties due to the presence of chitosan what make it proper for medical device applications. The presence of castor oil and chitosan confers special characteristics to this material. Arévalo-Alchiquire and co-workers (Arévalo-Alquichire et al., 2018) made a study of the physicochemical properties, hardness, in vitro degradation and cell viability of a PU material produced from CO, CH and IPDA. The results showed high viability to use the product as biomaterial. Díez-pascual and Díez-Vicente (Díez-Pascual & Díez-Vicente, 2015) developed a bio-nanocomposite based on CO polymeric PU matrix material and CH-ZnO modified nanoparticles. The material exhibited good cytocompatibility for antibacterial wound dressings.

Due to environmental and health concerns, research on polyurethanes have focused on water-based polyurethanes, commonly named as waterborne polyurethanes. PU conventional routes, as well as NIPU route, have been studied with water as the reaction medium. On the conventional way, many research works deserve mention: (Bizet, 2020), (Bizet et al., 2021), (C.-Y. Li et al., 2008), (W. Zhang et al., 2019), (Meng et al., 2017), (Valério et al., 2015), (Zanetti-Ramos et al., 2006), (Honarkar,

2018). Zhang and colleagues (W. Zhang et al., 2021) developed a semi-interpenetrating polymer by blending carboxymethyl chitosan with a castor-oil based waterborne PU to produce a material with high storage stability and surface wettability, useful for coatings, adhesives and ink applications. Compatibility and stability of CO and CH emulsions has been proved. Tamilvanan and colleagues (Tamilvanan et al., 2010) developed a CO nanosized emulsion stabilized with a CH derivative for pharmaceutical applications.

In NIPU production there is a well identified problem: the low reactivity of cyclic carbonates in aminolysis reaction and the subsequent low molar mass obtained for the NIPU. As the aminolysis reaction advances, hydrogen bonding from the new OH groups causes a limitation in the diffusivity of the species hence a slowdown in the reaction and lower molar masses (Cornille, Blain, et al., 2017). Another Cornille and colleagues publication of the same year (Cornille, Auvergne, et al., 2017), offers an insight in reaction parameters like solvent, structures and substituent effects on the reaction. Nohra and colleagues published a complete review on the use of vegetable oils as carbonated substrate for NIPU production. Studies on reactivity, catalysts and reaction parameters were published (Nohra et al., 2013). Other very complete reviews on the NIPU reaction are: (Maisonneuve et al., 2015), (Rokicki et al., 2015), (Błażek & Datta, 2019). Maisonnueve published in her thesis a very complete review on NIPU production from vegetable oils (Maisonneuve, 2013). Lombardo and colleagues (Lombardo et al., 2015) proposed a catalytic dual system composed by Triazabicyclodecene (TBD) and Lithium triflate (LiTOf) which improved the reaction rate of aminolysis reaction between CC and amines.

Many vegetable oils have been used to produce NIPU's with different polyamines. One of the first reports used soybean oil. NIPU was prepared by mixing thoroughly carbonated soybean oil with ethylenediamine at 60 °C and then pouring the system in a mold at 70°C by 10 hours and then at 100 °C by 3 hours. A 4 mm thick, light-brown, transparent and flexible polymeric material was obtained. The same procedure was applied with other amines as hexamethylenediamine and tris(2-aminoehtyl) amine (TA). The materials were characterized by solvent extraction, dynamical mechanical analysis (DMA) and limited tensile testing. Since a tri-functional amine provides more functionality hence a more crosslinked network, TA-based NIPU's showed the least amount of soluble and dangling chain ends, the highest Tg value (43°C), the highest rubbery plateau modulus and the highest level of stress for a given strain (Tamami et al., 2004). Under the numbers US 7,045,577 B2 and WO 2004/074352 A2, the same authors published a patent, based on this work (Wilkes et al., 2006). Li and colleagues (Z. Li et al., 2008) produced also soybean-based NIPU by mixing CSBO with EDA at 60-80 °C for 2-5 minutes and then the system was poured into molds and cured at 90-100 °C for 20-30 hours. IR analysis showed the disappearance of carbonate-carbonyl group at 1805 cm^{-1} and the appearance of new bands at 1710, 1540 and 3337 cm^{-1} corresponding to urethane-carbonyl group absorption, urethane N-H deformation and hydroxyl group,

respectively. In this work, they established that mechanical properties of NIPU strongly depends on the CC concentration groups, it is, the ESBO to CSBO conversion degree. They found that a very high CC groups content (greater than 85,1%) is not essential for the preparation of NIPU with good mechanical properties since such a high quantity can cause steric hindrance and the unreacted amine acts as plasticizer, leading to poor mechanical properties. Conversions under 74,3% can lead also to inferior mechanical properties.

Other authors mention those factors impacting the mechanical behavior of the NIPU. For example, Javni and colleagues (Javni et al., 2008) mentioned that fatty acid chains with unreacted epoxy groups act as plasticizers decreasing Tg and modulus of the NIPU. They prepared NIPU's from CSBO and various amines: 1,2-ethylenediamine (EDA), 1,4-butylendiamine (BDA) and 1,6-hexamethylenediamine (HMDA) with carbonate/amine molar ratios of 1:0.5, 1:1 and 1:2. The NIPU samples were analyzed by thermal, mechanical, swelling and FTIR methods. They found that stoichiometric carbonate/amine ratio produced a polymer network with the highest density, Tg, hardness and tensile strength. Another interesting finding was that the amine-excess ratio (1:2) causes the undesirable lateral reaction between the glyceride ester and amine toward amide formation. This amide formation decreases the crosslinking density producing a material with lower Tg, hardness and tensile strength but the highest elongation compared with the 1:1-molar-ratio material. This amidation reaction was always present in all molar ratios because the reaction temperature of 70-100 °C for urethane formation promoted also amidation and ester cleavage. On the other hand, the molecular weight of the amine affected the properties in different ways. EDA produced the NIPU with the highest hardness and tensile strength while HMDA produced the material with the highest elongation. The influence of some reaction parameters on the physicochemical and mechanical behavior of the NIPU was studied by Zalewski and colleagues through a Box-Behnken experimental design (Zalewski et al., 2022). They determined that viscosity was influenced by reaction time, temperature and reagents' molar ratio while mechanical properties as glass transition temperature were affected only by reagents' molar ratio. In the model validation, they reported that the experimental shear strenght and glass transition temperature deviated from the computed value by 15% and 7%, respectively.

Parzuchowski and colleagues (Parzuchowski et al., 2006) produced CSBO for modifying a bisphenol-A epoxy-based resin using polyamine hardeners (1,6 Hexanediamine, triethylenetetraamine, diethylenetriamine and isophoronediamine) for curing. First they produced CSBO and on what they called the "two-step method", CSBO was reacted with amine at 70 °C for 3 hours to produce a NIPU adduct and then it was added to a bisphenol-A epoxy-based resin. The obtained product was a brown-transparent polymer which it was characterized by spectroscopy and thermal and mechanical techniques. Boyer and co-workers (Boyer et al., 2010) polymerized sunflower oil-derived carbonated fatty acid diester with terminal and internal

carbonate groups and two amines: EDA and IPDA. The highest molecular weight NIPU was obtained with terminal-carbonated diester / IPDA monomer couple at 110 °C (Mw: 13500 g/mol) with a narrow poly-dispersity index below 1,5. Lower molecular weights were obtained with internal-carbonated diester monomer. It is clear that terminal carbonate groups are more reactive than internal ones so a higher crosslinking is reached hence, higher molecular weights. This was confirmed by thermal analysis: NIPU from internal-carbonated diester monomer exhibited lower Tg than that from terminal-carbonated diester due to the lower molecular weight of the former but also the presence of pendant chains which can act as plasticizers. Aminolysis of CSBO has been used also for surface modification of silica nanoparticles for nanocomposite materials application (Türünç et al., 2008) .

Bähr and Mülhaupt (Bähr & Mülhaupt, 2012) developed a NIPU material based on CSBO, CLSO and blends of both components. The carbonate content was tuned by blending CSBO and CLSO in determined proportions and the blends were cured with different amines: 1,2 ethane diamine (EDA), 1,4-butanediamine (BDA) and isophorone diamine (IPDA). The curing was performed for 10 hours at 70 °C and 3 hours at 100 °C until complete conversion of carbonate, determined by FTIR. The results showed that high carbonate content brings enhanced crosslinking density but also a high troublesome viscosity and shorter gel times, especially when curing with reactive diamines such as EDA and BDA. Viscosity is correlated with carbonate content. Tg, Young's modulus, stiffness and tensile strength increase with carbonate content whereas elongation at break decreases. IPDA affords a much higher stiff material with a Young's modulus improved by three orders of magnitude when increasing the carbonate content. Water-swelling content increases also with carbonate content.

Until this time no one but Mahendran and colleagues (Mahendran et al., 2012) had used a bio-based polyamine for NIPU. They were the first to report a completely bio-based NIPU from carbonated linseed oil and an alkylated phenolic polyamine (phenalkamine) from cashew nut shell liquid (*Anacardium occidentale*). Phenalkamines are a kind of Mannish base obtained by reacting cardanol from cashew nut, an aldehyde and an amine. Through FTIR, rheological and DSC measurements and using Vyazovkin's free kinetic method involving apparent activation energy of reaction they concluded that the aminolysis reaction rate start to decrease after 65% conversion since the longer polymer chains restricted the mobility of the system reducing the availability and contact between carbonate and amine reactive groups, increasing the activation energy at the same time. Interestingly, other authors used also the cashew nut shell liquid not as the polyamine adduct but as the cyclic carbonated substrate.

Kathalewar and colleagues (Kathalewar et al., 2014) developed NIPU´s from a carbonated epoxy commercial resin derived from cardanol and two different difunctional amines: hexamethylene diamine (HMDA) and isophorone diamine (IPDA) at 120°C and 150 °C of reaction temperature. They demonstrated that HMDA

produced faster reaction rates at both temperatures than IPDA because the aliphatic amines are more reactive than the aromatic or cycloaliphatic ones. They found also that these NIPU's applied as coatings showed some superior mechanical and physical properties as compared as the epoxy-based coatings formulated with the same amines. On a patent of 2012 Birukov and coworkers (Birukov et al., 2012b) developed hybrid NIPU's (HNIPU) from ESBO partially carbonated at 35%, 60% and 85% conversion. The polymerization was carried out with different amines as N-Octylamine, 2,2,4-trimethylhexamethylenediamine, isophorone diamine, 1,8 diamino-3,6-dioxaoctane and commercial epoxy resins as DER® 331 and DEN® 431. They obtained HNIPU and characterized them through hardness, tensile strength, elongation and chemical resistance tests. Lee and Deng produced an NIPU elastomer from CSBO, 3-aminopropyltriethoxysilane and lignin (Lee & Deng, 2015). The aminolysis reaction was catalyzed by 5 mol% of LiCl and carried out at 70 °C for 3 hours under stirring. Then, a THF/water-lignin solution was added and the reaction mixture was stirred for 12 hours and then poured into a mold and dried for 2 hours followed by curing at 60 °C for 7 hours. The addition of lignin showed an improvement on the tensile strength of the material.

Pathak and co-workers produced a NIPU from dehydrated castor oil fatty acid modified with 2-hydroxy ethyl isocyanurathe (Pathak et al., 2015). This product was cured with different amines like IPDA and HMDA to obtain NIPU coatings. The results showed that coatings cured with aromatic and ciclo-aliphatic amines resulted in better mechanical, chemical, thermal and anticorrosive properties than coatings cured with aliphatic amines. Pitaksanon and colleagues (Piyataksanon et al., 2022) used also CSBO for NIPU production with 3-aminopropyltriethoxysilane and diethylenetriamine. They added also lignin alkali to the formulation but no improvement in terms of adhesive peel strength. Poussard and colleagues (Poussard et al., 2016) produced NIPU from CSBO using an amino-telechelic oligoamide prepared from fatty acid dimer compound Pripol 1013® and short diamines as 1,2-diaminoethane, 1,4-diaminebutane and 1,5 diaminepentane also. The polymer was prepared in an internal kneader (Brabender plastograph) by melt copolymerization. CSBOs with different CC content were produced by varying the time reaction and then used for formulating NIPUs. It was found that NIPUs formulated with CSBO and short diamines revealed poor mechanical properties due to the high crosslinking. On the other hand, NIPUs with the amino-telechelic oligoamide showed improved elongation break and elastomeric behavior proper from partially cross-linked polymeric materials. They report also improved thermal stability compared to conventional petroleum or vegetable oil-derived PUs reported in the literature. Undecenoic, oleic and sebacic acid-based cyclic carbonates were used along with 1,10-diaminodecane and/or 1,3 cyclohexane-bis(methylamine) in DMF at 1 $mol.L^{-1}$, 70 °C and no catalyst, to produce NIPU. They confirmed urethane formation by the identification of the CH_2-NHC(O)O HNMR protons at 2.98 ppm. Besides aminolysis reaction they detected also amidation reaction which tended to decrease molar masses and to increase the dispersity by cleaving the polymer

chains. Tg in the ranges -26° to -10 °C and molar masses between 8800-12000 $g.mol^{-1}$ were obtained. Vegetable oils have been used not only as carbonated substrate but as precursor of amine substrate. It is the case of Duval and colleagues (Duval et al., 2016). In their work, through esterification reaction between sebacid acid and glycerol carbonate, they produce a bifunctional carbonate substrate. On the other hand they used methyl ricinoleate to produce a fatty difunctional amine. Other linear renewable amines were used also, like putrescine, cadaverine and 1,10-Decanediamine (from castor oil), and branched PRIAMINE 1074® (from oleic and linoleic acid). Linear NIPU showed semi-cristaline behavior while branched were totally amorphous. All polymers were thermally stable until 200 °C.

Jatropha oil has been used for NIPU production. Haniffa and co-workers (Haniffa et al., 2017) produced carbonated jatropha oil and an alkyd resin based on jatropha oil for NIPU formulation with isophorone diamine and 1,3-diaminopropane. The reaction mixture was heated to 70 °C for 8 hours and to 100 °C for 10 hours with continuous stirring at 600 RPM. Then the resulting mixture was placed overnight into an oven at 55 °C and then applicated onto a Teflon sheet and cured at 70 °C for 10 hours and 120 °C for 4 hours. They found that oil-alkyd resin-based NIPU had better thermal, mechanical, solvent and chemical resistance than the oil-based NIPU, it is, the addition of the jatropha-based alkyd resin improves the performance characteristics of the NIPU. Farhadian and colleagues (Farhadian et al., 2018) produced an hybrid NIPU network polymeric material from carbonated sunflower oil and different bio-based amines from castor oil, sunflower oil and oleic acid. The NIPU polymeric material was prepared by mixing the carbonated sunflower oil and the amines (Tri-ester Amide/amine, poly amine poyol and Di-amine amide) in stoichiometric ratio. After mixing monomers by 5 minutes the system is cast on Teflon panels and heated at 90 °C by 24 hours. They found materials with improved thermal stability and molecular weight than conventional PU's. Carbonated oligomeric ricinoleic acid was cured with IPDA and HMDA by Ren and colleagues (Ren et al., 2021). It was demonstrated that NIPU's derived from IPDA had higuer strength than the ones from HMDA due to the presence of cyclo-aliphatic structures which imparts rigidity to the cured backbone of the polymer. IPDA conferred also ductile behavior while HMDA gave brittle behavior. Higuer thermal stability was observed also with IPDA.

Mokhtari and colleagues (Mokhtari et al., 2019) put pendant cyclic carbonate groups on jojoba and castor oil by thiol-ene coupling with thioglycolic acid followed by esterification with glycerol carbonate. Then, these CC moieties were reacted with 1,4-diaminobutane and m-xylylenediamine to produce NIPU materials with molar masses between 6100 -7100 g/mol, Tg -46 to 20 °C and gel contents higher than 90% which correspond to highly crosslinked network materials. Pouladi and colleagues (Pouladi et al., 2021) produced a NIPU from carbonated linseed oil at different carbonate content and diethylenetriamine as hardener. It was found that the NIPU from the 75%-conversion carbonated oil showed the optimum performance in

coating and anticorrosive applications. Yu and coleagues (Yu et al., 2018) prepared CSBO-based NIPU coatings using tris(2-aminoethyl) amine as crosslinking agent, TBD and LiTOf catalysts at 120 °C and 3 hours of curing. Studies on catalyst, solvent and temperature on the mechanical and physicochemical characteristics of the NIPU resin, were carried out. It was found that the addition of LiTOf addition as a secondary catalyst, improved the solvent resistance of the coating.

Das and colleagues (Das et al., 2020) claimed the production of a sustainable bio-based NIPU from chitosan and CSBO in a bulk polyaddition. NIPU was prepared by adding 5% of lithium chloride (CSBO-based) to a defined mass of CSBO. Chitosan is dissolved apart in a 0,5 M AA solution and stirred for 5-6 hours at 85 °C. Then, the chitosan solution was poured into the CSBO/LiCl mixture in different weight ratios, the temperature was increased to 80 °C and the system was stirred by 12 hours. The obtained product was then poured on a Petri dish and kept overnight in an oven at 70 °C and then 5hours at 100 °C. FTIR characterization of the product showed signals at 1739 cm^{-1} assigned to C=O urethane stretching vibration and peaks at 1655-1660 cm^{-1} and 1557 cm^{-1} due to urethane C-O-C stretching vibration and both N-H bending and C-N vibration respectively. Castor-based materials have been produced also in the work of Ren and colleagues (Ren et al., 2021). Carbonated oligomeric methyl ricinoleate was cured with HMDA or IPDA. A series of PHU's were obtained. PHU FTIR characterization showed the following vibration bands: 3300-3400 cm^{-1} due to superposition of -OH and -NH groups, 1690-1720 cm^{-1} due to urethane carbonyl stretch, 1652 and 1536 cm^{-1} due to N-H bending of urethane group. The PHU's obtained based on IPDA showed higher strength than those based on HMDA due to the presence of cyclo-aliphatic structure which imparts rigidity to the backbone of the structure. This rigid structure gives to the material a higher thermal stability too. Heptanal, a CO derivative was used by Ruiz and colleagues for producing a NIPU material with potential application on catalysis and drug delivery systems (Ruiz et al., 2017).

NIPU route has been studied also in water medium. It is the case of Ochiai and colleagues (Ochiai et al., 2005). The reaction was conducted using 1,0 mL of water, 500 μmol of bifunctional carbonate and diamines, at temperatures between 50 and 100 °C and 24 hours of time reaction. They demonstrated that the key factors to ensure high conversion and selectivity are: hydrophobicity of carbonated substrate to guarantee heterogeneity to avoid carbonate hydrolysis from water, and high nucleophilicity of the amine. Bizet and colleagues (Bizet, 2020) published a nice review on water-based NIPU's. Rix and colleagues (Rix et al., 2016) used three different bis-CC monomers for NIPU production in bulk and micro-emulsion systems. The first one, called "BCC", was produced from vinyl ethylene carbonate and 1,4 butanedithiol through thiol-ene addition reaction. The other ones were produced from commercial dicarboxylic fatty acids, including Pripol ® 1009 and a poly (ricinoleic acid) diacid. They concluded that NIPUs prepared in mini-emulsion exhibited lower molar masses than the ones formed in bulk, phenomenon explained

by the partial hydrolysis of CC. They claimed also that fatty acid-derived CC's showed faster kinetics in the bulk polymerization reaction (87-99% CC conversion after 2 h at 90-130 °C) since ester linkages at the β position of the carbonate ring, make easier the ring-opening by amines, compared with BCC that is a bis-CC with a thio-eter linkage located at the γ position of the CC group. As a key factor in the mini-emulsion system, they found that a solid content not exceeding 30% wt. leads to the more stable and mono-disperse mini-emulsions and particle latexes. Above this value no stable mini-emulsion or latex could be obtained.

4. RAW MATERIAL CHARACTERIZATION

4.1 Castor oil

CO was obtained from a local supplier: Químicos JM S.A. A Product with lot number:1612038-2 was purchased as the main raw substrate material for the current research work; it was characterized through according to the following analytical tests.

For determining the fatty acid composition, CO was trans-esterified according a procedure based on the literature (see Appendix 6.1) and the obtained COFAME were analyzed by gas chromatography-Mass spectrometry (GC-MS) coupled technique, on an AGILENT 7890A chromatograph-5975C VL triple axis mass detector with a 30 m x 250 µm x 0,5 µm HP INNOWAX column. Figure 9 shows the GC spectrum of esterified castor oil fatty acids to get the fatty acid profile of the CO triglyceride. At a retention time of 19,05 minutes it can be identified the signal peak of palmitic acid. The other identified fatty acids are: stearic (21,747 min), oleic (22,069 min), 10-Octadecenoic or Isooleic (22,166 min), Linoleic (22,739 min), Linolenic (23,672 min), 11-Eicosenoic or Gondoic (24,944 min) and Ricinoleic (31,602 min). The appendix 6.2 shows the complete results obtained from the GS-MS analysis. With the areas of the signal peaks it was possible to estimate an average fatty acid profile of the CO triglyceride as it is shown in Table 6. Whit this composition it was possible to estimate an average CO Mw of 923,71 g/mol according to appendix 6.3.

Infrared spectroscopy (FTIR) and proton nuclear magnetic resonance (HNMR) analyses were applied on CO. A typical infrared spectrum of castor oil is showed in Figure 10.

The mark A shows the tension of the hydroxyl (OH) group around 3400 cm^{-1}. The mark B around 3080-3100 cm^{-1} points to the absorption band of the asymmetric stretch of the =CH portion of the DB. Ester triglyceride carboxylic group stretch is tagged with mark C around 1750 cm^{-1}. Figure 11 shows the HNMR spectrum of CO, where it is possible to identify the signal of the OH group near to 3,5 ppm. Triglyceride-glycerol, another typical functional group, has two chemical shift peaks between 4,0-4,5 ppm. The chemical shift signals around 5,2-5,5 ppm are from DB protons. Based on the three triglyceride CH_3 terminal groups (signal around 0,8 ppm) it is possible to quantify the number of hydroxyl groups per triglyceride molecule by integrating the areas, giving a value of 2,38 hydroxyl groups per molecule. According to this value, it is possible to estimate a hydroxyl value for the castor oil of 145,15 g/mol (see Appendix 6.4).

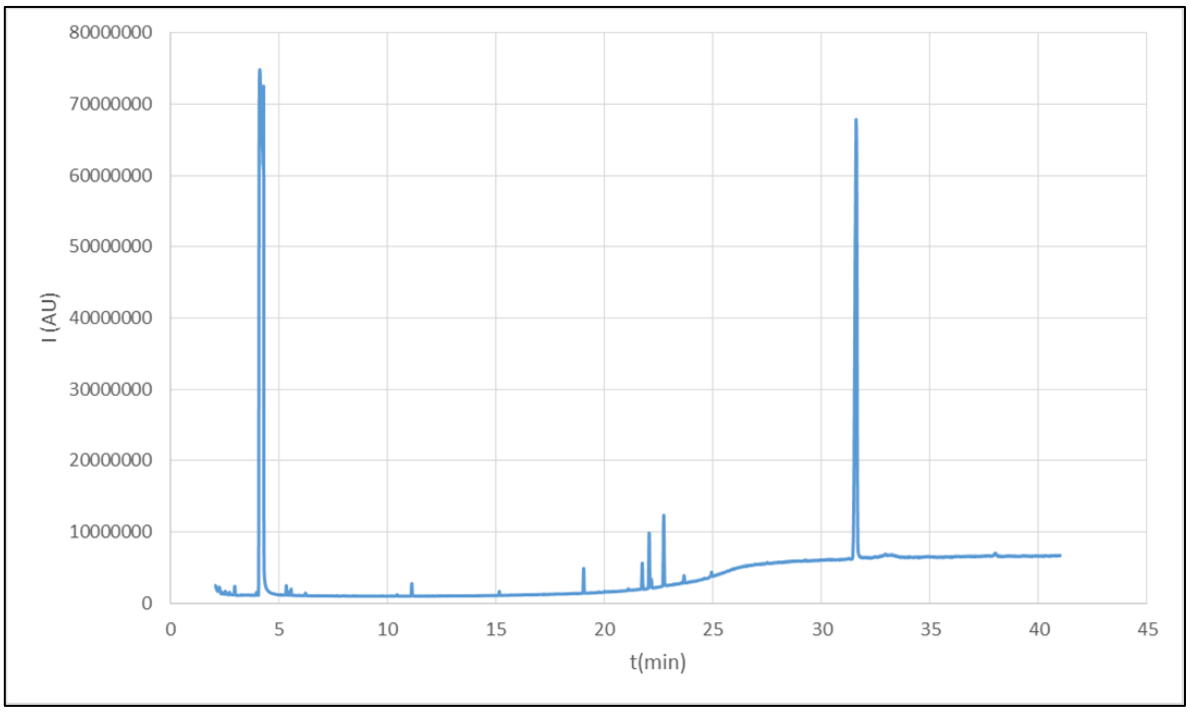

Figure 9. GC spectrum of CO methyl ester

Table 6. Estimated CO fatty acid profile

Fatty Acid	Composition (%)
Ricinoleic	85,04 %
Linoleic	5,49 %
Oleic	4;26 %
Stearic	1,89 %
Palmitic	1,59 %
10-Octadecenoic (Isooleic)	0,67%
Linolenic	0,58 %
Eicosenoic (Gondoic)	0,48 %

Acid value (AV) and Iodine value (IV) were determined according to the ASTM standards ASTM D1908 and ASTM D5554, respectively (ASTM, 1998, 2006). The dynamic viscosity was measured on a rotary viscometer (Lamy Rheology®, model: B One Plus). Density was measured according to the ASTM D891 standard (ASTM, 2018). Table 7 shows the estimated physicochemical properties of CO.

Table 7. Castor oil estimated physicochemical properties

Property	Value	Units
Acid Value	2,4	mg KOH/g
Iodine Value	86,08	g I_2/100g
Hydroxyl value	145,15	mg KOH/g
Density (23 °C)	0,9554	g/cm^3
Viscosity (23 °C)	873	cP
Molecular mass	923,71	g/mol

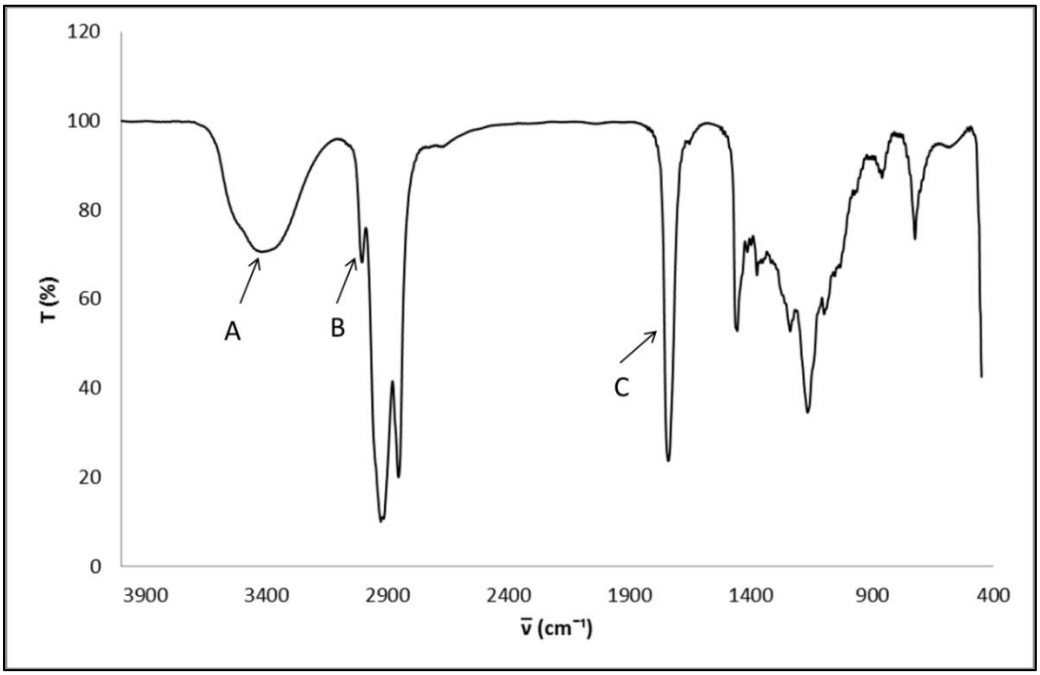

Figure 10. Infrared spectrum of Castor Oil

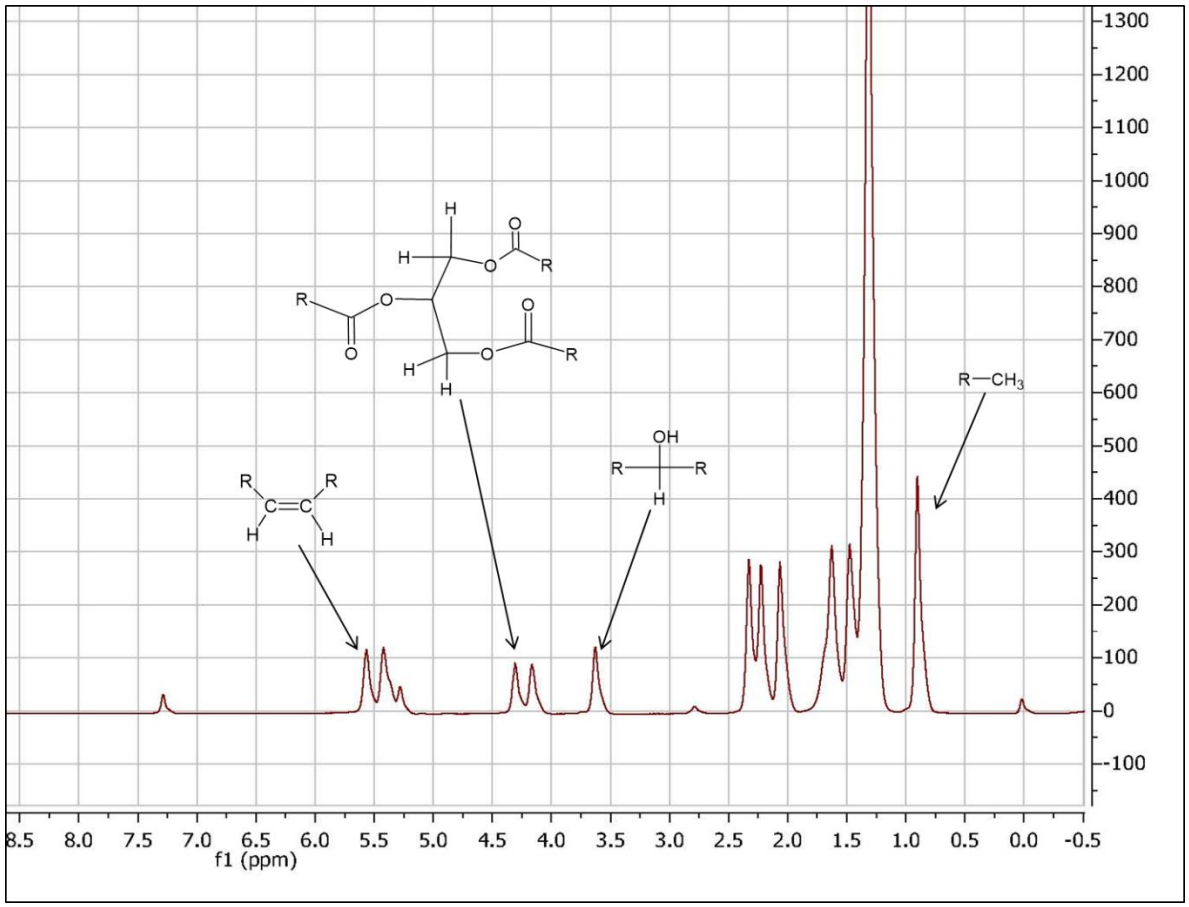

Figure 11. HNMR spectrum of Castor Oil

4.2 Chitosan

Alfa Aesar® 85% de-acetylated CH was obtained with product number: J64143 and lot number: Z13D046 (Aesar, 2009, 2018, 2022). The measured FTIR spectrum for CH is showed in Figure 12. Bands between 3000-3600 cm^{-1} (A) corresponds to the overlapped N-H and O-H stretching signals. Around 1670 cm^{-1} (B) it is the amide C=0 group stretching and around 1650 cm^{-1} (D) the overlapped bending of amide and amine N-H groups. Signal at 1360 cm^{-1} (C) is typical from the amine N-C(aryl) group stretching. Signals around 1430 cm^{-1} and 2900 cm^{-1} (E) are C-H, CH_2 and CH_3 groups vibrations (Abdelhalim, 2006; Skoog et al., 2000).

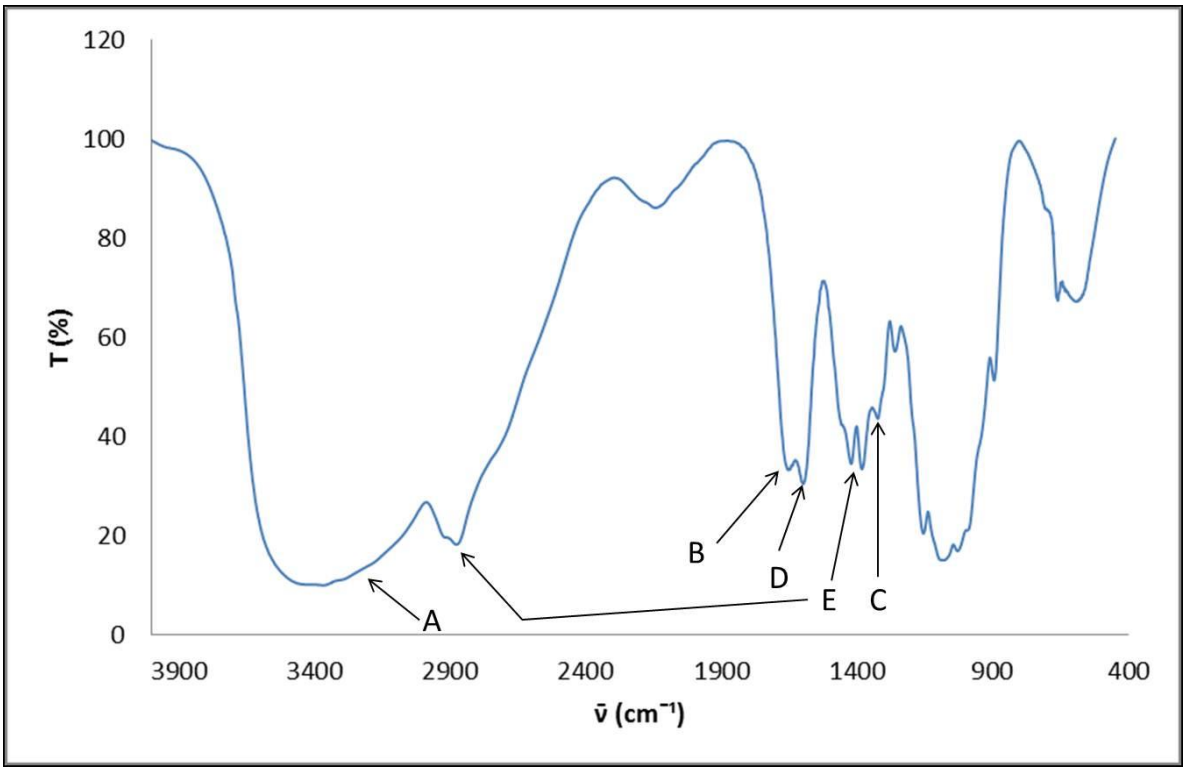

Figure 12. Chitosan FTIR spectrum

Elemental analysis of chitosan was carried out at the laboratory of Energy Sciences of the National University of Colombia, and the obtained results are show in Table 8.

Table 8. Chitosan elemental analysis

C	40,68
H	615
N	7,79
Residual	45,36*

*including oxygen, sulfur and ashes.

The certificate of analysis provided by the supplier is shown in Table 9 (Aesar, 2018).

Table 9. Supplier's chitosan certificate of analysis

Appearance	White powder
Moisture	8.97%
Heavy Metals	< 1 ppm
Arsenic	0.02%
Ash	0.75%
Insolubles	0.20%

A total nitrogen content analysis was conducted by the Water-Laboratory team of PQI research group with a reported value of 67839,63 mg N/Kg of sample.

The degree of acetylation (DA) of the CH used in this work has been calculated by elemental and potentiometric analysis. Some clarifications were made in order to bring clarity about the definition of some equations and calculations.

Kasaai and colleagues (Kassai et al., 2000) proposed a way to calculate DA from the carbon/nitrogen (C/N) ratio, since it is 5,145 in completely de-acetylated chitosan and 6,861 in fully acetylated chitin:

$$DA=\frac{C/N-5,145}{1,716}*100 \quad (2)$$

Using values from Table 8, equation (2) gives a DA of 4,49% and from equation (1), DD is equal to 95,5%, around 10% above the nominal value of 85%. Taking into account that the nitrogen content in fully de-acetylated chitosan is 8,695% and in fully acetylated chitin is 6,896%, Alvarenga (Alvarenga, 2022) proposed the estimation of degree of acetylation (DA) from the nitrogen content in the organic fraction %Norg, as:

$$DA=\frac{8,695-\%Norg}{1,779\%}*100 \quad (3)$$

According to the data in Table 9, an estimation of the chitosan elemental nitrogen content in organic base is:

$$\%Norg=\frac{7,79}{(100-0,75-8,97)}*100=8,63\% \quad (4)$$

Replacing the value from equation (4) in equation (3) gives a DA of 3,72%,then from equation (1), DD=96,27%, value in the same order than the obtained in the previous reference.

Gupta and colleagues (Gupta & Jabrail, 2006) proposed two ways of calculating DA from carbon and nitrogen elemental content through two equations (equations 4 and 5 in page 45 of the reference). Using carbon and nitrogen content from Table 8, DA

values of 55,79 % and 49,37% were obtained. As it is evident, the obtained values are very different from the expected values, as well as the obtained through the work of the previous authors. Those values would give DD's of 44,21% and 50,63%, very different from the nominal expected value. Indeed, revising this work on a deeper way, some "dark" facts were found: first, they claimed that the formulas to calculate DA from the carbon and nitrogen content come from the structural analysis of chitosan and they use a self-reference to a non-existing publication about which they assure it was submitted for publication. No signals on the web were found about such publication. Furthermore, validating the formulas with their proper values of carbon and nitrogen content (tables 1 and 2 page 48 of the reference) it was found that just the results obtained with the equation using nitrogen content are consistent (equation 5 of the reference). They report other DA values that are not possible to reach with the equation using the carbon content (equation 4 of the reference) and more strange even is that according with the report, this calculation seems to be based on the work of Mi and colleagues (Mi et al., 2002) while this publication is not related to DA calculation or something similar.

The potentiometric method was also applied to estimate DA of chitosan. For this purpose, two samples of chitosan (sample 1= 0.118 g, sample 2=0,109 g) were dissolved in 20 ml of a 0,1699 N HCl solution and 25 mL of distilled water were added. The system was stirred overnight at room temperature. Then, another 25 mL of water and a determined amount of KCl to ensure an ionic strength of 0,1 N, were added. A strong ionic content guarantees a greater stability in the pH measurement according to the Debbi-Huckel theory of electrolytes. The system is titrated with a 0,1062 N NaOH solution by adding 0,5 mL at once and waiting pH to stabilize. The titration plot (pH vs NaOH volume) allowed to identify the inflection points: the first determines the titration of the acid excess and the second one the de-protonation of amino groups. The difference between them is a quantification of the free-amino groups. Plotting the numerical derivative, it is easier to identify the volume corresponding to the two inflection points. Figure 13(a) shows the pH vs NaOH volume curve for sample 1. Figure 13(b) plots the numerical derivative $\Delta pH/\Delta V$ vs NaOH volume for sample 1. With the NaOH volumes at the inflection points (V_1=25 mL and V_2=30,5 mL for both samples) it is possible to determine the DD according to different authors. The complete set of data is shown

Parada and coleagues (Parada et al., 2004) propose the estimation of the free amino groups content in page 14 of their publication. They claimed that NaOH concentration is in molarity and no specification of the volume units were found. Even if the volume units were in liters in order to match with molarity, the obtained value would be a fraction but not a percentage, so it is evident the absence of the 100% term. It is clear also that 16,1 accounts for the molecular mass of the free amino group, so with this relationship it is intended to make a ratio between the mass of free amino group and the total mass of the sample. It is important to remark that this free amino group percentage is not the same DD of CH. It is the mass percentage

of the free amino groups respect to the mass of the sample which is not a 100%-purity chitosan mass so the ash and moisture content must be taken into account. Hence assuming the volumes come in milliliters as it is natural from a laboratory titration and considering the 100% term and the moisture and ash content, the following corrections are proposed, and the result is shown in equation (5).

$$\%NH_2=\frac{16{,}1(V_2-V_1)}{1000\ \frac{w}{100}(100-\%H_2O-\%Ash)}C_{NaOH}*100$$

$$\%NH_2=\frac{161(V_2-V_1)}{w(100-\%H_2O-\%Ash)}C_{NaOH} \qquad (5)$$

Where:

$\%NH_2$: Free amino group–mass percentage in the sample

V_2: Volume of NaOH in mL added until the second inflection point

V_1: Volume of NaOH in mL added until the first inflection point

C_{NaOH}: Concentration of NaOH solution in mol/L

W: sample mass in grams

$\%H_2O$: Mass percentage of water in sample

%Ash: Mass percentage of ash in sample

%NH2 would be useful to calculate DD considering the mass percentage of a 100% completely de-acetylated chitosan. From Figure 6 it is clear that the molar mass of a glucosamine monomer unit is 161,17 g/mol so the theoretical free amino content of a 100% de-acetylated CH with 100% purity is 16,1/161,17*100= 9,98%. DD could be calculated as it is shown in equation (6):

$$DD=\frac{\%NH_2}{9{,}98}*100 \qquad (6)$$

From the obtained values for sample 1, and the data in Table 9, $\%NH_2$ calculated with equation (5) gives a value of 8.83% and DD from equation (6) gives a value of 88.45%. In this sense Sweidan and colleagues (Sweidan et al., 2011) develop a similar calculation scheme. Equation 5 from page 21 of that work proposes a way to calculate the amino group mass percentage. As well as the case of Parada and colleagues, it was necessary to apply some corrections in order to make the units to match. The obtained corrected equation is shown as equation (7)(6).

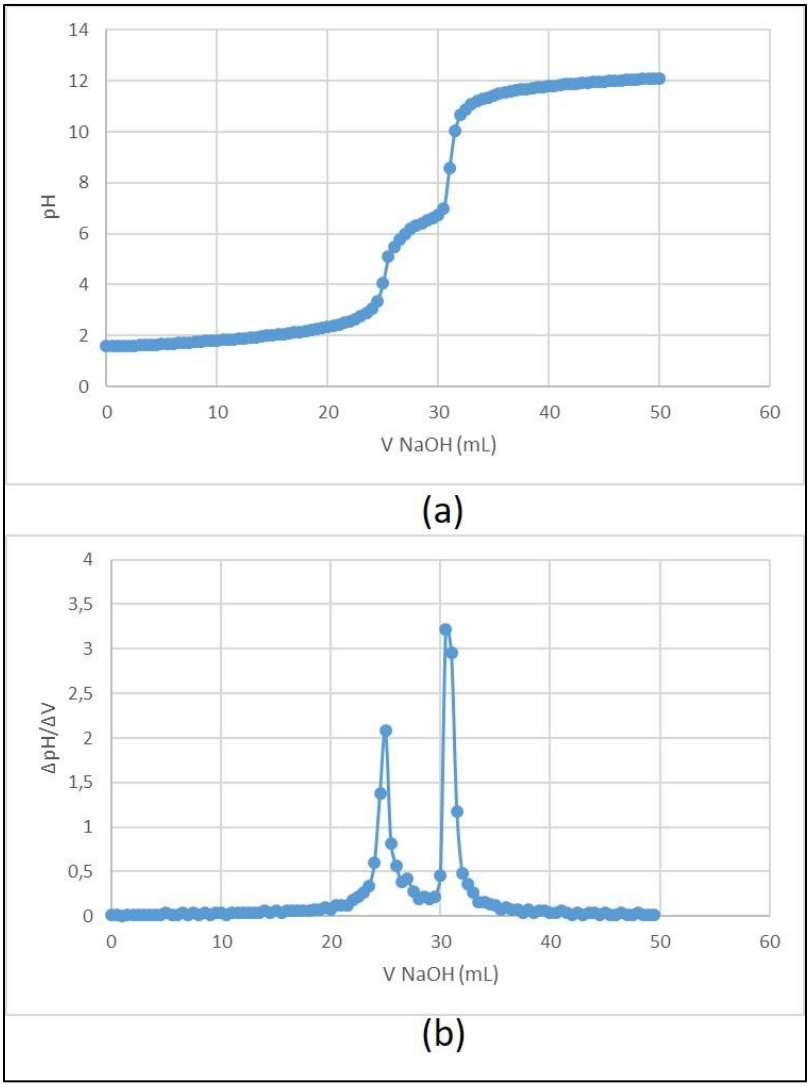

Figure 13. Potentiometric Chitosan DD determination for CH sample 1

$$\%NH_2 = \frac{\frac{16C_{NaOH}(V_2-V_1)}{1000}}{\frac{w(100-\%H_20)}{100}} * 100$$

$$\%NH_2 = \frac{160C_{NaOH}(V_2-V_1)}{w(100-\%H_20)} \qquad (7)$$

They propose also the calculation of DD as it is shown in equation (8), essentially the same equation (6).

$$DD = \frac{\%NH_2}{9,94} * 100 \qquad (8)$$

Using the values for sample 1 and the data in Table 9, the following values were obtained from equations (7) and (8): $\%NH_2$=8.70% and DD=87.53%.

The work of Gupta and colleagues referenced before (Gupta & Jabrail, 2006) uses in this part, a more reliable way to calculate DD from potentiometric analysis, according to equations (9) and (10). Equation (10) is a modification from the original adapted to the volume units in milliliters where the constants 203 and 42 come from and the molecular masses of N-acetyl-glucosamine (203,21 g/mol) and glucosamine monomer (161,17 g/mol) units and the difference between them (42,04 g/mol). Boudouaia and colleagues (Boudouaia et al., 2019) used a similar equation yielding and identical DD.

$$DD=\left(\frac{203Q}{1+42Q}\right)*100 \qquad (9)$$

$$Q=\frac{C_{NaOH}\,(V_2-V_1)}{1000*w} \qquad (10)$$

Replacing the corresponding values for sample 1, a DD of 83,19% is obtained.

Czechowska-Biskup and colleagues (Czechowska-Biskup et al., 2012) used a similar way of calculation of DD according to equation (11). The volumes in milliliters and the mass of the sample in grams, match perfectly. Replacing the values for sample 1, a DD of 79,13% was obtained.

$$DD=2{,}03\,\frac{V_2-V_1}{m+0{,}0042(V_2-V_1)} \qquad (11)$$

As a summary, the table

Table **10** shows all DD values calculated for elemental analysis (only one sample was used for determining elemental method) and for both samples used with the potentiometric method. Through methods, the values obtained by both, elemental and potentiometric, have a great consistency as it is possible to see in the simple descriptive statistical analysis showed in Table 11. For potentiometric, the averages are close to the nominal commercial value of 85% with coefficients of variation (CV) around 4,4%, confirming a high precision between the values, hence, it is reasonable to admit the potentiometric method as a reliable method to estimate the CH DD wit very similar ways of calculation proposed by various authors. The elemental analysis shows indeed a higher precision (CV=0,56%) confirming the high accuracy of the method since it uses less “human-influential steps” in the process which bring more experimental error.

Table 10. Summary of CH DD values obtained according to different methods and authors

Value (%)		Method	Author(s)	Observations/ Modifications
95,5		Elemental analysis	(Kassai et al., 2000)	Calculation based on C/N ratio.
96,27		Elemental analysis	(Alvarenga, 2022)	%NH2 in organic base calculated by subtracting ash and moisture content
Sample 1	**Sample 2**			
88,45	86,28	Potentiometric	(Parada et al., 2004)	Corrections applied on unit correspondence and moisture-ash-free-base. The author does not propose DD calculation just $\%NH_2$.
87,53	94,76	Potentiometric	(Sweidan et al., 2011)	Corrections applied on unit correspondence. Calculation based on $\%NH_2$.
83,19	88,78	Potentiometric	(Boudouaia et al., 2019; Gupta & Jabrail, 2006)	Calculation based on the basic definition: glucosamine moles/total moles
79,13	86,60	Potentiometric	(Czechowska-Biskup et al., 2012)	Calculation based on the basic definition: glucosamine moles/total moles

Table 11. Descriptive statistical analysis of DD results from elemental and potentiometric methods

	Elemental	Potentiometric	
		Sample 1	Sample 2
Average	95,89	84,29	90,94
Standard deviation	0,54	3,77	4,05

Coefficient of variation (%)	0,56	4,47	4,46

As a remarkable fact it can be noticed that there is a notorious difference between the values obtained from the elemental analysis (around 95-96%) and those from potentiometric methods (around 84-90%). At this point it is important to analyze the forms of the calculation of each method to understand the most probable cause of this difference. The elemental analysis uses as a basis, the distance or difference between the carbon or nitrogen weight composition in 100% de-acetylated and acetylated theoretical molecules. DD calculation is based on the degree of compliance of the sample with this basis as it can be seen in equations (2) and (3). On the other hand, the potentiometric method uses the basic definition of DD: the ratio between the de-acetylated glucosamine moles and the total (acetylated and de-acetylated glucosamine) moles (Balázs & Sipos, 2007; Czechowska-Biskup et al., 2012). Furthermore, potentiometric DD uses the sample mass and its impurities as calculation basis (equations (5)-(11)). This is the reason why both methods cannot be considered equivalents and it is necessary to express on an explicit way which method was used to estimate DD.

****

Viscous average molecular weight of chitosan was determined following a well-known procedure used by various authors (Chattopadhyay & Inamdar, 2010; Costa et al., 2015; Czechowska-Biskup et al., 2018; Kassai et al., 2000; Knaul et al., 1998; Lu et al., 2003; Rinaudo et al., 1993; Rinaudo, 2006; Tolaimate et al., 2000). Chitosan was dissolved in different concentrations (C) (0.001, 0.002, 0.003, 0.004 and 0.006 g/mL) on a AA 0,2 M/CH_3COONa 0,2 M buffer solution and then viscosity of each solution was measured three times at 30 °C on a Cannon-Fenske viscometer, as capillary flow time. Table 12 shows the results with their respective statistics. With these flow times it is possible to estimate the relative viscosity (η_r) of each solution as the ratio of the flow time of each solution to that of the solvent (0 g/mL concentration). This relative viscosity is approximately the same real ratio between dynamic viscosities (μ) (Czechowska-Biskup et al., 2018). Specific viscosity (η_{sp}) can be estimated as it is shown in equation (12) and the reduced viscosity defined as the ratio of η_{sp} to C is related to the intrinsic viscosity ([η]) according to the Huggins relationship shown in equation (13) where k_H is the Huggins coefficient related with the strength of the solvent. The obtained viscosities are shown in Table 13. The plot of C vs η_{sp}/C in Figure 14 gave a linear relationship from where it was possible to extract [η] as the intercept with a value of 513,18. According to the Mark-Howink relationship showed in equation (14), [η] is related with the viscous molecular mass Mv through some specific parameters K and α which depend on factors like type of solvent, temperature and DD of chitosan. For the solvent, temperature and DD of this experience, K=0,014 and α= 0,83 (Chattopadhyay & Inamdar, 2010; Lyalina et al., 2017). With these values it was

possible to estimate Mv for chitosan from equation (14), yielding a value of 315475,68 g/mol.

$$\eta_{sp} = \eta_r - 1 \quad (12)$$

$$\frac{\eta_{sp}}{C} = [\eta]_h + k_H [\eta]_h^2 C \quad (13)$$

$$[\eta] = K M v^{\alpha} \quad (14)$$

Table 12. Capillary flow time and statistics of chitosan solutions

C (g/mL)	t (min)	Average	SD	s.e
0	1,517	1,508	0,008	0,004
	1,505			
	1,502			
0,001	2,633	2,632	0,006	0,003
	2,626			
	2,637			
0,002	4,130	4,136	0,011	0,006
	4,148			
	4,129			
0,003	5,784	5,778	0,007	0,004
	5,779			
	5,771			
0,004	8,321	8,322	0,012	0,007
	8,3345			
	8,3107			
0,006	16,082	16,047	0,042	0,024
	16,059			
	16,000			

Table 13. Viscosity estimation for chitosan solutions

C (g/mL)	t (min)	η_r	η_{sp}	η_{sp}/C
0	1,508	1,00	0,00	-
0,001	2,632	1,75	0,75	745,40
0,002	4,136	2,74	1,74	849,91
0,003	5,778	3,83	2,83	913,31
0,004	8,322	5,52	4,52	1102,03

0,0061	16,047	10,64	9,64	1567,61

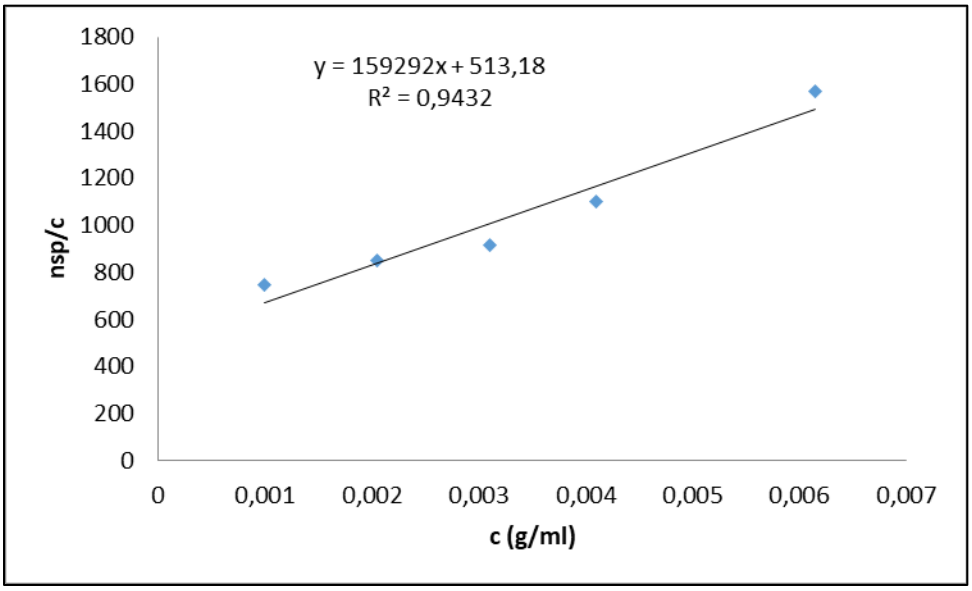

Figure 14. Linear regression of C vs η_{sp}/C

4.3 Final values

From **Table 11** it can be estimated an average DD for the chitosan and from the intrinsic viscosity estimation it was possible to estimate a viscous molecular mass (Mv) from equation (14). Results are summarized in **Table 14**.

Table 14. Characterization experimental values for chitosan

Parameter	Value	Units
DD	87,62	%
Mv	315475,68	g/mol
Total N	67839,63	mg N/kg

These values will be used in the preparation of the aqueous chitosan solution for the aminolysis of CCO.

5. CASTOR OIL PROCESSING EXPERIMENTAL WORK

5.1 CASTOR OIL EPOXIDATION METODOLOGY

CO epoxidation reaction was developed according to the previously well discussed Prilechajew reaction method with Amberlite® IR 120 IER heterogeneous catalyst (see 3.3 EPOXIDATION OF CASTOR OIL) as it was developed by various authors (Goud et al., 2006; Janković et al., 2014; Park et al., 2004; Sinadinović-Fišer et al., 2012). The procedure followed for this project is as follows: CO, HP, AA (molar ratio DB:HP:AA = 1:1,5:0,5), 80-100% HEX and 10% IER catalyst (%wt. oil base) were put together on a three neck round flask with mechanical/magnetic stirring, reflux condensation and controlled heating (Picture 1, photographic record). Temperature reaction is between 40-60 °C, velocity of stirring is between 300-900 rpm and time reaction is 6 to 9 hours. The reaction product is separated from the heterogeneous catalyst and the aqueous phase by filtration and decantation. Then the organic layer is washed 3-4 times with warm water (40 °C). Then, it is dried in rotary evaporator and by Na_2SO_3 treatment. Iodine value (IV) is measured to determine conversion and oxirane-oxygen content (OOC)is measured to determine selectivity. To confirm the identity of the product, analytical techniques as FTIR, HNMR, IV and OOC were performed to the ECO product. Since there is an important presence of hydroxyl groups in castor oil due to its natural composition (around 90% ricinoleic acid), conventional epoxidation using formic acid or a homogeneous catalyst like H_2SO_4 has proven to be counterproductive because such hydroxyl groups make castor oil more compatible with aqueous phases so oxirane rings formed during the reaction can be cleaved by the same action of the acids present in the reaction. This is the reason why a process with a heterogeneous catalyst was chosen for the epoxidation of castor oil. The previous experience has showed that heterogeneous catalyzed epoxidation of castor oil keeps selectivity to oxirane rings in good levels.

With the CO mass (CO_M) and the CO IV (IV_i), the necessary amounts of AA and PH were calculated according to the equations (15), (16) and (17). With the final IV of ECO (IV_f) and the OOC, it was possible to estimate %C and %S according to the equations (18) and (19). %Y and OOC_T were calculated according to equations (20) and (21), respectively.

$$\mathrm{DB_n} = \frac{\mathrm{CO_M} * \mathrm{IV_i}}{25380} \qquad (15)$$

$$AA_n = 0{,}5 * DB_n \qquad (16)$$

$$PH_n = 1{,}5 * DB_n \qquad (17)$$

$$\%C = \frac{IV_i - IV_f}{IV_i} * 100 \qquad (18)$$

$$\%S = \frac{1586{,}25 * OOC}{IV_i - IV_f} \qquad (19)$$

$$\%Y = \frac{OOC_T}{OOC} * 100 \qquad (20)$$

$$OOC_T = \frac{100 * IV_i}{(1586{,}25 + IV_i)} \qquad (21)$$

The derivation of the more non-intuitive equations can be found in appendix 6.5

As such, this methodology was applied for three different goals:

- Determination of the external mass transfer limitations of the IER Amberlite ® IR120 in the CO epoxidation
- Determining the process factors significances
- Producing ECO on a pilot scale

For the first two goals, the process was carried out in 150 mL rounded reaction flask as it is shown in picture 1 of the appendix 6. For the pilot scale stage, the process was carried out in a 5 L rounded reaction flask with an in-line temperature measurement system as it is shown in picture 2 of the photographic record.

DETERMINATION OF THE EXTERNAL MASS TRANSFER LIMITATIONS IN EPOXIDATION OF CASTOR OIL WITH ION EXCHANGE RESIN

The exchange activity of different size fractions of IER catalyst was measured by mixing a defined mass of Amberlite® IER catalyst with an aqueous solution of sodium chloride and mixing by 10 minutes. This causes the interchange of the Na^+ ions in the solution with the H^+ ions in the catalyst. Then, the H^+ ions realized from the IER catalyst were titrated with a sodium hydroxide (NaOH) solution. The sodium solution must contain an excess of Na^+ equivalents (eq) compared to the H^+ eq content of the IER catalyst sample, so, it is necessary to determine the minimum amount of sodium chloride in the solution. This is determined with the nominal exchange capacity provided by the specification data sheet of the manufacturing company with a value of 1,91 eq/L. It was necessary to determine also the apparent density of the resin. This was made with the help of a graduated cylinder in which it was packed the catalyst until a determined volume in the cylinder. The apparent density is calculated with the IER catalyst mass and the volume in the graduated cylinder. Then with an approximated IER catalyst mass it is possible to determine the mass of sodium chloride in the solution and the exchange capacity as it is shown in equations (22) and (23):

$$NaCl_M = \frac{IER_M \ * 1{,}91 \frac{eq}{L} * 58{,}44 \frac{g\ NaCl}{eq}}{AD} \qquad (22)$$

$$EC = \frac{NaOH_V * [NaOH] * AD.}{IER_M} \qquad (23)$$

For determining the possibility of the mass transfer limitations in the CO epoxidation with Amberlite® IER catalyst, a completely randomized one factor experimental design was done with the particle size as the main factor and %C as the response variable. For preparing the experimental design, the IER catalyst was sieved using adequate stainless-steel sieves of different sizes and the sieving process was made with the help of an electric stirring plate. For each run, the round glass reactor was charged with around 20 grams of CO along with the IER catalyst of a specific particle size and then this system was heated to 50 °C. PH and AA were mixed previously on a beaker and then added directly to the reaction system. Then the system reacts for 5 hours at 650 RPM of stirring speed with a magnetic bar. Reflux condensation in the reactor is ensured during the whole reaction. After the reaction time, the system was filtered with a stainless-steel mesh to separate the catalyst and the liquid is collected in a separation glass funnel. The two phases were separated and the upper one was washed with distilled water until no traces of acid can be observed in the washing water. It could take around 5-6 times if a good stirring is provided. The solvent and the remainder water were removed by rotating evaporation and drying salt (sodium sulfate) treatment.

DETERMINATION OF EPOXIDATION PROCESS FACTORS SIGNIFICANCE

For establishing the significance and importance of the process factors over the %C and %C of CO epoxidation with the Amberlite IR-120 ® IER catalyst, a 2^3 factor factorial design was done. The studied factors and their respective levels and labels, were: temperature (40-60 °C - T), time (6-9 hours - t) and stirring speed (300-900 RPM - SS). The response variables were %C and %S of the process. Since the %Y is related to %S according to the relationship in appendix 6.5, it is enough to study one of the two variables. The molar ratios of reactants were set on the following values: AA/DB=0.5, HP/DB= 1,5. The amounts of IER catalyst and HEX were respectively 10% and 100%, based on the CO mass. The HP concentration was 30%. Those values were set on constant values also in order to focus the study on the process factors of the experimental design since there is not enough information about the incidence and significance of them on this process.

It was made a pure curvature-quadratic analysis supported on the 2^2 factorial design by adding central point runs to the experimental design, it means, making experiments at 50 °C and 7,5 hours. In this case, 6 replicas in this point were carried out. With the information obtained it was possible to do an ANOVA analysis with a second order model to estimate the significance of a pure quadratic term in the response surface.

5.2 RESULTS ON CASTOR OIL EPOXIDATION

Figure 15 shows the ECO FTIR spectrum. Compared with Figure 10, the disappearing of DB signal around 3000-3100 cm^{-1} (signal A) confirms DB conversion and the tightening of the signal around 870 cm^{-1} (signal B) confirms the oxirane group formation. Figure 16 shows the HNMR of ECO. Compared with Figure 11, the disappearing of double bond signal at 5,5 ppm confirms the DB conversion and the appearing of a double signal around 3,0 ppm confirms the oxirane group formation. Oxirane ring opening can be observed by the appearing of a multiple signal around 3,8 ppm corresponding to the new OH groups generated.

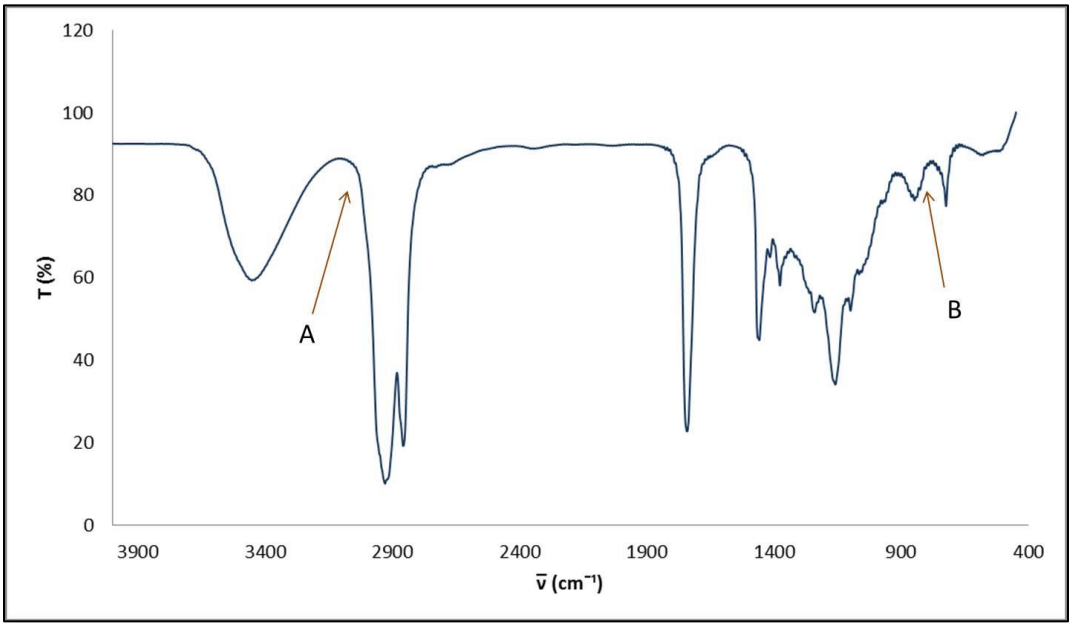

Figure 15. Infrared spectrum of Epoxidized Castor Oil

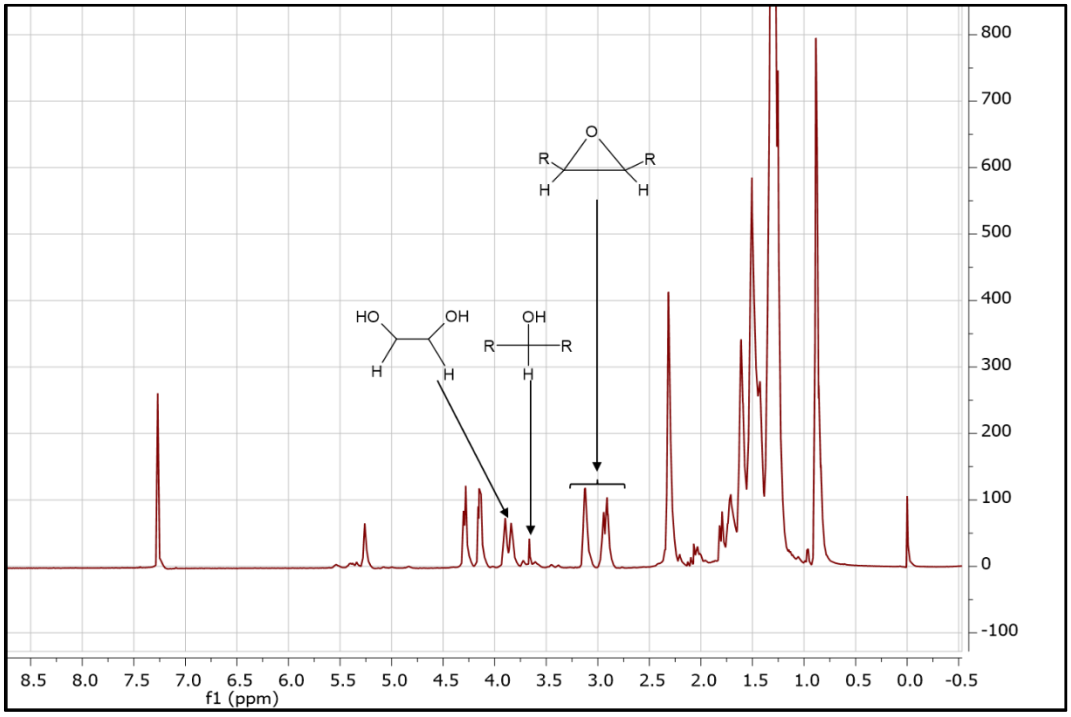

Figure 16. HNMR spectrum of Epoxidized Castor Oil

MASS TRANSFER LIMITATIONS IN EPOXIDATION OF CASTOR OIL

The sieving process of the Amberlite® catalyst was made with four different sieve sizes: “#35” (500 µm), “#50” (300 µm), “#100” (150 µm) and “>100” (< 150 µm). The average weight composition of each fracción is shown in Table 15.

Table 15. Weight composition percentage of different particle sizes in the Amberlite® IR 120 catalyst

Size	Weight composition %
>100	0,08
#100	1,37
#50	3,37
#35	94,14

Table 15 shows that the composition of the “>100” fraction is very low compared to the other ones, so it is possible to consider negligible its effect on the catalytic activity of the whole ion exchange resin. This can be confirmed by the results obtained from

the measurement of the exchange capacity of the different fractions of the Amberlite® IR-120 (H) catalyst, as it is shown in Table 16.

Table 16. Catalytic activity of the different fractions of Amberlite® IR-120 (H)

Catalyst fraction	Catalyst size (μm)	Exchange capacity (eq/L)
#35	500	3,16
#50	300	3,08
#100	150	3,00
>100	<150	2,64

It can be observed that the exchange capacity of the smallest fraction is lower than the other ones which their capacities are essentially the same. Figure 17 shows a microscopy picture of the different fractions of the catalyst. It can be seen that the ">100" smallest fraction has a morphology totally different from the other sizes. It looks like a set of shell-shaped particles. Since the Amberlite® catalyst comes from a polymerization that mostly produces catalytic sphere-shaped particles, it is reasonable to think that, as almost every chemical process, this one is not 100% homogeneous and it produces on a minimum way, some particles with different morphology, chemical structure and catalytic activity. On the other hand, this different morphology of the smallest fraction suggests also that it could come from crushing, friction or any other similar physical effect over the catalytic spheres because of the catalyst manipulation in the sieving or weighing processes. These processes can produce the degradation of some spherical catalyst particles and generating a residual smaller fraction that is not representative of the whole catalyst behavior. Because of its low weight composition, low exchange capacity and different morphology, from now on, the ">100" smallest fraction is not considered in the evaluation of the performance on the epoxidation conversion of each size catalyst fraction. Only the #35, #50 and #100 fractions were considered for doing the completely randomized one factor experimental design with the particle size as the main factor and %C as the response variable. The results of the experimental design are shown in Table 17 and the corresponding ANOVA is shown in Table 18, where it can be concluded that there is not a statistical significant difference in the mean reaction conversion of castor oil epoxidation with Amberlite® IR-120 (H) at different catalyst particle sizes at $\alpha=0,01$ with $p=0,0985$.

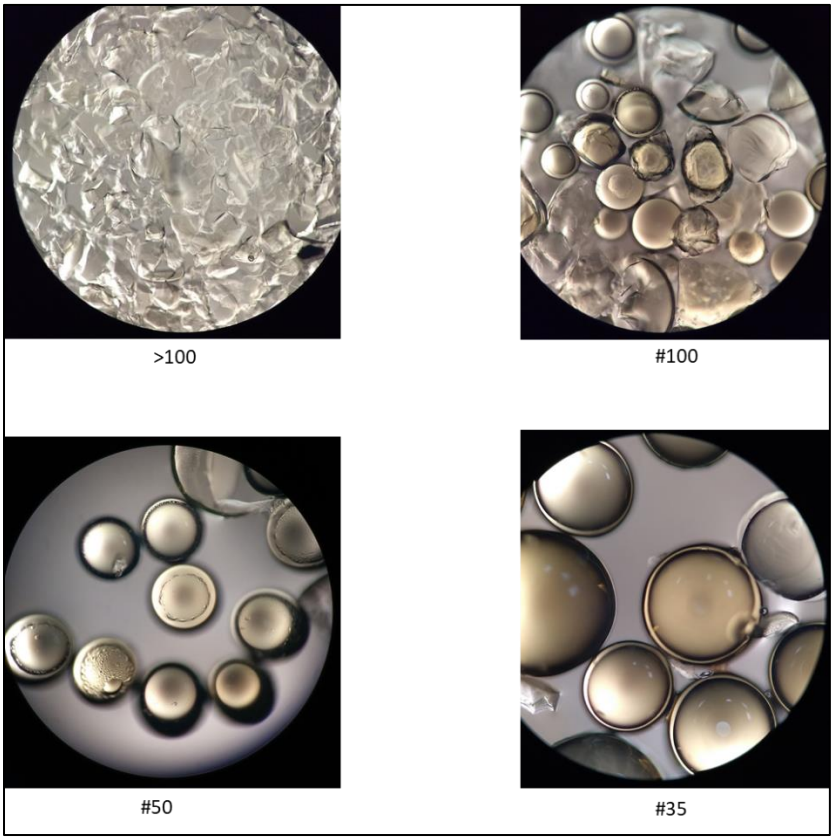

Figure 17. Microscopy pictures of the morphology of the different catalyst fractions

Table 17. Conversion percentage of castor oil epoxidation at different particle sizes

	%C		
Size	**1**	**2**	**3**
#100	62,69	67,89	66,14
#50	64,61	60,66	63,92
#35	62,144	61,14	60,43

Table 18. ANOVA of the particle size one factor experimental design

	DF	Sum Sq.	Mean Sq	F-Value	P
Size	2	28,43	14,214	3,497	0,0985
Residuals	6	24,39	4,056		

The graphic ANOVA in Figure 18 shows a slight tendency of %C decreasing with the increasing in the particle size. Although this trend is not detected by the statistic test, it is in the same way of what it is expected about the behavior of solid catalysts: the smaller the size of the particle the higher the mass transfer of the reactants to the active sites of the catalyst, which is the cause of a higher %C. Anyway, it is possible to conclude graphically that the differences in the heights of the boxes are not significative since always there is an interception of the boxes or whiskers with each other when they are projected laterally, therefore the catalytic activity of the resin in the epoxidation reaction of castor oil doesn't depend on the catalyst particle size and there is not external mass transfer limitations in the kinetics of the epoxidation of castor oil catalyzed by Amberlite® IR120 (H) ion exchange resin.

The ANOVA assumptions of variance equality, independency and residual normality are shown in appendix 6.6. They ensure the validity of the ANOVA analysis.

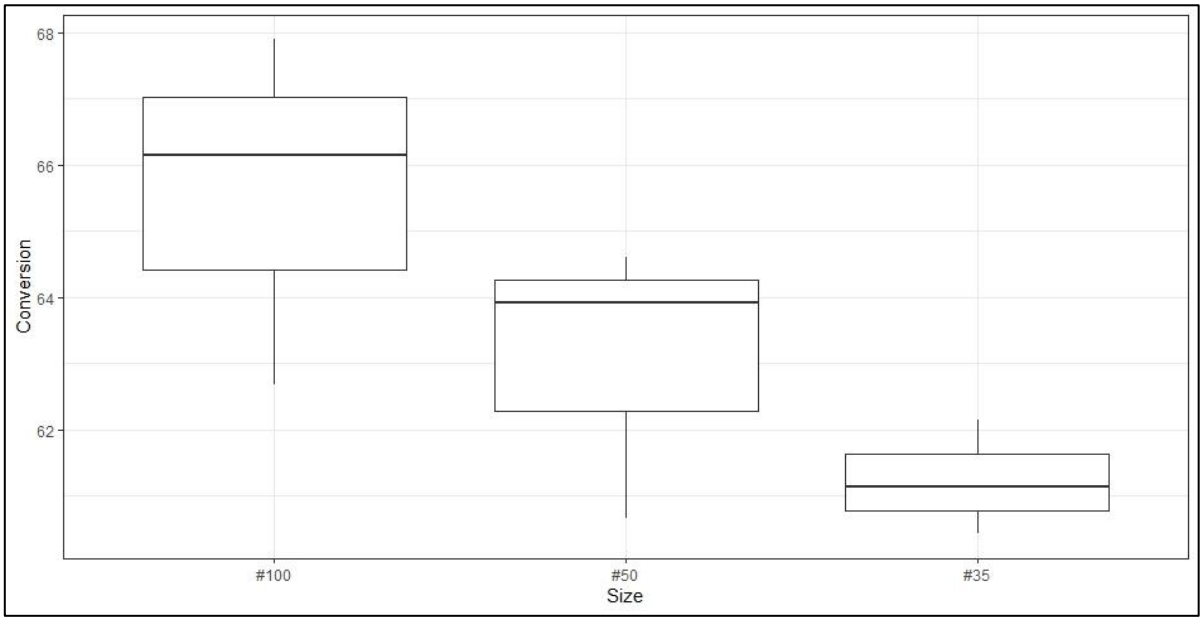

Figure 18. Graphic ANOVA of the particle size one factor experimental design

PROCESS FACTORS SIGNIFICANCE

Results of the experimental design of the 3-factors experimental design for the epoxidation process are shown in Table 19. The ANOVA for conversion and selectivity are shown in Table 20 and Table 21, respectively. The residual analysis and the normal probability plots for this ANOVA model are shown in appendix 6.7 and they validate the adequacy of the model.

Table 19. Factorial experimental design for epoxidation process

T	t	SP	%C	%S
40	9	900	68.77	59.75
60	6	300	78.61	71.73
40	6	900	53.73	57.62
60	9	300	91.09	56.24
60	6	900	80.14	71.28
40	9	300	70.18	64.07
60	9	900	74.39	53.87
40	6	300	59.21	58.20

Table 20. ANOVA for conversion in the 3-factor factorial experimental design

	Df	Sum Sq	Mean Sq	F value	P
T	1	654,1	654,1	10,523	0,190
t	1	134,0	134,0	2,155	0,381
SS	1	60,8	60,8	0,979	0,503
T:t	1	46,5	46,5	0,774	0,546
T:SS	1	8,6	8,6	0,138	0,774
t:SS	1	25,1	25,1	0,403	0,640
Residuals	1	62,2	62,2		

Model: Adjusted R^2=0.561, p-value=0.561

Table 21. ANOVA for selectivity in the 3-factor factorial experimental design

	Df	Sum Sq	Mean Sq	F value	Pr(>F)
T	1	22,71	22,71	54,858	0,0854
t	1	77,50	77,50	187,178	0,0464
SS	1	7,45	7,45	17,993	0,1474
T:t	1	209,10	209,10	505,014	0,0283
T:SS	1	0,54	0,54	1,306	0,4576
t:SS	1	4,00	4,00	9,671	0,1981
Residuals	1	0,41	0,41		

Model: Adjusted R^2=0.991, p-value=0.06721

From the p-values in Table 20 none of the factors has a significant effect over the conversion of double bonds in the epoxidation process of castor oil, with a significance value of 0,05. There is also no effect of any interaction over the conversion. However, the p-value for temperature is 0,190 with a correspondent F-Value of 10,523 showing a closeness with the significance limit point (p=0,05). Table 21 shows a significant effect of time and its interaction with temperature, over selectivity, and a possible effect of the stirring speed and its interaction with time (p-values of 0,1474 and 0,1981). Table 22 shows the main effect values of each factor over each response variable. It can be seen that although stirring speed has a notable effect over conversion (-5,516%) (i.e. conversion shows an average decreasing of 5,516% when the stirring speed is increased from 300 to 900 RPM), this is not a significant effect due to their high p-value on Table 20 (0,503). Furthermore, from a chemical process point of a view, it does not make sense since it is almost always expected to get higher conversion with higher stirring speeds, due to the greater homogeneity in the reaction system allowing an intimate contact between reactants, catalysts and solvents. Since the ANOVA in Table 20 says that this factor does not have a significant effect on the conversion, this behavior showed by the effect in Table 22 cannot be distinguished from the residual random variability of the conversion inherent in the process, so, according to the statistical analysis, it is a result of the random behavior and it would not have origin on a phenomenological fact. For selectivity, although mixing velocity has a p-value closer to the significance value of 0,05 (0,1474 in Table 21) it does not have a notable effect (-1,935 in Table 22) and this could be perfectly attributed to the random behavior. With all this in mind, it is possible to conclude that the evidence is stronger on the way of no rejecting the idea that the stirring speed does not have a significant effect over conversion.

Table 22. Main effect values for the 2^3 factorial design

Factor	Conversion	Selectivity
T	18,085	3,370
t	8,158	-6,225
SS	-5,516	-1,935

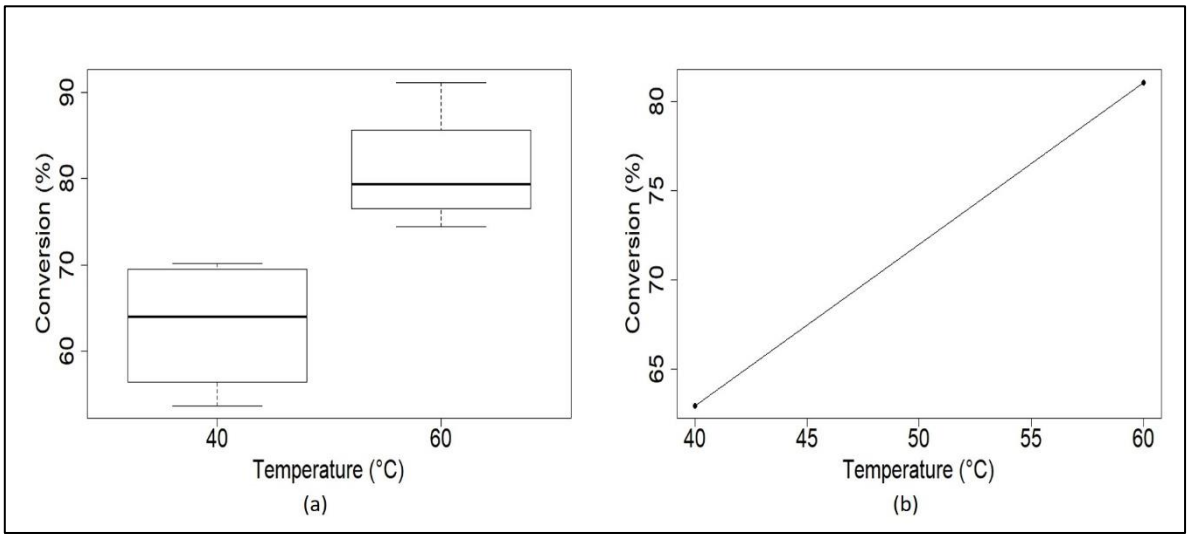

Figure 19. Conversion of double bonds by temperature (a) Boxplot, (b) Main effect plot

On the other hand, temperature has an average effect of 18,85% over conversion but it showed no significant effect, according to Table 20. The boxplot of Figure 19-a shows that the distribution of values at each temperature are located at different well-defined heights and there is not a possible intersection between their projections what is an indicative of a possible significant difference. The main-effect plot of Figure 19-b confirm this behavior since there is a considerable increasing in the average conversion with the increasing the temperature from 40 °C to 60 °C. This contradiction could be caused by the lack of degrees of freedom for the error, to achieve a high resolution in the results. This situation could be solved easily by removing the stirring speed from the analysis of the data, what increases the degrees of freedom for the residual error, it means, to do the ANOVA analysis as a 2^2 factorial design with temperature and time as factors. The residual plot analysis of this model in the appendix 6.8 shows a considerable heteroscedasticity in the residuals what indicates a deficient adequacy of the model. It means that is not a good practice to take the conclusions of the ANOVA with this model. This can be

solved by transforming the response variables and checking the residual analysis. After many try-and-failure tests, it was found that $y' = 1/y\text{^}2$ is a good transformation for doing again the ANOVA analysis, where y' is the response variable transformed and y is the original value of the response variable (%C and %S). The appendix 6.9 shows the complete converted data, the complete ANOVA and model analysis, and the residual graphical analysis where acceptable results[1] can be observed in terms of residual behavior.

Table 23. ANOVA for conversion in the 2-factor factorial with data transformation

	Df	Sum Sq	Mean Sq	F value	P
T	1	$2{,}28*10^{-8}$	$2{,}28*10^{-8}$	24,449	0,00779
t	1	$6{,}81*10^{-9}$	$6{,}81*10^{-9}$	7,296	0,05403
T:t	1	$5{,}04*10^{-9}$	$5{,}04*10^{-9}$	5,400	0,08080
Residuals	4	$3{,}73*10^{-9}$	$9{,}34*10^{-10}$		

Model: Adjusted R^2=0.8299, p-value=0.01714

Table 24. ANOVA for selectivity in the 2-factor factorial with data transformation

	Df	Sum Sq	Mean Sq	F value	P
T	1	$5{,}82*10^{-10}$	$5{,}82*10^{-10}$	2,132	0,21803
t	1	$4{,}84*10^{-9}$	$4{,}84*10^{-9}$	17,760	0,01354
T:t	1	$1{,}464*10^{-8}$	$1{,}464*10^{-8}$	53,688	0,00185
Residuals	4	$1{,}091*10^{-9}$	$2{,}73*10^{-10}$		

Model: Adjusted R^2=0.9098, p-value=0.004898

Table 25. Main and interaction effects for the 2^2 factorial design

Factor	Conversion	Selectivity
T	18,085	3,370
T	8,185	-6,225
Tt	-2,41	-5,1125

[1] Althougt the residual vs time plot shows an important heteroscedasticity, the other residual plots were improved with the data transformation.

Table 23 shows the ANOVA analysis for the transformed conversion data. It can be seen that temperature is a significant factor with a p-value of 0.00779. The higher the temperature the larger the conversion since there is more mobility of the molecules in the reacting system. Furthermore, time, with a value of 0.05403, approaches to the significance value 0,05, indicating a possible significant effect on the conversion. This might be possible from the fact that the PAA formation is the step which determine the overall kinetic of the process, since it is the slowest step. There is not significant interaction between temperature and time to affect %C. The adjusted square R value indicates that the linear model explains 82,99% of the variability in the conversion. The p-value of 0.01714 for the model indicates that the linear model is significant in order to explain the conversion. Table 24 shows that the time-temperature interaction has significant effect over selectivity with a value of 0.00185. The adjusted square R value indicates that the linear model explains 90,98% of the variability in selectivity. The p-value 0.004898 for the model indicates that the linear model with interaction effect is significant in order to explain the selectivity.

Table **25** shows the main and interaction effect values of the factors over the response variables and it confirms the results obtained in the ANOVA analysis.

The results matrix of the 2^2 with the center points for curvature analysis, is shown in Table 26. The pure quadratic curvature ANOVA analysis for the transformed response variables is shown in Table 27 and Table 28 for conversion and selectivity, respectively. The appendix 6.10 shows the table of transformed data as well as the complete ANOVA analysis.

Table 26. Factorial experimental design with center points for epoxidation

Temp	Time	Conv	Selec
40	9	68.77	59.75
50	7.5	81.91	72.21
50	7.5	81.04	69.58
60	6	78.61	71.73
40	6	53.73	57.62
60	9	91.09	56.24
50	7.5	83.24	68.85
60	6	80.14	71.28
50	7.5	79.9	57.19
50	7.5	72.24	69.63
40	9	70.18	64.07
60	9	74.39	53.87
50	7.5	74.77	58.91
40	6	59.21	58.20

Table 27. Pure quadratic curvature ANOVA analysis for conversion

	Df	Sum Sq	Mean Sq	F value	P
T	1	$2{,}28*10^{-8}$	$2{,}28*10^{-8}$	37,35	0,000177
t	1	$6{,}812*10^{-9}$	$6{,}812*10^{-9}$	11,15	0,008680
I (T^2)	1	$7{,}248*10^{-9}$	$7{,}248*10^{-9}$	11,86	0,007347
T:t	1	$5{,}042*10^{-9}$	$5{,}04*10^{-9}$	8,25	0,018409
Residuals	9	$5{,}50*10^{-9}$	$6{,}11*10^{-10}$		

Model: Adjusted R^2=0.8325, p-value=0.0003066

Table 28. Pure quadratic curvature ANOVA analysis for selectivity

	Df	Sum Sq	Mean Sq	F value	P
T	1	$5{,}82*10^{-10}$	$5{,}82*10^{-10}$	0,403	0,5416
t	1	$4{,}845*10^{-9}$	$4{,}845*10^{-9}$	3,353	0,1003
I (T^2)	1	$4{,}593*10^{-9}$	$4{,}593*10^{-9}$	3,179	0,1083
T:t	1	$1{,}464*10^{-8}$	$1{,}464*10^{-8}$	10,137	0,0111
Residuals	9	$1{,}300*10^{-8}$	$1{,}445*10^{-9}$		

Model: Adjusted R^2=0.5014, p-value=0.03292

Table 27 explains that the pure quadratic term with a p-value of 0.007347 indicates the evidence of the presence of a second order curvature for conversion in the explored region. The other terms are important also for the model. The t-test for significance of all the terms on the model, the complete ANOVA analysis and the lack-of-fit test are shown in appendix 8.10, for all response variables. In Table 28, the quadratic term with a p-value of 0.1083 suggests no strong evidence against not to reject the idea that the quadratic coefficient is equal to zero, this is, the quadratic term is not significant in the model. With this in mind, it is necessary to add axial experimental points to complete a central composite experimental design for establishing an adequate model. The axial points were defined with an axial distance equal to 1.41 units (coded variables) according to the characteristics defined by the central composite designs (rotability and orthogonality). Appendix 8.11 shows the data table of the central composite design as well as the complete response surface methodology analysis. It can be seen that for conversion the second order model has an adjusted R-squared of 0.8352 and a lack-of-fit test with a p-value of 0.90

meaning the model fits well to the experimental data. The predicted stationary point is: Temperature= 56,94°C and Time= 8.8 h with negative eigenvalues what it means that it is a maximum. This is the predicted stationary point to obtain the highest value of conversion. For selectivity, the adjusted R-squared is 0.4253. This result suggests that there are other factors not involved in the experimental design with a significant effect over the selectivity. The lack-of-fit test of the model has a p-value of 0.16785 indicating that the second order model fits well to the experimental data. The predicted stationary point is: Temperature= 49.55 °C, time= 8,6 h with a negative and a positive eigenvalue what it means it is a saddle point. This is the predicted stationary point to obtain the highest value of selectivity. It is possible to see that both stationary points are very similar so it is convenient to establish an only stationary point to validate experimentally.

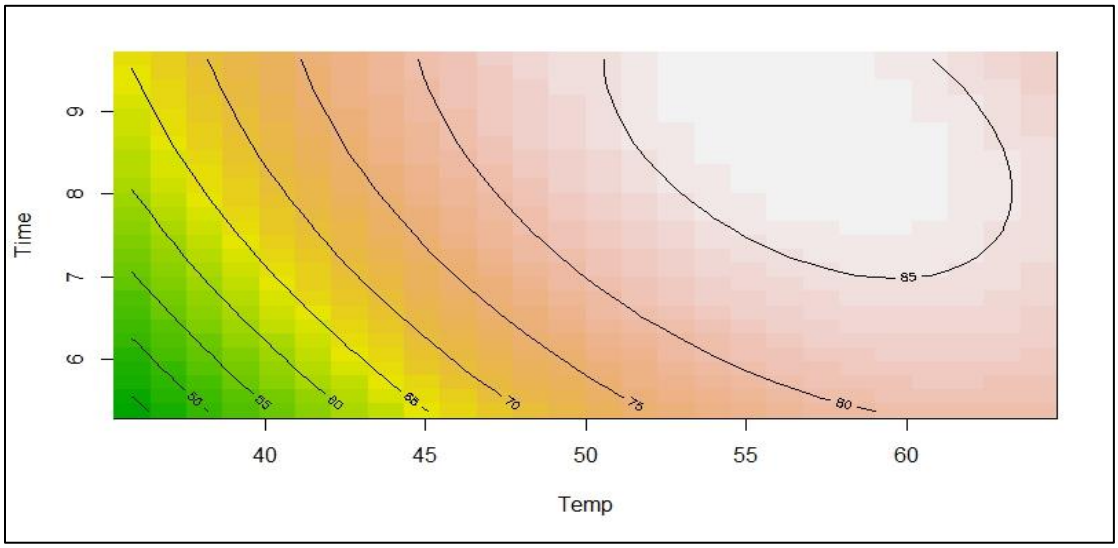

Figure 20. Contour plot of conversion

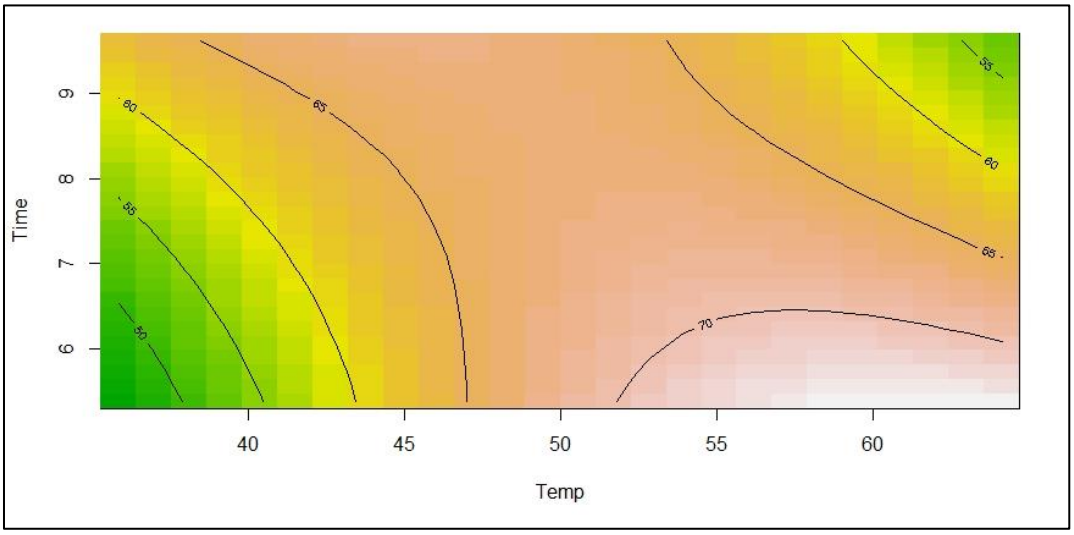

Figure 21. Contour plot for selectivity

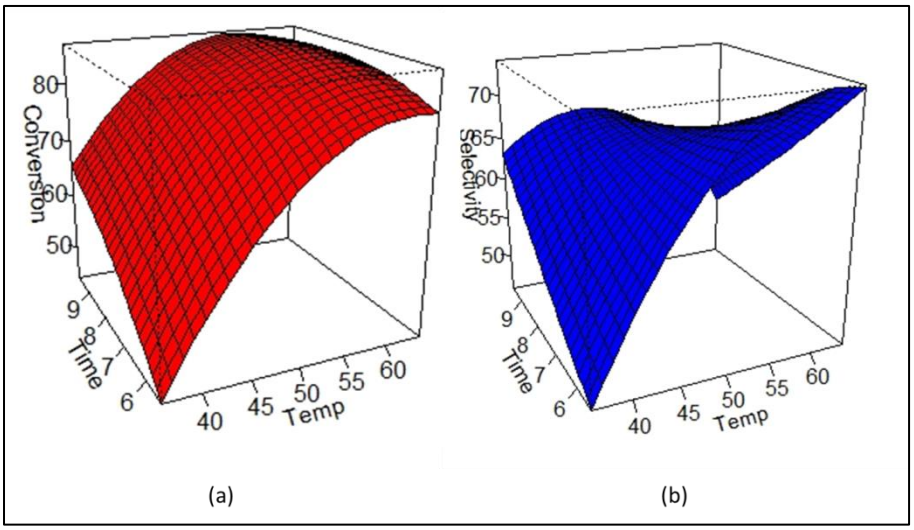

Figure 22. Response surfaces for (a) conversion (b) selectivity

Figure 20 shows the contour plot for conversion versus time and temperature. It can be seen that there is a predicted maximum conversion around 89.6% in the area surrounding the stationary point. For selectivity, Figure 21 shows that there is a predicted maximum value around 65.7% at the vicinity of the stationary point. In Figure 22 the response surfaces for conversion and selectivity show the shape of the predicted response surfaces obtained from the experimental data. There were made two validation experiments at a point near to both stationary points of the models (Temperature= 53 °C and Time= 8,7h). The obtained conversion and selectivity are showed in Table 29.

Table 29. Conversion and selectivity of the validation experiments

Experiment	Conversion (%)	Selectivity (%)
1	81,91	78,74
2	86,41	84,09
Average(%)	84,16	81,42
Stnd. Dev.(%)	3,18	3,78
Var. Coef.(%)	3,78	4,65

The low variation coefficients for both response variables are evidence of the high precision in the experience. The average conversion of 84,16% is close to the predicted one by the model (89,6%). This can be explained by the high value of the R^2 determination coefficient of the model (0,8352). It is not the best, but it provides nice prediction of the model. On the other hand, the average selectivity of 81,42% is far from the predicted one (65,7%). This is the evidence of the low R^2 determination

coefficient of the model (0,4253). Although this is not the optimal point, it is the best one that it is possible to obtain with the defined experimental design and the selected process factors.

PRODUCING EPOXIDIZED CASTOR OIL IN A PILOT SCALE

Two experiences were carried out where all liquid reactants and solvent (CO, HP, AA and HEX) were put together in the reaction flask and the system was heated until the desired temperature (run 1: 35°C and run 2: 26°C). Then, the IER catalyst Amberlite® was added and the temperature was monitored. Figure 23 shows this behavior. Both experiences reached a temperature around 54,1 °C starting from different temperatures. Because of the highly exothermic nature of the Prilezhaev reaction the system could reach an uncontrollable temperature increasing or thermal runaway but the reflux effect of HEX solvent keeps the system under isothermal conditions around this temperature. This isothermal condition can be demonstrated by the statistic of the temperature data in Table 30. The small values for SD and CV in both runs indicate that the average temperature is an excellent representative for the data. The skewness and kurtosis coefficient shows evidence that the temperature samples come from normal distributions and it is possible to estimate through 95% confidence intervals the mean temperature of the process after stabilization as it is shown in Table 31. 54,1 °C is a temperature near to the optimum temperatures found at the previous section so it is a very nice finding in terms of practical pilot and industrial scales Avoiding the time-consuming drip addition of HP to the system and at the same time reaching an optimum process temperature, this methodological approach is feasible to carry out on a safe way, with very good epoxidation results.

Table 30. Descriptive Statistics for temperature in CO epoxidation

Run	AverageTemperature	s	CV	s.e	Skew	Krt	n
1	54,10	0,32	0,59	0,0132	0,463	-0,305	594
2	54,14	0,17	0,31	0.009248	-0,684	1,67	334

Table 31. 95% confidence interval for temperature in CO Epoxidation

Run	Lower limit	upper limit
1	54,07	54,13
2	54,12	54,16

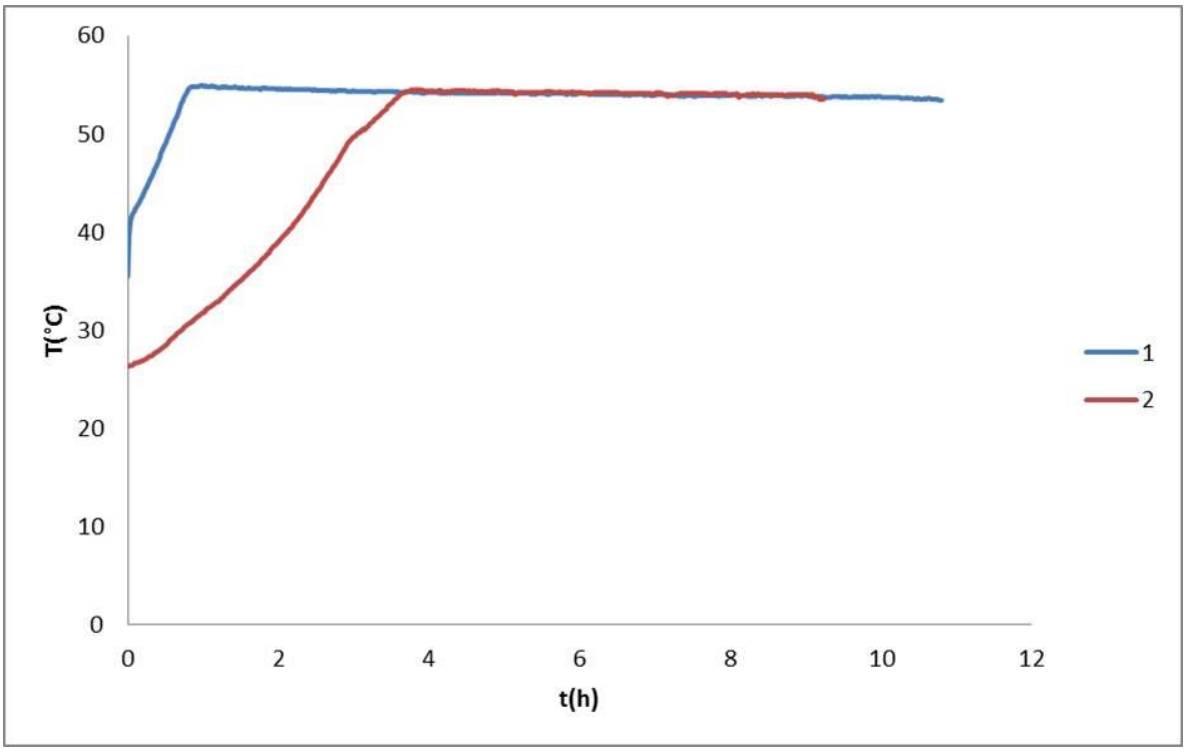

Figure 23. Temperature evolution of pilot epoxidation of CO

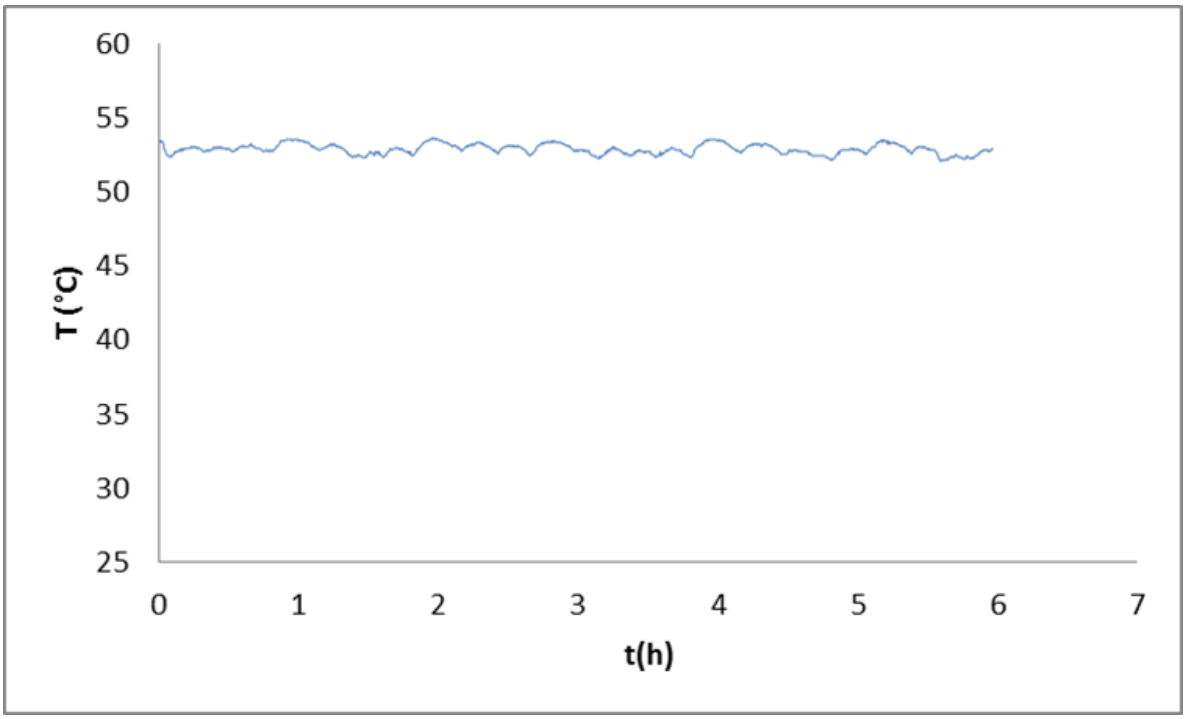

Figure 24. Temperature evolution of PAA production reaction

In order to clear out, it is important to establish that the reaction step that is exothermic enough to rise the system temperature until unsafe levels, is the Prilezhaev reaction of DB epoxidation with reported values of reaction enthalpy of -230 ±3,8 (J. L. Zheng et al., 2015). Although peracetic acid production seems to be exothermic too, as Dul'neva and colleagues reported, with a reaction enthalpy of -13,7±0,1 kJ/mol (Dul'neva & Moskvin, 2005), it is not powerful enough to increase the temperature of the system on a significant mode. It was corroborated by experimental way by measuring the temperature of a HP-AA system at certain temperature (53 °C, near the optimum for CO epoxidation) before and after the addition of the Amberlite ® IER. Figure 24 shows that temperature kept itself stable around this value, with an average temperature of 52,85 °C; s= 0,3371 and CV= 0,64%. These phenomenological and theoretical bases, support the proposition of this approach as a very nice option for pilot and industrial scale.

5.3 CARBONATION OF EPOXIDIZED CASTOR OIL EXPERIMENTAL WORK

METHODOLOGY

Carbonation of castor oil was carried out following a well-known methodoly reported by various authors (Bähr & Mülhaupt, 2012; Birukov et al., 2012b; Boyer et al., 2010; X. Cai et al., 2017; Doll & Erhan, 2005; Haniffa et al., 2017; Javni et al., 2008; Z. Li et al., 2008; Mahendran et al., 2012; Poussard et al., 2016; Tamami et al., 2004; C. Zhang et al., 2015; L. Zhang et al., 2014). The procedure is as follow: in a high pressure – 250 mL PARR® reactor, the epoxidized castor oil (around 120 g) is loaded with 5 % mol of TBABr catalyst and pressurized to 50 bar CO_2. Temperature is raised until 120 °C and the system is vigorously stirred (500 RPM) for 9 hours. After the reaction, the product is characterized without further purification. OOC is determined for conversion calculation. FTIR and HNMR analysis were done over the product also for confirmation of its identity. An important value can be extracted here for the aminolysis formulation: the concentration of cyclic carbonate groups. A convenient unit would be mol CC groups/100 g of carbonated oil. The calculation of this value is according to equation 24.

$$[CC] = \frac{Mol_{CC}}{\left(M_{ECO} + \frac{OCC * M_{ECO} * \%C * 44}{10000 * 16}\right)} * 100 \qquad (24)$$

Where…

$$Mol_{CC} = \frac{M_{ep} * \%C}{100} \qquad (25)$$

$$M_{ep} = \frac{M_{ECO} * OCC}{100 * 16} \qquad (26)$$

$[CC]$: Concentration of CC groups in mol CC/100 g

Mol_{CC}: Mol of CC groups estimated by equation 25

M_{ECO}: Mass of epoxidized castor oil used in the reaction (g)

OCC: Oxirane-oxygen content (%)

$\%C$: Conversion degree of the carbonation reaction (%)

M_{ep}: Mol of epoxy groups in ECO calculated with equation 26.

10000: comes from dividing two times by 100, because OCC and %C

16: comes from the molecular weight of the monoatomic oxygen.

44: comes from the molecular weight of the cyclic carbonate portion.

Since the kinetics of this reaction was studied previously, other interesting aspect is intended to be studied in this chapter. Some previous works have reported the improving effect of adding water to the carbonation of vegetable oils, mainly soybean oil, so, an appropriate goal of this project at this point would be to verify this improving effect with castor oil.

To determine the effect of water on the behavior of the epoxidized castor oil (ECO) carbonation, a follow up of a series of experiments with different amounts of water was carried out, defining as the ratio mol water/mol epoxy groups the following values: 0/1, 1/3 and 1:1, These amounts are defined based on previous experiments (Jian et al., 2009; Mazo & Rios, 2012, 2013). With the OOC measurement at different time intervals it was possible to determine the behavior of the reaction. Each configuration was run twice and the average OCC was used as the indicator value.

RESULTS

Figure 25 shows the FTIR spectra for the CCO. Compared with the ECO FTIR spectra of Figure 15, it is remarkable the appearing of a signal peak around 1870 cm^{-1} (pointed with letter A) due to the C=O group of CC. Figure 26 shows the ^{1}HNMR spectra of CCO. Compared with the ECO ^{1}HNMR spectra in Figure 16, it is noticeable the disappearing of the oxirane protons signals around 3 ppm and the appearing of signals around 4,5 and 5,0 ppm attributed to cyclic carbonate protons.

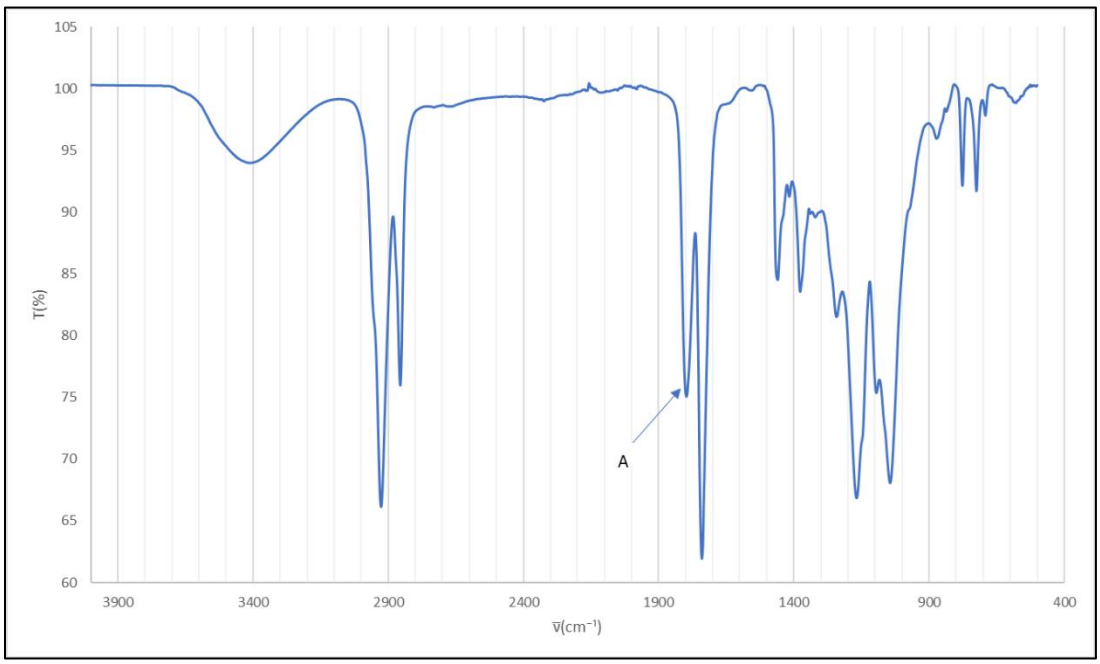

Figure 25. Infrared spectrum of Carbonated Castor Oil

The calculated CC concentration with equations 24 to 26 from a typical experience yielded a value of **0,1974 mol CC/ 100 g.** This value will be useful for the formulation of the aminolysis of CCO with CH.

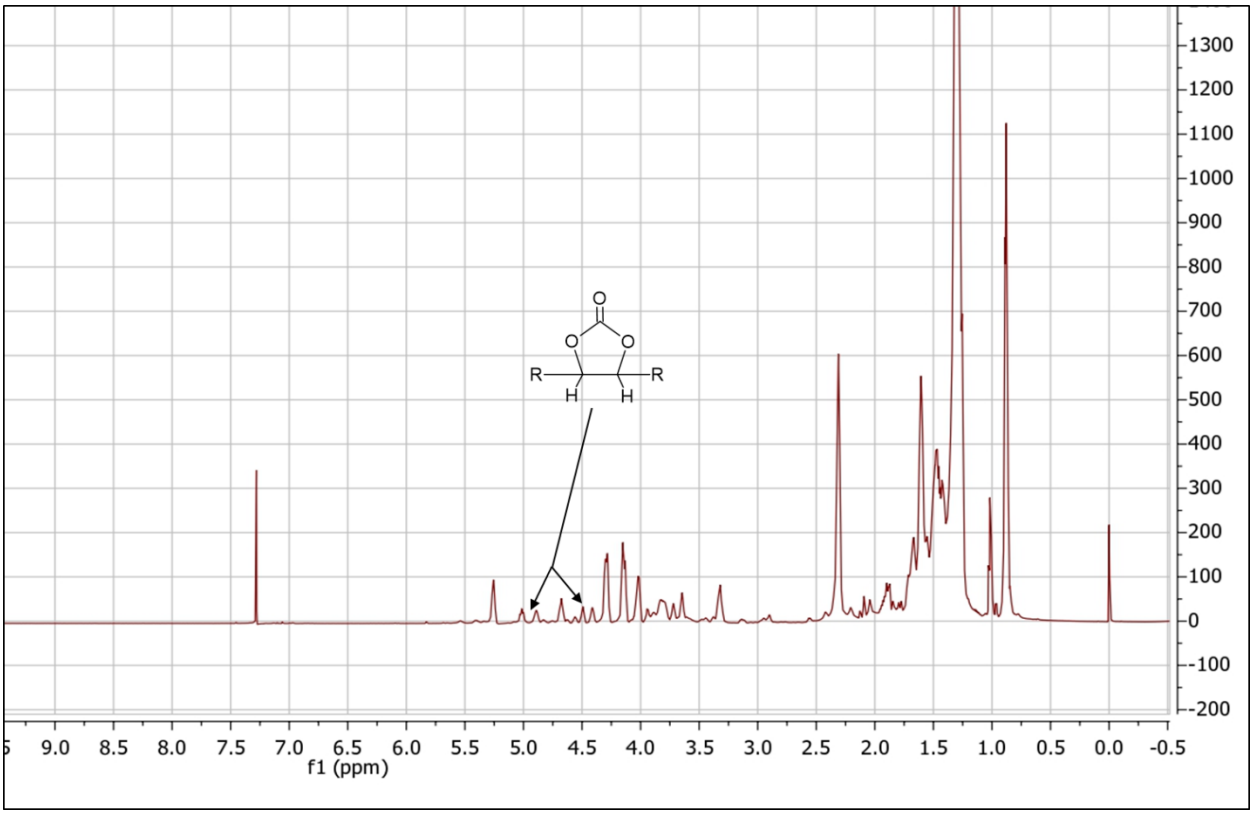

Figure 26. HNMR spectrum of Carbonated Castor Oil

The results of the OOC for the different water to epoxy ratios in the determination of the water effect on the carbonation of ECO are shown in Table 32. Figure 27 shows the evolution of the OOC through time for the different water to epoxy ratios. According to this figure, there is not a noticeable difference between the CCO evolution for the different water to epoxy ratios. It means that water does not have an apparent effect on the conversion of epoxy groups to carbonate groups. There is no evidence to support that water addition has an improving effect in terms of conversion or time reaction. This is the first time that a study of water effect on the carbonation of epoxidized castor oil is reported. All the publications that reported a successful improvement in the process by adding water were carried out with substrates different from castor oil. Jian and colleagues (Jian et al., 2009) used propylene oxide and Mazo and Rios (Mazo & Rios, 2012, 2013) used epoxidized soybean oil. As it has been discussed previously, castor oil is a special vegetable

oil. The presence of natural-occurrence hydroxyl groups in the fatty acid chains confer to the oil special features like water-affinity and higher viscosity what make it different from the other common vegetable oils like palm or soybean. It is possible that this behavior makes difficult the improvement effect of water on the carbonation reaction. Because the affinity, the hydroxyl groups could immobilize the water molecules interfering in the synergistic effect of them and the Lewis base (catalyst) as it is explained in the work of Jian an colleagues (Jian et al., 2009). That is the most plausible reason for the lack of evidence of kinetic improvement on the carbonation of ECO with water addition.

Table 32. OOC values for different water-to-epoxy ratio formulations in the determination of the water effect on the carbonation of ECO

	0:1 molH2O/molEpox				1:3 molH20/molEpox				1:1 molH2O/molEpox			
Time	**Run 1**	**Run 2**	**Average**	**S.D**	**Run 1**	**Run 2**	**Average**	**S.D**	**Run 1**	**Run 2**	**Average**	**S.D**
0	3,61	3,61	3,61	0,00	3,16	3,16	3,16	0,000	3,16	3,16	3,16	0,00
1	3,42	2,46	2,94	0,68	2,59	2,14	2,37	0,318	2,4	2,04	2,22	0,25
2	1,91	1,79	1,85	0,08	1,74	1,77	1,76	0,021	1,99	1,73	1,86	0,18
3	1,51	1,28	1,40	0,16	1,5	1,35	1,43	0,106	1,63	1,65	1,64	0,01
4	1,2	1,16	1,18	0,03	1,25	1,07	1,16	0,127	1,39	1,09	1,24	0,21
5	0,97	0,92	0,95	0,04	1	0,86	0,93	0,099	1,06	0,89	0,98	0,12
6	0,83	0,79	0,81	0,03	0,83	0,72	0,78	0,078	0,9	0,71	0,81	0,13
7	0,68	0,58	0,63	0,07	0,75	0,52	0,64	0,163	0,86	0,55	0,71	0,22
8	0,57	0,48	0,53	0,06	0,61	0,39	0,50	0,156	0,68	0,45	0,57	0,16
9	0,52	0,43	0,48	0,06	0,527	0,33	0,43	0,139	0,56	0,41	0,49	0,11

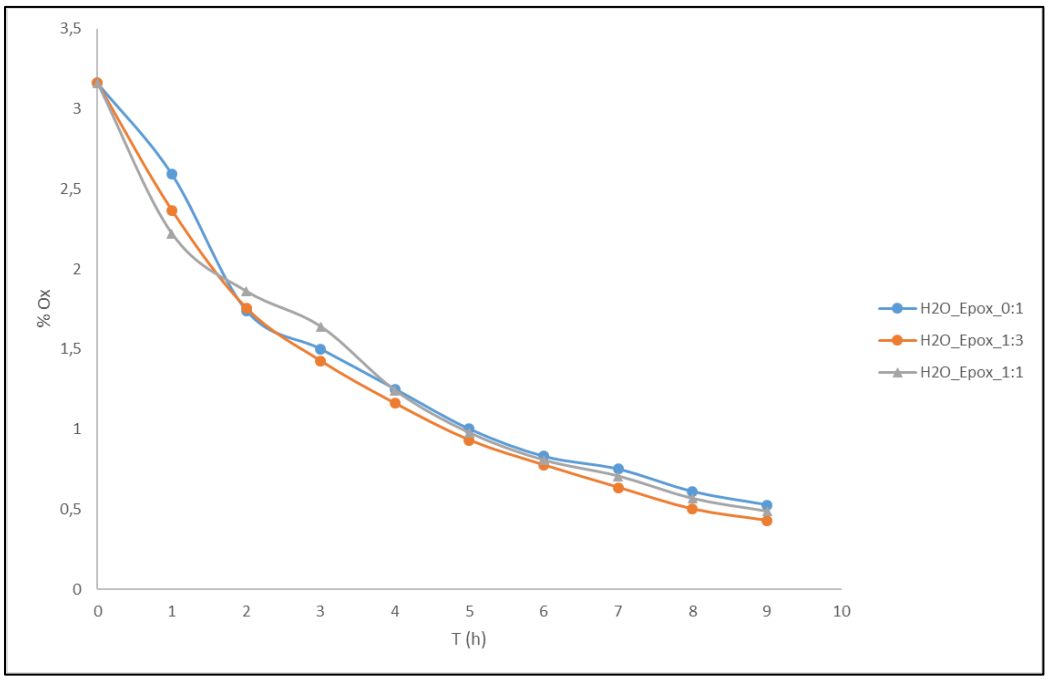

Figure 27. Average OOC evolution for different water to epoxide ratios in the determination of the water effect on the carbonation of ECO

6. AMINOLYSIS REACTION FOR NIPU PRODUCTION AND NIPU APPLICATION

6.1 METHODOLOGY

Aminolysis was studied first from simple and fundamental molecules of both principal functional groups: CC and amine to large molecules as castor oil and chitosan. It starts with carbonated methyl oleate (CMO) as carbonated oleaginous substrate model. It was studied the aminolysis of CMO with different amines: n-butylamine (BA), methyl-butylamine(MBA), ethyl-butylamine (EBA) and dibutylamine (DBA). These amine were selected due to their availability in the laboratory, their easiness to react as well as the fact that it was pretended to carry out a study of the steric hindrance effect on the aminolysis reaction. Following the gradual approach to the final process, CMO was reacted with glucosamine hydrochloride (GLH) as the monomeric unit of chitosan. Those two substrates are the simplest system one can imagine before the final reaction, since CMO is a simple oleaginous carbonated substrate and GLH is a simple saccharide-aminated substrate. Since there is no previous reports in aminolysis of these two compound families, the processes were carried out at this point and from now on just only using FTIR and HNMR analysis for looking for evidence of the reaction. At this point, a deeper study of different aspects like kinetics, reactivity and so for so on, would be a topic for another PhD thesis.

The kinetic of the reaction was followed by FTIR. The concentration of carbonate and ester groups was followed through FTIR calibration curves. Reactions were carried out in a 500 mL glass reactor equipped with mechanical stirring, heating glass jacket and reflux condenser (Picture 3-Photographic record). Experiments were conducted in batch mode under isothermal conditions. At the beginning of any kinetic experiments, there was no amide group or methanol molecule, so at time zero, their concentrations were zero. One should keep in mind that the selectivity of the double bond to the epoxide group was lower than 100% during the epoxidation stage and the epoxide conversion and selectivity of epoxide to cyclic carbonate were also lower than 100%. These experimental results explain the fact that the ratio initial ester concentration to the initial carbonated group concentration is ca. 0,5. A turbine stirrer was used, and the optimum agitation, i.e., avoiding vortex formation, was found to be 500 RPM. Despite the presence of a reflux condenser, the reaction temperature was lower than the boiling point of the amines to avoid amine evaporation during the reaction. It was noticed that as the size of the amine substituent increases, one needs to increase the reaction temperature to observe a significant conversion of the carbonated group. For experiments carried out with BA and MBA, it was possible to observe significant carbonated group conversions at reaction temperatures lower than their boiling points. However, for kinetic experiments carried out with EBA, at reaction temperatures lower than its boiling point, i.e., 381.15K, it was not possible to observe a significant conversion of the carbonated group. For that reason, a reaction temperature slightly above the EBA

boiling point was used for the experiment carried out with this amine. The boiling point of DBA is 432.15K, but the heating system used in this study could not stabilize the reaction temperature when it was higher than 413.15K. If the reaction temperature was lower than 403.15K for experiments carried out with DBA, then one could not observe a significant carbonated group conversion. For these reasons, two reaction temperatures were tested: 403.15 and 413.15K. **Table 33** shows the complete experimental matrix for the aminolysis of CMO with BS, MBA, EBA and DBA.

Table 33. Experimental matrix for CMO aminolysis experiments with BA, MBA, EBA and DBA

	Initial concentration mol/L			**T (K)**
	Ester	**Amine (BA)**	**Carbonated MO**	
RUN1	2.87	3.4	1.23	313.78
RUN2	2.74	3.44	1.23	323.79
RUN3	2.75	3.36	1.21	334.07
	Initial concentration mol/L			**T (K)**
	Ester	**Amine (MBA)**	**Carbonated MO**	
RUN4	2.86	2.97	1.75	344.88
RUN5	2.57	2.95	1.7	355.13
RUN6	2.49	2.93	1.7	364.84
	Initial concentration mol/L			**T (K)**
	Ester	**Amine (EBA)**	**Carbonated MO**	
RUN7	2.68	2.8	1.35	382.15
	Initial concentration mol/L			**T (K)**
	Ester	**Amine (DBA)**	**Carbonated MO**	
RUN8	2.19	2.52	1.15	413.15
RUN9	2.22	2.53	1.19	403.15

For preparing the carbonate calibration curve, samples at different times were taken from a typical carbonation reaction. For each sample, the oxirane value was measured, and the difference between the initial and final oxirane values allows knowing the carbonate concentration. Then for each sample, an FTIR run was taken, and the absorbance for carbonate group at 1800 cm-1 and a reference group like –CH vibration at 2920 cm-1 were measured. The calibration curve was obtained from a linear regression of the arranged data: ratio carbonate absorbance/-CH absorbance vs. concentration of the carbonate group. For preparing the ester

calibration curve, different mixes of oleic acid (OA) and methyl oleate (MO) were prepared. With the known masses and average molecular weights of OA and MO, it is possible to calculate the concentration of each sample. Then for each sample, an FTIR run was taken, and the absorbances for the ester group at 1750 cm-1 and a reference group like –CH vibration at 2920 cm-1 were measured. The calibration curve was obtained from a linear regression of the arranged data: ratio ester absorbance/-CH absorbance vs. concentration of ester group.

Glucosamine hydrochloride (GLH) as amine-based fundamental molecule was studied. GLH was reacted with CMO and CCO. In a typical experience, 6,532 g of GLH, 0664 g of LiCl and 0,64 g of tensoactive Tween 80 were dissolved in 50 mL of water in a bottom-rounded reaction flask. The system was heated in an oil bath at 60 °C with constant mechanical stirring. Apart, 12,35 g of CMO and 5,39 g of isopropanol were mixed in a beaker and added drop by drop to the aqueous system whit high speed stirring (1400 RPM). A similar procedure was followed in the aminolysis with CCO. The products were analiyzed by FTIR, HNMR and CNMR.

The aminolysis reaction between the CCO and chitosan was tackled from different fronts: A first one called “bulk reaction” between CCO and solid chitosan, then, a second one named “emulsion reaction” between CCO and aqueous chitosan where two types of emulsion were produced: oil in water (o/w) and water in oil w/o emulsions. The “bulk reaction” consisted in mixing the CCO with solid chitosan, LiCl catalyst and 2-octanol as solvent in a rounded glass reactor equipped with mechanical stirring and oil bath. The system was run for 21 hours at 150 °C. The “o/w emulsion bulk reaction” was based on the CO emulsion work developed by Zhang and colleagues (D. Zhang et al., 2011) and the emulsion-NIPU reaction published by Rix and Colleagues (Rix et al., 2016) and (Das et al., 2020). For preparing the CH solution, CH was dissolved in acidified water taking into account the criteria exposed in the chitosan theoretical review of section 3.5. The aqueous chitosan solution was prepared based on the work of Rinaudo and colleagues (Rinaudo et al., 1999). They found that CH is completely soluble in aqueous-acidic-media at degree of protonation of NH_2 groups larger or equal to 50%, with [AA]/[NH_2] molar ratio of 0,6. This apparently let around 40% of NH_2 groups available for aminolysis reaction. Considering previous experiences with the viscosity of dissolved chitosan, the experimental run was fixed at the following values: concentration around 0,5 g/mL ([AA]/[NH_2] molar ratio of 0,7 in a 0,11 M AA aqueous solution). The acetic acid was dissolved in water and then the corresponding chitosan quantity was added slowly with a vigorous mechanical stirring. The system was let overnight at 40 °C and 150 RPM.

With the data characterization of Table 14 it is possible to calculate the stoichiometric amounts of reactants for the reaction as follows:

With the total nitrogen content, it is possible to calculate the mol of nitrogen per gram of chitosan:

$$67839{,}63\,\frac{mgN}{1\ kg\ CH} * \frac{1\ kg\ CH}{1000\ g\ CH} * \frac{1\ g\ N}{1000\ mg\ N} * \frac{1\ mol\ N}{14\ g\ N} = 4{,}85 * 10^{-3}\,\frac{mol\ N}{g\ CH} \quad (27)$$

With this value of concentration of N per gram of chitosan and the DD it is possible to determine the effective available amount of NH_2 groups for solubilization and aminolysis reaction:

$$4{,}85 * 10^{-3}\,\frac{mol\ N}{g\ CH} * 0{,}8762 = 4{,}25 * 10^{-3}\,\frac{mol\ N}{g\ CH} \quad (28)$$

It is important to determine also, the range of molecular weight of CH. This is because high molecular weight CH generates more viscous aqueous solution and a high viscosity of this solution could be problematic for the aminolysis step, since it is required as much as possible, to generate affinity of the CCO oleaginous phase and CH aqueous phase. Then, for high molecular CH the author recommends to prepare low concentration CH aqueous solution in order to have fluid systems easy to mix. If the total concentration of nitrogen ($4{,}85 * 10^{-3}$ mol N/g CH) is multiplied by the viscous molecular weight (315475,68 g/mol ≈ 315,5 kDa) a value of 1530,06 mol N/ mol CH is obtained. This is an estimate of the number monomeric glucosamine units per average filament molecule of CH. It means that each CH molecule-filament is composed by approximately 1530,06 units of acetylated and de-acetylated glucosamine units. The work of Zhang (H. Zhang et al., 2016) and colleagues may serve as reference as follows: if this number of glucosamine monomeric units is multiplied by its length one can obtain the length of a molecule-filament of CH. The authors report that one monomeric unit is 0,52 nm long, so a CH molecule would be 795,63 nm. If this value is located in a plot of the statistical distribution curve of CH filament length (figure 3-b of Zhang's work), it would fall at the right-heavy-tailed side of the distribution. This is evidence of the fact that CH used in this work is composed by long filaments, causing a high molecular weight. If this value is projected to a graphic of the statistical distribution of molecular weight (figure 3-c of Zhang´s work) it can be confirmed that molecular weight would be also at the right-heavy-tailed side of the distribution, around 300 kDa, what it is alike to the Mv value obtained experimentally in this work. All this evidence allows to conclude that the chitosan used is a high molecular weight product and low concentration aqueous solutions must be prepared in order to facilitate the fusion of the phases in the aminolysis step of CCO and CH.

The o/w emulsion was prepared as follows: in 100 mL of a 0.0075 g/mL CH solution in 0,11 M aqueous AA, 0,2617 g of LiCl catalyst, 0,257 g of Tween 80 and 1,54 g of Na_2CO_3 were dissolved. The system was heated in oil bath at 70 °C with constant mechanical stirring. Apart, 5,14 g of CCO were dissolved in 10 mL of isopropanol. Then, this CCO solution was dropped in 30 minutes to the aqueous system while it was stirred at 1400 RPM. After the CCO addition the temperature was raised to 90°

and the system was maintained for 24 hours. The product was characterized by FTIR analysis.

The w/o emulsion was typically prepared as follows: 31,12 g of CCO are weighted in a round-bottomed reaction flask. Then, 16,7 mL of a 0,047 g/mL CH solution prepared as it was previously described was dropped to the CCO system with constant mechanical stirring at 1400 RPM. Then, 0.1706 g of Na_2CO_3 and 1,60 g of LiCl were added to the system. The reaction is maintained at 70 °C for 20 hours. A sample was taken at this point. To guarantee a higher crosslinking of the product, 3.94 g of EDA were added, temperature was raised to 94 °C and the process was maintained for 4 hours. The product was characterized by FTIR, HNMR, CNMR, TGA and DTA. Finally, the product was tested in an acrylic emulsion adhesive substrate - AUTOADHESAN® from ANDERCOL enterprises, an AKZO-NOBEL Medellín-based company. 5% w/w of the product was added to the acrylic adhesive AUTOADHESAN® and FINAT adhesive tests were run for comparison: Peel adhesion (180°) test (FTM1), Loop tack measurement test (FTM) and resistance to shear from a standard surface test (FTM8).

6.2 RESULTS ON AMINOLYSIS REACTION

Aminolysis with CMO

During the aminolysis process, there are two reactions: aminolysis producing urethane group and amidation leading to amide group. The latter reaction is reversible. As carbonated methyl oleate is used, then methanol is produced with an amide group. For a complete kinetic model, one must consider the reactivity of the two reaction centers, as shown in **Figure 28**.

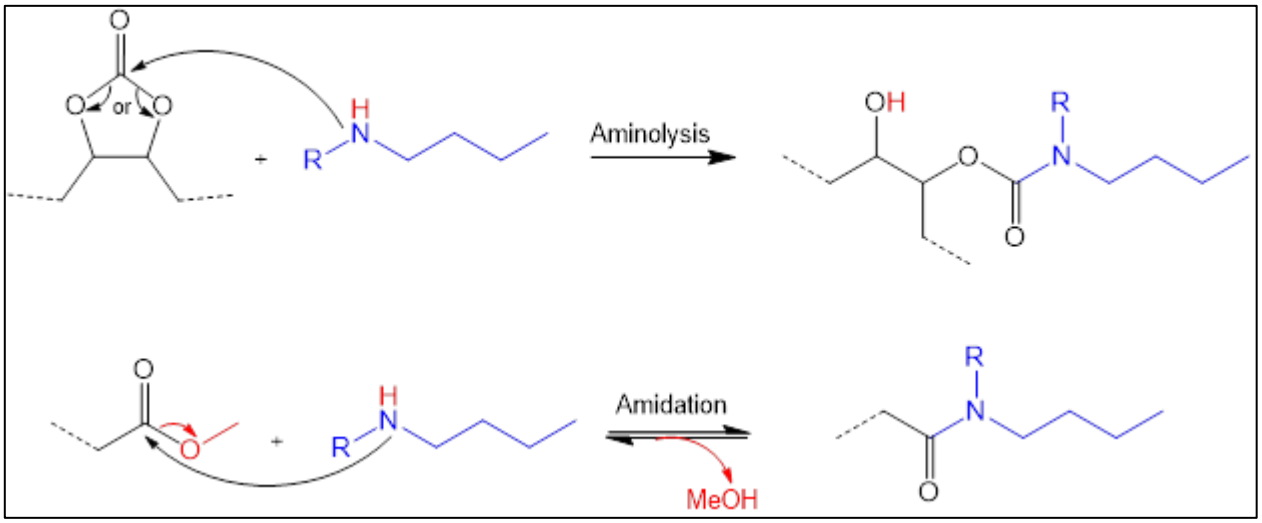

Figure 28. Reaction scheme for aminolysis and amidation reaction

As shown in the article by Perez-Sena (Pérez-Sena et al., 2018) the kinetic expressions for these two reactions can be expressed as:

$$\mathrm{R}_{Aminolysis} = k_{Aminolysis} \cdot [Carbonated] \cdot [Amine] \quad (29)$$

$$\mathrm{R}_{Amidation} = k_{Amidation} \cdot \left([Ester] \cdot [Amine] - \frac{1}{\mathrm{K}_{Amidation}} [Amide] \cdot [Methanol] \right) \quad (30)$$

The amidation equilibrium constant $\mathrm{K}_{Amidation}$ was assumed to be temperature-independent for the aminolysis by butylamine and methylbutylamine. Based on the experimental data, the aminolysis of CMO by ethylbutylamine and dibutylamine revealed the amidation reaction was quasi-inexistent. This low reactivity might be linked to thermodynamic limitation.

The material balances for the different compounds in the isothermal batch reactor can be written as:

$$\frac{[Carbonated]}{dt} = -\mathrm{R}_{Aminolysis} \quad (31)$$

$$\frac{[Urethane]}{dt} = \mathrm{R}_{Aminolysis} \quad (32)$$

$$\frac{[Amine]}{dt} = -\mathrm{R}_{Aminolysis} - \mathrm{R}_{Amidation} \quad (33)$$

$$\frac{[Ester]}{dt} = -\mathrm{R}_{Amidation} \quad (34)$$

$$\frac{[Amide]}{dt} = \mathrm{R}_{Amidation} \quad (35)$$

$$\frac{[Methanol]}{dt} = \mathrm{R}_{Amidation} \quad (36)$$

For kinetic modeling, ModEst software was used. The ordinary differential equations (3126)-(36) were solved numerically by ODESSA solver implemented in the ModEst software. Non-linear regression was used to estimate the parameters. The concentrations of ester and carbonated groups were used as observables in the regression analysis.

The objective function OF was minimized by the Simplex and Levenberg-Marquardt algorithms,

$$OF = \sum \left(C_{i,exp} - C_{i,sim}\right)^2 \qquad (37)$$

where, Ci,exp is the experimental concentration, and $C_{i,sim}$ is the concentration simulated by the model. The coefficient of determination evaluated the reliability of the models to the experimental data,

$$\mathrm{R}^2 = 1 - \frac{\sum \left(C_{i,exp} - C_{i,sim}\right)^2}{\sum \left(C_{i,exp} - \bar{C}_{i,exp}\right)^2} \qquad (38)$$

where, $\bar{C}_{i,exp}$ is the average value of the experimental concentrations. In the estimation of the kinetic constants the modified Arrhenius equation was used, in order to suppress the natural correlation between the pre-exponential factor and the activation energy,

$$k_R(T) = k_R\left(T_{Ref}\right) * \exp\left(\frac{-E_{a_R}}{R}\left(\frac{1}{T} - \frac{1}{T_{Ref}}\right)\right) \qquad (39)$$

where, T_{Ref} is a reference temperature. The standard errors of the parameters were estimated within the confidence interval of 95%.

Aminolysis of carbonated methyl oleate (CMO) by n-butylamine

Table 34 shows the results of the parameter estimation stage. The estimated results are in the same order of magnitude compared to our previous study (Pérez-Sena et al., 2018). The standard deviation of the estimated constant is low. The coefficient of determination was found to be 99.77%, indicating the reliability of the model.

Table 34. Kinetic constants estimated at Tref=333.15K and statistical data for aminolysis by BA.

	Estimated	**Standard deviation %**
$k_{Amidation}\left(T_{Ref}\right)$ (L·mol^{-1}·s^{-1})	9,39*10^{-6}	12,90
$Ea_{Amidation}$ (J·mol^{-1})	45400	16,40
$k_{Aminolysis}\left(T_{Ref}\right)$ (L·mol^{-1}·s^{-1})	6,16*10^{-5}	4,70
$Ea_{Aminolysis}$ (J·mol^{-1})	42100	7,50
$K_{Amidation}$	3,03*10^{-2}	16,90

Table 35 shows the correlation matrix of the estimated parameters. One can notice that correlation between the rate constants and their activation energies is quite moderate.

Table 35. Correlation matrix of the estimated parameters for aminolysis by BA.

	$k_{Amidation}\left(T_{Ref}\right)$	$Ea_{Amidation}$	$Ea_{Aminolysis}$	$k_{aminolysis}\left(T_{Ref}\right)$	$K_{amidation}$
$k_{Amidation}\left(T_{Ref}\right)$	1.00				
$Ea_{Amidation}$	0.74	1.00			
$Ea_{Aminolysis}$	0.03	0.06	1.00		
$k_{Aminolysis}\left(T_{Ref}\right)$	0.04	0.04	0.77	1.00	
$K_{amidation}$	-0.48	-0.09	0.02	0.03	1.00

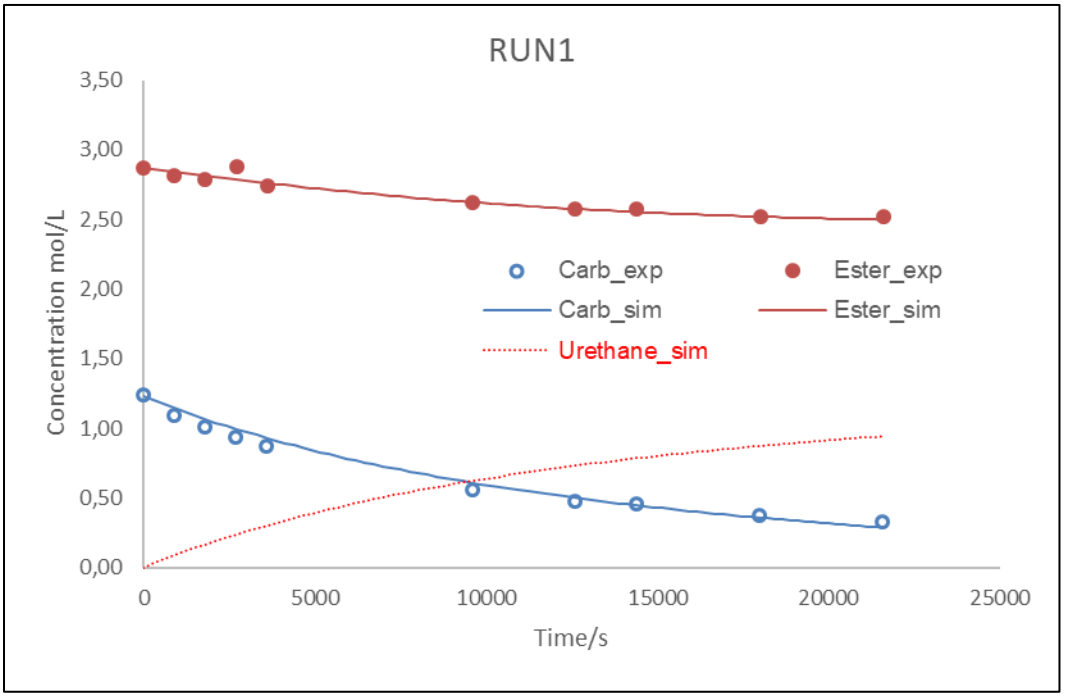

Figure 29. Fit of the model to the experimental observation for Run 1

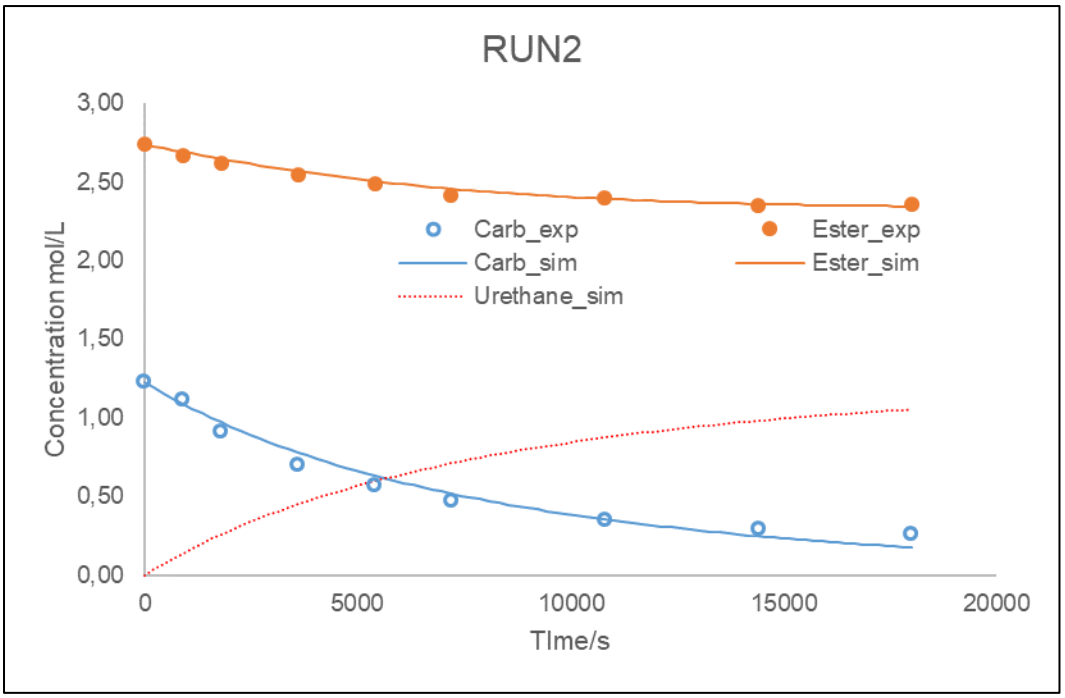

Figure 30. Fit of the model to the experimental observation for Run 2

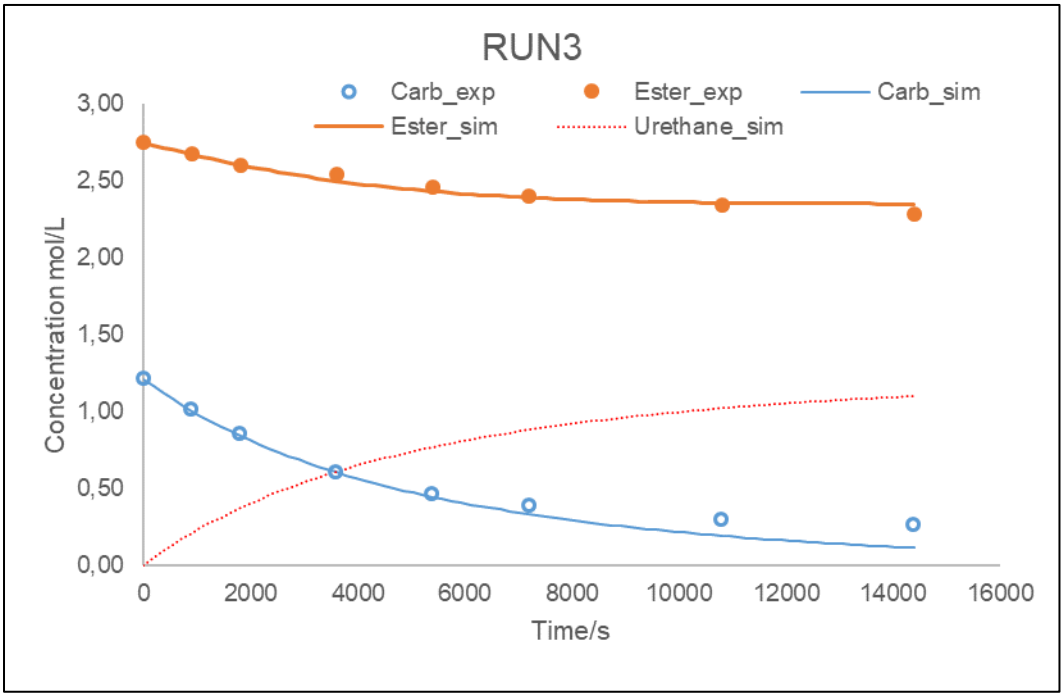

Figure 31. Fit of the model to the experimental observation for Run 3

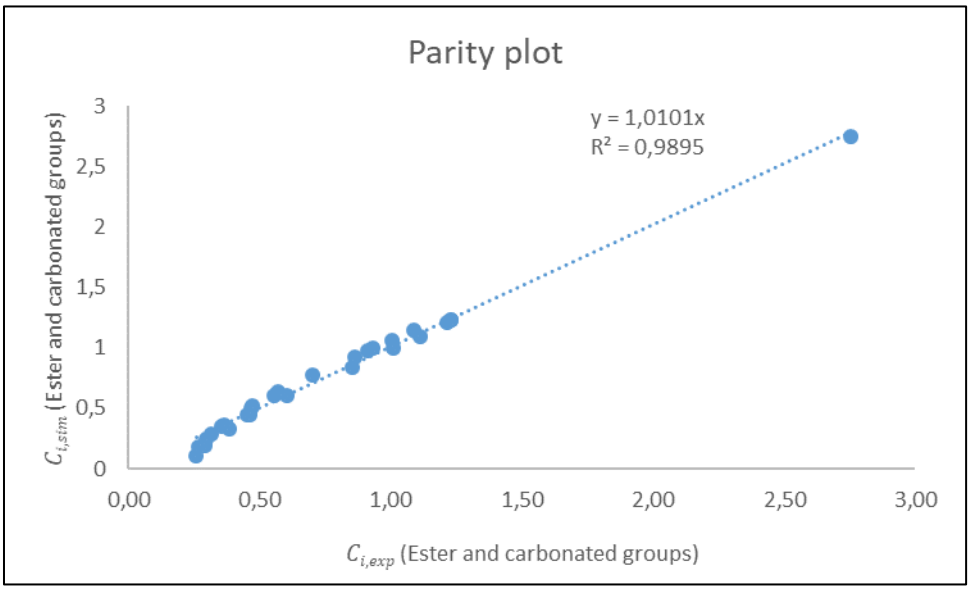

Figure 32. Parity plot between estimated and experimental concentrations for the aminolysis by BA.

The fit of the model for the RUNS 1,2 and 3 and the parity plot are shown in Figure 29, Figure 30, Figure 31 and Figure 32, respectively. One can notice that the fit of the model to the experimental data is very good.

Aminolysis of carbonated methyl oleate (CMO) by methylbutylamine (MBA)

The estimated parameters with the standard deviations are shown in Table 36. One can notice that the standard deviations are less than 30%, indicating a relatively good estimation of these parameters. The coefficient of determination was calculated to be 99.50%. The correlation between the estimated parameters was very low (Table 37), except between the amidation rate constant at Tref and the equilibrium constant. The moderate correlation between these parameters can be explained by the fact that for this system, the equilibrium constant dependence towards temperature is higher. The model fits perfectly the experimental concentrations (Figure 33, Figure 34, Figure 35 and Figure 36).

Table 36. Kinetic constants estimated at Tref=354.35K and statistical data for aminolysis by MBA.

	Estimated	**Standard deviation %**
$k_{Amidation}\left(T_{Ref}\right)$ (L·mol^{-1}·s^{-1})	3,16*10^{-06}	10,20
$Ea_{Amidation}$ (J·mol^{-1})	40000	24,80
$k_{Aminolysis}\left(T_{Ref}\right)$ (L·mol^{-1}·s^{-1})	2,02*10^{-05}	2,30
$Ea_{Aminolysis}$ (J·mol^{-1})	40000	7,50
$K_{Amidation}$	3,50*10^{-02}	28,30

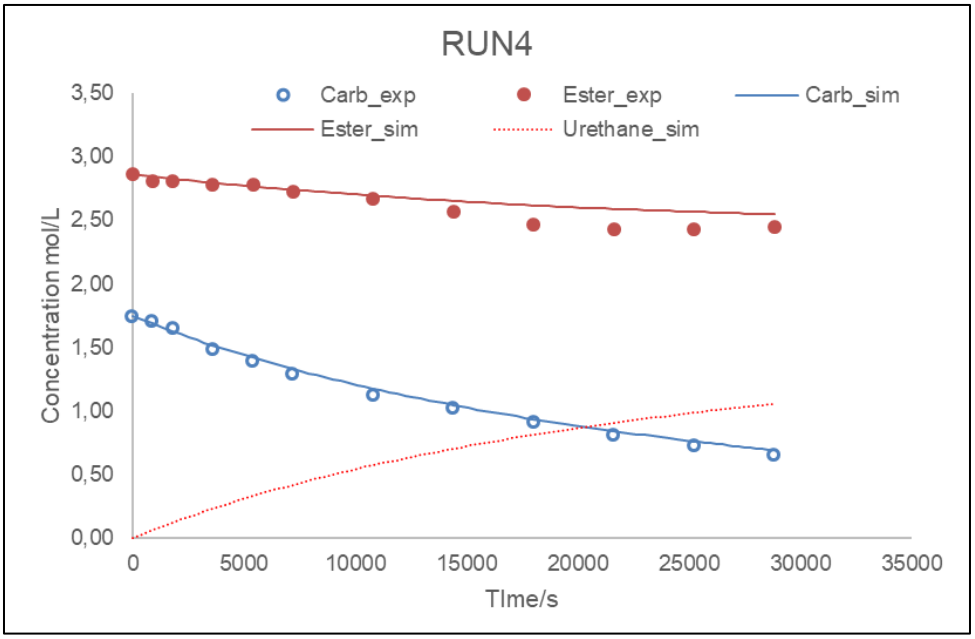

Figure 33. Fit of the model to the experimental observation for Run 4.

Table 37. Correlation matrix of the estimated parameter for aminolysis by MBA.

	$k_{Amidation}$ (T_{Ref})	$Ea_{Amidation}$	$Ea_{Aminolysis}$	$k_{Aminolysis}$ (T_{Ref})	$K_{Amidation}$
$k_{Amidation}$ (T_{Ref})	1.00				
$Ea_{Amidation}$	0.25	1.00			
$Ea_{Aminolysis}$	-0.01	0.05	1.00		
$k_{Aminolysis}$ (T_{Ref})	0.03	-0.01	-0.09	1.00	
$K_{Amidation}$	**-0.69**	-0.29	0.02	0.03	1.00

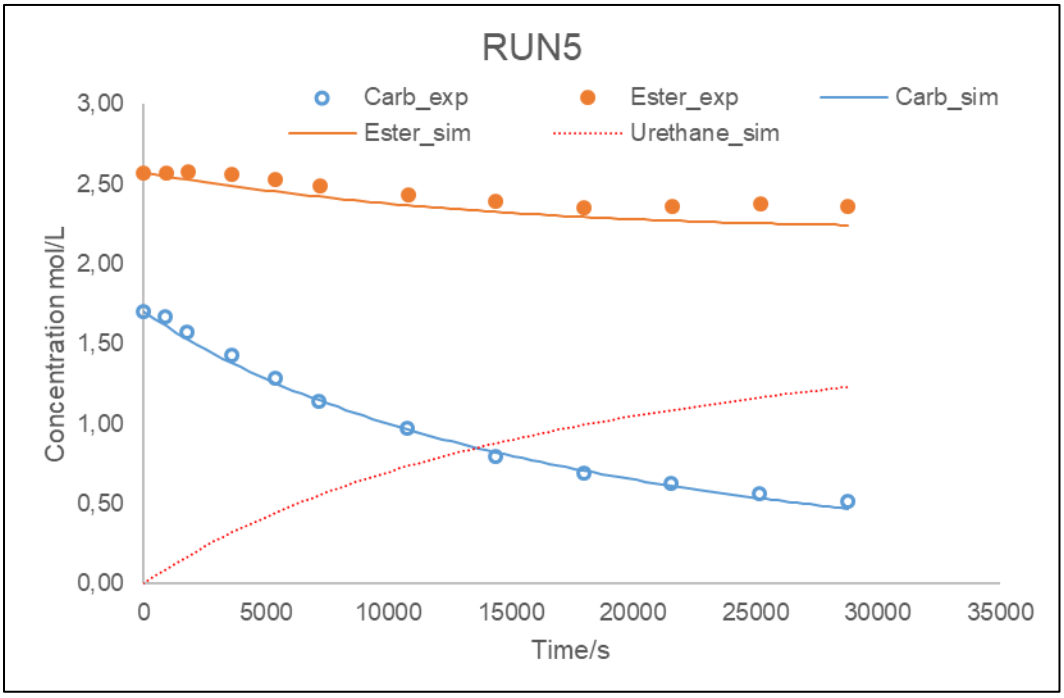

Figure 34. Fit of the model to the experimental observation for Run 5.

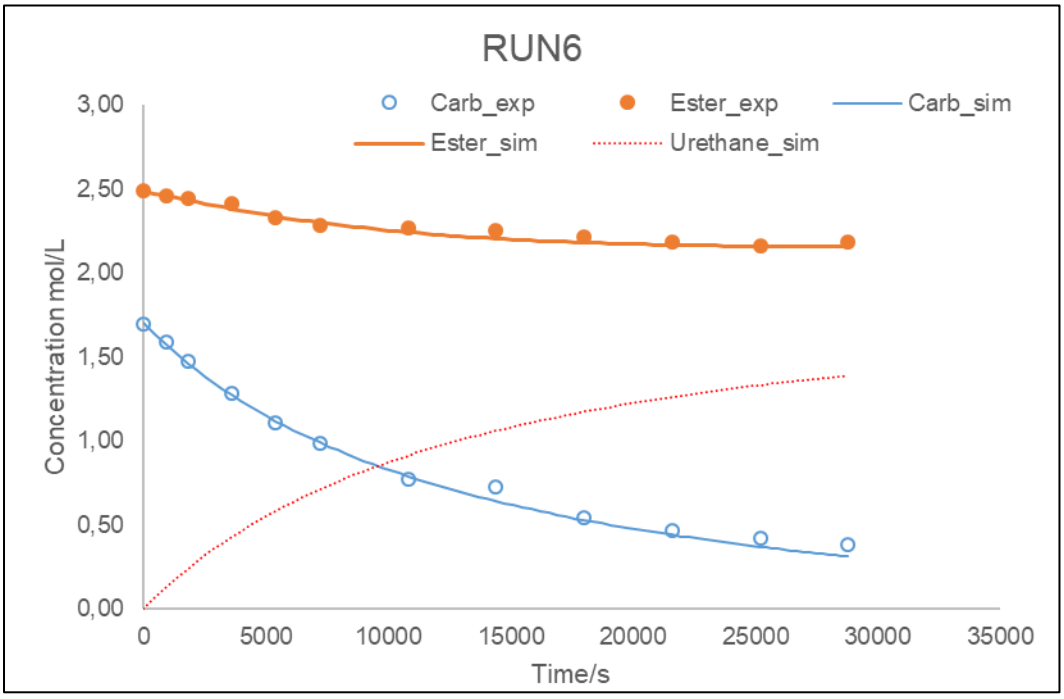

Figure 35. Fit of the model to the experimental observation for Run 6.

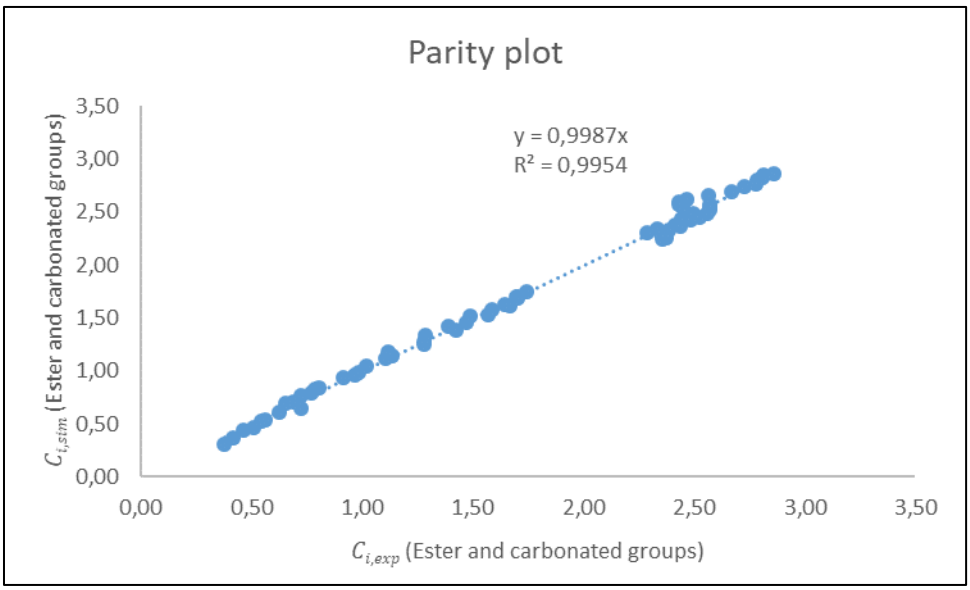

Figure 36. Parity plot between estimated and experimental concentrations for the aminolysis by MBA.

Aminolysis of carbonated methyl oleate (CMO) by ethylbutylamine (EBA)

Table 38 shows that the rate constant at 382.15K was estimated to be $2.92 \cdot 10^{-6}$ $L.mol^{-1}s^{-1}$. The coefficient of determination was found to be 98.30%. Figure 37 shows the fit of the model to the experimental data. The parity plot figure is displayed in Figure 38.

Table 38. Kinetic constants estimated at T_{ref}=382.15K and statistical data for the aminolysis by EBA.

	Estimated	Standard deviation %
$k_{Aminolysis}\left(T_{Ref}\right)$ (L·mol^{-1}·s^{-1})	$2.92 \cdot 10^{-6}$	2.6

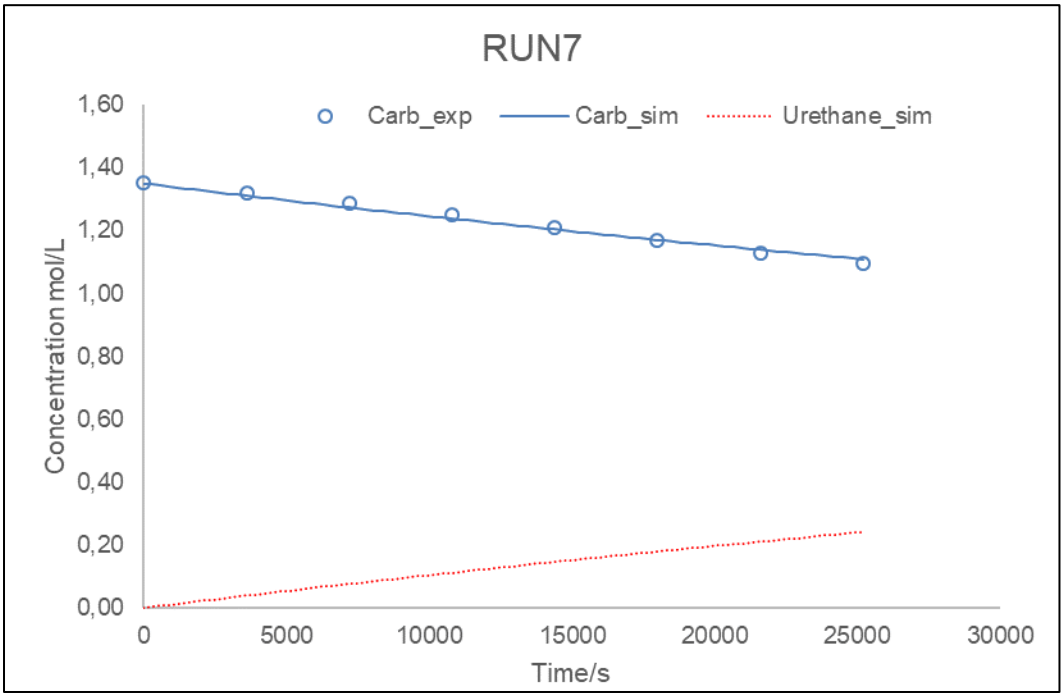

Figure 37. Fit of the model to the experimental observation for Run 7

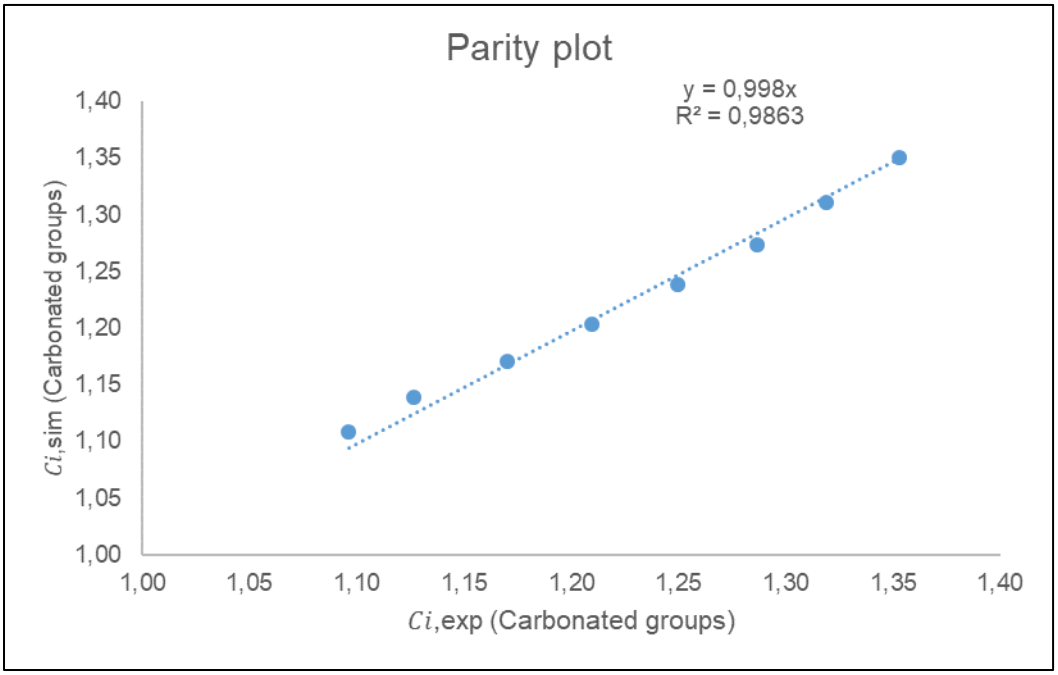

Figure 38. Parity plot between estimated concentration versus experimental concentration for aminolysis by EBA.

Aminolysis of carbonated methyl oleate (CMO) by dibutylamine (DBA)

Table 39 shows the estimated parameters along with the standard deviations. It can be noticed that the standard deviations are very low, confirming a relatively good estimation of these parameters. The coefficient of determination was calculated to be 99.09%. The correlation between the rate constant and the activation energy was very low, i.e., -0.22. The model fits perfectly the experimental data (Figure 39, Figure 40 and Figure 41).

Table 39. Kinetic constants estimated at T_{ref}=408.15K and statistical data for aminolysis by DBA.

	Estimated	**Standard deviation %**
$k_{Aminolysis}\ (T_{Ref})$ (L·mol^{-1}·s^{-1})	4,16*10^{-06}	1,60
$Ea_{Aminolysis}$ (J·mol^{-1})	52900	8,50

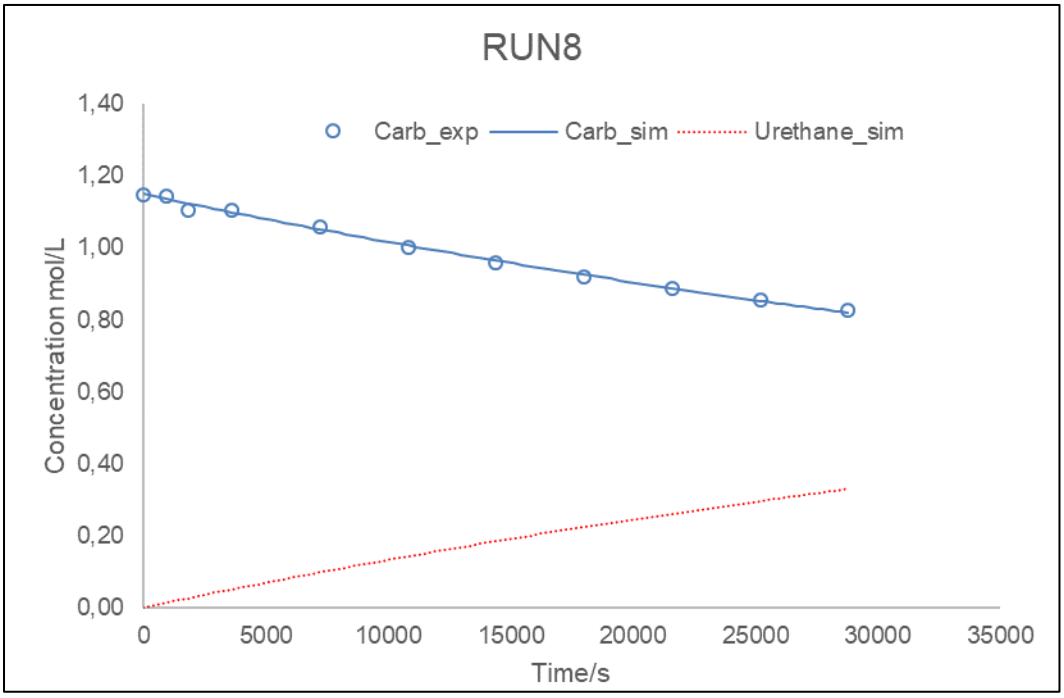

Figure 39. Fit of the model to the experimental observation for Run 8

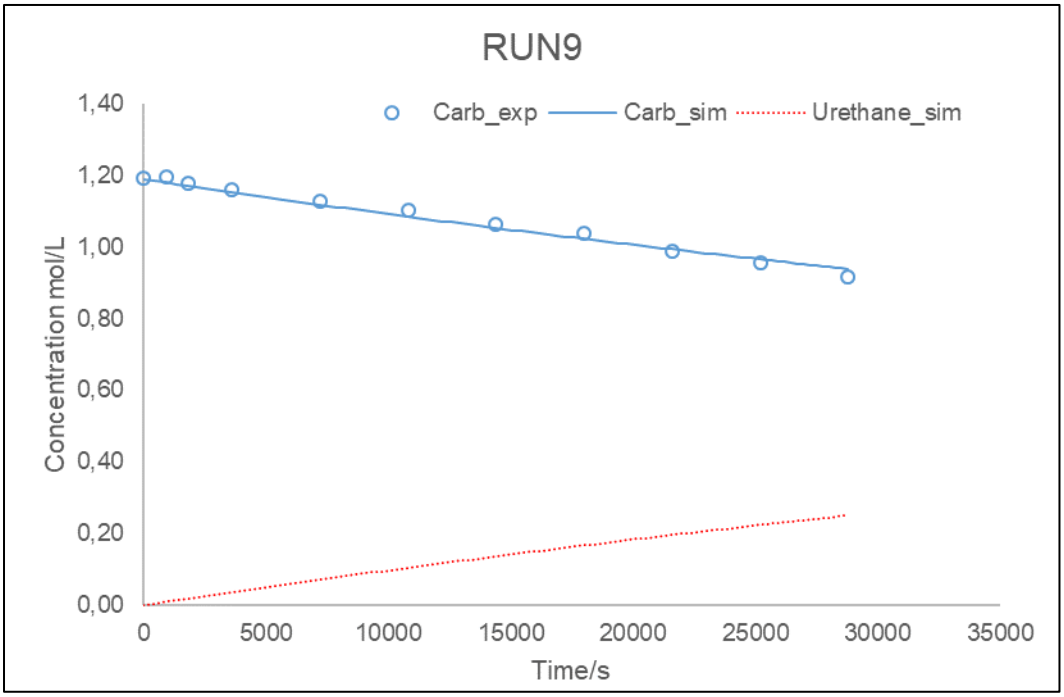

Figure 40. Fit of the model to the experimental observation for Run 9.

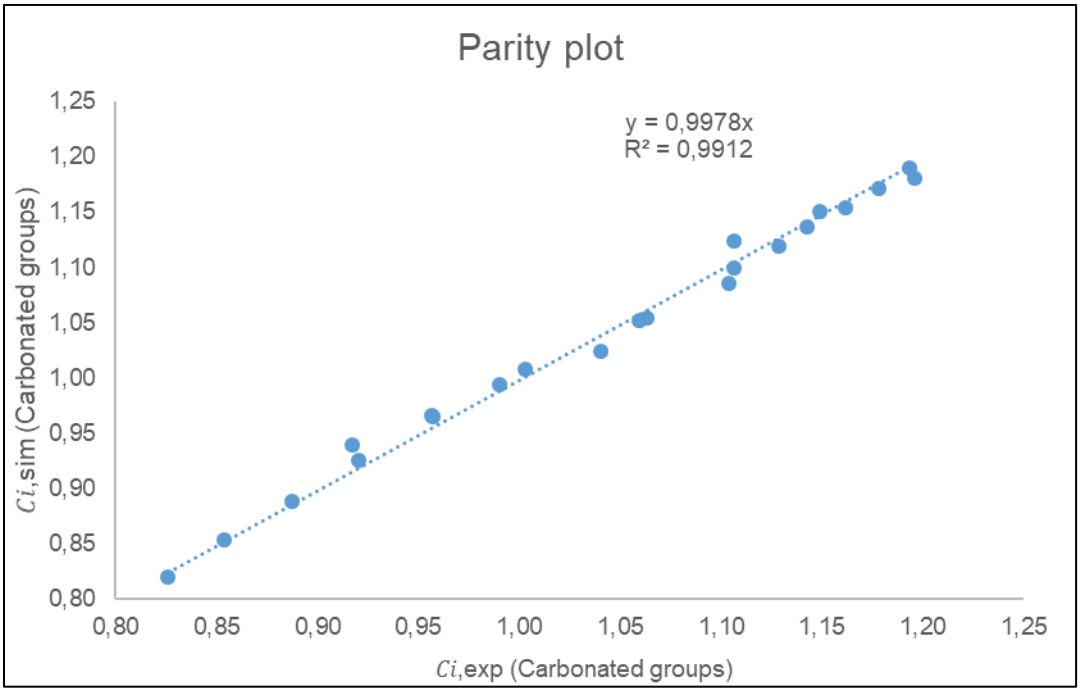

Figure 41. Parity plot between estimated and experimental concentrations for the aminolysis by DBA.

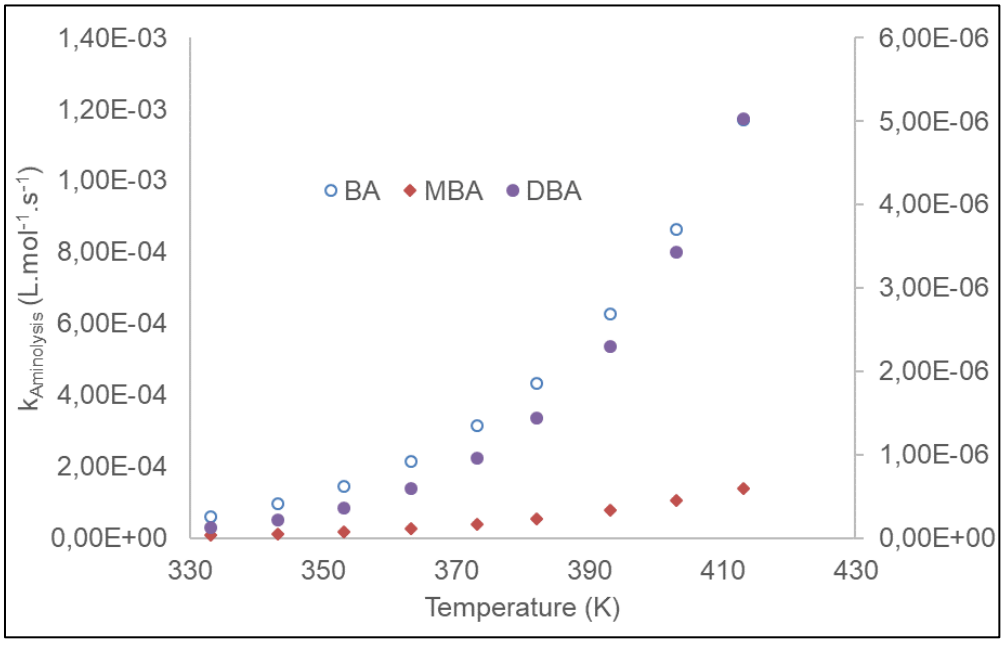

Figure 42. Evolution of aminolysis rate constants at different temperatures and substituents.

Figure 42 shows the evolution of the aminolysis rate constants at different temperatures for BA, MBA and DBA. It can be noticed that the rates of aminolysis increase in the following way: $R_{Aminolysis\ by\ BA} > R_{Aminolysis\ by\ MBA} > R_{Aminolysis\ by\ DBA}$ at any temperatures. At 382.15 K, the rate increases in the following way $R_{Aminolysis\ by\ BA} > R_{Aminolysis\ by\ MBA} > R_{Aminolysis\ by\ EBA} > R_{Aminolysis\ by\ DBA}$. As the steric hindrance substituent increases, the kinetics of aminolysis decreases.

In this study, a linear free energy relationship was used to find a relationship (Eq. 32) between the substituent reactant and kinetics.

$$log(k_X) = a \cdot b_x + c \quad (32)$$

The coefficient b_x depends on the substituents –H (for BA), -Me (for MBA), -Et (for EBA) and –Bu (for DBA). This coefficient represents the total steric effect of the substituent.

Table 40 displays the values of b_x tested in this study. Figure 43 demonstrates that equation 32 using values from Table 40, is correct at different temperatures. A value of 3 for b_x was given for Bu- substituent because it gives the best statistical results. One can notice that the values of *a* and *c* are temperature dependent. Figure 43 shows that equation 32 establishes a correlation between reaction rates and substituent for aminolysis reaction. This study shows that the aminolysis reaction depends on the steric hindrance of amine substituent. By increasing the reaction temperature, the importance of the steric effect on the reaction series, i.e., the absolute values of *a* and *c* decrease with the increase of reaction temperature.

Table 40. Values of b_x from Eq. (11)

Substituents	**b_x**
H-	0
Me-	1
Et-	2
Bu-	3

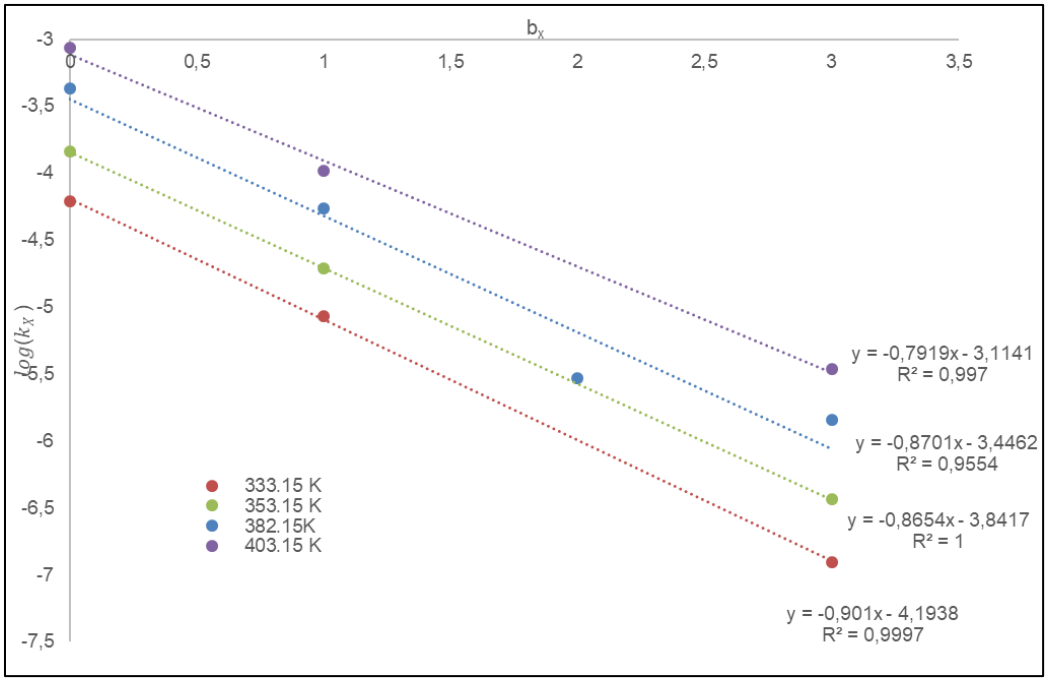

Figure 43. Application of Eq. (11) to the aminolysis system.

A direct comparison between the kinetics with these amines is not possible, because the optimum reaction temperature is not the same. Hence, a kinetic model was developed for each aminolysis system, and it was found that as the steric hindrance of amine increases, the rate constant is smaller. It was found that the amidation reaction is negligible for the aminolysis by ethyl-butyl-amine and dibutyl-amine. As expected, activation energies are quite similar, within 45000-52900 $J \cdot mol^{-1}$, indicating that the decrease in the rate constants is indeed due to the increase in the steric hindrance of the amines that leads to a lower probability of collisions. A relationship between substituent structure and reactivity was found for the aminolysis reaction by using the concept of the linear free energy relationship. The logarithm of the aminolysis rate constant can be expressed by a linear function with b_x, which measures the steric hindrance of the amine substituent. It was demonstrated that the two other parameters *a* and *c* are temperature dependent. More investigation on the theoretical interpretation of b_x, *a* and *c* are needed in order to be able to predict the reactivity of different amines for the aminolysis reaction. Such an approach could contribute to finding adequate diamine and optimum operating conditions for the production of Non-isocyanate polyurethane.

Aminolysis with GLH

Aminolysis of GLH with CMO produced an emulsified system that can be identified after a gravity separation of the water excess, as it can be seen in picture 4-Appendix 6. Figure 44 shows the HNMR spectra of the product from CMO-GLH aminolysis reaction. It can be observed the following results: δ=5,3 ppm (s) and δ=4,70 ppm (d). Wang (G. Wang et al., 2009) reported the following results: δ=5,55 ppm (s, -NH urethan) and δ=5,08 ppm (d, -NH urethan, J=6,6 Hz) and Bietsch (Bietsch et al., 2023) reported the following: δ=5,50ppm (s, 1H) and δ=5,05 ppm (d, 1H, J=6,5 Hz). From the comparation of the results, it can be concluded that, at least, the aminolysis reaction between $-NH_2$ group of GLH and CC group of CMO, took place. FTIR spectra of Figure 45 shows three peaks: one between 1500-1600 cm^{-1} according to the bibliography, due to the -N-H urethane group vibration, another around 1650 cm^{-1} due to -C-O-C amide group vibration and another one around 1700 cm^{-1} due to C=O urethane vibration. No signals around 1750 cm^{-1} (C=O ester group) and 1800 cm^{-1} (CC group) are observed what can be interpreted as that total amidation and aminolysis took place. Increased signal around 3300-3400 cm^{-1} suggests new -OH groups from aminolysis reaction as well as the proper ones from GLH molecule.

Figure 46 and Figure 47 show HNMR and FTIR spectra for the reaction product from CCO and GLH. Results show a singlet at δ=5,3 ppm most probably from -NH urethane proton and a little bit displaced compared to the signal of CMO. Doublet signal from NH-carbamate proton can be identified at 4,53 ppm. FTIR spectra shows the same pattern of Figure 45 (urethane and amide signals) indicating complete amidation and aminolysis reactions on CC and ester C=O groups of CCO.

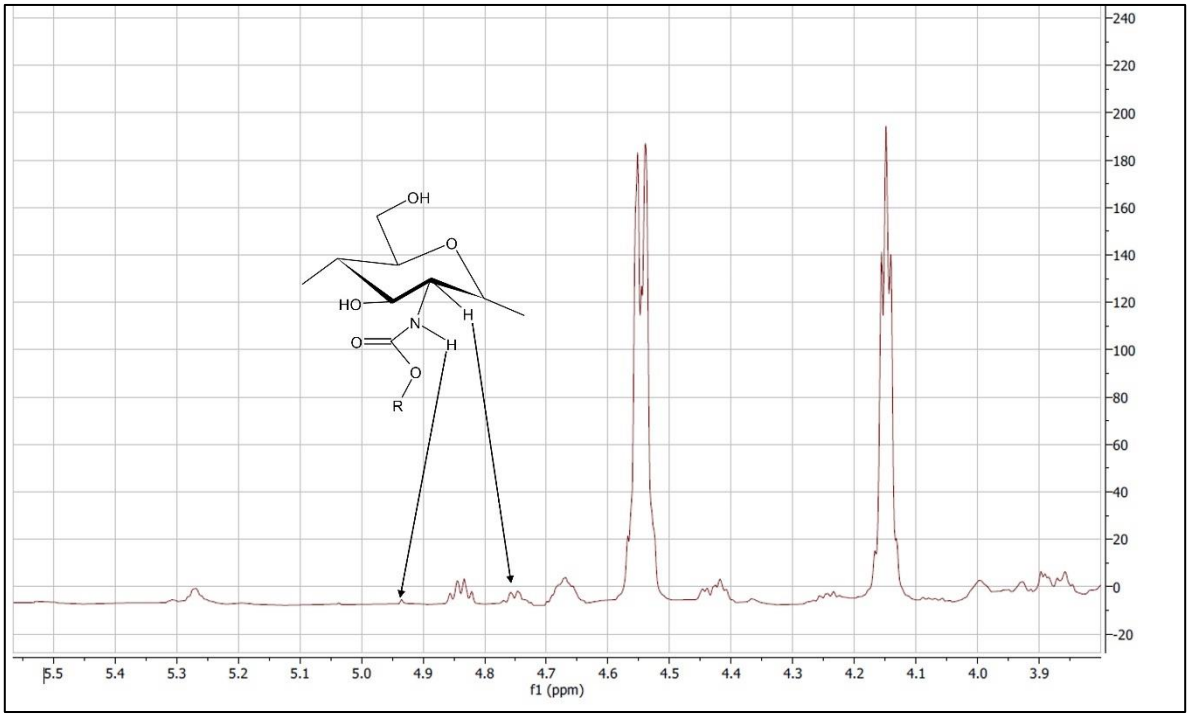

Figure 44. HNMR spectra of aminolysis product between GLH and CMO

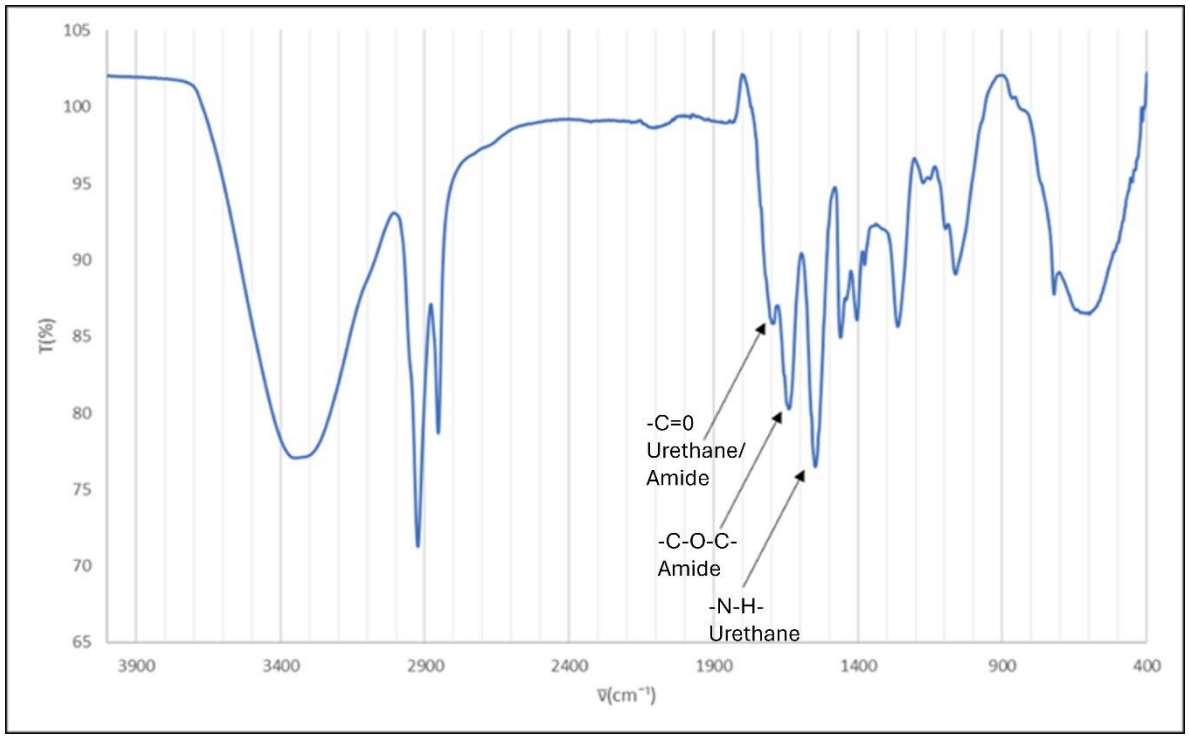

Figure 45. FTIR spectra for aminol product between GLH and CMO

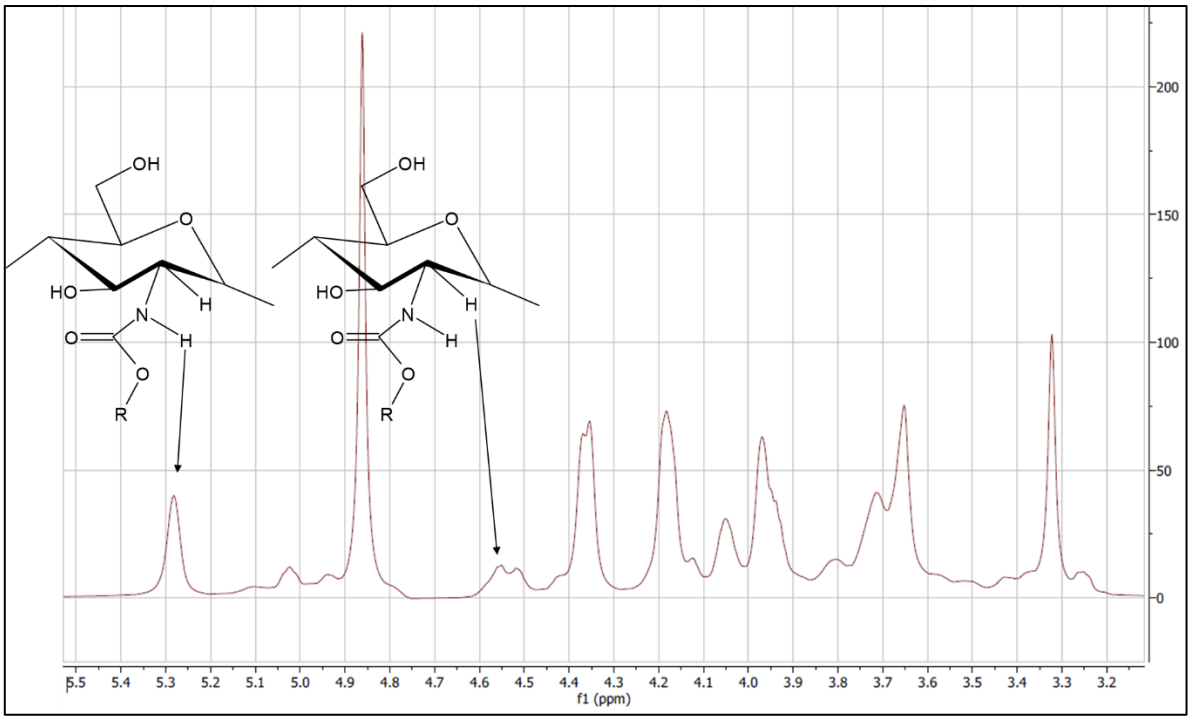

Figure 46. HNMR spectra of aminolysis product between GLH and CCO

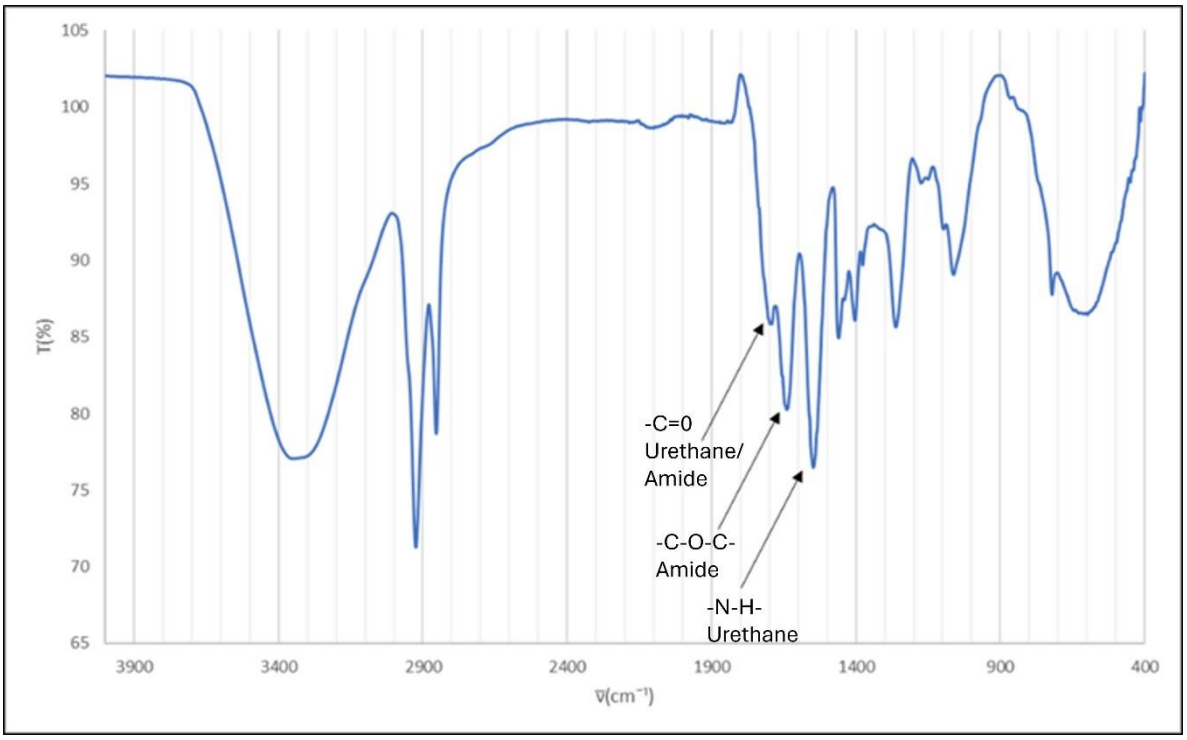

Figure 47. FTIR spectra for aminol product between GLH and CCO

Aminolysis with CCO and CH

The bulk reaction yielded a dark sticky sludge (Picture 5- Photographic record). It is like a pasty mass that it can be molded. It does not seem like a useful polymerization product. Figure 48 shows that carbonate signal around 1800 cm^{-1} decreased considerably compared to the carbonate signal of the CCO (Figure 25). Signal between 1500-1600 cm^{-1} is also an evidence of reaction and it could be from N-H or C-N bond of urethane group. This is a remarkable result in order to propose that the aminolysis reaction between cyclic carbonate group of castor oil and amino group from chitosan, is possible. Although the reaction took place, the system seems to be not adequate for plasticizer or adhesive application since it is not a completely homogeneous material and it looks like a sticky colloidal heterogeneous mass. Then, an “emulsion bulk reaction” was carried out.

In Picture 6 of the Photographic record, it is possible to observe that o/w emulsion is not a homogeneous system since it shows film appearance in some areas but the rest is a sticky mix of oil and solid grains of chitosan. This product seems also not proper for the scope of this work. A FTIR analysis showed that aminolysis reaction took place along with amidation of glyceride-ester groups. Figure 49 shows the evolution of the emulsion-bulk reaction through time. There are signals suggesting the evolution of the aminolysis reaction, like the growing signal around 3400 cm^{-1}

corresponding to the -OH groups. Around 1540 cm^{-1} (urethane -NH vibration) there is also a growing signal although it appears overlapped with other neighbor signal around 1650 cm^{-1} (C-O-C amide vibration). This evidence suggests the occurring of amidation non-desirable side reaction along with aminolysis of CC group (decreasing signal around 1800 cm^{-1}). The decreasing of gryceride-ester group signal around 1750 cm^{-1} it's a very strong evidence also for the occurring of amidation reaction.

The w/o emulsion product obtained it's a sticky viscous white-yellowish product as it is shown in picture 7- Photographic record. HNMR spectra (Figure 50) of this product shows the following signals: δ=5,8 ppm (s, 1H) that can be related to the -NH proton of carbamate function and δ=5,02 ppm (d, 1H) related to the alpha proton of the carbamate function. It is not possible to observe the duplet signal of the -NH carbamate group due to the complexity of the signals between 5,25-5,50 ppm. CNMR analysis (Figure 51) shows a signal around 157 ppm from C=O carbamate carbon.

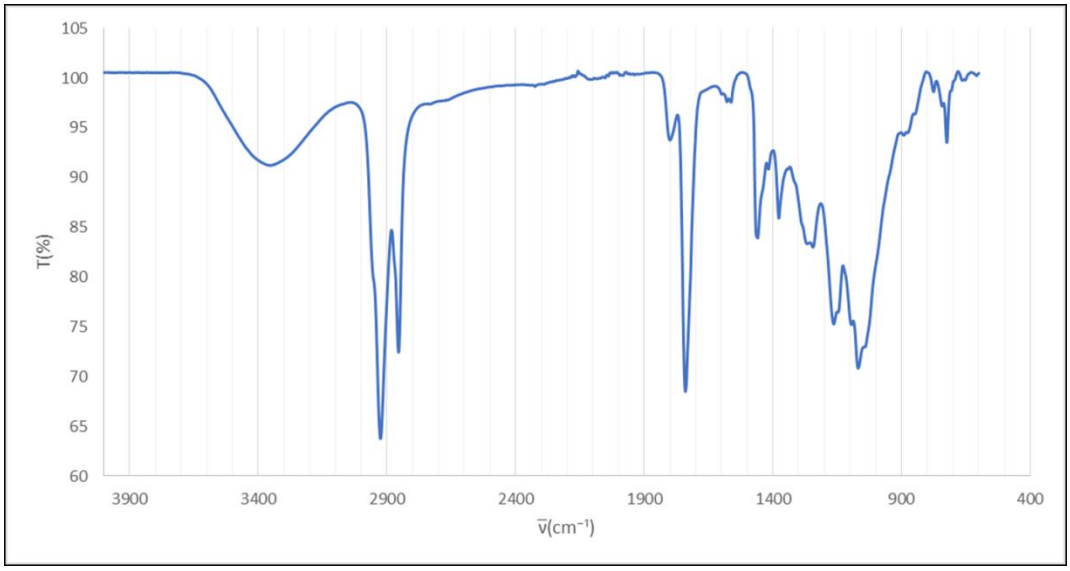

Figure 48. FTIR spectra for bulk reaction

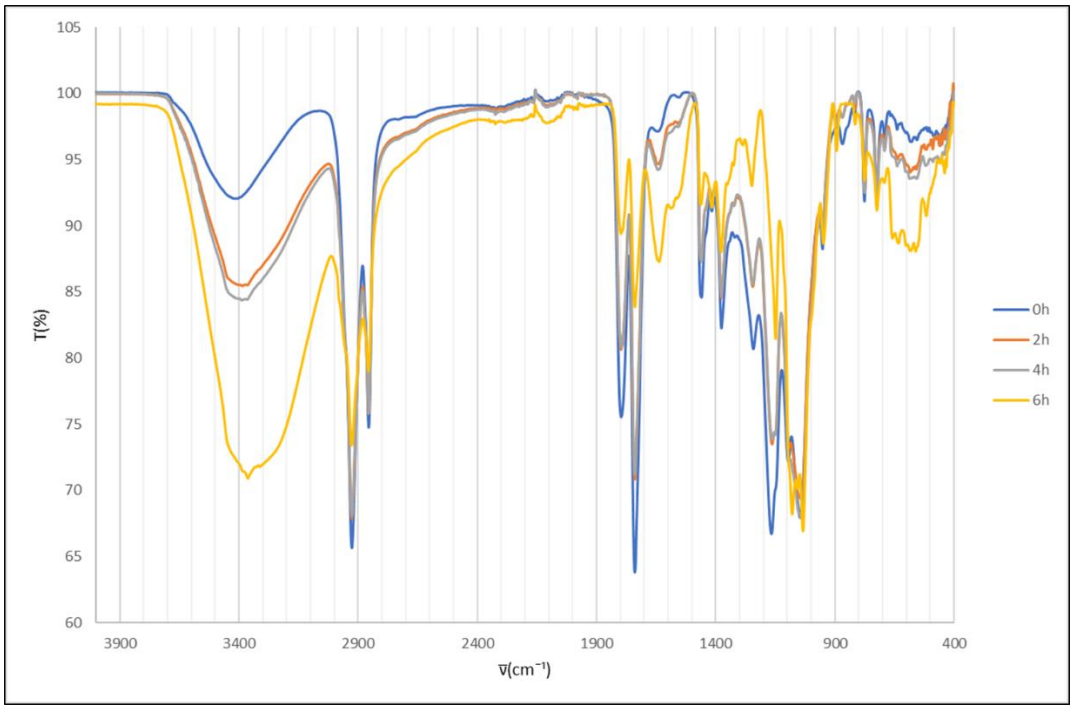

Figure 49. FTIR spectra for " o/w emulsion reaction"

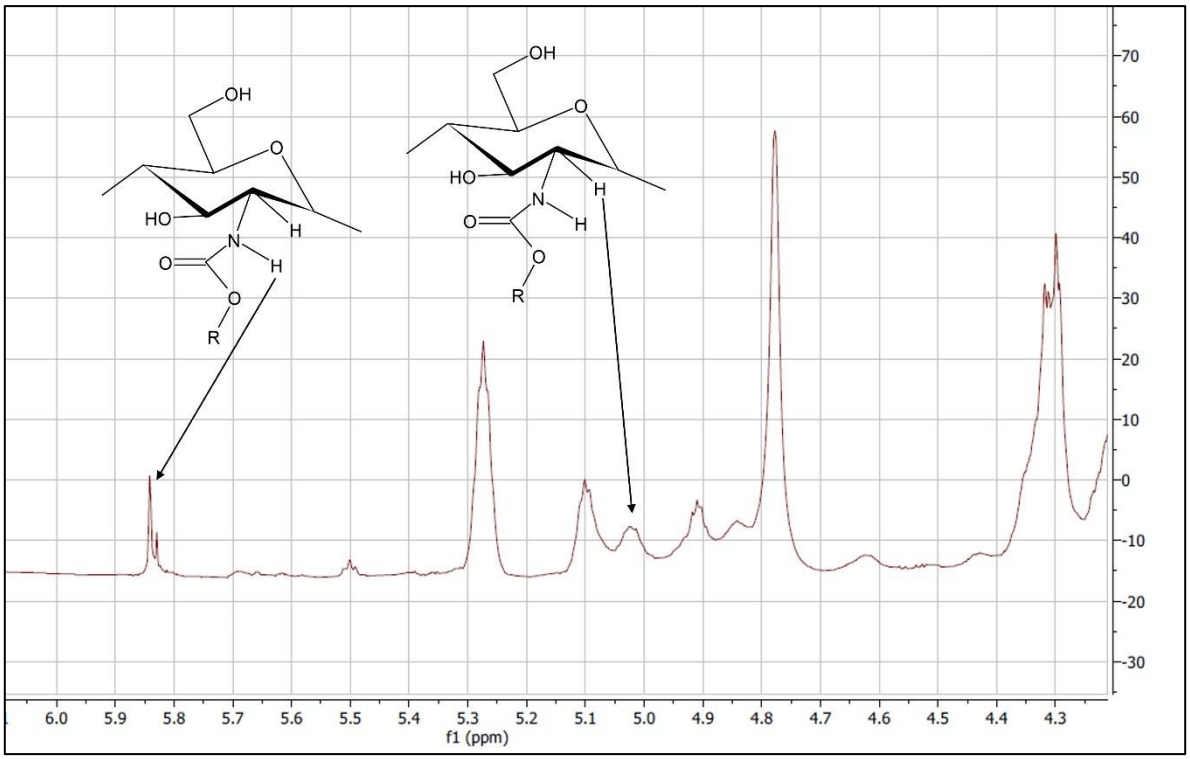

Figure 50. HNMR for w/o emulsion CCO-CH NIPU

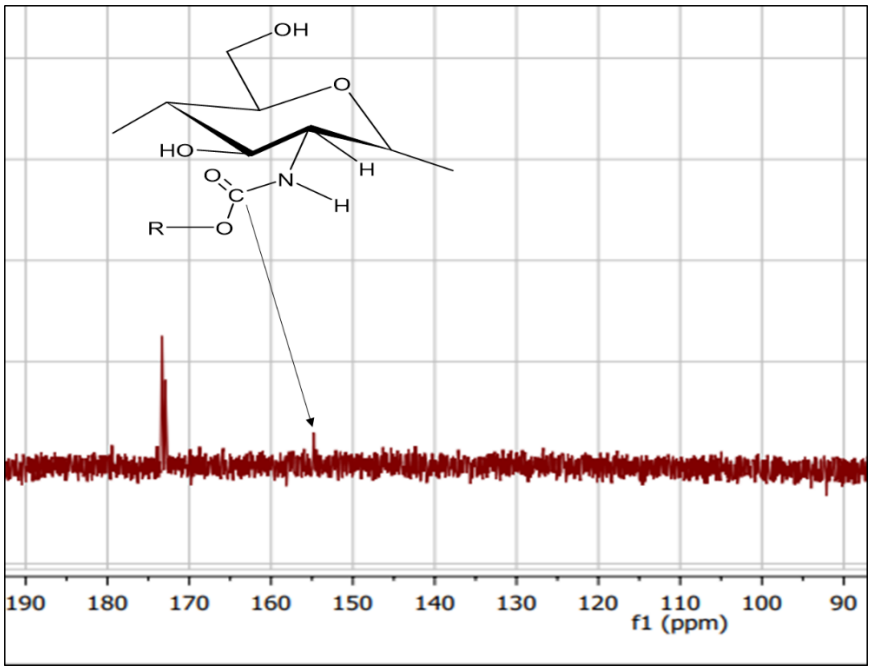

Figure 51. CNMR for for w/o emulsion CCO-CH NIPU

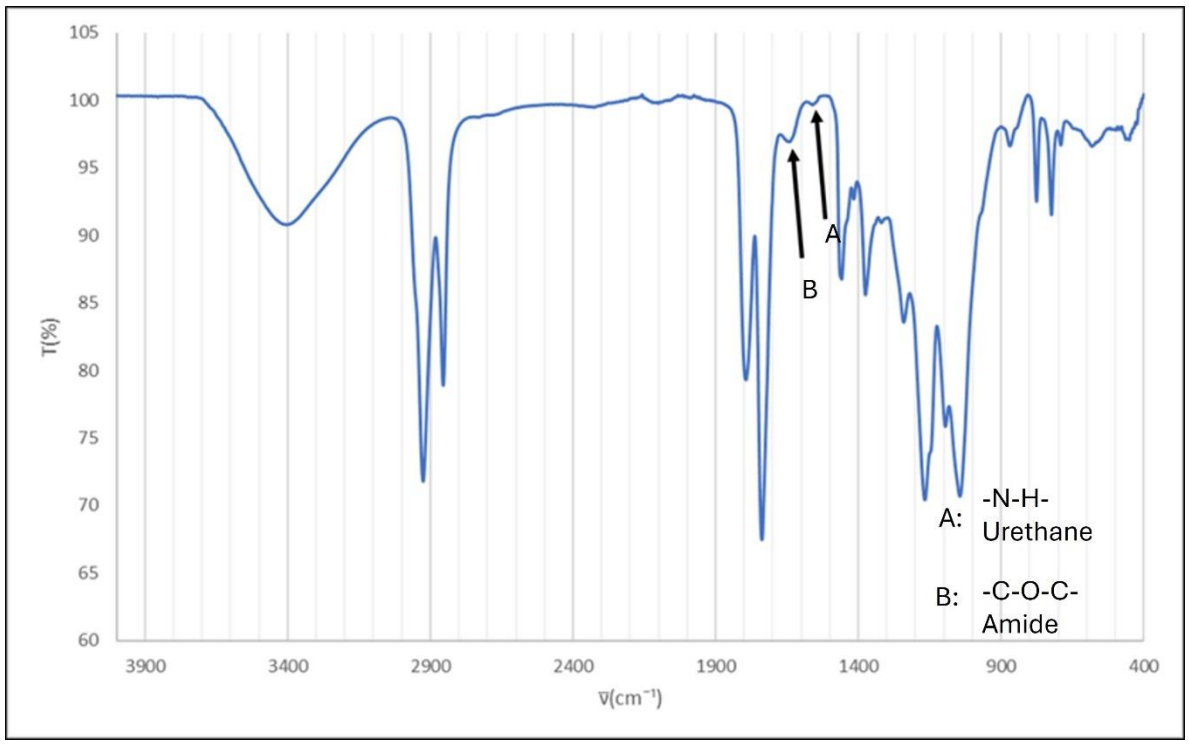

Figure 52. FTIR for for w/o emulsion CCO-CH NIPU (20 hours, 70°C)

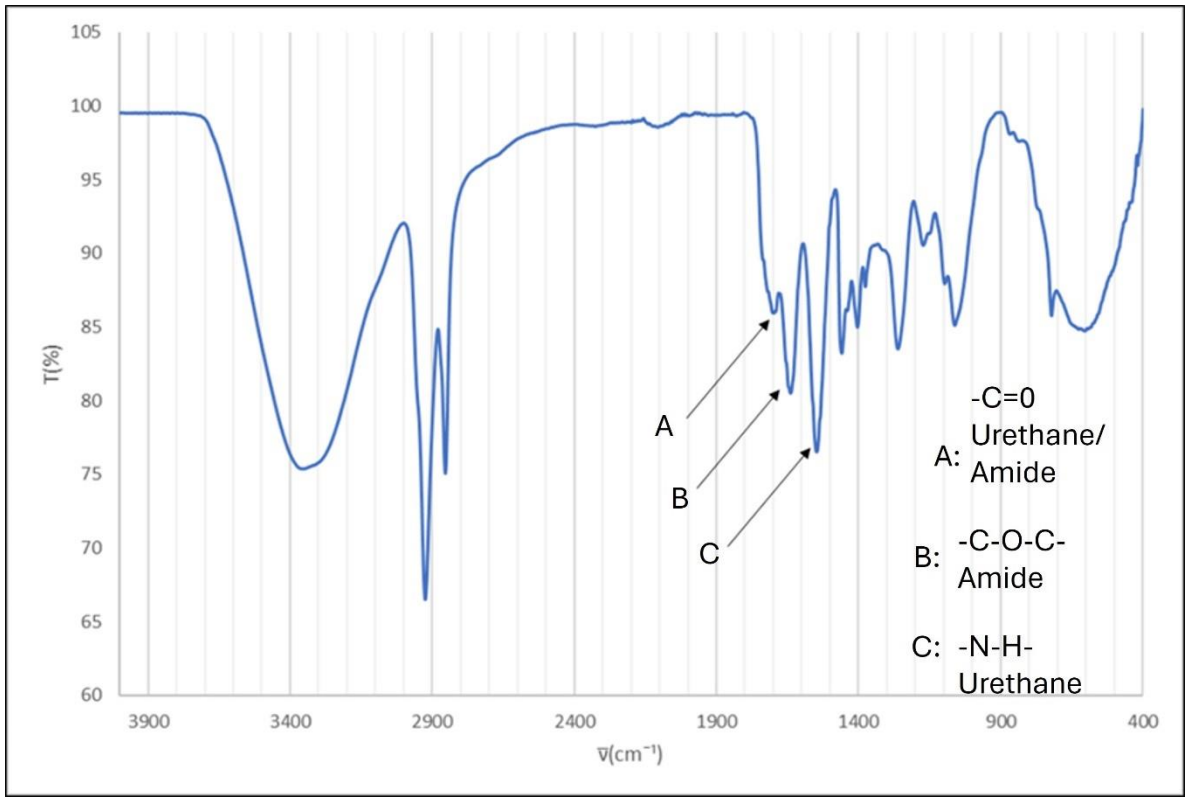

Figure 53. FTIR for w/o emulsion CCO-CH NIPU Final product

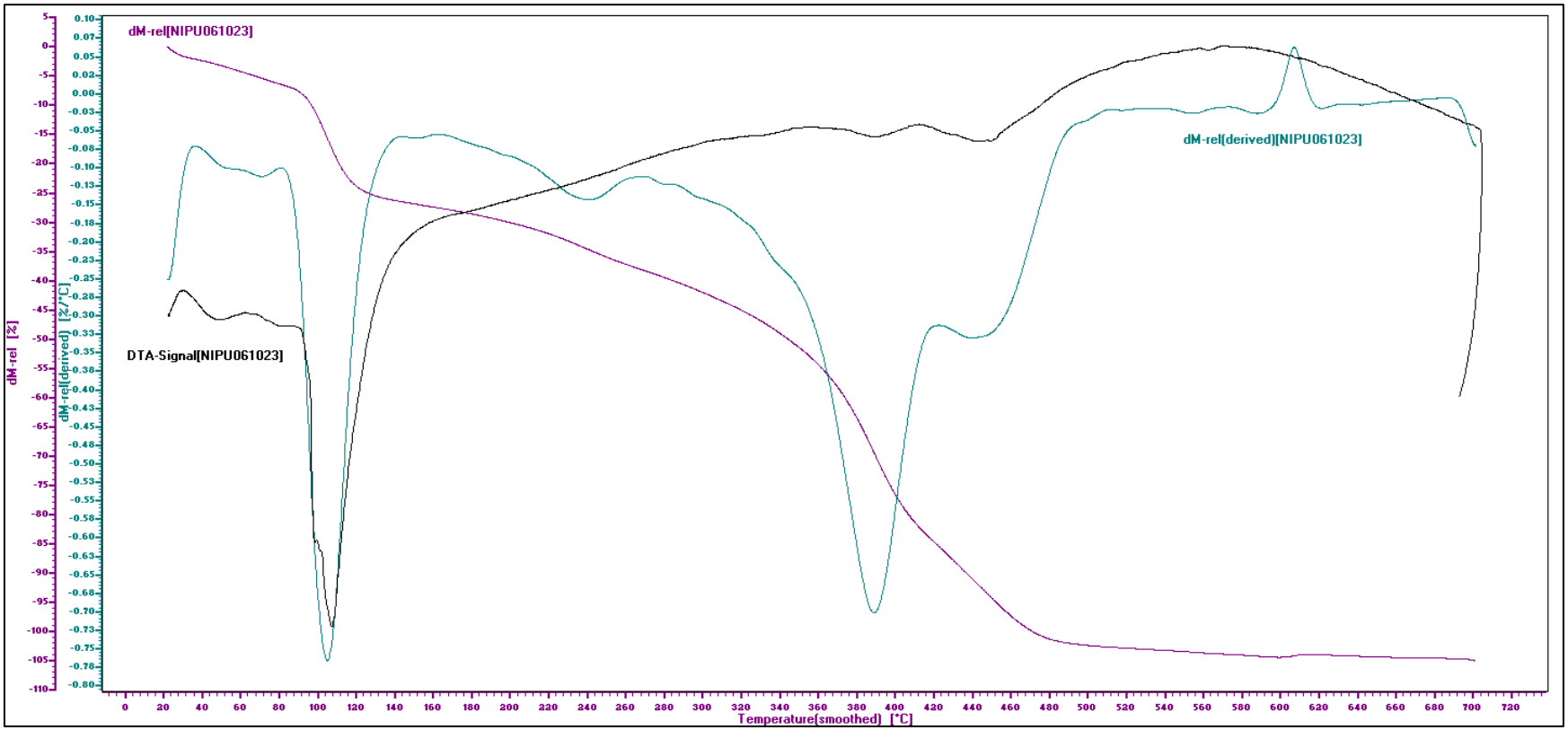

Figure 54. TGA and DTA for w/o emulsion CCO-CH NIPU Final product

Figure 52 shows the FTIR spectra of the CCO-CH NIPU after 20 hours of reaction at 70 °C. Signal around 1550 cm^{-1} shows the urethane -NH group vibration so, it is a confirmation of the aminolysis reaction between CH-NH_2 group and CCO-CC group. Signal around 1650 cm^{-1} is an evidence of the amidation reaction between CH-NH_2 group and triglyceride -C=O group. It is clear that coupling between CH and CCO is possible through carbamate bond. Crosslinking trough amide bond is also occurring so it is not also exclusively a polyurethane but a polyamide material. Figure 53 shows the final product after EDA addition. The following signals can be noticed: 1500-1600 cm^{-1} due to the -N-H urethane group vibration, 1650 cm^{-1} due to -C-O-C amide group vibration and around 1700 cm^{-1} due to C=O urethane vibration. No signals around 1750 cm^{-1} (C=O ester group) and 1800 cm^{-1} (CC group) are observed what can be interpreted as total amidation and aminolysis took place. Figure 54 shows the thermal analysis of the CCO-CH NIPU final product. It is evident an important mass loss approximately of 20% around 100 °C mainly attributed to the water evaporation. After 160 °C until around 380 °C it is possible to observe a progressive mass loss from an apparent exothermic character phenomenon according to the DTA signal. This could be explained by a possible combination of curing reaction and cracking processes of the substrate. This part of the TGA signal is very similar to the one reported by Das and colleagues (Das et al., 2020) for a similar material they produced. After 380 °C to 500 °C there is another notorious weight loss of around 50%. This is, with no doubt, the final combustion of the material.

Application on acrylic adhesive AUTOADHESAN®

Picture 8 of the photographic record shows the visual aspect of the AUTOADHESAN® adhesive. It is a white low-viscosity liquid. When 5% w/w of CCO-CH NIPU is added, the viscosity increases almost inmediately as it can be seen in picture 9 of the photographic record. The product shows rheological-modifying properties over AUTOADHESAN®. Blanc and modified adhesives were applied on 50 µm bio-oriented polypropylene substrates as it can be seen in pictures 10, 11 and 12 of Photographic record and let to dry at room temperature overnight. Samples of the applications were tested for loop tack test (picture 13- Photographic record), hold-shear test (picture 14- Photographic record) and 180° peel test (picture 15- Photographic record). The obtained results are shown in Table 41. A two-tailed t-statistic test was run for the mean difference of the response variables for the two samples. The results are shown in Table 42. P-values for the three tests were less than 0,05 so it can be claimed that there is a significant statistical difference between the adhesive tests for the blank AUTOADHESAN® sample and the AUTOADHESAN®+%5 CCO-CH NIPU sample. FTM 8 hold test measures the cohesion of the sample. It is defined as the time required to allow a given area of self-adhesive material to shear from a standard surface by loading parallel to the surface. AUTOADHESAN® sample showed an average time of 172,48 min while

AUTOADHESAN®+%5 CCO-CH NIPU sample yielded 18,67. It means the additive caused a significant decreasing on the cohesive forces of the adhesive, it is, the additive is not good for applications where high tear resistance is needed. On the other hand, FTM 1 peel test measures the permanence of adhesion or peelability of self-adhesive pressure sensitive materials. Peel adhesion is defined as the force required to remove pressure sensitive coated material, which has been applied to a standard test plate under specific conditions, from the plate at a specified angle and speed. Table 41 shows that added AUTOADHESAN® shows an average force of 10,98 N and blank material is 7,94 N. Since t-test concluded that there is a significant difference between the mean force, it can be concluded that the addition of CCO-CH NIPU improved the adhesive performance of the material. FTM 9 loop-tack results are in the same sense. The loop tack value of a pressure sensitive materials is the force required to separate, at a specific speed, a loop of material which has been brought into contact with a specific area of standard surface. Table 41 shows an average force of 1,32 kgf/in² for modified material compared to 1,05 kgf/in² of the blank material, a statistically significant difference according to Table 42. This is another test evidence for the improvement of the adhesive properties of the AUTOADHESAN® adhesive. In general terms, according to the experience of the colleagues in the company, improving one characteristic of the adhesive, adhesion or cohesion, will cause a depletion on the other one. It means, and additive improving the adhesion of an adhesive will cause a weakening on its cohesive behavior and vice versa. That is the case of the CO-CH based NIPU additive produced in this project: it caused a notorious improvement in the adhesion behavior with a cost in the cohesive properties of the additive.

Table 41. FINAT Adhesive tests results

	AUTOADHESAN®			AUTOADHESAN® + 5% CCO-CH NIPU		
	Test	**Value**	**Average**	**Test**	**Value**	**Average**
	FTM 8 Hold (1/2 x 1/2 x 1000) [min]	121,6	172,48	FTM 8 Hold (1/2 x 1/2 x 1000) [min]	13,6	18,67
		359,93			16,73	
		283,42			18,72	
		61,6			15,83	
		84,23			16,17	
		124,08			28,25	
					21,4	
s.d		120,382		**s.d**	4,882	
CV		69,796		**CV**	26,148	
	FTM 1 Peel FINAT 180° [N]	7,912	7,64	FTM 1 Peel FINAT 180° [N]	10,963	10,98
		7,749			10,859	
		7,236			11,296	
		7,662			10,809	
					10,96	
s.d		0,288		**s.d**	0,190	
CV		3,775		**CV**	1,731	
	FTM 9 Loop Tack [kgf/in²]	1,065	1,05	FTM 9 Loop Tack [kgf/in²]	1,182	1,32
		1,074			1,418	
		0,934			1,364	
		1,132			1,321	
s.d		0,084		**s.d**	0,101	
CV		7,954		**CV**	7,641	

Notes: * Label substrate is in bi-oriented polypropylene-50 µm thickness
* All test surfaces are stainless steel
*Adhesive application is 22-24 g/m²

Table 42. Two tailed t-statistic tests for mean difference

	FTM 8	FTM 1	FTM 9
Hypothetic mean difference (Ho)	0	0	0
Degrees of freedom	11	7	6
t-statistic	3,40	-20,97	-4,12
P(T<=t) two tails	0,005899	1,408E-07	0,006221

7. CONCLUSIONS

Castor oil processing

It was demonstrated in the castor oil epoxidation that the catalytic activity of the Amberlite® IR 120 resin doesn't depend on the catalyst particle size, therefore, there is not external mass transfer limitations in the kinetics of the epoxidation of castor oil catalyzed by Amberlite® IR120 (H) ion exchange resin. This is an important assumption when kinetic modeling of this reaction is pretended to be obtained. Temperature has a significant direct effect on the conversion of DB. It means, higher temperatures favor higher conversions. On the other hand, reaction time is the parameter that has a significant inverse effect on selectivity. Longer reaction time causes the decreasing of the selectivity and the effect seems to be more severe when it is combined with high temperatures. On the conquest of a successful process, it is necessary to achieve an equilibrium considering these principles. Theoretical maximum conversion and selectivity are 89,6% and 65,7 %, respectively, at 53 °C and 8,7 hours of reaction. Validation experiments showed the following values: 84,16% conversion and 81,42% selectivity, a nice equilibrated combination considering the difficulty of the process and the complicated and unique nature of the castor oil as oleaginous raw material with a non-common behavior. It was also demonstrated that the reaction step that is exothermic enough to rise the system temperature until unsafe levels, is the Prilezhaev reaction on DB and not the peracetic acid formation as it is claimed in many repots of vegetable oil epoxidation. This insight on the thermodynamic behavior could be useful for a better understanding of the kinetics of the reaction. For practical purposes, it was demonstrated in a pilot scale that the presence of a solvent like hexane helps to avoid the time-consuming drip addition of HP since it can absorb the heat released in the reaction until its boiling point (near to the optimum process temperature ≈ 54 °C) and maintaining at the same time the thermal equilibrium of the system. One-pot addition of all reactants and catalyst in the presence of a solvent like hexane is feasible to carry out on a safe way, with very good epoxidation results. Hexane also avoids the emulsification of the system and the subsequent loss in selectivity because of the epoxide ring cleavage.

Contrary to some cases where the improvement on the kinetics of vegetable oil carbonation with water addition is reported for species like soybean, for castor oil is not the case. No kinetic improvement was observed. As it has been discussed previously, castor oil is a special vegetable oil. The presence of natural-occurrence hydroxyl groups in the fatty acid chains confer to oil, special features like water-affinity and higher viscosity what make it different from the other common vegetable oils like palm or soybean. This feature of castor oil may block the improvement effect of water observed on the carbonation of other vegetable oils. Because the affinity,

the hydroxyl groups could immobilize the water molecules interfering in the synergistic effect of them and the Lewis base (catalyst) as it is explained in the work of Jian an colleagues (Jian et al., 2009). That is the most plausible reason for the lack of evidence of kinetic improvement on the carbonation of ECO with water addition.

Aminolysis reaction, NIPU production and application

In aminolysis reaction between amine and cyclic carbonate groups, it was found that as the steric hindrance of amine increases, the rate constant is smaller. Amidation reaction is negligible for the aminolysis by ethyl-butyl-amine and dibutyl-amine. By using the concept of the linear free energy relationship, it was possible to describe the reactivity of an amine in terms of its substituent, in the aminolysis reaction. The logarithm of the aminolysis rate constant can be expressed by a linear function with b_x, which measures the steric hindrance of the amine substituent. It was demonstrated that the two other parameters *a* and *c* are temperature dependent. More investigation on the theoretical interpretation of b_x, *a* and *c* are needed in order to be able to predict the reactivity of different amines for the aminolysis reaction. Such an approach could contribute to finding adequate diamine and optimum operating conditions for the production of Non-isocyanate polyurethane. Evidence showed the occurring of amidation non-desirable side reaction in the aminolysis with glucosamine and chitosan with cyclic carbonated oleaginous substrates like methyl oleate and castor oil.

NIPU material based on castor oil and chitosan showed a significant improvement in the adhesive performance of a commercial pressure sensitive adhesive AUTOADHESAN®. This improvement causes a depletion on cohesive properties.

General conclusion

It was demonstrated in this project that it is possible to carry out the aminolysis of fatty cyclic carbonated material with amine functionalities from polysaccharides like chitosan to generate NIPU materials for adhesive and possibly plasticizer applications. As the best of the knowledge of the author, no previous report on this technique was published before. It can be the entrance door for future investigations working on related aspects as kinetic, thermodynamical, process optimization and new applications.

8. APPENDIX

8.1 Trans-esterification method for castor oil

To make the CO trans-esterification some previous works were consulted.

Reference	KOH catalyst (%w/w)	Metanol (molar ratio metanol/oil)	Temp. (°C)	Time (min)	Yield
(Conceição et al., 2007)	1% w/w	5,8:1	Tamb	30	98%
(Canoira et al., 2010)	1% w/w	5:1	40 °C	60	96%
(Benavides et al., 2007)	0,8% w/w	9:1	Tamb	120	90%

Taking into account this information and the previous experience at the research group in producing vegetable oil biodiesel, the procedure of CO transesterification was as follows: in a glass reaction recipient equipped with reflux system, a known mass of castor oil was placed and heated until a temperature of 60-65 °C. In another recipient, 0,8% (oil weight) of KOH catalyst was dissolved in 5:1 (methanol:oil) moles of methanol. It is important to take into account the free fatty acids (FFA) of the oil in the calculation of the KOH catalyst amount. When the oil is at the reaction temperature, the catalyst-methanol solution was added. The system was allowed to react for 2h with constant reflux and stirring. After the reaction time, the system was placed in a separation funnel. If the FFA content is considerable it is possible not to observe methyl ester-glycerol phase separation in the funnel because of the tensoactive effect of the soap generated from FFA. The upper layer was washed with distilled water until neutrality of the washing water. After that, the COFAME were dried on a rotary evaporator and anhydrous sodium sulfate. The identity of the COFAME was determined by HNMR analysis according to Figure 55. Compared with the HNMR spectrum for CO (Figure 11) it is evident the almost disappearing of the triglyceride-glycerol signal between 4,1-4,3 ppm and the appearance of an ester signal around 3,74 ppm.

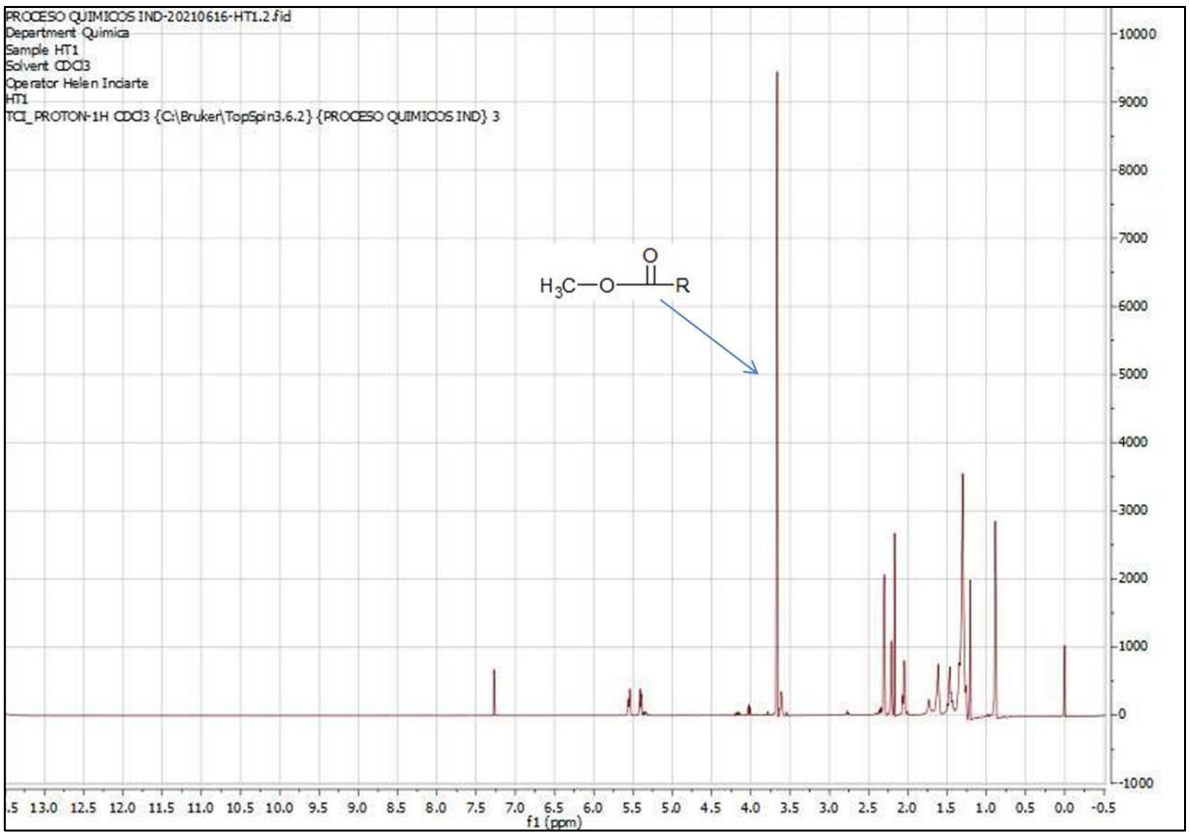

Figure 55. HNMR spectrum for COFAME

8.2 GC-MS results for COFAME

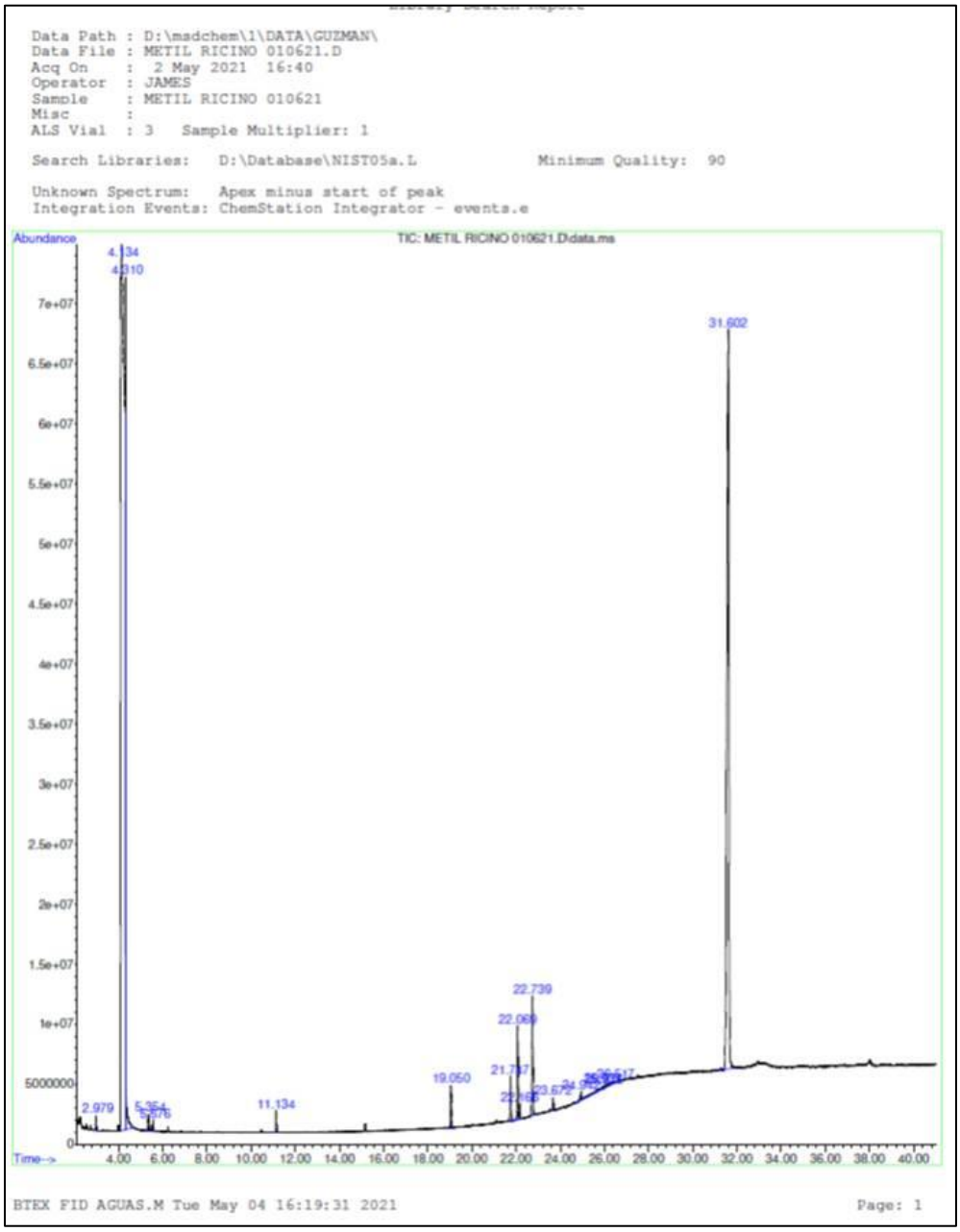

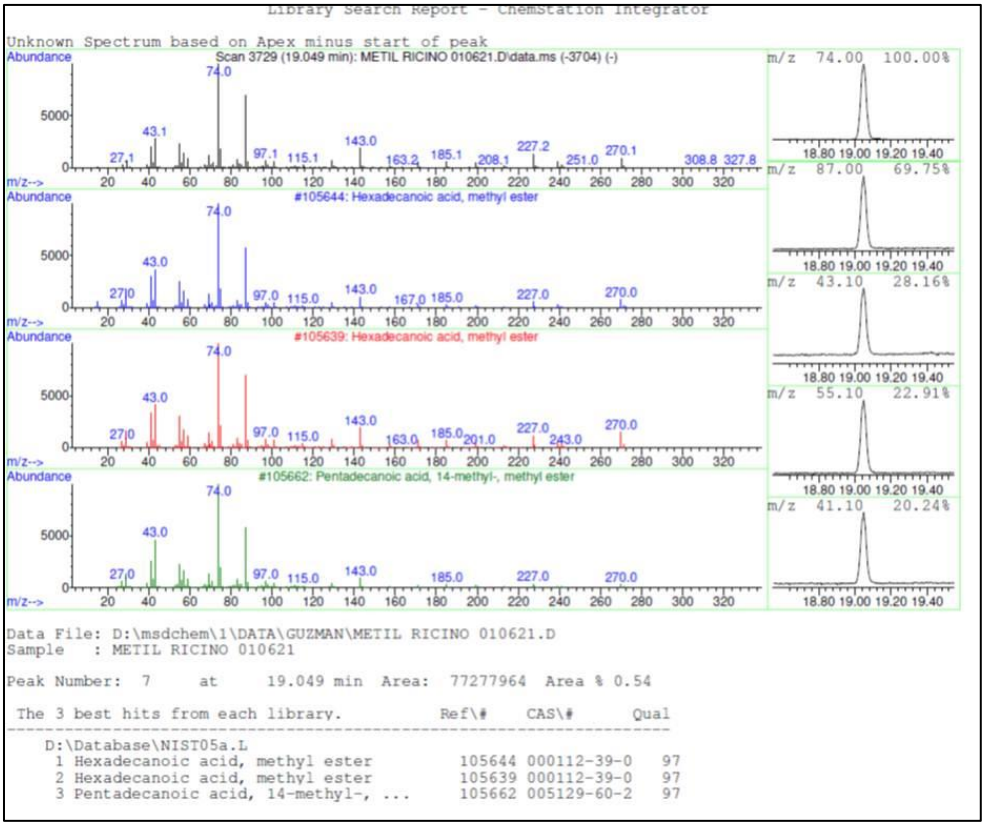
Library Search Report - ChemStation Integrator
Unknown Spectrum based on Apex minus start of peak
Abundance
Scan 3729 (19.049 min): METIL RICINO 010621.D\data.ms (-3704) (-)
#105644: Hexadecanoic acid, methyl ester
#105639: Hexadecanoic acid, methyl ester
#105662: Pentadecanoic acid, 14-methyl-, methyl ester
m/z-->
m/z 74.00 100.00%
m/z 87.00 69.75%
m/z 43.10 28.16%
m/z 55.10 22.91%
m/z 41.10 20.24%
18.80 19.00 19.20 19.40
Data File: D:\msdchem\1\DATA\GUZMAN\METIL RICINO 010621.D
Sample : METIL RICINO 010621
Peak Number: 7 at 19.049 min Area: 77277964 Area % 0.54
The 3 best hits from each library. Ref\# CAS\# Qual
D:\Database\NIST05a.L
1 Hexadecanoic acid, methyl ester 105644 000112-39-0 97
2 Hexadecanoic acid, methyl ester 105639 000112-39-0 97
3 Pentadecanoic acid, 14-methyl-, ... 105662 005129-60-2 97

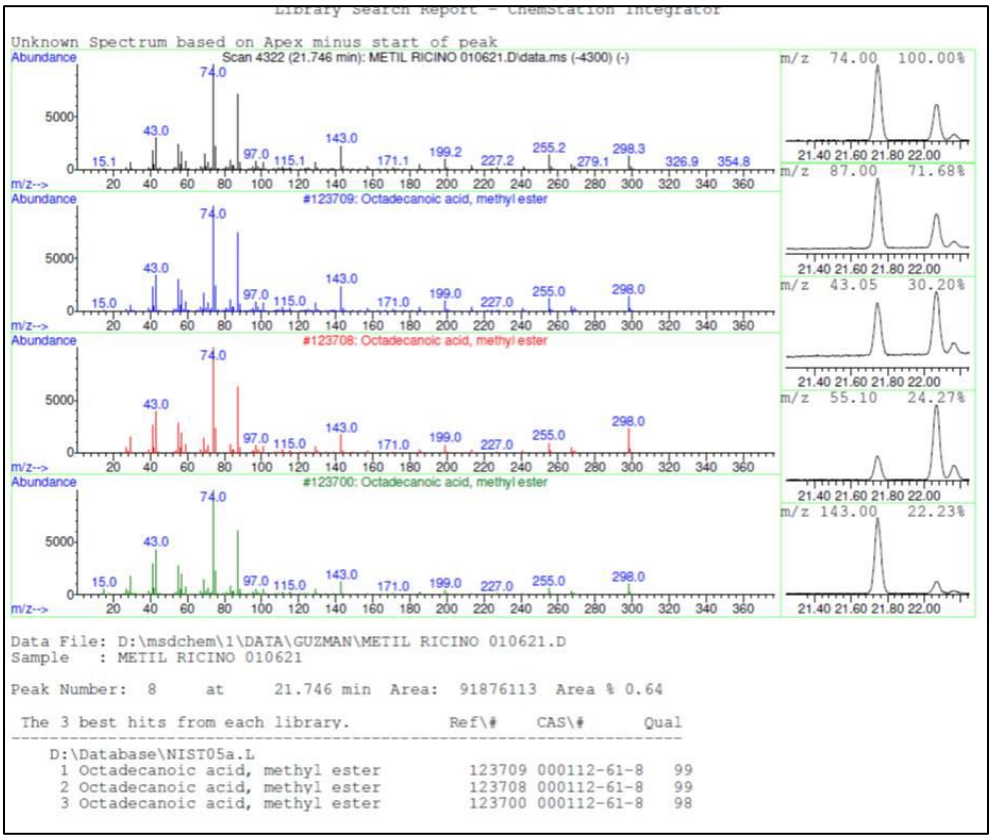
Library Search Report - ChemStation Integrator
Unknown Spectrum based on Apex minus start of peak
Abundance
Scan 4322 (21.746 min): METIL RICINO 010621.D\data.ms (-4300) (-)
#123709: Octadecanoic acid, methyl ester
#123708: Octadecanoic acid, methyl ester
#123700: Octadecanoic acid, methyl ester
m/z-->
m/z 74.00 100.00%
m/z 87.00 71.68%
m/z 43.05 30.20%
m/z 55.10 24.27%
m/z 143.00 22.23%
21.40 21.60 21.80 22.00
Data File: D:\msdchem\1\DATA\GUZMAN\METIL RICINO 010621.D
Sample : METIL RICINO 010621
Peak Number: 8 at 21.746 min Area: 91876113 Area % 0.64
The 3 best hits from each library. Ref\# CAS\# Qual
D:\Database\NIST05a.L
1 Octadecanoic acid, methyl ester 123709 000112-61-8 99
2 Octadecanoic acid, methyl ester 123708 000112-61-8 99
3 Octadecanoic acid, methyl ester 123700 000112-61-8 98

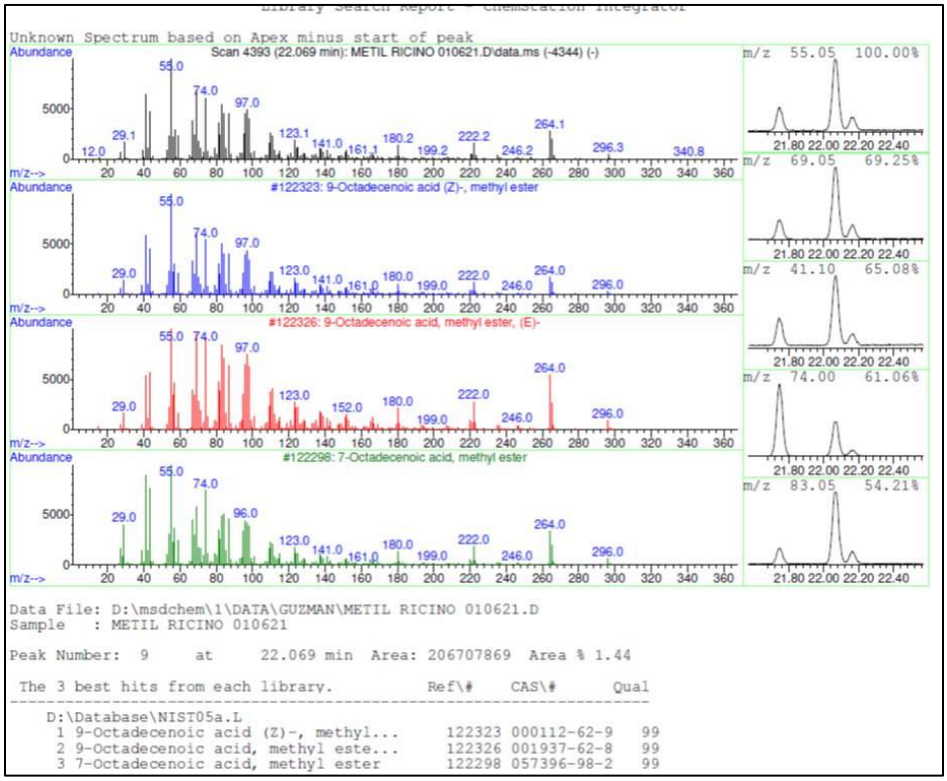
Unknown Spectrum based on Apex minus start of peak
Scan 4393 (22.069 min): METIL RICINO 010621.D\data.ms (-4344) (-)
#122323: 9-Octadecenoic acid (Z)-, methyl ester
#122326: 9-Octadecenoic acid, methyl ester, (E)-
#122298: 7-Octadecenoic acid, methyl ester
m/z 55.05 100.00%
m/z 69.05 69.25%
m/z 41.10 65.08%
m/z 74.00 61.06%
m/z 83.05 54.21%
Data File: D:\msdchem\1\DATA\GUZMAN\METIL RICINO 010621.D
Sample : METIL RICINO 010621
Peak Number: 9 at 22.069 min Area: 206707869 Area % 1.44
The 3 best hits from each library. Ref\# CAS\# Qual
D:\Database\NIST05a.L
1 9-Octadecenoic acid (Z)-, methyl... 122323 000112-62-9 99
2 9-Octadecenoic acid, methyl este... 122326 001937-62-8 99
3 7-Octadecenoic acid, methyl ester 122298 057396-98-2 99

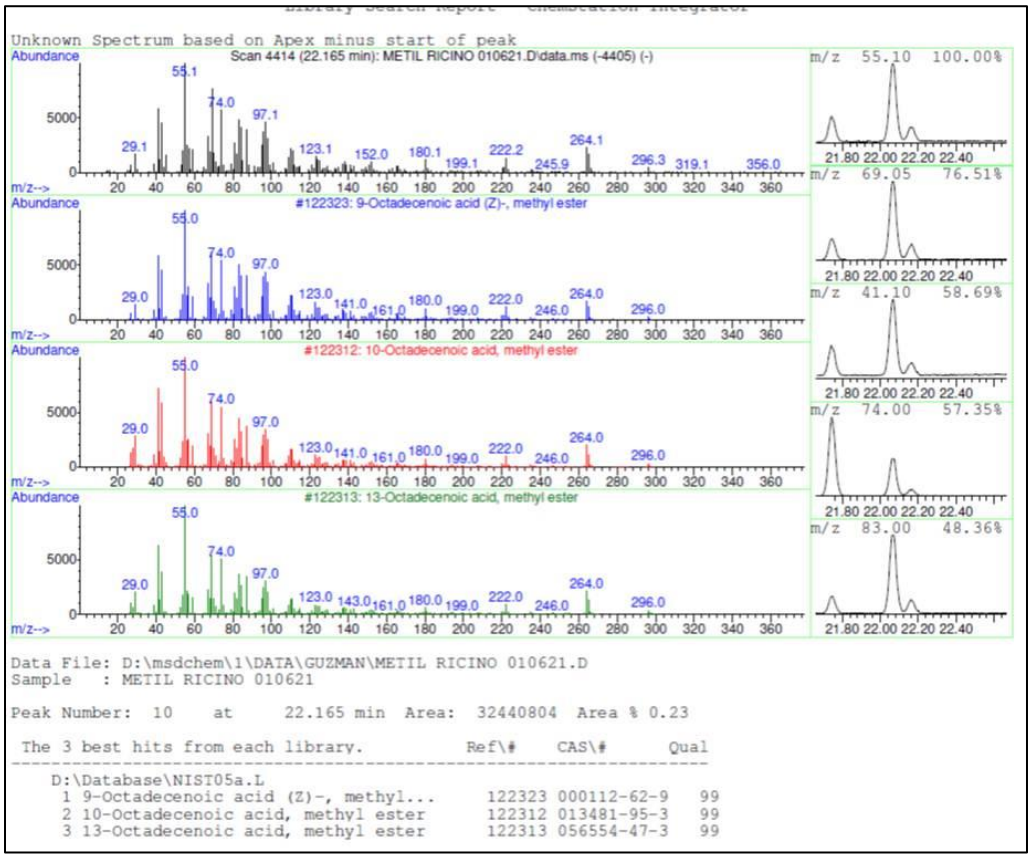
Unknown Spectrum based on Apex minus start of peak
Scan 4414 (22.165 min): METIL RICINO 010621.D\data.ms (-4405) (-)
#122323: 9-Octadecenoic acid (Z)-, methyl ester
#122312: 10-Octadecenoic acid, methyl ester
#122313: 13-Octadecenoic acid, methyl ester
m/z 55.10 100.00%
m/z 69.05 76.51%
m/z 41.10 58.69%
m/z 74.00 57.35%
m/z 83.00 48.36%
Data File: D:\msdchem\1\DATA\GUZMAN\METIL RICINO 010621.D
Sample : METIL RICINO 010621
Peak Number: 10 at 22.165 min Area: 32440804 Area % 0.23
The 3 best hits from each library. Ref\# CAS\# Qual
D:\Database\NIST05a.L
1 9-Octadecenoic acid (Z)-, methyl... 122323 000112-62-9 99
2 10-Octadecenoic acid, methyl ester 122312 013481-95-3 99
3 13-Octadecenoic acid, methyl ester 122313 056554-47-3 99

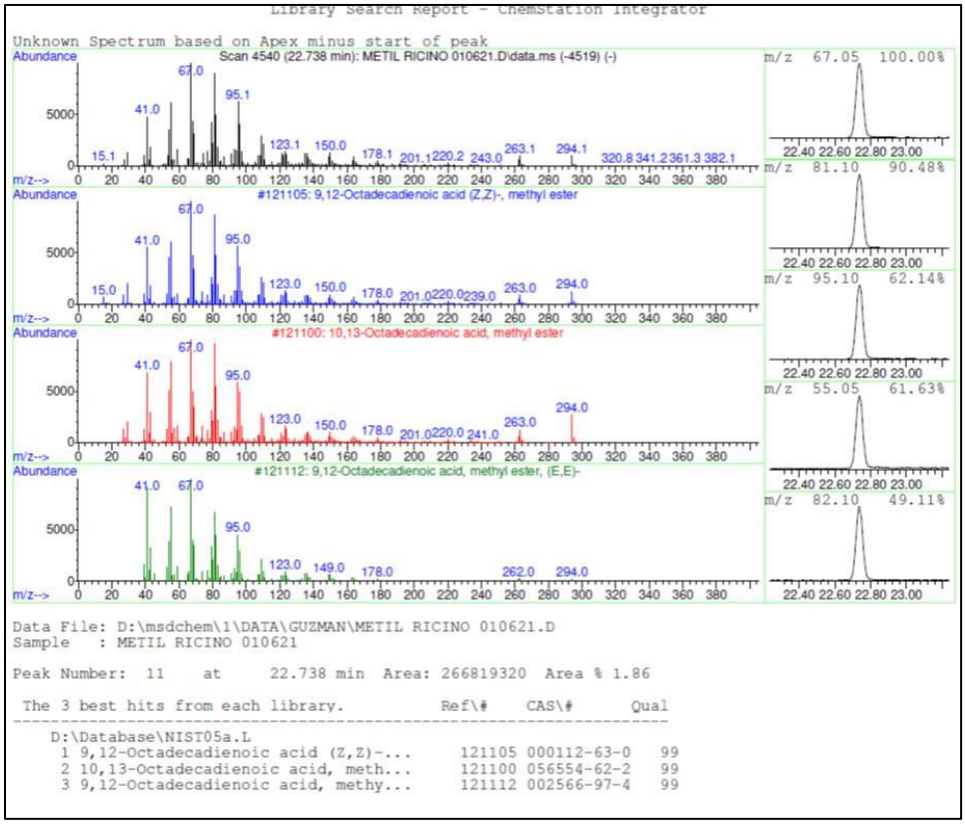
Library Search Report - ChemStation Integrator
Unknown Spectrum based on Apex minus start of peak
Abundance
Scan 4540 (22.738 min): METIL RICINO 010621.D\data.ms (-4519) (-)
#121105: 9,12-Octadecadienoic acid (Z,Z)-, methyl ester
#121100: 10,13-Octadecadienoic acid, methyl ester
#121112: 9,12-Octadecadienoic acid, methyl ester, (E,E)-
m/z-->
m/z 67.05 100.00%
m/z 81.10 90.48%
m/z 95.10 62.14%
m/z 55.05 61.63%
m/z 82.10 49.11%
22.40 22.60 22.80 23.00
Data File: D:\msdchem\1\DATA\GUZMAN\METIL RICINO 010621.D
Sample : METIL RICINO 010621
Peak Number: 11 at 22.738 min Area: 266819320 Area % 1.86
The 3 best hits from each library. Ref\# CAS\# Qual
D:\Database\NIST05a.L
1 9,12-Octadecadienoic acid (Z,Z)-... 121105 000112-63-0 99
2 10,13-Octadecadienoic acid, meth... 121100 056554-62-2 99
3 9,12-Octadecadienoic acid, methy... 121112 002566-97-4 99

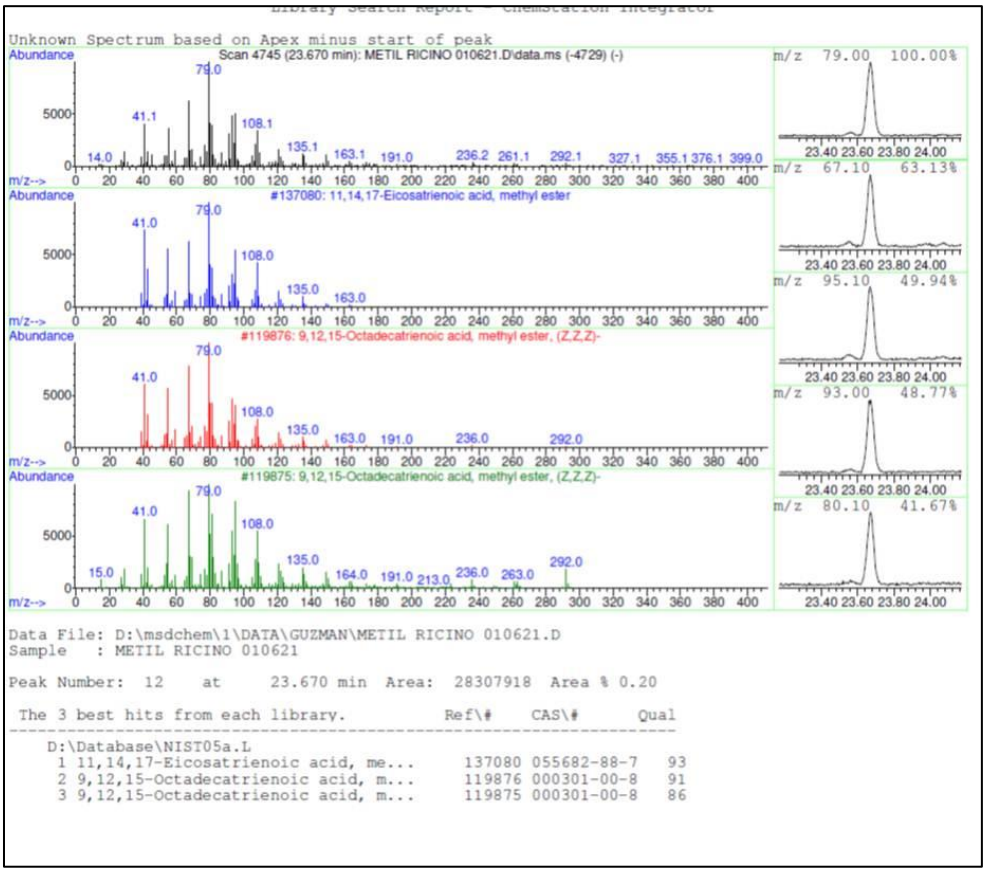
Unknown Spectrum based on Apex minus start of peak
Abundance
Scan 4745 (23.670 min): METIL RICINO 010621.D\data.ms (-4729) (-)
#137080: 11,14,17-Eicosatrienoic acid, methyl ester
#119876: 9,12,15-Octadecatrienoic acid, methyl ester, (Z,Z,Z)-
#119875: 9,12,15-Octadecatrienoic acid, methyl ester, (Z,Z,Z)-
m/z-->
m/z 79.00 100.00%
m/z 67.10 63.13%
m/z 95.10 49.94%
m/z 93.00 48.77%
m/z 80.10 41.67%
23.40 23.60 23.80 24.00
Data File: D:\msdchem\1\DATA\GUZMAN\METIL RICINO 010621.D
Sample : METIL RICINO 010621
Peak Number: 12 at 23.670 min Area: 28307918 Area % 0.20
The 3 best hits from each library. Ref\# CAS\# Qual
D:\Database\NIST05a.L
1 11,14,17-Eicosatrienoic acid, me... 137080 055682-88-7 93
2 9,12,15-Octadecatrienoic acid, m... 119876 000301-00-8 91
3 9,12,15-Octadecatrienoic acid, m... 119875 000301-00-8 86

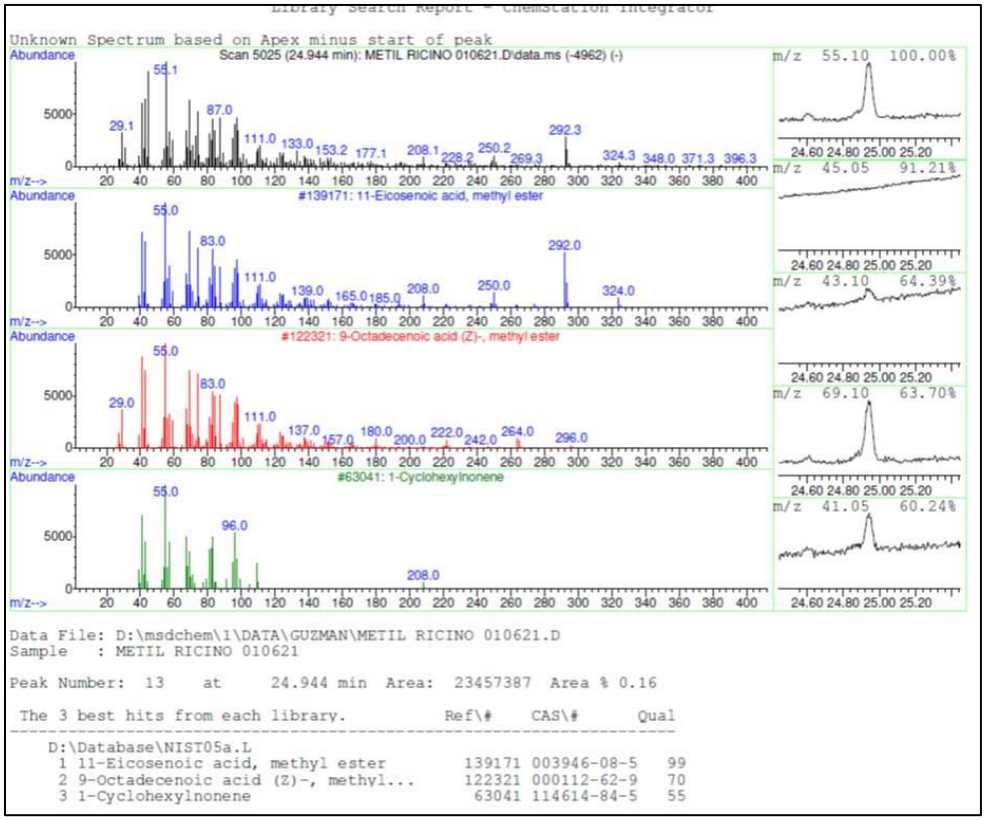
Library Search Report - ChemStation Integrator
Unknown Spectrum based on Apex minus start of peak
Abundance
Scan 5025 (24.944 min): METIL RICINO 010621.D\data.ms (-4962) (-)
#139171: 11-Eicosenoic acid, methyl ester
#122321: 9-Octadecenoic acid (Z)-, methyl ester
#63041: 1-Cyclohexylnonene
m/z-->
m/z 55.10 100.00%
m/z 45.05 91.21%
m/z 43.10 64.39%
m/z 69.10 63.70%
m/z 41.05 60.24%
24.60 24.80 25.00 25.20
Data File: D:\msdchem\1\DATA\GUZMAN\METIL RICINO 010621.D
Sample : METIL RICINO 010621
Peak Number: 13 at 24.944 min Area: 23457387 Area % 0.16
The 3 best hits from each library. Ref\# CAS\# Qual
D:\Database\NIST05a.L
1 11-Eicosenoic acid, methyl ester 139171 003946-08-5 99
2 9-Octadecenoic acid (Z)-, methyl... 122321 000112-62-9 70
3 1-Cyclohexylnonene 63041 114614-84-5 55

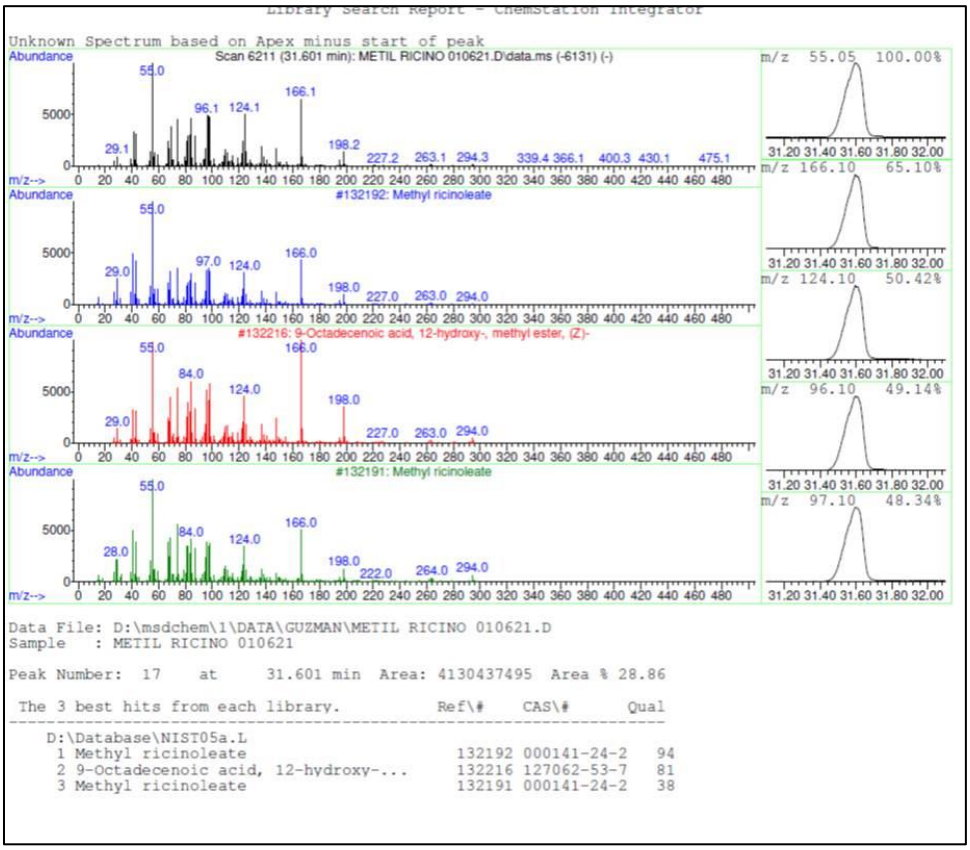
Library Search Report - ChemStation Integrator
Unknown Spectrum based on Apex minus start of peak
Abundance
Scan 6211 (31.601 min): METIL RICINO 010621.D\data.ms (-6131) (-)
#132192: Methyl ricinoleate
#132216: 9-Octadecenoic acid, 12-hydroxy-, methyl ester, (Z)-
#132191: Methyl ricinoleate
m/z-->
m/z 55.05 100.00%
m/z 166.10 65.10%
m/z 124.10 50.42%
m/z 96.10 49.14%
m/z 97.10 48.34%
31.20 31.40 31.60 31.80 32.00
Data File: D:\msdchem\1\DATA\GUZMAN\METIL RICINO 010621.D
Sample : METIL RICINO 010621
Peak Number: 17 at 31.601 min Area: 4130437495 Area % 28.86
The 3 best hits from each library. Ref\# CAS\# Qual
D:\Database\NIST05a.L
1 Methyl ricinoleate 132192 000141-24-2 94
2 9-Octadecenoic acid, 12-hydroxy-... 132216 127062-53-7 81
3 Methyl ricinoleate 132191 000141-24-2 38

8.3 Castor Oil molecular mass estimation from GC analysis

The CO Mw can be estimated with the fatty acid composition of **Table 6** as follows:

Considering the glycerin portion and taking out the hydrogen of bonding, a triglyceride composed by one of the fatty acids has a Mw of:

$41 + (Mw_i - 1) * 3$ where Mw_i is the molecular mass of the i[th] fatty acid.

The estimated castor oil molecular mass of (Mw_{CO}) can be calculated with the composition-weighted sum of all triglyceride molecular weights:

$$Mw_{CO} = \sum_{i=1}^{n} X_i[41 + (Mw_i - 1) * 3]$$

Where X_i is the fraction composition of the i[th] fatty acid.

8.4 Castor Oil Hydroxyl value estimation

$$2{,}39\frac{OH}{molec} * \frac{6{,}02 * 10^{23}\ molec}{1\ mol\ \ molec} * \frac{1\ mol\ OH}{6{,}02 * 10^{23}\ OH} * \frac{1\ mol\ KOH}{1\ mol\ OH} * \frac{56{,}1\ g\ KOH}{1\ mol\ KOH} *$$
$$\frac{1000\ mg\ KOH}{1\ g\ KOH} * \frac{1\ mol\ molec}{923{,}71\ g} = 145{,}15\ \frac{mg\ KOH}{g}$$

8.5 Derivation of some equations for CO epoxidation calculations

DB mol

$$DB_n = CO_M\ g * \frac{IV\ gI}{100\ g} * \frac{1\ mol\ I}{126.9\ gI} * \frac{1\ mol\ DB}{2\ mol\ I} = \frac{CO_M * IV}{25380}$$

Selectivity

In this work, selectivity is defined as the ratio between the moles of epoxide groups (desired product) produced and the moles of double bonds reacted (limiting reactant):

$$\%S = \frac{E_n}{DB_n\ reacted}$$

This definition can be found in different sources in the literature (Coker, 2001; Doraiswamy & Uner, 2013; Harriot, 2003; Missen et al., 1999; Nauman, 2007).

This is for holding the useful relationship:

$$Yield = \%C * \%S$$

There are different definitions for selectivity and conversion. For a deep discussion about this topic, see (Pirola et al., 2013).

Since the oxirane-oxygen content is a percentage, the moles of epoxide groups per 100 grams of oil can be calculated from the oxirane value as follows:

$$E_n = OOC * \frac{1\ mol\ O}{16\ g\ O} * \frac{1\ mol\ Epox}{1\ mol\ O} = \frac{OOC}{16}$$

Since the iodine value has unit of grams of iodine per 100 grams of oil, the moles of double bonds reacted per 100 g of oil are:

$$\left(IV_i - IV_f\right) * \frac{1\ mol\ I}{126{,}9\ g\ I} * \frac{1\ mol\ DB}{2\ mol\ I} = \frac{\left(IV_i - IV_f\right)}{253{,}8}$$

Then, the selectivity is

$$\%S = \frac{\frac{OOC}{16}}{\frac{\left(IV_i - IV_f\right)}{253{,}8}} * 100 = \frac{1586{,}25 * OOC}{IV_i - IV_f}$$

Theoretical Oxirane-Oxygen Content

If 100 g of an unsaturated substrate with an iodine value of IV_i are epoxidized with 100% of conversion, they are obtained…

$\left(100g + DB_n * 16\ \frac{g\ O}{mol\ O}\right)$g of epoxidized substrate, where

With a 100% conversion, DB_n are the same moles of epoxide groups produced and they can be estimated as follows:

$$DB_n = IV_i * \frac{1\ mol\ I}{126{,}9\ g\ I} * \frac{1\ mol\ DB}{2\ mol\ I} = \frac{IV_i}{253{,}8}$$

Since the oxirane value is the weight percentage of oxirane-oxygen, it is:

$$OOC_T = \frac{\frac{IV_i}{253{,}8} mol\ O * 16\ \frac{g\ O}{mol\ O}}{\left(100g + \frac{IV_i}{253{,}8} mol\ O * 16\ \frac{g\ O}{mol\ O}\right)} * 100 = \frac{100 * IV_i}{(1586{,}25 + IV_i)}\ \%$$

8.6 Validation of ANOVA assumptions in particle size experiment

```
Code for particle sizes:
X1= #100
X2= #50
X3= #35

Call:
lm(formula = Conv ~ Size, data = diseño)

Coefficients:
(Intercept)       SizeX2       SizeX3
     65.573       -2.510       -4.335

Coefficients:
            Estimate Std. Error t value Pr(>|t|)
(Intercept)   65.573      1.164  56.336  2.1e-09 ***
SizeX2        -2.510      1.646  -1.525   0.1781
SizeX3        -4.335      1.646  -2.634   0.0389 *
---
Signif. codes:  0 ‘***’ 0.001 ‘**’ 0.01 ‘*’ 0.05 ‘.’ 0.1 ‘ ’ 1

Residual standard error: 2.016 on 6 degrees of freedom
Multiple R-squared:  0.5382,Adjusted R-squared:  0.3843
F-statistic: 3.497 on 2 and 6 DF,  p-value: 0.09845
```

- Shapiro-Wilk normality test

```
data:  diseño$resid
W = 0.93394, p-value = 0.5198
```

- Levene's Test for Homogeneity of Variance (center = median)

```
      Df F value Pr(>F)
group  2  0.5036 0.6278
       6
```

- Independence test

```
data:  as.factor(diseño$resid > median(diseño$resid))
Standard Normal = 1.1245, p-value = 0.2608
alternative hypothesis: two.sided
```

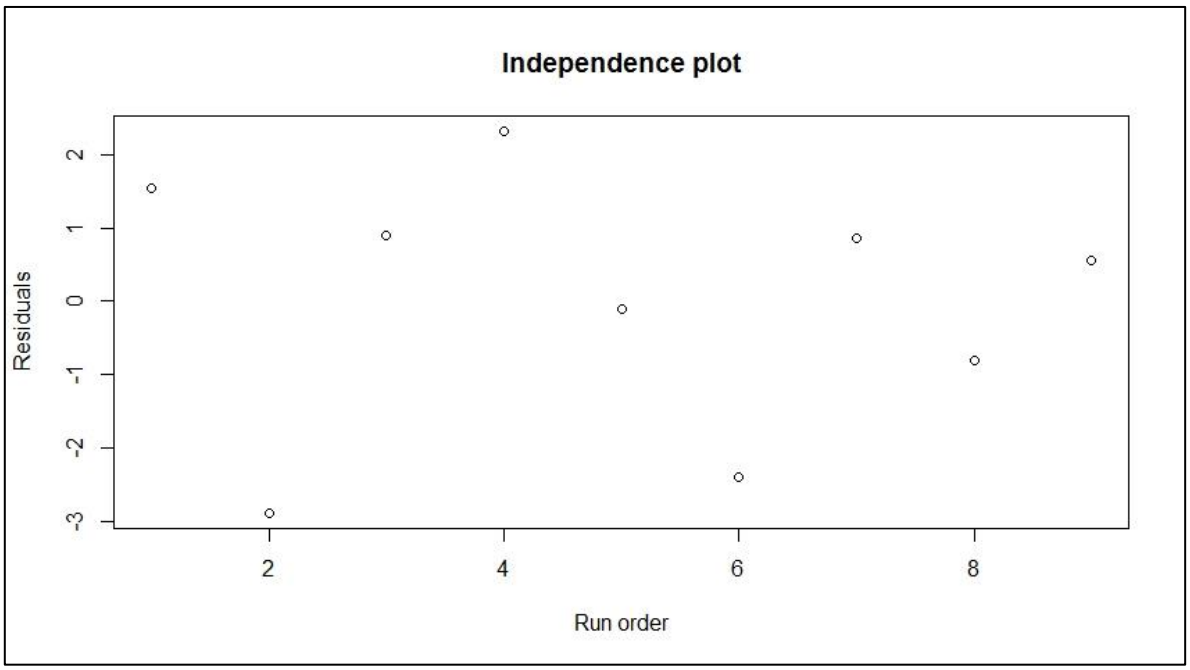

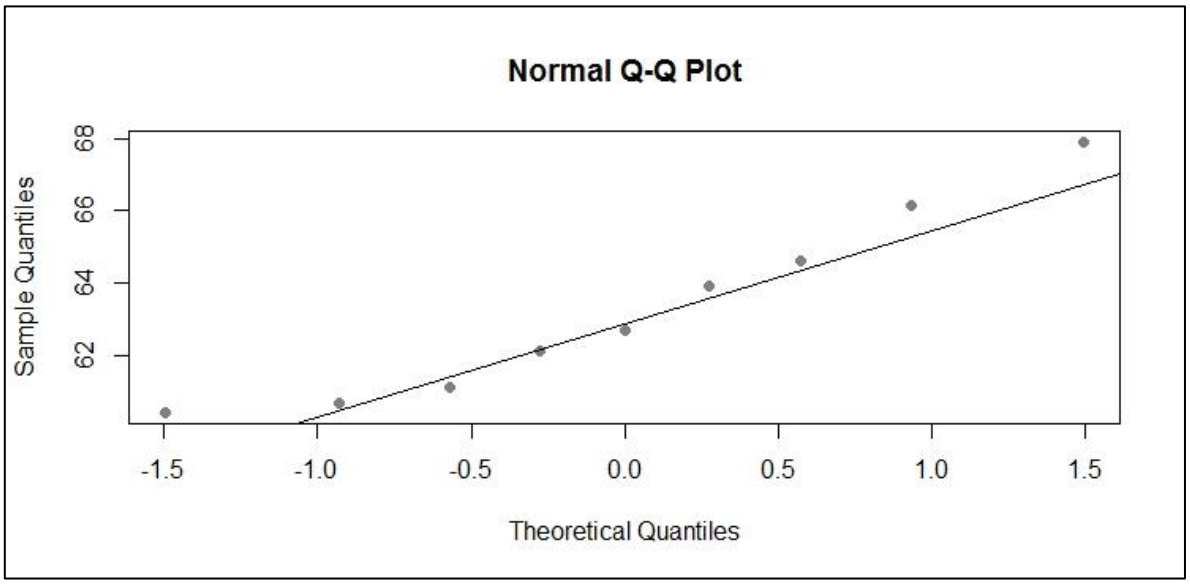

8.7 Residual and normal probability plots for 2^3 ANOVA

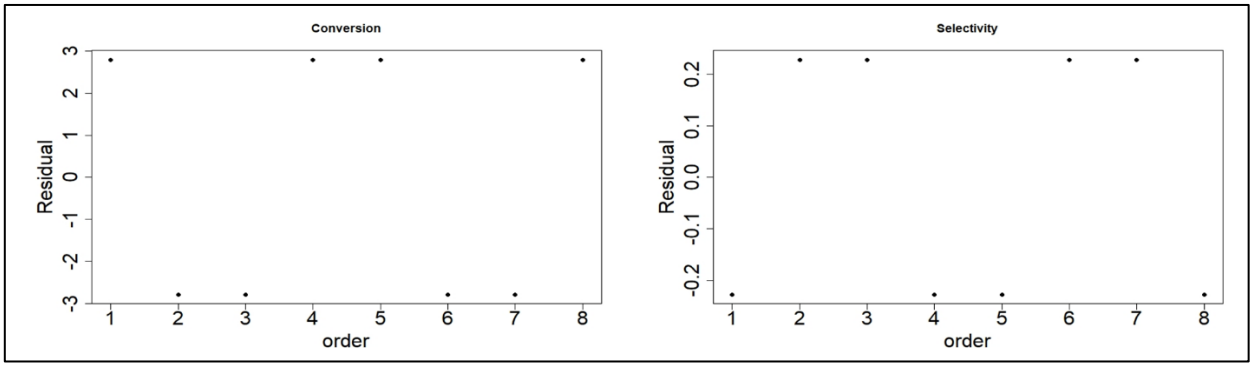
Conversion
Residual
order
Selectivity
Residual
order

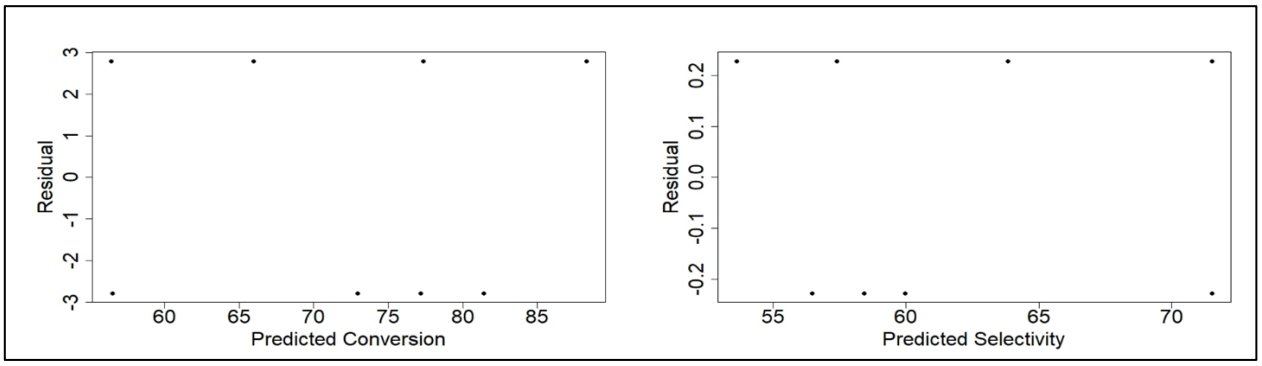
Residual
Predicted Conversion
Residual
Predicted Selectivity

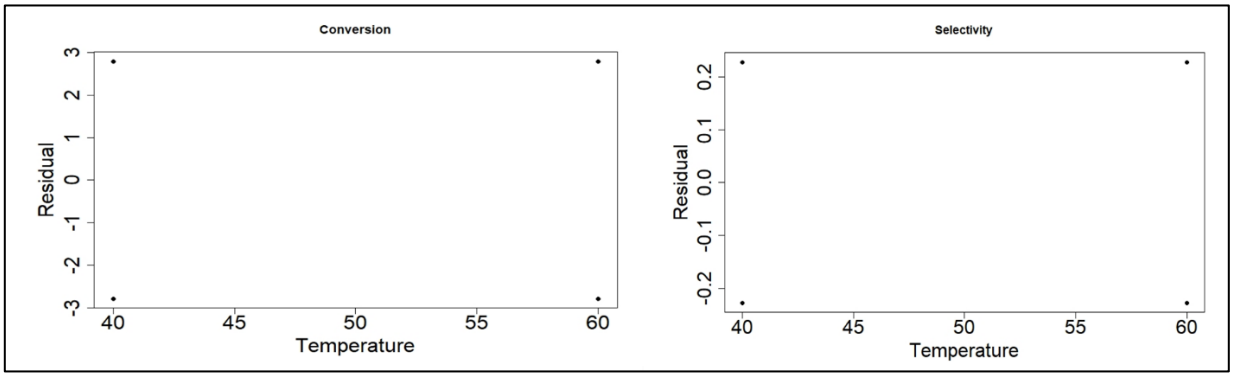
Conversion
Residual
Temperature
Selectivity
Residual
Temperature

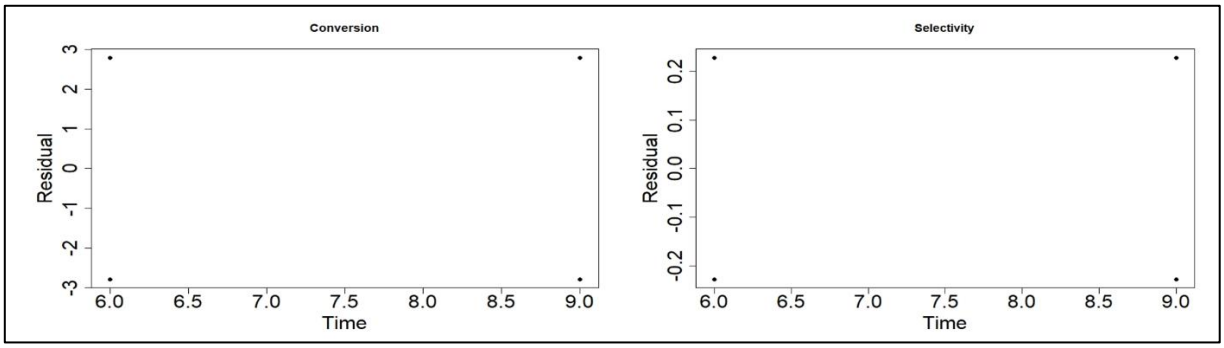
Conversion
Residual
Time
Selectivity
Residual
Time

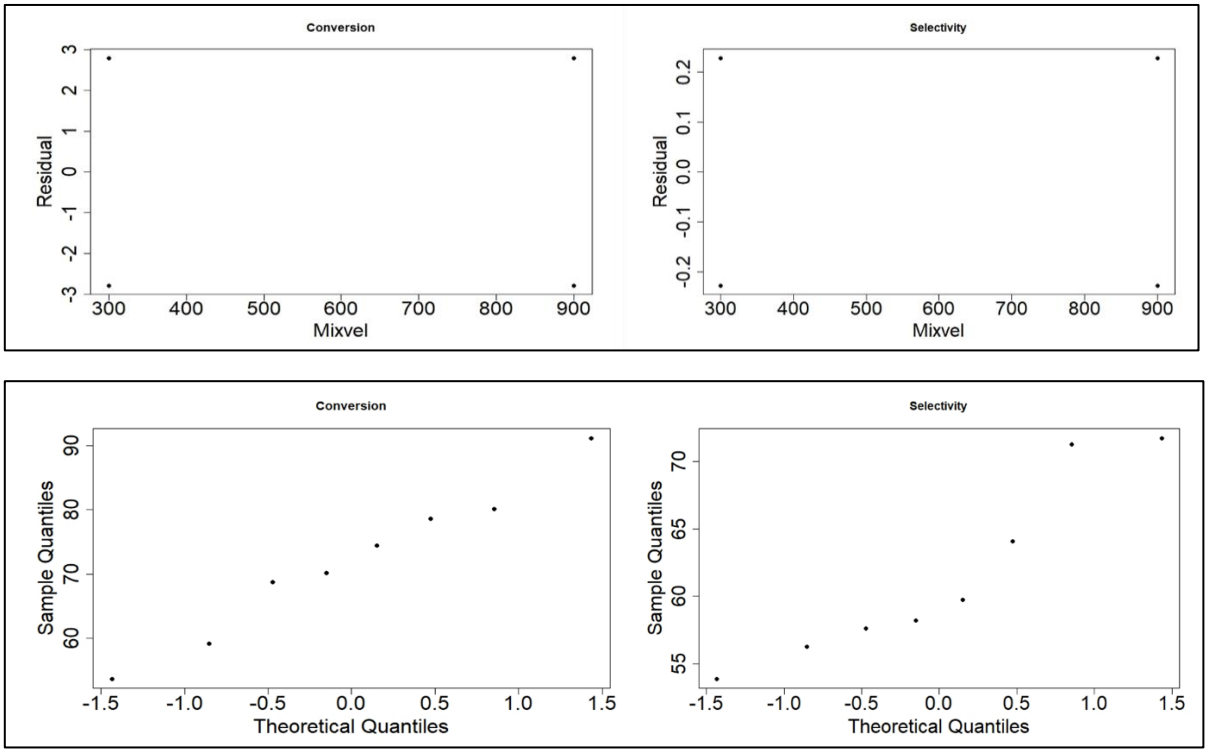

8.8 Residual and normal probability plots for 2^2 ANOVA

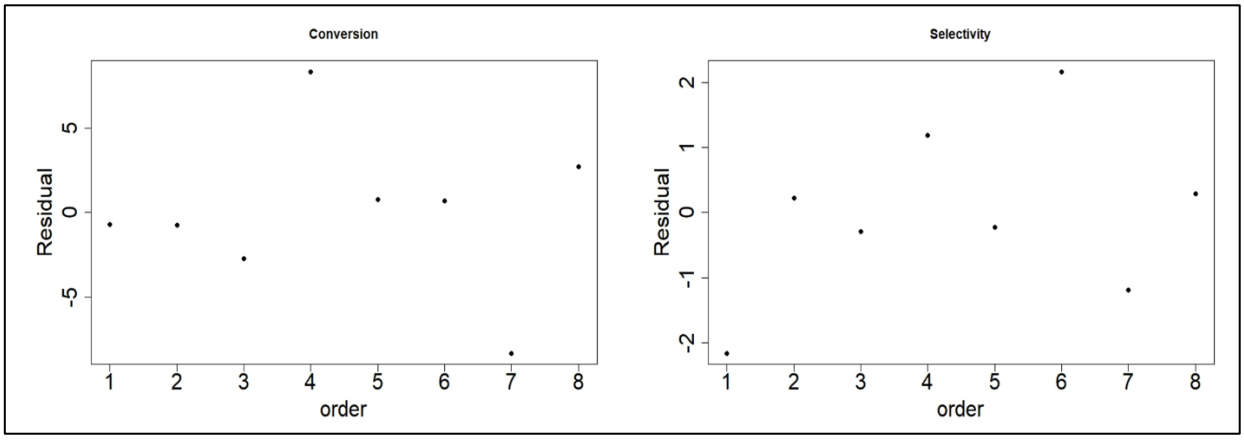

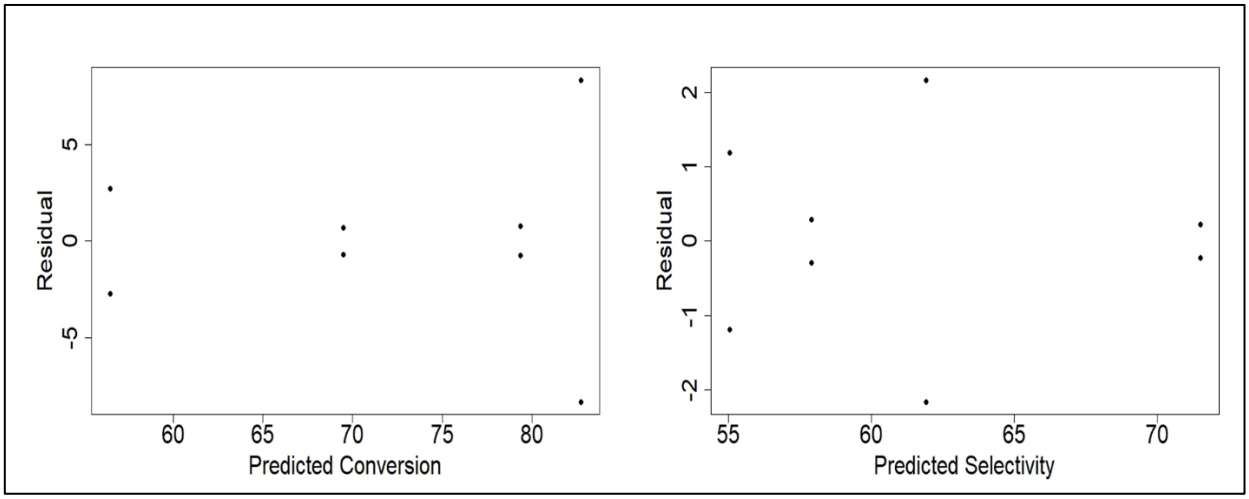
Residual
5
0
-5
60
65
70
75
80
Predicted Conversion
Residual
2
1
0
-1
-2
55
60
65
70
Predicted Selectivity

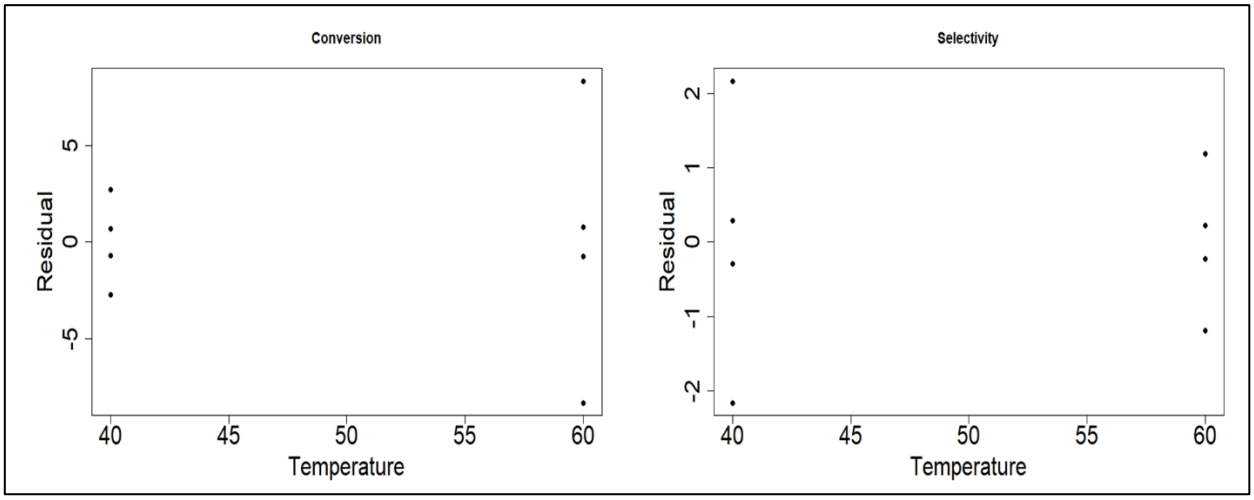
Conversion
Residual
5
0
-5
40
45
50
55
60
Temperature
Selectivity
Residual
2
1
0
-1
-2
40
45
50
55
60
Temperature

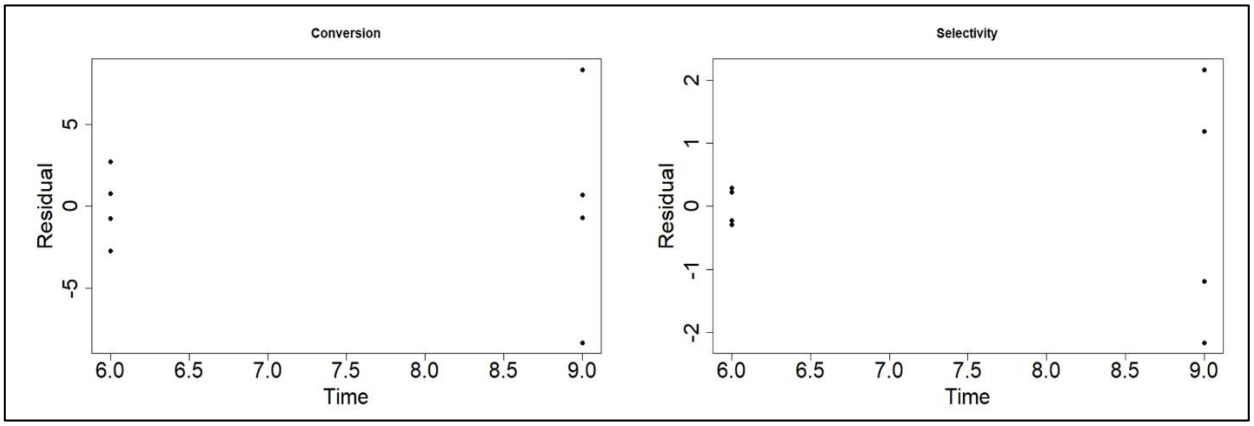
Conversion
Residual
5
0
-5
6.0
6.5
7.0
7.5
8.0
8.5
9.0
Time
Selectivity
Residual
2
1
0
-1
-2
6.0
6.5
7.0
7.5
8.0
8.5
9.0
Time

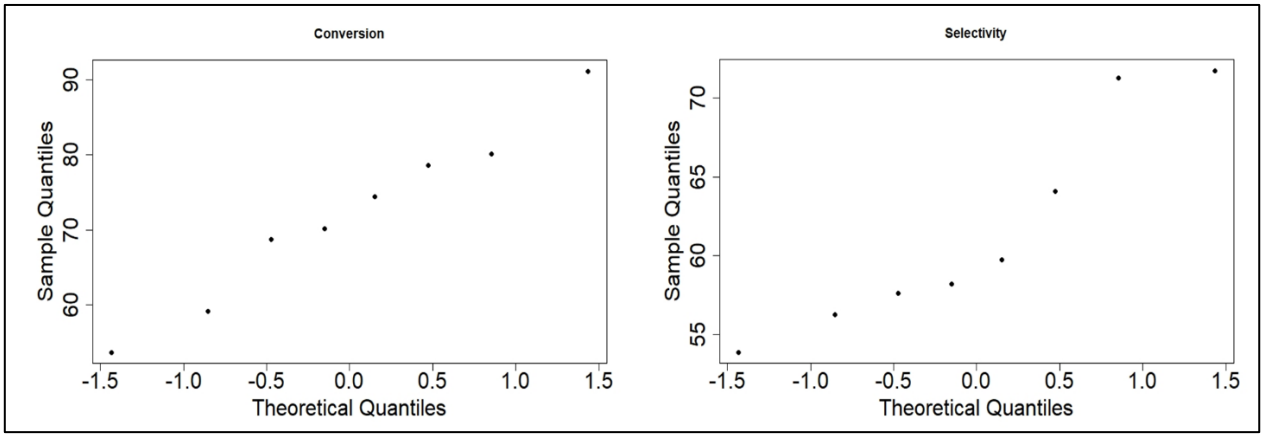

8.9 2^2 factorial design data transformed ($y' = 1/y$^2) and residual analysis

Table A1.Response variable data converted

Run.Ord.	Stn.Ord.	Temp	Time	Conv	Selec
1	7	40	9	0.0002114472	0.0002801071
2	2	60	6	0.0001618245	0.0001943562
3	5	40	6	0.0003463908	0.0003011990
4	4	60	9	0.0001205199	0.0003161618
5	6	60	6	0.0001557046	0.0001968179
6	3	40	9	0.0002030361	0.0002436074
7	8	60	9	0.0001807053	0.0003445927
8	1	40	6	0.0002852396	0.0002952256

```
Call:
lm(formula = Conv7 ~ Temp + Time + Temp:Time, data = fact7r)

Coefficients:
(Intercept)         Temp         Time    Temp:Time
  1.249e-03   -1.789e-05   -1.031e-04    1.674e-06

            Df    Sum Sq   Mean Sq F value  Pr(>F)
Temp         1 2.283e-08 2.283e-08  24.449 0.00779 **
Time         1 6.812e-09 6.812e-09   7.296 0.05403 .
Temp:Time    1 5.042e-09 5.042e-09   5.400 0.08080 .
Residuals    4 3.735e-09 9.340e-10
---
Signif. codes:  0 ‘***’ 0.001 ‘**’ 0.01 ‘*’ 0.05 ‘.’ 0.1 ‘ ’ 1

Call:
lm(formula = Conv7 ~ Temp + Time + Temp:Time, data = fact7r)
```

```
Residuals:
  1             2          3         4           5         6
4.206e-06  3.060e-06  3.058e-05 -3.009e-05 -3.060e-06 -4.206e-06
   7          8
3.009e-05 -3.058e-05

Coefficients:
              Estimate Std. Error t value Pr(>|t|)
(Intercept)  1.249e-03  2.809e-04   4.446   0.0113 *
Temp        -1.789e-05  5.509e-06  -3.248   0.0314 *
Time        -1.031e-04  3.673e-05  -2.808   0.0484 *
Temp:Time    1.674e-06  7.202e-07   2.324   0.0808 .
---
Signif. codes:  0 ‘***’ 0.001 ‘**’ 0.01 ‘*’ 0.05 ‘.’ 0.1 ‘ ’ 1

Residual standard error: 3.056e-05 on 4 degrees of freedom
Multiple R-squared:  0.9028,    Adjusted R-squared:  0.8299
F-statistic: 12.38 on 3 and 4 DF,  p-value: 0.01714

Call:
lm(formula = Selec7 ~ Temp + Time + Temp:Time, data = fact7r)

Coefficients:
(Intercept)         Temp         Time    Temp:Time
  1.261e-03   -2.225e-05   -1.262e-04    2.852e-06

            Df    Sum Sq   Mean Sq F value  Pr(>F)
Temp         1 5.820e-10 5.820e-10   2.132 0.21803
Time         1 4.845e-09 4.845e-09  17.760 0.01354 *
Temp:Time    1 1.464e-08 1.464e-08  53.688 0.00185 **
Residuals    4 1.091e-09 2.730e-10
---
Signif. codes:  0 ‘***’ 0.001 ‘**’ 0.01 ‘*’ 0.05 ‘.’ 0.1 ‘ ’ 1

Call:
lm(formula = Selec7 ~ Temp + Time + Temp:Time, data = fact7r)

Residuals:

   1          2          3          4          5          6
1.825e-05 -1.231e-06   2.987e-06 -1.422e-05   1.231e-06 -1.825e-05
   7          8
1.422e-05 -2.987e-06

Coefficients:
              Estimate Std. Error t value Pr(>|t|)
(Intercept)  1.261e-03  1.518e-04   8.304  0.00115 **
Temp        -2.225e-05  2.977e-06  -7.471  0.00172 **
Time        -1.262e-04  1.985e-05  -6.358  0.00314 **
Temp:Time    2.852e-06  3.893e-07   7.327  0.00185 **
---
```

```
Signif. codes:  0 ‘***’ 0.001 ‘**’ 0.01 ‘*’ 0.05 ‘.’ 0.1 ‘ ’ 1

Residual standard error: 1.652e-05 on 4 degrees of freedom
Multiple R-squared:  0.9484,    Adjusted R-squared:  0.9098
F-statistic: 24.53 on 3 and 4 DF,  p-value: 0.004898
```

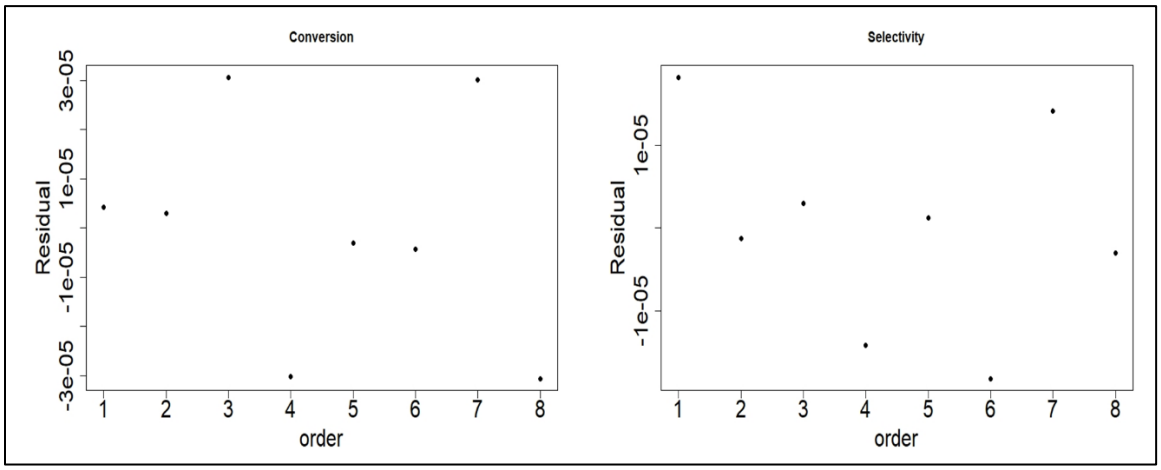

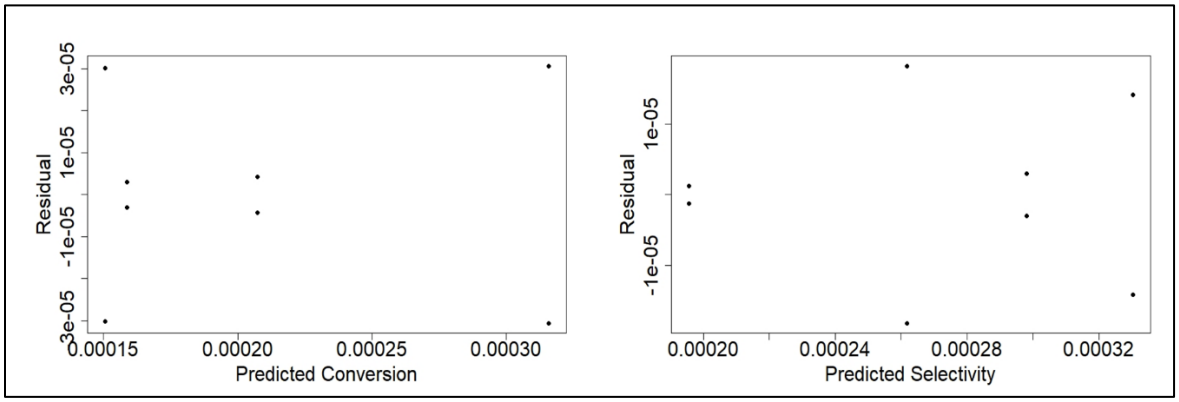

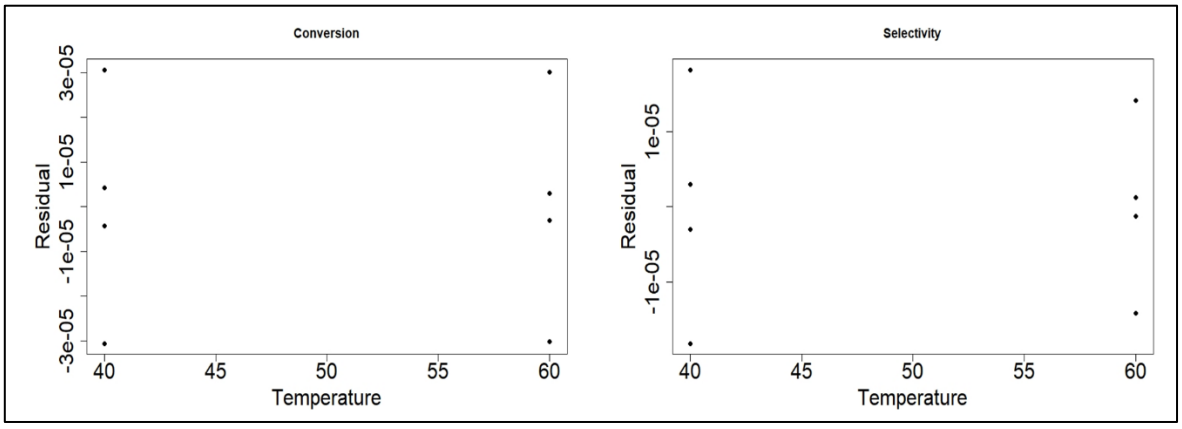

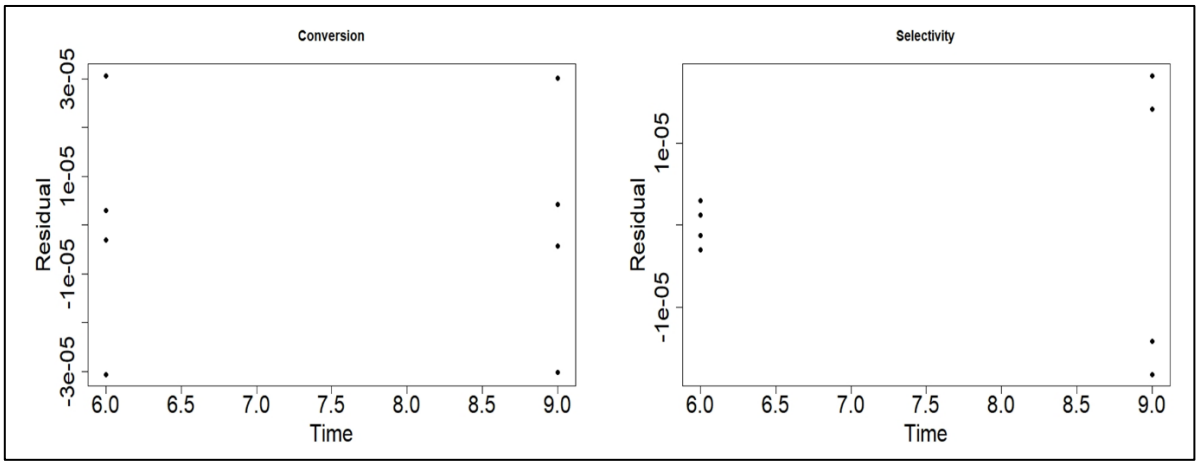

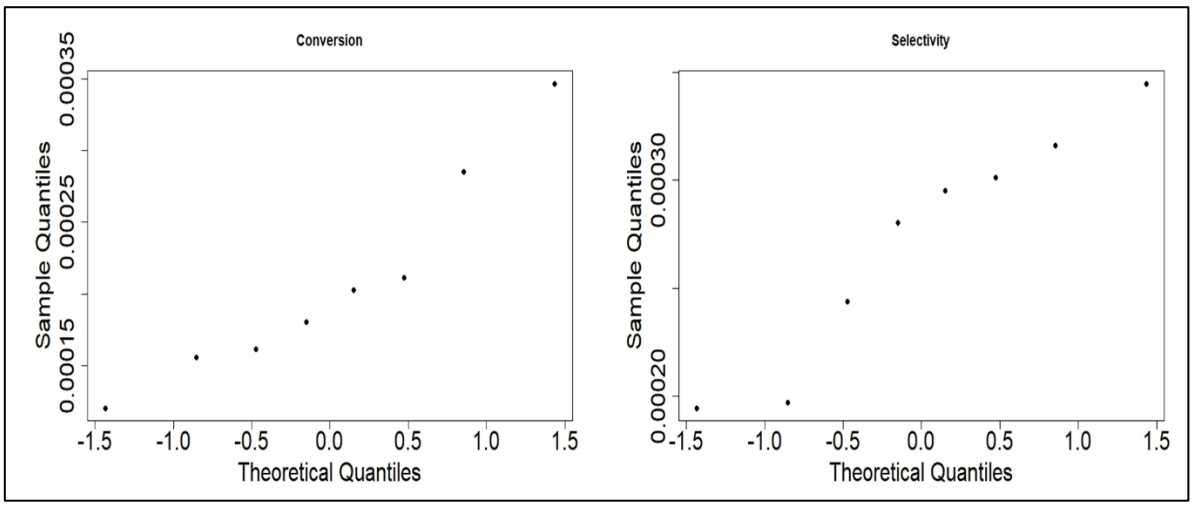

8.10 PURE QUADRATIC CURVATURE ANAYSIS FOR THE 2^2 EXPERIMENTAL DESIGN

Run.Ord.	Stn.Ord.	Temp	Time	Conv	Selec
1	7	40	9.0	0.0002114472	0.0002801071
2	10	50	7.5	0.0001490480	0.0001917809
3	13	50	7.5	0.0001522654	0.0002065528
4	2	60	6.0	0.0001618245	0.0001943562
5	5	40	6.0	0.0003463908	0.0003011990
6	4	60	9.0	0.0001205199	0.0003161618
7	12	50	7.5	0.0001443231	0.0002109561
8	6	60	6.0	0.0001557046	0.0001968179
9	9	50	7.5	0.0001566414	0.0003057453
10	11	50	7.5	0.0001916216	0.0002062563

11	3	40	9.0	0.0002030361	0.0002436074
12	8	60	9.0	0.0001807053	0.0003445927
13	14	50	7.5	0.0001788732	0.0002881522
14	1	40	6.0	0.0002852396	0.0002952256

```
Call:
lm(formula = Conv ~ Temp + Time + Temp:Time + I(Temp^2) +
I(Time^2),
    data = fact6r)

Coefficients:
(Intercept)  Temp        Time       I(Temp^2) (Time^2) Temp:Time
2.352e-03   -6.387e-05  -1.031e-04  4.598e-07  NA      1.674e-06

            Df    Sum Sq   Mean Sq F value   Pr(>F)
Temp         1 2.283e-08 2.283e-08   37.35 0.000177 ***
Time         1 6.812e-09 6.812e-09   11.15 0.008680 **
I(Temp^2)    1 7.248e-09 7.248e-09   11.86 0.007347 **
Temp:Time    1 5.042e-09 5.042e-09    8.25 0.018409 *
Residuals    9 5.501e-09 6.110e-10
---
Signif. codes:  0 ‘***’ 0.001 ‘**’ 0.01 ‘*’ 0.05 ‘.’ 0.1 ‘ ’ 1

Call:
lm(formula = Conv ~ Temp + Time + Temp:Time + I(Temp^2) +
I(Time^2),
    data = fact6r)

Residuals:
       Min         1Q     Median         3Q        Max
-3.058e-05 -1.228e-05 -3.633e-06  1.361e-05  3.058e-05

Coefficients: (1 not defined because of singularities)
              Estimate Std. Error t value Pr(>|t|)
(Intercept)  2.352e-03  3.975e-04   5.918 0.000224 ***
Temp        -6.387e-05  1.408e-05  -4.538 0.001410 **
Time        -1.031e-04  2.971e-05  -3.471 0.007035 **
I(Temp^2)    4.598e-07  1.335e-07   3.444 0.007347 **
I(Time^2)           NA         NA      NA       NA
Temp:Time    1.674e-06  5.827e-07   2.872 0.018409 *
---
Signif. codes:  0 ‘***’ 0.001 ‘**’ 0.01 ‘*’ 0.05 ‘.’ 0.1 ‘ ’ 1

Residual standard error: 2.472e-05 on 9 degrees of freedom
Multiple R-squared:  0.884,     Adjusted R-squared:  0.8325
F-statistic: 17.15 on 4 and 9 DF,  p-value: 0.0003066
```

```
Call:
lm(formula = Selec1 ~ Temp + Time + Temp:Time + I(Temp^2) +
I(Time^2),
    data = fact6r)

Coefficients:
(Intercept)   Temp      Time       I(Temp^2)  I(Time^2) Temp:Time
2.139e-03  -5.885e-05  -1.262e-04   3.660e-07   NA       2.852e-06

            Df    Sum Sq   Mean Sq F value Pr(>F)
Temp         1 5.820e-10 5.820e-10   0.403 0.5416
Time         1 4.845e-09 4.845e-09   3.353 0.1003
I(Temp^2)    1 4.593e-09 4.593e-09   3.179 0.1083
Temp:Time    1 1.464e-08 1.464e-08  10.137 0.0111 *
Residuals    9 1.300e-08 1.445e-09
---
Signif. codes:  0 ‘***’ 0.001 ‘**’ 0.01 ‘*’ 0.05 ‘.’ 0.1 ‘ ’ 1

Call:
lm(formula = Selec1 ~ Temp + Time + Temp:Time + I(Temp^2) +
I(Time^2),
    data = fact6r)

Residuals:
       Min         1Q     Median         3Q        Max
-4.313e-05 -2.253e-05 -2.109e-06  1.141e-05  7.084e-05

Coefficients: (1 not defined because of singularities)
             Estimate Std. Error t value Pr(>|t|)
(Intercept)  2.139e-03  6.111e-04   3.500  0.00672 **
Temp        -5.885e-05  2.164e-05  -2.719  0.02364 *
Time        -1.262e-04  4.568e-05  -2.763  0.02201 *
I(Temp^2)    3.660e-07  2.053e-07   1.783  0.10826
I(Time^2)           NA         NA      NA       NA
Temp:Time    2.852e-06  8.959e-07   3.184  0.01112 *
---
Signif. codes:  0 ‘***’ 0.001 ‘**’ 0.01 ‘*’ 0.05 ‘.’ 0.1 ‘ ’ 1

Residual standard error: 3.801e-05 on 9 degrees of freedom
Multiple R-squared:  0.6548,    Adjusted R-squared:  0.5014
F-statistic: 4.268 on 4 and 9 DF,  p-value: 0.03292


Lack of fit test for conversion

Model 1: Conv ~ Temp + Time + Temp:Time
Model 2: Conv ~ Temp + Time + Temp:Time + I(Temp^2) + I(Time^2)
  Res.Df        RSS Df  Sum of Sq     F   Pr(>F)
1     10 1.2749e-08
2      9 5.5007e-09  1 7.2485e-09 11.86 0.007347 **
---
Signif. codes:  0 ‘***’ 0.001 ‘**’ 0.01 ‘*’ 0.05 ‘.’ 0.1 ‘ ’ 1
```

```
Lack of fit test for selectivity
Model 1: Selec1 ~ Temp + Time + Temp:Time
Model 2: Selec1 ~ Temp + Time + Temp:Time + I(Temp^2) + I(Time^2)
  Res.Df        RSS Df  Sum of Sq      F Pr(>F)
1     10 1.7596e-08
2      9 1.3003e-08  1 4.5931e-09 3.1792 0.1083
```

8.11 CENTRAL COMPOSITE DESIGN ANALYSIS FOR EPOXIDATION OF CASTOR OIL

Temp	Time	Conv	Selec	Block
50,0	7,5	81,91	72,21	1
50,0	7,5	81,04	69,58	1
40,0	6,0	53,73	57,62	1
40,0	6,0	59,21	58,2	1
50,0	7,5	83,24	68,85	1
50,0	7,5	79,9	57,19	1
40,0	9,0	68,77	59,75	1
60,0	6,0	78,61	71,73	1
50	7,5	72,24	69,63	1
50	7,5	74,77	58,91	1
60	6	80,14	71,28	1
60	9	91,09	56,24	1
60	9	74,39	56,79	1
40	9	70,18	64,07	1
35,9	7,5	58,84	52,5	2
50	9,6	90	67,99	2
50	5,4	77,74	67,47	2
50	5,4	72,82	65,1	2
64,1	7,5	87,09	71,6	2
35,9	7,5	60,13	53,96	2
64,1	7,5	88,65	59,39	2
50	9,6	85,29	73,57	2

```
Call:
rsm(formula = Conv ~ Block + SO(x1, x2), data = CCDcomp)

            Estimate Std. Error t value  Pr(>|t|)
```

```
(Intercept)  78.8500     1.7670 44.6243 < 2.2e-16 ***
Block2        5.5550     2.1641  2.5669  0.021466 *
x1            9.5391     1.0820  8.8157 2.554e-07 ***
x2            4.2321     1.0820  3.9112  0.001389 **
x1:x2        -2.4100     1.5302 -1.5749  0.136129
x1^2         -5.3637     1.3969 -3.8397  0.001607 **
x2^2         -1.4712     1.3969 -1.0532  0.308915
---
Signif. codes:  0 '***' 0.001 '**' 0.01 '*' 0.05 '.' 0.1 ' ' 1

Multiple R-squared:  0.8823,    Adjusted R-squared:  0.8352
F-statistic: 18.73 on 6 and 15 DF,  p-value: 3.492e-06

Analysis of Variance Table

Response: Conv
            Df  Sum Sq Mean Sq F value    Pr(>F)
Block        1   35.10   35.10  1.8736  0.191214
FO(x1, x2)   2 1742.47  871.23 46.5074 3.712e-07
TWI(x1, x2)  1   46.46   46.46  2.4803  0.136129
PQ(x1, x2)   2  281.39  140.69  7.5103  0.005496
Residuals   15  281.00   18.73
Lack of fit  2    4.26    2.13  0.1000  0.905541
Pure error  13  276.74   21.29

Stationary point of response surface:
       x1        x2
0.6937506 0.8700612

Stationary point in original units:
     Temp      Time
56.937506  8.805092

Eigenanalysis:
eigen() decomposition
$values
[1] -1.128414 -5.706586

$vectors
        [,1]      [,2]
x1  0.273651 -0.961829
x2 -0.961829 -0.273651



Call:
rsm(formula = Selec ~ Block + SO(x1, x2), data = CCDcomp)

            Estimate Std. Error t value  Pr(>|t|)
(Intercept) 66.06167    2.10928 31.3195 4.401e-15 ***
Block2       1.98750    2.58333  0.7694   0.45363
x1           3.19317    1.29166  2.4721   0.02589 *
```

```
x2          -0.57914    1.29166 -0.4484   0.66030
x1:x2       -4.74750    1.82669 -2.5990   0.02014 *
x1^2        -4.34333    1.66753 -2.6046   0.01991 *
x2^2         0.24167    1.66753  0.1449   0.88670
---
Signif. codes:  0 ‘***’ 0.001 ‘**’ 0.01 ‘*’ 0.05 ‘.’ 0.1 ‘ ’ 1

Multiple R-squared:  0.5895,    Adjusted R-squared:  0.4253
F-statistic:  3.59 on 6 and 15 DF,  p-value: 0.02077

Analysis of Variance Table

Response: Selec
            Df Sum Sq Mean Sq F value  Pr(>F)
Block        1   0.27   0.268  0.0101 0.92145
FO(x1, x2)   2 168.51  84.254  3.1562 0.07177
TWI(x1, x2)  1 180.31 180.310  6.7546 0.02014
PQ(x1, x2)   2 225.86 112.929  4.2305 0.03492
Residuals   15 400.42  26.694
Lack of fit  2  96.14  48.069  2.0537 0.16785
Pure error  13 304.28  23.406

Stationary point of response surface:
         x1          x2
-0.04510916  0.75513731

Stationary point in original units:
     Temp      Time
49.548908  8.632706

Eigenanalysis:
eigen() decomposition
$values
[1]  1.249204 -5.350871

$vectors
         [,1]       [,2]
x1  0.3907114 -0.9205132
x2 -0.9205132 -0.3907114
```

9. PHOTOGRAPHIC RECORD

Picture 1

Picture 2

Picture 3

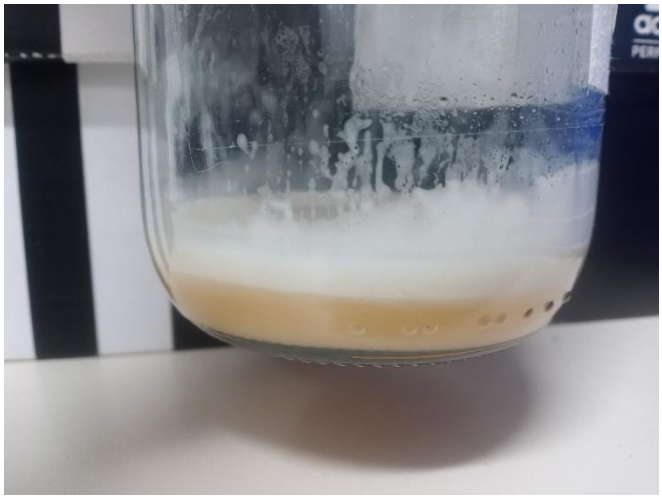

Picture 4

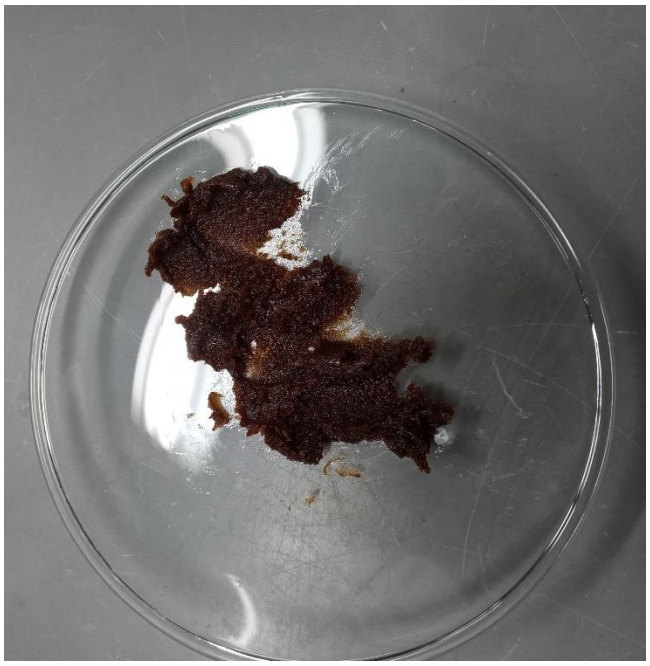

Picture 5

Picture 6

Picture 7

Picture 8

Picture 9

Picture 10

Picture 11

Picture 12

Picture 13

Picture 14

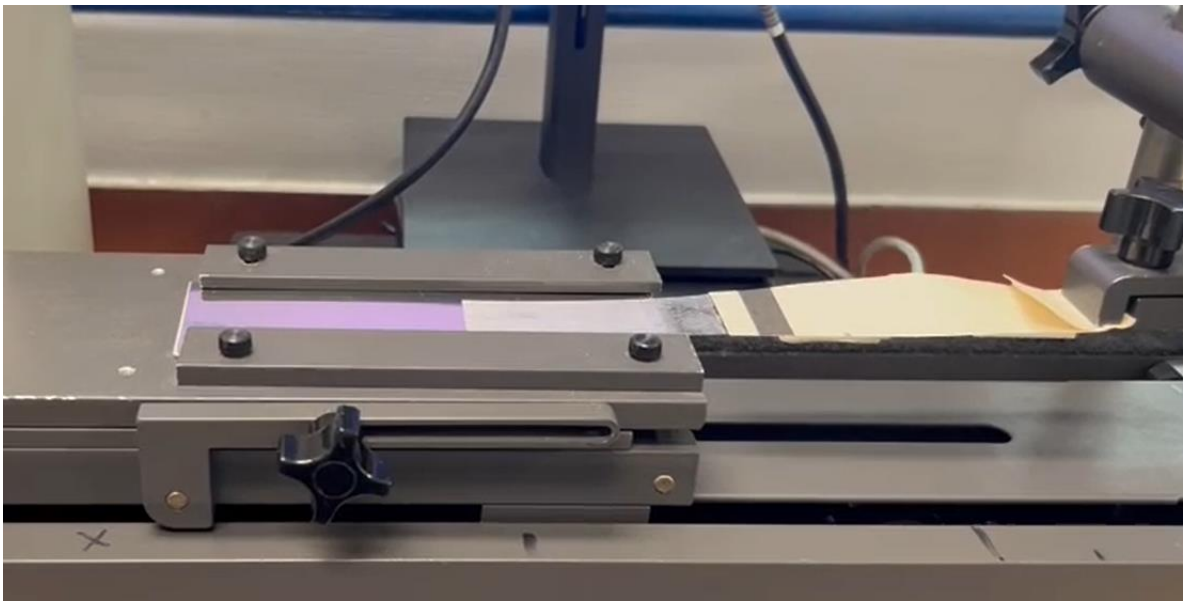

Picture 15

10. REFERENCES

Abdelhalim, I. M. E.-S. (2006). Preparation, Characterization and In-Vitro Evaluation of Chitosan: Vol. PhD. At Massey University.

Aesar, A. (2009). Chitosan Safety Datasheet.

Aesar, A. (2018). Chitosan Certificate of Analysis.

Aesar, A. (2022). Chitosan Product Especification.

Ahmadi, F., Oveisi, Z., Samani, S. M., & Amoozgar, Z. (2015). Chitosan based hydrogels: Characteristics and pharmaceutical applications. Research in Pharmaceutical Sciences, 10(1), 1-16.

Aiba, S. (1989). Studies on chitosan: 2. Solution stability and reactivity of partially N-acetylated chitosan derivatives in aqueous media. International Journal of Biological Macromolecules, 11(4), 249-252. https://doi.org/10.1016/0141-8130(89)90077-9

Aiba, S. (1991). Studies on chitosan: 3. Evidence for the presence of random and block copolymer structures in partially N-acetylated chitosans. International Journal of Biological Macromolecules, 13(1), 40-44. https://doi.org/10.1016/0141-8130(91)90008-I

Aiba, S. (1993). Studies on chitosan 5. Reactivity of partially N-acetylated chitosan in aqueous media. Die Makromolekulare Chemie, 194(1), 65-75. https://doi.org/10.1002/macp.1993.021940105

Akpan, U. G., Jimoh, A., & Mohammed, A. D. (2006). Extraction, characterization and modification of castor seed oil. Leonardo Journal of Sciences, 8, 43-52.

Alvarenga, E. S. de. (2022). Biotechnology of Biopolymers (E. S. de Series Alvarenga, Ed.). INTECH. https://www.intechopen.com/books/158

Alvárez-Paino, M., Juan-Rodríguez, R., Cuervo-Rodríguez, R., Muñoz-Bonilla, A., & Fernández-García, M. (2014). Preparation of amphiphilic glycopolymers with flexible long side chain and their use as stabilizer for emulsion polymerization. Journal of Colloid and Interface Science, 417, 336-345. https://doi.org/10.1016/j.jcis.2013.11.048

Alves, M., Grignard, B., Gennen, S., Detrembleur, C., Jerome, C., & Tassaing, T. (2015). Organocatalytic synthesis of bio-based cyclic carbonates from CO2 and vegetable oils. RSC Advances, 5(66), 53629-53636. https://doi.org/10.1039/C5RA10190E

Anthonsen, M. W., Vårum, K. M., & Smidsrød, O. (1993). Solution properties of chitosans: Conformation and chain stiffness of chitosans with different degrees of

N-acetylation. Carbohydrate Polymers, 22(3), 193-201. https://doi.org/10.1016/0144-8617(93)90140-Y

Aomchad, V., Cristòfol, À., Della Monica, F., Limburg, B., D'Elia, V., & Kleij, A. W. (2021). Recent progress in the catalytic transformation of carbon dioxide into biosourced organic carbonates. Green Chemistry, 23(3), 1077-1113. https://doi.org/10.1039/D0GC03824E

Aranaz, I., Alcántara, A. R., Civera, M. C., Arias, C., Elorza, B., Caballero, A. H., & Acosta, N. (2021). Chitosan: An Overview of its Properties and Applications. Polymers, 13(3256). https://doi.org/10.3390/polym13193256

Arévalo-Alquichire, S., Ramírez, C., Andrade, L., Uscategui, Y., Diaz, L. E., Gómez-Tejedor, J. A., Vallés-Lluch, A., & Valero, M. F. (2018). Polyurethanes from modified castor oil and chitosan: Synthesis, characterization, in vitro degradation, and cytotoxicity. Journal of Elastomers & Plastics, 50(5), 419-434. https://doi.org/10.1177/0095244317729578

ASTM. (1998). Standard Test Method for Acid Value of Fatty Acids and Polimerized Fatty Acids (ASTM D1980).

ASTM. (2004a). Standard Test Method for Epoxy Content of Epoxy Resins (Vol. D1652).

ASTM. (2004b). Standard Test Method for Epoxy Content of Epoxy Resins (ASTM D 1652-04).

ASTM. (2006). Standard Test Method for Determination of the Iodine Value of Fats and Oils (ASTM D5554).

ASTM. (2018). Standard Test Method for Determination of the Iodine Value of Fats and Oils (ASTM D891).

Bähr, M., & Mülhaupt, R. (2012). Linseed and soybean oil-based polyurethanes prepared via the non-isocyanate route and catalytic carbon dioxide conversion. Green Chemistry, 14(2), 483-489. https://doi.org/10.1039/C2GC16230J

Balázs, N., & Sipos, P. (2007). Limitations of pH-potentiometric titration for the determination of the degree of deacetylation of chitosan. Carbohydrate Research, 342, 124-130.

Bauer, T., Tarasiuk, J., & Paśniczek, K. (2002). Highly enantioselective diethylzinc addition to aldehydes catalyzed by d-glucosamine derivatives. Tetrahedron: Asymmetry, 13(1), 77-82. https://doi.org/10.1016/S0957-4166(02)00053-8

Benavides, A., Benjumea, P., & Pashova, V. (2007). El Biodiesel de Aceite de Higuerilla Como Combustible Alternativo Para Motores Diesel. Dyna, 74(153), 141-150.

Bhaskar, T., Pandey, A., Mohan, S. V., Lee, D.-J., & Khanal, S. K. (2018). Waste Biorefinery. Elsevier.

Bietsch, J., Baker, L., Duffney, A., Mao, A., Foutz, M., Ackermann, C., & Wang, G. (2023). Para-Methoxybenzylidene Acetal-Protected D-Glucosamine Derivatives as pH-Responsive Gelators and Their Applications for Drug Delivery. Gels (Basel, Switzerland), 9(6). https://doi.org/10.3390/gels9060445

Birchall, L. S., Roy, S., Jayawarna, V., Hughes, M., Irvine, E., Okorogheye, G. T., Saudi, N., De Santis, E., Tuttle, T., Edwards, A. A., & Ulijn, Rein. V. (2011). Exploiting CH-π interactions in supramolecular hydrogels of aromatic carbohydrate amphiphiles. Chemical Science, 2(7), 1349-1355. https://doi.org/10.1039/C0SC00621A

Birukov, O., Figovsky, O., Leykin, A., Potashnikov, R., & Shapovalov, L. (2012a). Method of producing hybrid polyhydroxyurethane network on a base of carbonated-epoxidized unsaturated fatty acid triglyceride (Patent US 2012/0208967 A1).

Birukov, O., Figovsky, O., Leykin, A., Potashnikov, R., & Shapovalov, L. (2012b). Method of producing hybrid polyhydroxyurethane network on a base of carbonated-epoxidized unsaturated fatty acid triglycerides (Office, United States Patent Patent US 2012/0208967 A1).

Bizet, B. (2020). Design of Waterborne Isocyanate -free Poly (Hydroxy Urethane)s-Poly (Butyl Methacrilate) Hybrids via Miniemulsion and Properties of the Cast Films [PhD]. Université de Bordeaux-Universidad del País Vasco.

Bizet, B., Grau, E., Cramail, H., & Asua, J. M. (2021). Crosslinked isocyanate-free poly(hydroxy urethane)s – Poly(butyl methacrylate) hybrid latexes. European Polymer Journal, 146, 110254. https://doi.org/10.1016/j.eurpolymj.2020.110254

Błażek, K., & Datta, J. (2019). Renewable natural resources as green alternative substrates to obtain bio-based non-isocyanate polyurethanes-review. CRITICAL REVIEWS IN ENVIRONMENTAL SCIENCE AND TECHNOLOGY.

Borugada, V. B., & Goud, V. V. (2014). Epoxidation of castor oil fatty acid methyl esters (COFAME) as a lubricant base stock using heterogeneous ion-exchange resin (IR-120) as a catalyst. Energy Procedia, 54, 75-84.

Boudouaia, N., Bengharez, Z., & Jellali, S. (2019). Preparation and characterization of chitosan extracted from shrimp shells waste and chitosan film: Application for Eriochrome black T removal from aqueous solutions. Applied Water Science, 9(91). https://doi.org/10.1007/s13201-019-0967-z

Boyer, A., Cloutet, E., Tassaing, T., Gadenne, B., Alfos, C., & Cramail, H. (2010). Solubility in CO2 and carbonation studies of epoxidized fatty acid diesters:

Towards novel precursors for polyurethane synthesis. Green Chemistry, 12, 2205-2213.

Büttner, H., Grimmer, C., Steinbauer, J., & Werner, T. (2016). Iron-Based Binary Catalytic System for the Valorization of CO2 into Biobased Cyclic Carbonates. ACS Sustainable Chemistry & Engineering, 4(9), 4805-4814. https://doi.org/10.1021/acssuschemeng.6b01092

Cai, T., Liu, J., Cao, H., & Cui, C. (2020). Synthesis of bio-based cyclic carbonate from vegetable oil methyl ester by CO2 fixation with acid-base pair MOFs. Industrial Crops and Products, 145, 112155. https://doi.org/10.1016/j.indcrop.2020.112155

Cai, X., Zheng, J. L., Wärnå, J., Salmi, T., Taouk, B., & Leveneur, S. (2017). Influence of gas-liquid mass transfer in kinetic modeling: Carbonation of epoxidized vegetable oils. Chemical Engineering Journal, 313, 1168-1183.

Campanella, A., & Baltanás, M. A. (2004). Degradation of the oxirane ring of epoxidized vegetable oils with solvated acetic acid using cation exchange-resins. European Journal of Lipid Science and Technology, 106, 524-530.

Campanella, A., & Baltanás, M. A. (2005). Degradation of the oxirane ring of epoxidized vegetable oils in liquid-liquid systems: II. Reactivity with solvated acetic and peracetic acids. Latin American Applied Research, 35, 211-216.

Campanella, A., Fontanini, C., & Baltanás, M. A. (2008). High yield epoxidation of fatty acid methyl esters with performic acid generated in situ. Chemical Engineering Journal, 144, 466-475.

Canoira, L., Galeán, J. G., Alcántara, R., Lapuerta, M., & García-Contreras, R. (2010). Fatty acid methyl esters (FAMEs) from castor oil: Production process assesment and synergistic effects in its properties. Renewable Energy, 35, 208-217.

Cárdenas, G., Paredes, J. C., Cabrera, G., & Casals, P. (2002). Synthesis and characterization of chitosan alkyl carbamates. Journal of Applied Polymer Science, 86(11), 2742-2747. https://doi.org/10.1002/app.11252

Carré, C., Ecochard, Y., Caillol, S., & Avérous, L. (2019). From the Synthesis of Biobased Cyclic Carbonate to Polyhydroxyurethanes: A Promising Route towards Renewable Non-Isocyanate Polyurethanes. ChemSusChem, 12(15), 3410-3430. https://doi.org/10.1002/cssc.201900737

Chattopadhyay, D. P., & Inamdar, M. S. (2010). Aqueous Behaviour of Chitosan. International Journal of Polymer Science, 2010(Article ID 939536), 7 pages.

Chauke, N. P., Mukaya, H. E., & Nkazi, D. B. (2019). Chemical Modifications of castor oil: A review. Science Progress, 102, 199-217.

Coker, K. A. (2001). Modeling of Chemical Kinetics and Reactor Design. Gulf Professional Publishing.

Conceição, M. M., Candeia, R. A., Silva, F. C., Bezerra, A. F., Jr., V. J. F., & Souza, A. G. (2007). Thermoanalytical characterization of castor oil biodiesel. Renewable and Sustainable Energy Reviews, 11, 964-975.

Cornille, A., Auvergne, R., Figovsky, O., Boutevin, B., & Caillol, S. (2017). A perspective approach to sustainable routes for non-isocyanate polyurethanes. European Polymer Journal, 87, 535-552. https://doi.org/10.1016/j.eurpolymj.2016.11.027

Cornille, A., Blain, M., Auvergne, R., Andrioletti, B., Boutevin, B., & Caillol, S. (2017). A study of cyclic carbonate aminolysis at room temperature: Effect of cyclic carbonate structures and solvents on polyhydroxyurethane synthesis. Polymer Chemistry, 8, 592-604.

Costa, C. N., Teixeira, V. G., Delpech, M. C., Souza, J. V. S., & Costa, M. A. S. (2015). Viscometric Study of Chitosan Solutions in acetic acid/sodium acetate and acetic acid/sodium chloride. Carbohydrate Polymers, 133, 245-250.

Crivello, J. v., & Chakrapani, S. (2000). Epoxidation of Ricin Compounds using a Phase Transfer Catalyst (Patent US 6051725).

Czechowska-Biskup, R., Jarosińska, D., Rokita, B., Ulański, P., & Rosiak, J. M. (2012). Determination of degree of deacetylation of chitosan-Comparision of methods. Progress on Chemistry and Application of Chitin and its Derivatives, 17, 5-20.

Czechowska-Biskup, R., Wach, R. A., Rosiak, J. M., & Ulański, P. (2018). Procedure for determination of the molecular weight of chitosan by viscometry. Progress on Chemistry and Application of Chitin and its Derivatives, 23(DOI: 10.15259.PCACD.23.04).

Das, M., Mandal, B., & Katiyar, V. (2020). Environment-friendly synthesis of sustainable chitosan-based nonisocyanate polyurethane: A biobased polymeric film. Journal of Applied Polymer Science, 137(36), 49050. https://doi.org/10.1002/app.49050

Díez-Pascual, A. M., & Díez-Vicente, A. L. (2015). Wound Healing Bionanocomposites Based on Castor Oil Polymeric Films Reinforced with Chitosan-Modified ZnO Nanoparticles. Biomacromolecules, 16(9), 2631-2644. https://doi.org/10.1021/acs.biomac.5b00447

Doll, K. M., & Erhan, S. Z. (2005). Synthesis of Carbonated Fatty Methyl Esters Using Supercritical Carbon Dioxide. Journal of Agricultural and Food Chemistry, 53, 9608-9614.

Domard, A. (1987). pH and c.d. Measurements on a fully deacetylated chitosan: Application to CuII—polymer interactions. International Journal of Biological Macromolecules, 9(2), 98-104. https://doi.org/10.1016/0141-8130(87)90033-X

Doraiswamy, L. K., & Uner, D. (2013). Chemical Reactor Engineering (1.a ed.). CRC Press.

dos Santos, V. H. J. M., Pontin, D., Rambo, R. S., & Seferin, M. (2020). The Application of Quantitative Structure–Property Relationship Modeling and Exploratory Analysis to Screen Catalysts for the Synthesis of Oleochemical Carbonates from CO2 and Bio-Based Epoxides. Journal of the American Oil Chemists' Society, 97(8), 817-837. https://doi.org/10.1002/aocs.12361

Dul'neva, L. V., & Moskvin, A. V. (2005). Kinetics of Formation of Peracetic Acid. Russian Journal of General Chemistry, 75(7), 1125-1130.

Duval, C., Kébir, N., Jauseau, R., & Burel, F. (2016). Organocatalytic synthesis of novel renewable non-isocyanate polyhydroxyurethanes. Journal of Polymer Science Part A: Polymer Chemistry, 54(6), 758-764. https://doi.org/10.1002/pola.27908

El-Adly, R. A., Shoaib, A. M., A., I. E., & Modather, F. (2014). Optimum Operating Conditions for Epoxidation Reaction of Jojoba and Castor Oil. International Journal of Engineering Research and Applications, 4(3), 816-822.

FAO. (2024). Food and Agriculture Organization of the United Nations Statistics [Dataset]. http://www.fao.org/faostat/en/#data

Farhadian, A., Ahmadi, A., Omrani, I., Miyardan, A. B., Varfolomeev, M. A., & Nabid, M. R. (2018). Synthesis of fully bio-based and solvent free non-isocyanate poly (ester amide/urethane) networks with improved thermal stability on the basis of vegetable oils. Polymer Degradation and Stability, 155, 111-121. https://doi.org/10.1016/j.polymdegradstab.2018.07.010

Fu, Q., Long, Y., Gao, Y., Ling, Y., Qiang, H., Wang, F., & Zhu, X. (2019). Synthesis and properties of castor oil based plasticizers. Royal Society of Chemistry Advances, 9, 10049-10057.

Gallego, R., Arteaga, J. F., Valencia, C., & Franco, J. M. (2013). Isocyanate-functionalized chitin and chitosan as gelling agents of castor oil. Molecules (Basel, Switzerland), 18(6), 6532-6549. https://doi.org/10.3390/molecules18066532

González Martínez, D. A., Vigueras Santiago, E., & Hernández López, S. (2021). Yield and Selectivity Improvement in the Synthesis of Carbonated Linseed Oil by Catalytic Conversion of Carbon Dioxide. Polymers, 13(6). https://doi.org/10.3390/polym13060852

Goud, V. V., Patwardhan, A. V., & Pradhan, N. C. (2006). Strongly Acidic Cation Exchange Resin of Sulphonated Polyestyrene Type used as Catalist for Epoxidation of Castor oil with Peracetic acdi and Performic Acid. Solid State Science and Technology, 14(1), 62-68.

Gupta, K. C., & Jabrail, F. H. (2006). Effects of degree of deacetylation and cross-linking on physical characteristics, swelling and release behavior of chitosan microspheres. Carbohydrate Polymers, 66, 43-54.

Guzmán, A. F. (2016). Formulación y Aplicaciones de un Poliuretano sin Isocianato Basado en Aceite de Higuerilla y Glicerol Subproducto del Biodiesel. En Chemical Engineering: Vol. Master of Engineering. University Of Antioquia.

Haniffa, Mhd. Abd. C. M., Ching, Y. C., Chuah, C. H., Kuan, Y. C., Liu, D.-S., & Liou, N.-S. (2017). Synthesis, Characterization and the Solvent Effects on Interfacial Phenomena of Jatropha Curcas Oil Based Non-isocyanate Polyurethane. Polymers, 9(162). https://doi.org/10.3390/polym9050162

Harriot, P. (2003). Chemical Reactor Design. Marcel Dekker.

Hernandez, N. L. P., Bonon, A. J., Bahú, J. O., Barbosa, M. I. R., Maciel, M. R. W., & Filho, R. M. (2017). Epoxy monomers obtained from castor oil using a toxicity-free catalytic system. Journal of Molecular Catalysis A: Chemical, 426, 550-556.

Higashi, S. L., & Ikeda, M. (2021). Development of an Amino Sugar-Based Supramolecular Hydrogelator with Reduction Responsiveness. JACS Au, 1(10), 1639-1646. https://doi.org/10.1021/jacsau.1c00270

Holser, R. A. (2007). Carbonation of Epoxy Methil Soyate at Atmosferic Pressure. Journal of Oleo Science, 56(12), 629-632.

Honarkar, H. (2018). Waterborne polyurethanes: A review. Journal of Dispersion Science and Technology, 39(4), 507-516. https://doi.org/10.1080/01932691.2017.1327818

Ikeda, D., Tsuchiya, T., & Umezawa, S. (1971). Studies on Aminosugars. XXVIII. Synthesis of β-L-Idopyranosides through the Corresponding 5-Enopyranosides. Bulletin of the Chemical Society of Japan, 44(9), 2529-2537. https://doi.org/10.1246/bcsj.44.2529

Il'ina, A. V., & Varlamov, V. P. (2005). Chitosan-Based Polyelectrolyte Complexes: A Review. Applied Biochemistry and Microbiology, 41(1), 5-11.

Imoto, M., Yoshimura, H., Shimamoto, T., Sakaguchi, N., Kusumoto, S., & Shiba, T. (1987). Total Synthesis of Escherichia coli Lipid A, the Endotoxically Active Principle of Cell-Surface Lipopolysaccharide. Bulletin of the Chemical Society of Japan, 60(6), 2205-2214. https://doi.org/10.1246/bcsj.60.2205

Jalilian, M., Yeganeh, H., & Haghighi, M. N. (2008). Synthesis and properties of polyurethane networks derived from new soybean oil-based polyol and a bulky blocked polyisocyanate. Polymer International, 57, 1385-1394.

Janković, M. R., Sinadinović-Fišer, S., & Govedarica, O. M. (2014). Kinetics of the Epoxidation of Castor Oil with peracetic Acid Formed in situ in the Presence of an Ion-Exchange Resin. Industrial & Engineering Chemistry Research, 53, 9357-9364.

Javni, I., Hong, D. P., & Petrović, Z. S. (2008). Soy-Based Polyurethanes by Nonisocyanate Route. Journal of Applied Polymer Science, 108, 3867-3875.

Javni, I., Zhang, W., & Petrovic, Z. S. (2003). Effect of Different Isocyanates on the Properties of Soy-Based Polyurethanes. Journal of Applied Polymer Science, 88, 2912-2916.

Jian, S., Junyi, R., Zhang, S., & Weigo, C. (2009). Water as an efficient medium for the synthesis of cyclic carbonate. Tetrahedron Letters, 50, 423-426.

Jiang, X., Chen, L., & Zhong, W. (2003). A new linear potentiometric titration method for the determination of deacetylation degree of chitosan. Carbohydrate Polymers, 54, 457-463.

Kamphuis, A. J., Picchioni, F., & Pescarmona, P. P. (2019). CO2-fixation into cyclic and polymeric carbonates: Principles and applications. Green Chemistry, 21, 406-448.

Kasaai, M. R., Arul, J., & Charlet, G. (2000). Intrinsic Viscosity-Molecular weight Relationship for Chitosan. Journal of Polymer Science Part B: Polymer Physics, 38, 2591-2598.

Kassai, M. R., Arul, J., & Charlet, G. (2000). Intrinsic Viscosity-Molecular Weight Relationship for Chitosan. Journal of Polymer Science, 38, 2591-2598.

Kathalewar, M., Sabnis, A., & D'Mello, D. (2014). Isocyanate free polyurethanes form new CSNL based bis-cyclic carbonate and its application in coatings. European Polymer Journal, 57, 99-108.

Kathalewar, M., Sabnis, A., & Waghoo, G. (2013). Effect of incorporation of surface treated zinc oxide on non-isocyanate polyurethane based nano-composite coatings. Progress in Organic Coatings, 76(9), 1215-1229. https://doi.org/10.1016/j.porgcoat.2013.03.027

Khan, M., & Lo, I. M. C. (2016). A holistic review of hydrogel applications in the adsorptive removal of aqueous pollutants: Recent progress, challenges and perspectives. Water Research, 106, 259-271.

Kildeeva, N. R., Perminov, P. A., Vladimirov, L. V., Novikov, V. V., & Mikhailov, S. N. (2009). About Mechanism of Chitosan Cross-Linking with Glutaraldehyde. Russian Journal of Bioorganic Chemistry, 35(3), 360-369.

Knaul, J. Z., Kassai, M. R., Bui, V. T., & Creber, K. A. M. (1998). Characterization of deacetylated chitosan and chitosan molecular weight review. Canadian Journal of Chemistry, 76(11), 1699-1706.

Krajewska, B. (2004). Application of chitin- and chitosan-based materials for enzyme immobilizations: A review. Enzyme and Microbial Technology, 35, 126-139.

Kubota, N., & Eguchi, Y. (1997). Facile Preparation of Water-Soluble N-Acetylated Chitosan and Molecular Weight Dependence of Its Water-Solubility. Polymer Journal, 29(2), 123-127. https://doi.org/10.1295/polymj.29.123

Kurita, K., Sannan, T., & Iwakura, Y. (1977). Studies on chitin, 4. Evidence for formation of block and random copolymers of N-acetyl-D-glucosamine and D-glucosamine by hetero- and homogeneous hydrolyses. Die Makromolekulare Chemie, 178(12), 3197-3202. https://doi.org/10.1002/macp.1977.021781203

Lamarzelle, O., Durand, P.-L., Wirotius, A.-L., Chollet, G., Grau, E., & Cramail, H. (2016). Activated lipidic cyclic carbonates for non-isocyanate polyurethane synthesis. Polymer Chemistry, 7(7), 1439-1451. https://doi.org/10.1039/C5PY01964H

Langanke, J., Greiner, L., & Leitner, W. (2013). Substrate dependent synergetic and antagonistic interaction of ammonium halide and polyoxometalate catalysts in the synthesis of cyclic carbonates from oleochemical epoxides and CO2. Green Chemistry, 15(5), 1173-1182. https://doi.org/10.1039/C3GC36710J

Lee, A., & Deng, Y. (2015). Green polyurethane from lignin and soybean oil through non-isocyanate reactions. European Polymer Journal, 63, 67-73. https://doi.org/10.1016/j.eurpolymj.2014.11.023

Levina, M. A., Miloslavskii, D. G., Pridatchenko, M. L., Gorshkov, A. V., Shashkova, V. T., Gotlib, E. M., & Tiger, R. P. (2015). Green Chemistry of Polyurethanes:Synthesis, Structure and Functionality of Triglycerides of Soybean Oil wit Epoxy and Cyclocarbonate Groups-Renewable Raw Materials for New Urethanes. Polymer Science, 57(6), 584-592.

Li, C.-Y., Li, Y.-H., Hsieh, K.-H., & Chiu, W.-Y. (2008). High-molecular-weight polyurethanes prepared by one-step miniemulsion polymerization. Journal of Applied Polymer Science, 107(2), 840-845. https://doi.org/10.1002/app.25164

Li, Z., Zhao, Y., Yan, S., Wang, X., Kang, M., Wang, J., & Xiang, H. (2008). Catalytic Synthesis of Carbonated Soybean Oil. Catalysis Letters, 123, 246-251.

Liu, W., & Lu, G. (2018). Carbonation of Epoxidized Methyl Soyates in Tetrabutylammonium Bromide-Based Deep Eutectic Solvents. Journal of Oleo Science, 67(5), 609-616. https://doi.org/10.5650/jos.ess17194

Lombardo, V. M., Dhulst, E. A., Leitsch, E. K., Wilmot, N., Heath, W. H., Gies, A. P., Miller, M. D., Torkelson, J. M., & Scheidt, K. A. (2015). Cooperative Catalysis of Cyclic Carbonate Ring Opening: Application Towards Non-Isocyanate Polyurethane Materials. European Journal of Organic Chemistry, 2015(13), 2791-2795. https://doi.org/10.1002/ejoc.201500313

Longwitz, L., Steinbauer, J., Spannenberg, A., & Werner, T. (2018). Calcium-Based Catalytic System for the Synthesis of Bio-Derived Cyclic Carbonates under Mild Conditions. ACS Catalysis, 8(1), 665-672. https://doi.org/10.1021/acscatal.7b03367

Lu, S., Song, X., Cao, D., Che, Y., & Yao, K. (2003). Preparation of Water Soluble Chitosan. Journal of Applied Polymer Science, 91, 3497-3503.

Luo, Z., Shi, Y., Zhao, D., & He, M. (2011). Synthesis of epoxidatied castor oil and its effect on the properties of waterborne polyurethane. Procedia Engineering, 18, 31-36.

Lyalina, T., Zubareva, A., Lopatin, S., Zubov, V., Sizova, S., & Svirshchevskaya, E. (2017). Correlation Analysis of Chitosan Physicochemical Parameters Determined by Different Methods. Organic and Medicinal Chemistry International Journal, 1(3), 555562. DOI: 10.19080/OMCIJ.2017.01.555562.

Mahendran, A. R., Aust, N., Wuzella, G., Müller, U., & Kandelbauer, A. (2012). Bio-Based Non-Isocyanate Urethane Derived from Plant Oil. Journal of Polymers and the Environment, 20(4), 926-931. https://doi.org/10.1007/s10924-012-0491-9

Maisonneuve, L. (2013). Vegetable oils as a platform for the design of sustainable and non-isocyanate thermoplastic polyurethanes. Université Sciences et Technologies-Boudeaux.

Maisonneuve, L., Lamarzelle, O., Rix, E., Grau, E., & Cramail, H. (2015). Isocyanate-Free Routes to Polyurethanes and Poly(hydroxy Urethane)s. Chemical Reviews, 115(22), 12407-12439. https://doi.org/10.1021/acs.chemrev.5b00355

Mazo, P., & Rios, L. (2012). Improved synthesis of carbonates vegetable oils using microwaves. Chemical Engineering Journal, 210, 333-338.

Mazo, P., & Rios, L. (2013). Carbonation of Epoxidized Soybean Oil Improved by the Addition of Water. Journal of the American Oil Chemists Society, 90(5), 725-730.

Meng, L., Soucek, M. D., Li, Z., & Miyoshi, T. (2017). Investigation of a non-isocyanate urethane functional monomer in latexes by emulsion polymerization. Polymer, 119, 83-97. https://doi.org/10.1016/j.polymer.2017.05.006

Mi, F.-L., Tan, Y.-C., Liang, H.-F., & Sung, H.-W. (2002). In vivo biocompatibility and degradability of a novel injectable-chitosan-based implant. Biomaterials, 23, 181-191.

Miloslavskiy, D., Gotlib, E., Figovsky, O., & Pashin, D. (2014). Cyclic Carbonates Based on Vegetable Oils. International Letters of Chemistry, Physics and Astronomy, 8, 20-29.

Missen, R. W., Mims, C. A., & Saville, B. A. (1999). Introduction to Chemical Reaction Engineering and Kinetics. Jhon Wiley & Sons Inc.

Mitura, S., Sionkowska, A., & Jaiswal, A. (2020). Biopolymers for hydrogels in cosmetics: Review. Journal of Materials Science: Materials in Medicine, 31(50), https://doi.org/10.1007/s10856-020-06390-w.

Mokhtari, C., Malek, F., Manseri, A., Caillol, S., & Negrell, C. (2019). Reactive jojoba and castor oils-based cyclic carbonates for biobased polyhydroxyurethanes. European Polymer Journal, 113, 18-28. https://doi.org/10.1016/j.eurpolymj.2019.01.039

Mutlu, H., & Meier, M. A. R. (2010). Castor oil as a renewable resource for the chemical industry. European Journal of Lipid Science and Technology, 112, 10-30.

Nauman, E. B. (2007). Chemical Reactor Design, Optimization and Scaleup. Jhon Wiley & Sons Inc.

Nohra, B., Candy, L., Blanco, J.-F., Guerin, C., Raoul, Y., & Mouloungui, Z. (2013). From Petrochemical Polyurethanes to Biobased Polyhydroxyurethanes. Macromolecules, 46(10), 3771-3792. https://doi.org/10.1021/ma400197c

Nunes, M. R. dos S., Martinelli, M., & Pedroso, M. M. (2008). Epoxidacao do Oleo de Mamona e Derivados Empregando o Sistema Catalítico VO(acac)2/TBHP. Química Nova, 31(4), 818-821.

Ochiai, B., Satoh, Y., & Endo, T. (2005). Nucleophilic polyaddition in water based on chemo-selective reaction of cyclic carbonate with amine. Green Chemistry, 7(11), 765-767. https://doi.org/10.1039/B511019J

Ogunniyi, D. S. (2006). Castor oil: A vital industrial raw material. Bioresource Techonology, 97, 1086-1091.

Parada, L. G., Crespín, G. D., Miranda, R., & Katime, I. (2004). Caracterización de quitosano por viscosimetría capilar y valoración potenciométrica. Revista Iberoamericana de Polímeros, 5(1), 1-16.

Park, S.-J., Jin, F.-L., & Lee, J.-R. (2004). Synthesis and Thermal Properties of Epoxidized Vegetable Oil. Macromolecular Rapid Communications, 25, 724-727.

Parzuchowski, P. G., Jurzcyk-Kowalska, M., Ryszkowska, J., & Rokicki, G. (2006). Epoxy resin Modified with Soybean Oil Containing Cyclic Carbonate Groups. Journal of Applied Polymer Science, 102, 2904-2914.

Patel, V. R., Dumancas, G. D., Viswanath, L. C. K., Maples, R., & Subong, B. J. (2016). Castor oil: Properties, Uses and Optimization of Processing Parameters in Commercial Production. Lipid Insights, 9, 1-12.

Pathak, R., Kathalewar, M., Wazarkar, K., & Sabnis, A. (2015). Non-isocyanate polyurethane (NIPU) from tris-2-hydroxy ethyl isocyanurate modified fatty acid for coating applications. Progress in Organic Coatings, 89, 160-169. https://doi.org/10.1016/j.porgcoat.2015.08.015

Peña Carrodeguas, L., Cristòfol, À., Fraile, J. M., Mayoral, J. A., Dorado, V., Herrerías, C. I., & Kleij, A. W. (2017). Fatty acid based biocarbonates: Al-mediated stereoselective preparation of mono-, di- and tricarbonates under mild and solvent-less conditions. Green Chemistry, 19(15), 3535-3541. https://doi.org/10.1039/C7GC01206C

Pérez-Sena, W. Y., Cai, X., Kebir, N., Verniéres-Hassimi, L., Serra, C., Salmi, T., & Leveneur, S. (2018). Aminolysis of cyclic-carbonate vegetable oils as a non-isocyanate route for the synthesis of polyurethane: A kinetic and thermal study. Chemical Engineering Journal, 346, 271-280.

Pestov, A., Privar, Y., Slobodyuk, A., Boroda, A., & Bratskaya, S. (2022). Chitosan Cross-Linking with Acetaldehyde Acetals. Biomimetics, 7(1). https://doi.org/10.3390/biomimetics7010010

Pirola, C., Rossetti, I., & Ragaini, V. (2013). Are Conversion , seleCtivity And yield terms unAmbiguously defined in ChemiCAl And ChemiCAl engineering terminology ? https://api.semanticscholar.org/CorpusID:209543940

Piyataksanon, N., Suttiruengwong, S., & Seadan, M. (2022). Bio-based Polyurethane Derived from Carbon Dioxide and Epoxidized Soybean Oil. Suan Sunandha Science and Technology Journal, 9(2), 8-14. https://doi.org/10.53848/ssstj.v9i2.229

Pouladi, J., Mirabedini, S. M., Eivaz Mohammadloo, H., & Rad, N. G. (2021). Synthesis of novel plant oil-based isocyanate-free urethane coatings and study of their anti-corrosion properties. European Polymer Journal, 153, 110502. https://doi.org/10.1016/j.eurpolymj.2021.110502

Poussard, L., Mariage, J., Grignard, B., Detrembleur, C., Jérôme, C., Calberg, C., Heinrichs, B., Winter, J. D., Gerbaux, P., Raquez, J.-M., Bonnaud, L., & Dubois, Ph. (2016). Non-Isocyanate Polyurethanes from Carbonated Soybea Oil Using Monomeric or Oligomeric Diamines To Achieve Thermosets or Thermoplastics. Macromolecules, 49, 2162-2171.

Qian, X., & Hindsgaul, O. (1997). Use of the p-nitrobenzyloxycarbonyl group as an orthogonal amine protecting group in the synthesis of β-GlcNAc terminating glycosides. Chemical Communications, 11, 1059-1060. https://doi.org/10.1039/A700549K

Ren, F.-Y., You, F., Gao, S., Xie, W.-H., He, L.-N., & Li, H.-R. (2021). Oligomeric ricinoleic acid synthesis with a recyclable catalyst and application to preparing non-isocyanate polyhydroxyurethane. European Polymer Journal, 153, 110501. https://doi.org/10.1016/j.eurpolymj.2021.110501

Rihayat, T., Suryani, Riskina, S., Sirega, J. P., Jaafar, J., Cionita, T., & Fitria. (2020). Making Polyurethanes from castor oil with addition of Bentonite and Chitosan as coating paints on eco-friendly medical device applications. IOP Conference Series: Materials Science and Engineering, 788(1), 012046. https://doi.org/10.1088/1757-899X/788/1/012046

Rinaudc, M., Pavlov, G., & Desbrieres, J. (1999). Solubilization of Chitosan in Strong Acid Medium. International Journal of Polymer Analysis and Characterization, 5, 267-276. https://doi.org/10.1080/10236669908009742

Rinaudo, M. (2006). Chitin and chitosan: Properties and applications. Progress in Polymer Science, 31, 603-632.

Rinaudo, M., Milas, M., & Dung, P. L. (1993). Characterization of chitosan. Influence of ionic strenght and degree of acetylation on chain expansion. International Journal of Biological Macromolecules, 15, 281-285.

Rinaudo, M., Pavlov, G., & Desbrières, J. (1999). Influence of acetic acid concentration on the solubilization of chitosan. Polymer, 40(25), 7029-7032. https://doi.org/10.1016/S0032-3861(99)00056-7

Rix, E., Grau, E., Cholet, G., & Cramail, H. (2016). Synthesis of fatty acid-based non-isocyanate polyurethanes, NIPUs, in bulk and mini-emulsion. European Polymer Journal, 84, 863-872.

Rokicki, G., Parzuchowski, P. G., & Mazurek, M. (2015). Non-isocyanate polyurethanes: Synthesis, properties, and applications. Polymers for Advanced Technologies, 26(7), 707-761. https://doi.org/10.1002/pat.3522

Ruiz, L., Aghmiz, A., Masdeu-Bultó, A. M., Lligadas, G., Ronda, J. C., Galià, M., & Cádiz, V. (2017). Upgrading castor oil: From heptanal to non-isocyanate poly(amide-hydroxyurethane)s. Polymer, 124, 226-234. https://doi.org/10.1016/j.polymer.2017.07.070

Sadeghi, M., Hanifpour, F., Taheri, R., Javadian, H., & Gashemi, M. (2016). Comparisong of using formaldehyde and carboxy methyl chitosan in preparation of Fe3O4 superparamagnetic nanoparticles-chitosan hydrogel network: Sorption

behavior towrd bovine serum albumin. Process Safety and Environmental Protection, 102, 119-128.

Salimon, J., Salih, N., & Yousif, E. (2012). Biolubricant basestocks from chemically modified ricinoleic acid. Journal of King Saud University, 24, 11-17.

Schäffner, B., Blug, M., Kruse, D., Polyakov, M., Köckritz, A., Martin, A., Rajagopalan, P., Bentrup, U., Brückner, A., Jung, S., Agar, D., Rüngeler, B., Pfennig, A., Müller, K., Arlt, W., Woldt, B., Graß, M., & Buchholz, S. (2014). Synthesis and Application of Carbonated Fatty Acid Esters from Carbon Dioxide Including a Life Cycle Analysis. ChemSusChem, 7(4), 1133-1139. https://doi.org/10.1002/cssc.201301115

Shridhar, B. S., Beena, K. V., Anita, M. V., & Paramjeet, K. B. (2010). Optimization and Characterization of Castor Seed Oil. Leonardo Journal of Sciences, 17, 59-70.

Sinadinović-Fišer, S., Janković, M., & Borota, O. (2012). Epoxidation of castor oil with peracetic acid formes in situ in the presence of an ion exchange resin. Chemical Engineering and Processing: Process Intensification, 62, 106-113.

Sinadinovic-Fiser, S., Jankovic, M., & Petrovic, Z. S. (2001). Kinetics of in-situ Epoxidation of Soybean Oil in Bulk Catalyzed by Ion Exchange resin. Journal of the American Oil Chemists' Society, 78(7), 725-731.

Skoog, D. A., Haller, F. J., & Nieman, T. A. (2000). Principles of Instrumental Analysis (5.a ed.).

Steblyanko, A., Choi, W., Sanda, F., & Endo, T. (2000). Addition of five membered Cyclic Carbonate with Amine and its application to Polymer synthesis. Journal of Polymer Science, 38, 2375-2380.

Sudha, G. S., Kalita, H., Mohanty, S., & Nayak, S. K. (2017). Castor oil modified by epoxidation, transesterification and acrylation processes: Spectroscopic characteristics. International Journal of Polymer Analysis and Characterization, 22, 519-525.

Sweidan, K., Jaber, A.-M., Al-jbour, N., Obaidat, R., Al-Remawi, M., & Badwan, A. (2011). Further inverstigation on the degree of deacetylation of chitosan determined by potentiometric titration. Journal of Excipients and Food Chemicals, 2(16-25).

Tamami, B., Sohn, S., & Wilkes, G. L. (2004). Incorporation of Carbon Dioxide into Soybean Oil and Subsequent Preparation and Studies of Nonisocyanate Polyurethane Networks. Journal of Applied Polymer Science, 92(883-891).

Tamilvanan, S., Kumar, B. A., Senthilkumar, S. R., Baskar, R., & Sekharan, T. R. (2010). Stability assessment of injectable castor oil-based nano-sized emulsion

containing cationic droplets stabilized by poloxamer-chitosan emulsifier films. AAPS PharmSciTech, 11(2), 904-909. https://doi.org/10.1208/s12249-010-9455-3

Tan, S. C., Khor, E., Tan, T. K., & Wong, S. M. (1998). The degree of deacetylation of chitosan: Advocating the first derivative UV-spectrophotometry method of determination. Talanta, 45, 713-719.

Tenhumberg, N., Büttner, H., Schäffner, B., Kruse, D., Blumenstein, M., & Werner, T. (2016). Cooperative catalyst system for the synthesis of oleochemical cyclic carbonates from CO2 and renewables. Green Chemistry, 18(13), 3775-3788. https://doi.org/10.1039/C6GC00671J

Tiger, R., Zabalov, M., & Levina, M. (2021). Mechanisms of Reactions of Green Chemistry of Polyurethanes and Problems of Using Renewable Vegetable Raw Materials. Polymer Science, Series C, 63, 113-125. https://doi.org/10.1134/S1811238221020090

Tolaimate, A., Desbrières, J., Rhazi, M., Alagui, A., Vincendon, M., & Vottero, P. (2000). On the influence of deacetylation process on the physicochemical characteristics of chitosan from squid chitin. Polymer, 41, 2463-2469.

Tomita, H., Sanda, F., & Endo, T. (2001). Reactivity comparison of Five- and Six-Membered Cyclic Carbonates with Amines: Basic Evaluation for Synthesis of Poly(hydroxyurethane). Journal of Polymer Science Part A: Polymer Chemistry, 39, 162-168.

Türünç, O., Kayaman-Apohan, N., Kahraman, M., Menceloglu, Y., & Guengoer, A. (2008). Nonisocyanate based polyurethane/silica nanocomposites and their coating performance. Journal of Sol-Gel Science and Technology, 47, 290-299. https://doi.org/10.1007/s10971-008-1786-0

Ullah, F., Othman, M. B. H., Javed, F., Ahmad, Z., & Alkil, H. Md. (2015). Classification, processing and application of hydrogels: A review. Materials Science and Engineering C, 57, 414-433.

Uscátegui, Y. L., Díaz, L. E., Gómez-Tejedor, J. A., Vallés-Lluch, A., Vilariño-Feltrer, G., Serrano, M. A., & Valero, M. F. (2019). Candidate Polyurethanes Based on Castor Oil (Ricinus communis), with Polycaprolactone Diol and Chitosan Additions, for Use in Biomedical Applications. Molecules (Basel, Switzerland), 24(2). https://doi.org/10.3390/molecules24020237

Valério, A., Fortuny, M., Santos, A. F., Araújo, P. H. H., & Sayer, C. (2015). Poly(Urea–Urethane) Synthesis by Miniemulsion Polymerization Using Microwaves and Conventional Polymerization. Macromolecular Reaction Engineering, 9(1), 48-59. https://doi.org/10.1002/mren.201400029

Vårum, K. M., Anthonsen, M. W., Grasdalen, H., & Smidsrød, O. (1991a). 13C-n.m.r. Studies of the acetylation sequences in partially N-deacetylated chitins

(chitosans). Carbohydrate Research, 217, 19-27. https://doi.org/10.1016/0008-6215(91)84113-s

Vårum, K. M., Anthonsen, M. W., Grasdalen, H., & Smidsrød, O. (1991b). Determination of the degree of N-acetylation and the distribution of N-acetyl groups in partially N-deacetylated chitins (chitosans) by high-field n.m.r. Spectroscopy. Carbohydrate Research, 211(1), 17-23. https://doi.org/10.1016/0008-6215(91)84142-2

Wang, G., Cheuk, S., Yang, H., Goyal, N., Reddy, P. V. N., & Hopkinson, B. (2009). Synthesis and Characterization of Monosaccharide-Derived Carbamates as Low-Molecular-Weight Gelators. Langmuir, 25(15), 8696-8705. https://doi.org/10.1021/la804337g

Wang, J., Zhao, Y., Li, Q., Yin, N., Feng, Y., Kang, M., & Wang, X. (2012). Pt Doped H3PW12O40/ZrO2 as a Heterogeneous and Recyclable Catalyst for the Synthesis of Carbonated Soyeban Oil. Journal of Applied Polymer Science, 124, 4298-4306.

Wilkes, G. L., Sohn, S., & Tamami, B. (2006). Nonisocyanate Polyurethane Materials, and their Preparation from Epoxidized Soybean Oils, Incorporation of Carbon Dioxide into Soybean Oil, and Carbonation of Vegetable Oils (Office, United States Patent Patent US 7045577 B2).

Yeboah, A., Ying, S., Lu, J., Xie, Y., vAmoanimaa-Dede, H., Boateng, K. G. A., Chem, M., & Yin, X. (2020). Castor oil (Ricinus communis): A review on the chemical composition and physicochemical properties. Food Science and Technology. https://doi.org/10.1590/fst.19620

Yu, A. Z., Setien, R. A., Sahouani, J. M., Docken, J. S., & Webster, D. C. (2018). Catalyzed non-isocyanate polyurethane (NIPU) coatings from bio-based poly(cyclic carbonates). Journal of Coatings Technology and Research, 16, 41-57.

Zabalov, M., Levina, M., & Tiger, R. (2020). Various Reactivity of Cyclocarbonate-Containing Chains of Vegetable Oil Triglycerides as the Cause of the Abnormal Kinetics of Urethane Formation with Their Participation. Polymer Science, Series B, 62, 457-464. https://doi.org/10.1134/S1560090420050152

Zalewski, M. J., Mamiński, M. Ł., & Parzuchowski, P. G. (2022). Synthesis of Polyhydroxyurethanes—Experimental Verification of the Box–Behnken Optimization Model. Polymers, 14(21). https://doi.org/10.3390/polym14214510

Zalomaeva, O. V., Chibiryaev, A. M., Kovalenko, K. A., Kholdeeva, O. A., Balzhinimaev, B. S., & Fedin, V. P. (2013). Cyclic carbonates synthesis from epoxides and CO2 over metal-organic framework Cr-MIL-101. Journal of Catalysis, 298, 179-185.

Zalomaeva, O. V., Maksimchuk, N. V., Chibiryaev, A. M., Kovalenko, K. A., Fedín, V. P., & Balzhinimaev, B. S. (2013). Synthesis of cyclic carbonates from epoxides or olefins and CO2 catalyzed by metal-organic frameworks and quaternary ammonium salts. Journal of Energy Chemistry, 22, 130-135.

Zanetti-Ramos, B. G., Lemos-Senna, E., Soldi, V., Borsali, R., Cloutet, E., & Cramail, H. (2006). Polyurethane nanoparticles from a natural polyol via miniemulsion technique. Polymer, 47(24), 8080-8087. https://doi.org/10.1016/j.polymer.2006.09.057

Zhang, C., Madbouly, S. A., & Kessler, M. R. (2015). Biobased Polyurethanes Prepared from Different vegetable Oils. ACS Applied Materials & Interfaces, 7, 1226-1233.

Zhang, D., Lin, Y., Li, A., & Tarasov, V. V. (2011). Emulsification for castor biomass oil. Frontiers of Chemical Science and Engineering, 5(1), 96-101.

Zhang, H., Li, Y., Zhang, X., Liu, B., & Zhao, H. (2016). Directly determining the molecular weight of chitosanwith atomic force microscopy. Front Nanosci Nanotech 2. https://doi.org/10.15761/FNN.1000121

Zhang, L., Luo, Y., Huo, Z., He, Z., & Eli, W. (2014). Synthesis of Carbonated Cotton Seed Oil and Its Application as Lubricating Base Oil. Journal of the American Oil Chemists Society, 91, 143-150.

Zhang, W., Deng, H., Xia, L., Shen, L., Zhang, C., Lu, Q., & Sun, S. (2021). Semi-interpenetrating polymer networks prepared from castor oil-based waterborne polyurethanes and carboxymethyl chitosan. Carbohydrate Polymers, 256, 117507. https://doi.org/10.1016/j.carbpol.2020.117507

Zhang, W., Zhang, Y., Liang, H., Liang, D., Cao, H., Liu, C., Qian, Y., Lu, Q., & Zhang, C. (2019). High bio-content castor oil based waterborne polyurethane/sodium lignosulfonate composites for environmental friendly UV absorption application. Industrial Crops and Products, 142, 111836. https://doi.org/10.1016/j.indcrop.2019.111836

Zheng, J. L., Burel, F., Salmi, T., Taouk, B., & Leveneur, S. (2015). Carbonation of Vegetable Oils: Influence of Mass Transfer on Reaction Kinetics. Industrial & Engineering Chemistry Research.

Zheng, J.-L., Tolvanen, P., Taouk, B., Eränen, K., Leveneur, S., & Salmi, T. (2018). Synthesis of carbonated vegetable oils: Investigation of microwave effect in a pressurized continuous-flow recycle batch reactor. Chemical Engineering Research and Design, 132, 9-18. https://doi.org/10.1016/j.cherd.2017.12.037

Zheng, Y., Chen, X., & Shen, Y. (2008). Commodity Chemicals Derived from Glycerol, an Important Biorefinery Feedstock. Chemical Reviews, 108, 5253-5277.